



The EMPIR initiative is co-funded by the European Union's Horizon 2020 research and innovation programme and the EMPIR Participating States

17NRM03 EUCoM

Evaluating Uncertainty in Coordinate Measurement

GUIDELINES ON UNCERTAINTY OF COORDINATE MEASUREMENTS A PRIORI USING TYPE B EVALUATION

DELIVERABLE D2

Lead partner: NPL

Alistair Forbes, Wojciech Płowucha, Alessandro Balsamo

Deliverable Due Date: March 2021

Actual Submission Date: 2022-02-01

Table of Contents

1	Abstract	3
2	Introduction	3
2.1	Project background	3
2.2	Objective of <i>a priori</i> methods	3
3	<i>A priori</i> information available to type B methods	4
3.1	Input uncertainties.....	4
3.2	Sensitivity coefficients.....	5
4	Structure of this document	7
5	References.....	7
Section 1	Method B1 - An a priori method for CMM uncertainty evaluation based on approximate models of CMM behaviour	
Section 2	Method B2 - An a priori method for CMM uncertainty evaluation based on essential sets of measurement points	
	Conclusion	

1 Abstract

This document describes two *a priori* methods for evaluating the uncertainty of measurement in coordinate metrology. *A priori* means that the needed information is known *prior to* the actual measurement. This enables *predicting* the uncertainty and then comparing among possible different experimental plans to pursue one or more measurands. These methods are referred to as Methods B to reflect the type B evaluation of the uncertainty according to the GUM.

The main source of prior information is the set of metrological characteristics standardized in the EN ISO 10360 series of standards, which is well accepted and widely used in industry. Either the actual measured values or the specification on data sheets (the MPEs, *Maximum Permissible Errors*) of such metrological characteristics can be fed to the methods B.

To propagate the input uncertainties to the combined uncertainties, suitable sensitivity coefficients are needed, usually arranged in matrices. These matrices reflect the nominal geometry at hand, the sampling strategy and the sequence and choice of mathematical operators employed to derive the results. They are independent of actual measurements taken and hence predictable.

Two Methods B are described in this document, referred to as B1 and B2. The latter was not anticipated in the project protocol and is an extra result of the project. The two methods are similar in the evaluation of the input uncertainties but completely different and independent to each other in the sensitivity analysis, that is, in the way the input uncertainty are propagated to the combined uncertainties.

2 Introduction

2.1 Project background

EUCoM – Evaluating Uncertainties in Coordinate Measurement – is an EMPIR/Euramet-supported project to develop new methods for estimating the uncertainties of tactile measurements. There are two basic approaches, named methods A and B¹:

- **A posteriori** (Method A): Estimate uncertainties using experimental data from repeated measurements in four different orientations. A length and a sphere standard must also be measured.
- **A priori** (Method B): Estimate uncertainties using expert knowledge and performance characteristics of or prior experience with the CMM (coordinate measuring machine) being used.

In essence, method A is an empirical approach to measurement uncertainty. While it requires more measurement work to be done, it does not depend on any modelling of the particular measurement system used to obtain it. Method B is the exact opposite, requiring no prior data other than information that would usually be available from prior use of the system.

2.2 Objective of *a priori* methods

The main objective of *a priori* methods is to *predict* the uncertainty before any measurements are *taken*. This is useful for checking whether a perspective measurement strategy is adequate for a predefined target uncertainty and to compare among alternative CMMs and strategies. In this way, *a priori* methods are important design of experiment tools and important for constructing a measurement methodology that will be fit for purpose.

Another objective of *a priori* methods is to estimate the uncertainties associated with actual measurements based on information that is available prior to the measurements without the need for i) additional statistical analysis of the actual measurement results, which may require

¹ The methods are named “A” and “B” with reference to the types of evaluation of the uncertainty described in the GUM [3] 4.2 and 4.3.

resources that are not available, nor ii) additional experiments that are required by a *posteriori* methods.

The *a priori* nature of methods B imposes that the evaluation cannot count on experimental information derived from the specific measurement being evaluated, it can only on general information about the CMM and the environment. As a consequence, the information fed to methods B is likely weaker than to methods A: the uncertainty evaluated with methods B will likely be coarser. When both methods are applicable, methods B are recommended only when the target uncertainty is not tight, in view of the saving of the experimental effort.

3 A priori information available to type B methods

The ambition of methods B is to rely on information that is already available to the user with no or little extra experimental effort.

Two main sources of information are needed to evaluate the uncertainty according to the GUM: the input standard uncertainties and the sensitivity coefficients. The following sections address either one.

3.1 Input uncertainties

The main source of such information is the metrological characteristics of CMMs as defined in the EN ISO 10360 series of standards. This series provides a set of predefined indicators—the metrological characteristic—to measure the CMM performance. CMMs are versatile and re-programmable instruments able to perform a virtually infinite number of measurement tasks. Verify them all experimentally would not be viable for any standardized procedure. The approach of the EN ISO 10360 is to select a limited number of measuring tasks identified by the standard maker² as a reasonable compromise between thoroughness and coverage of the tests. These tasks are summarised by a set of metrological characteristics deemed as paradigmatic of the actual CMM performance. The most relevant for the methods B in this document—which is limited to tactile Cartesian CMMs—are defined in EN ISO 10360-2 [1] and EN ISO 10360-5 [2], namely:

- E_L , *length measurement error* (EN ISO 10360-2). This is the error of indication of a CMM when measuring a calibrated test length bi-directionally. A calibrated test length is implemented by means of either a material or an immaterial standard of size. Examples of material standards of size are gauge blocks and step gauges; examples of immaterial ones are a CMM rectilinear movement directly measured by interferometry. Bi-directionally means that the probing occurring at the opposite ends of the standard are along opposite directions. For instance, this is the natural case for gauge blocks, it is between an even and an odd face of a step gauges, and it is on the opposite faces of an auxiliary short gauge blocks sliding along a straight line whose displacement is measured interferometrically³. This metrological characteristic captures the CMM capability of measuring distances accurately regardless of their orientations in the measurement volume. It is a powerful indicator of how well-behaved the measurement volume is. The volume can be envisaged as a 3D grid of equally-spaced coordinate lines; only when the grid is perfectly straight, square and traceably sized, the distance between any points pair is without error. The errors are a good measure of how the actual volume deviates from the nominal, that is, how curved, oblique and expanded/compressed it is.
- P_{Size} , *size error* (EN ISO 10360-5). This is the error of indication of the diameter of a calibrated test sphere measured with one or more styli, each probing a predefined number of points (25) evenly spaced on a hemisphere.

² The competent standardization body is the ISO/TC 213 *Dimensional and Geometrical Product Specification and Verification*. The preparation work on this subject matter is assigned to the ISO/TC 213/WG 10 *CMMs*.

³ More examples and details are found in the Annex B of [2].

This metrological characteristic captures the CMM capability of a probing system of localising the probed points on the workpiece surface relative to a representative point of the ram whose coordinates are measured as the three scale readings. A positive error indicates that the surface is sensed as shifted out of the material and vice versa.

- P_{Form} , *form error* (EN ISO 10360-5). This is the form error (span of the radial distances of the measured points) of a calibrated test sphere measured with one or more styli, each probing a predefined number of points (25) evenly spaced on a hemisphere. As the actual form error of the test sphere is required to be small relative with the CMM performance, the measured form error is attributed to the CMM.

This metrological characteristic captures the CMM capability of a probing system of sensing the workpiece surface independently of its orientation, or equivalently, independently of the probing direction. Any anisotropy of the probing system results in a measured form error of the nearly perfectly-shaped test sphere.

- $L_{\text{Dia.5}\times 25}$, *multi-stylus location error* (EN ISO 10360-5). This is the 3D span⁴ of 5 test sphere centres measured with as many different styli (e.g., those of a star stylus system). When multiple styli are involved in a same measurement, the relative offsets of their tip centres are very relevant for the final accuracy and are taken care of automatically by the CMM. The offsets are derived experimentally beforehand in the qualification procedure of the probing system. Any error in determining such offsets results in measuring a same physical sphere at different locations.

This metrological characteristic captures the CMM capability of relating the measurements taken with different probe styli to each other.

The above metrological characteristics are subject to MPEs (*Maximum Permissible Errors*). They are set by the CMM manufacturer for acceptance testing and by the CMM user for reverification testing. In all cases, testing according to the EN ISO 10360 series requires that each metrological characteristic is assigned an MPE.

When applying methods B, the actual values of the metrological characteristics may or may not be available. A necessary condition for the former case is that the CMM is identified: different CMMs—even of the same model—may perform differently within the common MPEs. When a specific CMM is not defined instead (even if its model is), such values are not available. This situation may occur when several CMMs of the same model are available—for instance in a large laboratory or workshop—or when one or more models are being compared to each other based on a specific measurement task.

In all cases, MPEs are assumed to be available. They may be derived from the CMM data sheets, or from the purchase contract, or from company regulations aiming at guaranteeing that the CMM is fit for purpose.

When both the measured value and the MPE are available of a metrological characteristic, it is recommended that the former is fed to the methods B for the uncertainty evaluation. In fact, the measured values are more tailored to a specific CMM than the MPEs are, which applies to all CMMs of that model instead.

3.2 Sensitivity coefficients

The sensitivity coefficients express how the measurand varies when the input quantities vary: the more it does the larger the coefficients. Their fundamental role is in the propagation of the input uncertainties to the combined uncertainty.

When the measurand is scalar, i.e. when a single quantity is under measurement, the sensitivity coefficients are the partial derivatives of the measured quantity to the input quantities, see [3] 5.1.3. They collectively form a vector with as many components as input quantities. A convenient equation for the propagation is

⁴ More precisely, this is the diameter of the minimum circumscribed sphere encompassing all measured centres.

$$u_y^2 = \mathbf{c}^T \mathbf{V}_x \mathbf{c}, \quad c_j = \frac{\partial y}{\partial x_j}$$

where \mathbf{c} is the vector of the n sensitivity coefficients and \mathbf{V}_x the $(n \times n)$ variance matrix of the n input quantities, \mathbf{x} . This equation accounts for the possible correlation of the input quantities, manifested by non-null covariances appearing off-diagonal in \mathbf{V}_x .

Typical measuring tasks in coordinate metrology involve multiple measurands at the same time. For instance, the measurement of a cylinder involves a localisation point on and an orientation unit vector of its axis, and an intrinsic dimensional quantity such as the diameter⁵. The measurands are not a single scalar in this case, rather a vector of m quantities, \mathbf{y} , and the complete description of their uncertainties is an $(m \times m)$ variance matrix, \mathbf{V}_y . The sensitivity coefficients follow this increase in the dimension of the problem: the vector of coefficients becomes a $(m \times n)$ sensitivity matrix, $\mathbf{G}_{y|x}$ and the uncertainty propagation is

$$\mathbf{V}_y = \mathbf{G}_{y|x} \mathbf{V}_x \mathbf{G}_{y|x}^T, \quad (\mathbf{G}_{y|x})_{ij} = \frac{\partial y_i}{\partial x_j}$$

Usually, multiple geometric elements are involved at the same time with measurands derived from their combination. Some geometric features may be involved for the measurand even though they are not in the measurand. The typical case is that of datum features: they constrain relevant locations and orientations of the measurands but are not part of them. For instance, the orthogonality of the median line of a cylinder to a datum plane involves the distances of the centres of the nominally-circular sections of the cylinder, to a line orthogonal to the plane. The plane orientation plays an essential role in the measurement but is not a measurand. Obviously the plane orientation is relevant for the uncertainty but is not explicit in any variance matrix; it is rather “hidden” in the sensitivity matrix $\mathbf{G}_{y|x}$.

The sensitivity analysis is particularly suited for dealing with such cases. The chain rule of derivation enables expressing the overall sensitivity matrix as the product of sensitivity matrices relevant for intermediate calculations. In the above example, if \mathbf{a} is the unit vector normal to the plane, the overall sensitivity matrix can be derived as $\mathbf{G}_{y|x} = \mathbf{G}_{y|\mathbf{a}} \mathbf{G}_{\mathbf{a}|x}$, where $\mathbf{G}_{\mathbf{a}|x}$ is the sensitivity of the plane orientation to the probed points (no involvement of the cylinder) and $\mathbf{G}_{y|\mathbf{a}}$ that of the measurands to an orientation (no involvement of the plane): full decoupling of the two involved elements is achieved.

The sensitivity matrix depends only on the problem geometry, the sampling strategy and the choice and sequence of mathematical operator to derive the results. In principle, the *actual* geometry and sampling should be considered, with all their imperfections. However, the sensitivity is dominated by *macroscopic* quantities (such as distances between elements and extents of elements), whereas their *microscopic* imperfections are second-order. In conclusion, the sensitivity analysis requires detailed *prior* knowledge of the *nominal* geometry and sampling strategy and of the sequence of computation.

This knowledge is in fact embodied in the part programme of the measurement task. When one is available (for instance developed in a previous similar measurement), the needed information is all available and can be derived automatically (at least in principle, when suitable software tools are able to). In the most general scenario, no part programme is available. The nominal geometry is known, as defined by, e.g., drawings or CAD models. The sampling strategy and the computation is not. Deciding on them is a very important task of the metrologist's. The *a priori* Methods B helps in doing: alternatives are considered, their sensitivities are analysed, and one is selected as the best trade-off between small uncertainty and low measurement cost.

⁵ These measurands are the parameters of the parameterisation of the element. A set of standardised parametrisations is found in [4] Table 3.

4 Structure of this document

The EUCoM project aimed at developing one Method B. Its conceptual flow is anticipated in the project protocol.

In the course of the project, another method B was found. Both are *a priori*, that is, based on essentially the same or similar prior information on the CMM. Apart from that, the two methods are independent to each other and alternative, and exhibit different characteristics as to the treatment of data, the equations involved and the needed software.

For brevity, the two methods are referred to hereafter as Method B1 and B2, respectively: that originally foreseen in the project protocol is B1.

The following two Sections describes methods B1 and B2, respectively.

Some common conclusions follow at the end.

5 References

- [1] *EN ISO 10360-2:2009 Geometrical product specifications (GPS) - Acceptance and reverification tests for coordinate measuring machines (CMM) - Part 2: CMMs used for measuring linear dimensions, 2009.*
- [2] *EN ISO 10360-5:2020 Geometrical product specifications (GPS) - Acceptance and reverification tests for coordinate measuring systems (CMS) — Part 5: Coordinate measuring machines (CMMs) using single and multiple stylus contacting probing systems using disc, 2020.*
- [3] *JCGM 100: 2008 - Evaluation of measurement data – Guide to the expression of uncertainty in measurement, 2008.*
- [4] *ISO 10360-6:2001 Geometrical Product Specifications (GPS) — Acceptance and reverification tests for coordinate measuring machines (CMM) — Part 6: Estimation of errors in computing Gaussian associated features, 2001.*

SECTION I

METHOD B1

An a priori method for CMM uncertainty evaluation based on approximate models of CMM behaviour

I.1 Outline of this section (Method B1)

The section is organised as follows.

Section I.2 discusses the main elements of the approach based on the methodology underpinning the Guide to the Expression of Uncertainty [5], covering:

- what is meant by an *a priori* method,
- a summary of the GUM approach in terms of a functional relationship relating measurands and their influence factors, the statistical characterisation of the influence factors in terms of mean and variances, and how their statistical can be used to provide a statistical characterisation of the measurands,
- the application of the GUM methodology to CMM measurement to provide a statistical characterisation of point clouds and features derived from point clouds in terms of a statistical characterisation of the influence factors
- the influence factors important for CMM measurement discussed in this section
- how the CMM influence factors are characterised statistically in terms of statistical parameters, and
- how these statistic parameters can be assigned from prior knowledge.

Section I.3 describes the models for the influence and how uncertainties associated with the influence factors are propagated through to point clouds.

Section I.4 describes how the uncertainties associated with the influence factors propagate through to uncertainties associated with length measurement an how a statement of length measuring capability such as maximum permissible error can be used to guide the assignment of the statistical parameters for the influence factors.

Section I.5 describes how uncertainties associated with point clouds are propagated through to features extracted from the point clouds in terms of sensitivity matrices. The section describes how sensitivity matrices for least-squares element and surface fitting can be evaluated and how they can be approximated for standard measurement strategies. The section also

provides an analysis of how uncertainties associated with partial features behave and discusses uncertainty propagation associated with establishing a datum frame of reference.

Section I.6 gives a brief description of how workpiece form error influences featured derived from point clouds. Section I.7 discusses how a Monte Carlo method can be used to evaluate uncertainties associated with derived features, particularly those associated with Chebyshev/minimum zone fitting criteria.

I.1.1 Notation

General notation

Given coordinate data \mathbf{x}_i , $i = 1, 2, \dots, m$, then

$$\mathbf{x}_{1:m} = \begin{bmatrix} x_1 \\ y_1 \\ z_1 \\ x_2 \\ \vdots \\ y_m \\ z_m \end{bmatrix}, \quad \mathbf{x}_{p:q} = \begin{bmatrix} x_p \\ y_p \\ z_p \\ \vdots \\ x_q \\ y_q \\ z_q \end{bmatrix}, \quad q \geq p,$$

i.e., $\mathbf{x}_{1:m}$ represents the $3m \times 1$ vector of coordinates in the given order, etc.

Notation associated with statistical characterisation of CMM influence factors

Table I.1 gives a summary of the notation used in this document relating to CMM influence factors and associated statistical parameters.

Notation relating to variance matrices associated with coordinate data

Table I.2 gives a summary of the notation used in this document relating to variance matrices.

Symbol	Association, interpretation
MPE	Statement of maximum permissible error
A, B	Parameters characterising the MPE as a function of distance, $A + d/B$
R	Repeatability
σ_R	Standard deviation associated with repeatability
PQ	Probe qualification/location effects
σ_{PQ}	Standard deviation associated with probe qualification effects
S	Scale and squareness effects
σ_S	Standard deviation associated with a global scale effect
$\sigma_{S,a}$	Standard deviation associated with independent scale effects associated with each axis
σ_Q	Standard deviation associated with independent squareness effects
ET	Geometric location errors (local scale and straightness)
σ_{ET}	Standard deviation associated with spatially-correlated geometric location errors
λ_{ET}	Length scale parameter associated with the spatially-correlated geometric location errors
ER	Geometric rotation errors (roll, pitch and yaw)
σ_{ER}	Standard deviation associated with spatially-correlated geometric rotation errors
λ_{ER}	Length scale parameter associated with the spatially-correlated geometric rotation errors
P	Probing effects
σ_{P_0}	Standard uncertainty in the probe radius
σ_P	Standard deviation associated with spatially-correlated probing effects
λ_P	Length scale parameter associated with the spatially-correlated probing effects

Table I.1: Notation associated with CMM influence factors.

Symbol	Association, interpretation
V_A	variance matrix associated with quantities labelled 'A' due to all influence factors
$V_{A B}$	variance matrix associated with quantities labelled 'A' due to influence factors labelled 'B'
K_B	variance factor of V_B with $V_B = K_B K_B^\top$
D_C	diagonal variance factor of V_C with $V_C = D_C D_C^\top = D_C^2$
$G_{A B}$	sensitivity matrix of quantities labelled 'A' with respect to influence factors labelled 'B'

Table I.2: Notation associated with the variance matrices.

I.2 An *a priori* method based on the GUM methodology

I.2.1 Summary of the GUM methodology

The *a priori* uncertainty evaluation approach described in this report is based on the methodology described in the Guide to the Expression of Uncertainty in Measurement, the GUM, [2], specifically GUM Supplement 2 [4] which deals with multivariate outputs. A feature that distinguishes coordinate metrology from other areas of metrology is the fact that the measurands are usually multivariate, for example, a set of point coordinates, or are derived from multivariate quantities, e.g., the radius of a cylinder associated with a set of coordinates. The GUM methodology involves an input-output model in which the measurand(s) \boldsymbol{x} are described as having a functional relationship $\boldsymbol{x} = \boldsymbol{f}(\boldsymbol{b})$ on a set of inputs or *influence factors* \boldsymbol{b} . Any statistical characterisation of the influence factors \boldsymbol{b} defines a corresponding statistical characterisation of the outputs \boldsymbol{x} . In particular, if \boldsymbol{b} is associated with a (multivariate) probability distribution with mean $\hat{\boldsymbol{b}}$ and variance matrix V_B , the mean $\hat{\boldsymbol{x}}$ and variance matrix V_X associated with \boldsymbol{x} are completely defined by the functional relationship $\boldsymbol{x} = \boldsymbol{f}(\boldsymbol{b})$. If \boldsymbol{f} is a nonlinear function of \boldsymbol{b} , the mean and variance associated with \boldsymbol{x} may be difficult to compute exactly but can be approximated by linearising \boldsymbol{f} about $\hat{\boldsymbol{b}}$. If $G_{X|B}$ is¹ the *sensitivity matrix* of \boldsymbol{x} with respect to \boldsymbol{b} ,

$$G_{X|B}(i, j) = \frac{\partial f_i}{\partial b_j}$$

then the law of propagation of uncertainty (LPU, [10]) states that $\hat{\boldsymbol{x}}$ and V_X are approximated by

$$\hat{\boldsymbol{x}} \approx \boldsymbol{f}(\hat{\boldsymbol{b}}), \quad V_X \approx G_{X|B} V_B G_{X|B}^\top, \quad (\text{I.1})$$

a multivariate version of the well-known formula used in the GUM. The standard uncertainties $u(\boldsymbol{x})$ associated $\hat{\boldsymbol{x}}$ are given by the square roots of the diagonal elements of V_X .

If the inputs \boldsymbol{b} are associated with a multivariate Gaussian distribution²

$$\boldsymbol{b} \sim \mathcal{N}(\hat{\boldsymbol{b}}, V_B),$$

¹The symbol $X|B$ can be read as ‘ X given B ’.

²The symbol \sim can be read as ‘is distributed according to’.

then the distribution associated with \mathbf{x} is approximated by $\mathcal{N}(\hat{\mathbf{x}}, V_X)$. The LPU is exact for linear functions \mathbf{f} and in this case if \mathbf{b} is associated with a Gaussian distribution, \mathbf{x} is also associated with the given Gaussian distribution and no approximation is involved. For measurements that are associated with a number of influence factors, the distribution $\mathcal{N}(\hat{\mathbf{x}}, V_X)$ is usually a suitable approximation to the true distribution.

In coordinate metrology, relative accuracies are of the order of 1 part in 10^5 so that second order effects are of the order of 1 part in 10^{10} and can be ignored in almost all applications. This means that the linearisation of \mathbf{f} in (I.1) used to propagate the uncertainty information introduces no significant approximation error. One significant exception is in extracting features from point cloud data based on Chebyshev/minimum zone criteria and related criteria. In this case the functional \mathbf{f} relationship is nonlinear and, more challenging, the first order partial derivatives are not continuous so that evaluating the partial derivatives of \mathbf{f} at one estimate need not be a good guide to the partial derivatives at a nearby estimate.

Monte Carlo methods, as described in GUM Supplement 1 [3], can be used for problems for which a linearisation of the functional relationship is not effective. The concept is simple. If \mathbf{b}_q , $q = 1, \dots, M$, are samples from the multivariate probability distribution characterising the influence factors then,

$$\mathbf{x}_q = \mathbf{f}(\mathbf{b}_q), \quad q = 1, \dots, M, \quad (\text{I.2})$$

are samples from the probability distribution associated with the measurands \mathbf{x} . The mean and variance matrix associated with \mathbf{x} are estimated from the mean and variance matrix associated with the sample $\mathbf{x}_{1:M}$.

I.2.2 A GUM methodology applied to CMM measurement

To apply the GUM methodology, requires

- specifying the set of factors \mathbf{b} that influence the measurand(s) \mathbf{x} ,
- establishing the functional relationship of $\mathbf{x} = \mathbf{f}(\mathbf{b})$ how \mathbf{x} depends on the influence factors \mathbf{b} ,
- assigning estimates $\hat{\mathbf{b}}$ of the influence factors \mathbf{b} and the associated variance matrix V_B , and

- evaluating the sensitivity matrix G .

Once these steps have been completed, the LPU can be used to statistically characterise \mathbf{x} in terms of $\hat{\mathbf{x}}$ and V_X as in (I.1).

I.2.3 CMM influence factors

This report considers the following CMM measurement influence factors:

- Repeatability effects (R)
- Probe qualification/location effects (PQ)
- Scale and squareness effects (S)
- Kinematic/geometrical errors: straightness errors (ET)
- Kinematic/geometrical errors: angular/rotation errors (ER)
- Probing effects: probe radius, errors depending on probing direction (P)

The labels in brackets are used consistently in this report to denote the corresponding influence factor. Temperature effects are assumed to arise via changes in scale and machine geometry. Hysteresis effects are not covered in this report. The effects of workpiece form error is considered to some extent.

I.2.4 Functional relationship between influence factors and point coordinates and derived features, evaluated sensitivities

The evaluation uncertainties associated with geometric features \mathbf{a} derived from coordinate data $\mathbf{x}_{1:m}$ can generally be thought of as two stage process, the first in which a $3m \times 3m$ variance matrix V_X associated with the coordinate data $\mathbf{x}_{1:m}$ is evaluated, the second stage in which the uncertainties associated with $\mathbf{x}_{1:m}$ are propagated through to those for the features \mathbf{a} derived from $\mathbf{x}_{1:m}$. Hence there are two functional relationships to derive, the first from influence factors \mathbf{b} to point cloud $\mathbf{x}_{1:m}$, the second from point

cloud data to derived features. These functional relationships are generally straightforward to derive and are described in this report for the influence factors listed above and for features based on fitting a geometric element or design surface to a point cloud based on a least-squares criterion. Much of the technical elements of this report is given to deriving these functional relationships and corresponding sensitivities. All of the calculations are straightforward and can be implemented in a spreadsheet that supports basic matrix operations. No optimisation or Monte Carlo sampling is involved.

I.2.5 Statistical characterisation of the influence factors

The *a priori* nature of the methods described in this report arises in the the assignment of the statistical characterisation of the influence factors. All other aspects are more or less defined and follow standard mathematical/engineering practice. In order for the *a priori* method to be practical, it is necessary that the statistical characterisation requires the assignment of a modest number of parameter values, σ say, and that these values can be estimated straightforwardly based on information that is likely to be available, for example the statement of maximum permissible error (MPE) for measurement of length for the CMM. The MPE statement says that the difference between estimated distance \hat{d} derived from CMM measurement and the true distance d is bounded by a linear function of distance:

$$|\hat{d} - d| \leq A + d/B.$$

The MPE statement characterises CMM (length measuring) behaviour using two parameters A and B . The MPE statement can be re-interpreted in terms of uncertainty $u(d)$ associated with distance measurement,

$$Ku(d) \leq A + d/B, \tag{I.3}$$

where K (typically $K = 2$ or $K = 3$) ensures that the probability of exceeding an MPE statement is suitably small. Given any point cloud matrix $V_X = V_X(\sigma)$ it is very straightforward to evaluate the uncertainty $u(d_{ij}) = u(d_{ij}|\sigma)$ associated³ with the measurement of the distance between any two points \mathbf{x}_i and \mathbf{x}_j and therefore check if the variance matrix $V_X(\sigma)$ is consistent with the MPE statement. These issues are considered in detail in section I.4.

³The notation $u(d|\sigma)$ means the standard uncertainty associated with d , given the values σ of the statistical parameters.

The *a priori* method is being used to estimate the uncertainty contributions from the various influence factors, not to evaluate or estimate (and correct for) the influence factors themselves. This means that some of the complexity of error correction can be avoided. Most specific measuring tasks involve converting a set of measured coordinates to a small number of feature parameters, such as determining the radius of a cylinder from a set of point coordinates. The uncertainties associated with the computed parameters depends on the uncertainties associated with the point coordinates as encoded in the associated variance matrix. While the true variance matrix associated with the point cloud may be difficult to evaluate, a reasonable approximation can be determined using prior information and this approximation is likely to be sufficient to estimate uncertainties associated with the derived features.

MPE implies statistical correlation associated with a point cloud

If the MPE statement is a plausible characterisation of the length measuring capability of a CMM, then it can be used to guide the assignment of the statistical parameters used to evaluate V_X . The form of the MPE statement implies that the uncertainty associated with distance measurement has some dependence on the size of the distance. This fact immediately implies that the point cloud variance matrix V_X is not a diagonal matrix and that uncertainties associated with the coordinates \mathbf{x}_i are statistically correlated. Such correlation is to be expected since the point coordinates depend on a number of common influence factors such as scale and squareness effects. For this reason, the *a priori* method described here is based on the full multivariate version of the law of propagation of uncertainty (LPU) summarised by (I.1). Even if the variance matrix V_X associated with the point cloud can be approximated by a diagonal matrix, the variance matrix V_A associated with the derived features \mathbf{a} will be a full matrix and often represents strong correlation between different estimated parameters.

I.2.6 Main statistical parameters of the *a priori* method

The implementation of the *a priori* method described in this report involves the following main statistical parameters $\boldsymbol{\sigma} = (\sigma_R, \sigma_{PQ}, \sigma_S, \sigma_{S,a}, \sigma_Q)^\top$, $\boldsymbol{\sigma}_k^P = (\sigma_{P_0,k}, \sigma_{P,k})^\top$ and $\boldsymbol{\lambda} = (\lambda_{ET}, \lambda_{ER}, \lambda_P)^\top$ associated with the main influence factors listed in section I.2.3. The *a priori* information that can be used

to assign them is also discussed. Given values for these parameters, the point cloud matrix $V_X = V_X(\boldsymbol{\sigma}, \boldsymbol{\sigma}^P, \boldsymbol{\lambda})$ associated with a (proposed) set of measurements $\boldsymbol{x}_{1:m}$ can be evaluated directly propagated through to any derived features.

Repeatability (R)

Repeatability is characterised by one statistical parameter σ_R which represents the standard deviation of statistically independent random effects associated with each coordinate measurements. The standard deviation represents the likely variation in measured point coordinates if the same measurements were repeated under the same conditions. Repeatability contributes directly to the estimate of A in an MPE statement but has no distance-dependent component and does not contribute to B . A prior estimate of σ_R can be derived from repeatability experiments or estimated from the MPE statement. In order to be consistent with the MPE, $\sigma_R \leq A/K$ where K as in (I.3).

Repeatability influences all derived features including position, size and form error. The influence of repeatability on estimates of position and size are reduced as more measurements on an artefact are taken.

Probe location/qualification effects (PQ)

Probe qualification effects are characterised by one statistical parameter σ_{PQ} which represents the standard deviation of statistically independent random effects associated with estimation of the probe offset vector \boldsymbol{p} . A procedure for estimating σ_{PQ} for probe qualification experiments is given in section I.3.4. Probe qualification contributes directly to the estimate of A in an MPE statement but has no distance-dependent component and does not contribute to B . Probe qualification effects can contribute to all derived features including position and, if multiple probes are used, size and form error. If only one probe offset is used then probe qualification effects do not make a significant contribution to derived features. The influence of probe qualification effects on derived features are *not* reduced as more measurements on an artefact are taken.

Scale and squareness effects (S)

Scale and squareness effects are characterised by three statistical parameters σ_S , $\sigma_{S,a}$ and σ_Q . The first, σ_S , represents the standard deviation associated with a global scale effect, the second $\sigma_{S,a}$, represents the standard deviation associated with independent scale effects associated with each axis, while σ_Q represents the standard deviation associated with independent squareness effects.

Scale and squareness effects contribute directly to the estimate of B in an MPE statement but not to A . Scale and squareness effects influence all derived features including position, size and form error. The global scale effect makes negligible contribution to form error. Scale and squareness effects model non-isotropic CMM behaviour since squareness effects only influence length measurements that are not aligned with an axis. Section I.4.8 considers how these statistical parameters can be estimated from an MPE statement and how they are constrained by the value of B .

Geometric error, location effects (ET)

Geometric errors associated with location effects correspond to local scale and straightness effects for each axis, similar to those that appear in a CMM kinematic error model [32]. It is assumed that the CMM has already been corrected for kinematic errors and the location effects arise from the residual, uncorrected, kinematic errors that arise due to changes in the measuring environment, for example. The fact that the location effects correspond to residual, uncorrected errors means that there is no requirement to reflect the axis-upon-axis build up of errors that are present in standard kinematic error models.

The location effects are associated with two statistical parameters σ_{ET} and λ_{ET} . The first, σ_{ET} , represents the standard deviation associated with all local scale and straightness effects. The second, λ_{ET} , is a length scale parameter that controls the smoothness of the model for the location effects. If $\lambda_{ET} = 0$, then the effects are modelled as independent random effects and make the same type of uncertainty contribution as repeatability effects. If λ_{ET} is of the order of the length L_{\max} of the largest diagonal of the CMM, then the effects vary approximately linearly over the working volume and make a contribution similar to scale and squareness effects. A value

of $\lambda_{ET} = L_{\max}/5$ is appropriate in the absence of other information and models scale and straightness errors over short to medium length scales.

Spatially-correlated location effects contribute to both A and B in an MPE statement, with the balance depending of the value of λ_{ET} , with smaller values of λ_{ET} associated with a bigger contribution to A . Spatially-correlated location effects contribute to all derived features, including position, size and form error. The value of σ_{ET} can be estimated from measurements of calibrated artefacts with low form errors such as straight edges or ring gauges, or assigned using expert judgement.

Geometric error, rotation effects (ER)

Geometric errors associated with rotation effects correspond to local roll, pitch and yaw errors for each axis, similar to those that appear in a CMM kinematic error model. It is assumed that the CMM has already been corrected for kinematic errors and the rotation effects arise from the residual, uncorrected, kinematic errors that arise due to changes in the measuring environment, for example. The rotation effects are associated with two statistical parameters σ_{ER} and λ_{ER} . The first, σ_{ER} represents the standard deviation associated with all local rotational angles modelling the non-ideal rotational motion of the CMM. The second, λ_{ER} , is a length scale parameter that controls the smoothness of the model for the rotation effects. If $\lambda_{ER} = 0$, then the effects are modelled as independent random effects and make the same type of uncertainty contribution as repeatability effects. If λ_{ER} is of the order of the length L_{\max} of the largest diagonal of the CMM, then the effects are variance approximately linearly over the working volume and make a contribution similar to scale and squareness effects. A value of $\lambda_{ET} = L_{\max}/5$ is appropriate in the absence of other information. If only one probe is used, rotation effects make a similar contribution as location effects.

Spatially-correlated rotation effects contribute to both A and B in an MPE statement, with the balance depending of the value of λ_{ER} , with smaller values of λ_{ER} associated with a bigger contribution to A . Spatially-correlated rotation effects contribute to all derived features, including position, size and form error. The value of σ_{ER} can be estimated from measurements using an autocollimator or from measurements of calibrated artefacts with low form errors such as straight edges or ring gauges, or assigned using expert

judgement.

Probing effects (P)

The *a priori* method includes probe radius effects and probing effects that depend on probing direction. The probe radius effects are characterised by σ_{P_0} that represents the standard uncertainty associated with the probe radius. The probing effects that depend on probing direction are associated with two parameters. The first, σ_P , represents the standard uncertainty associated with spatially-correlated probing effects, while the second, λ_P , gives the spatial correlation length (relative to distances on the unit sphere) associated with the probing effects as a function of probing direction. The spatial correlation means that the probing effects are the same or similar if the probing directions are the same or similar (and cancel out for unidirectional length measurement) but that probing directions that are significantly different (and in particular in opposite directions) are uncorrelated (and do not cancel out for bi-directional length measurement).

Probing effects will be likely be different for different probe offsets and it may be advisable to assign different values of σ_{P_0} and σ_P for different probe offsets. A value of $\lambda_P = 0.5$ is appropriate in the absence of other information.

Probing effects contribute mainly to A in an MPE statement. Probe radius effects contribute to the size of derived features while probing effects contribute mainly to the form error associated with derived features.

I.2.7 Assigning statistical parameters based on an MPE statement

The statistical parameters described above (σ , σ^P and λ) can be related to the MPE statement through the evaluation of the uncertainties associated with distances between points. The relationship enables the MPE statement to be used to derive plausible values for the statistical parameters and rule out choices of parameter values that are not consistent with the MPE statement. Such an approach is described in section I.4.8 so that the uncertainties associated with derived features generated from measurements $\mathbf{x}_{1:m}$ can be estimated on the basis of an MPE statement alone. However, there are potentially significant limitations in basing estimating CMM uncertainties on

the basis of length measuring capability alone; see section I.2.9 below.

I.2.8 Assigning statistical parameters based on *a posteriori* information

Measurements of the same artefact in a number of different positions can be used to generate estimates of the repeatability component of CMM uncertainty and the component arising from geometric errors and other influence factors. The approach described in [39, 40] uses an analysis of variance methodology [36] to separate out and evaluate the contribution from repeatability effects and geometry effects. These estimates can be used to derive plausible values for the statistical parameters following similar principles to that for estimating them from an MPE statement.

I.2.9 Length measuring capability and three-dimensional measurement capability

This section illustrates the fact that CMM behaviour is not characterised by length measurement capability nor by its behaviour when measuring with a single probe. The *a priori* method described in this report attempts to characterise fully the three-dimensional nature of CMM measurement with multiple probes.

Length measuring capability does not define three dimensional measurement capability

The behaviour of a CMM cannot be characterised purely in terms of its length measuring capability, even if the length measuring capability is known completely. In general, length measurement capability provides only limited information about other derived features such as cylindricity, etc. In section I.4.3, it is shown how a combination of independent axes scale effects along with squareness effects provide exactly the same length measuring capability as that arising from a single global scale effect. Therefore, it is possible that two CMMs with exactly the same length measurement capability can perform significantly differently on other measurement tasks, such as the measurement of a ball plate [15]. It follows that an MPE statement can only be used to provide a plausible characterisation of CMM behaviour

and therefore plausible point cloud variance matrices. In deriving estimates of the statistical parameters described above in section I.2.6 from an MPE statement, there is a set of possible assignments that are potentially equally consistent with the MPE statement and it is as desirable to choose a set that is likely to be representative of a large class of CMMs. For example, a model in which there are independent axis scale errors and squareness errors covers a far larger class of CMM behaviours than a model for which there is only a single global scale effect.⁴

Measurement with a single probe does not define three dimensional measurement capability

The following example shows that completely characterising the behaviour of a CMM measurement using a single probe offset does not characterise CMM measurements using multiple measurements. In particular, experiments to estimate the kinematic errors of a CMM must involve multiple probe offsets [8].

Suppose a CMM has an error behaviour determined by roll about each axis that depends linearly on the length of travel along the axis. This behaviour can be modelled as

$$\tilde{\mathbf{x}} = \mathbf{x} + R(\kappa\mathbf{x})\mathbf{p},$$

where \mathbf{x} is the true position of (a fixed point on) the probe assembly, \mathbf{p} is the probe offset (from the fixed point) and $\tilde{\mathbf{x}}$ are the CMM coordinate measurements (scale readings), R is the linearised rotation matrix corresponding to roll about each axis given by

$$R(\mathbf{x}) = \begin{bmatrix} 1 & -z & y \\ z & 1 & -x \\ -y & x & 1 \end{bmatrix},$$

and $\kappa \approx 0$ is a parameter determining the rate of roll. Then

$$\tilde{\mathbf{x}} = \mathbf{x} + R(\kappa\mathbf{x})\mathbf{p} = \mathbf{x} + \mathbf{p} + \kappa\mathbf{x} \times \mathbf{p} = R(-\kappa\mathbf{p})\mathbf{x} + \mathbf{p}, \quad (\text{I.4})$$

where $\mathbf{x} \times \mathbf{p}$ is the vector cross-product of \mathbf{x} with \mathbf{p} . The relationship (I.4) shows that measurements of an artefact using a CMM with isotropic axis

⁴A potentially useful approach to determining a set of representative values of the statistical parameters would be to find, amongst all values consistent with the MPE statement, the values that maximise some measure of entropy [34] (or randomness) associated with a point cloud variance matrix

roll, i.e., having the same rate κ of roll along each axis, are the exactly same as those of the same artefact rotated by $R(-\kappa\mathbf{p})$ by a CMM with no axis roll (to first order). This equivalence means that, irrespective of measurement strategy and calibration information, a CMM cannot be completely characterised from the multiple measurement of calibrated artefacts such as ball plates and step gauges *unless* measurements are taken of the same artefact in the same position using more than one probe offset. In general, at least three probe offsets are required; by analogy, the location of three points are needed to track the position of a moving rigid body.

I.3 Point cloud uncertainty evaluation for CMM measurement

This section describes of models associated with the various influence factors that affect CMM behaviour listed in section I.2.3 and how uncertainties associated with these factors can be propagated through to point cloud variance matrices using the law of propagation of uncertainty (I.1).

I.3.1 A general model of CMM measurement

A general model of CMM measurement has the form

$$\mathbf{x}_i = \mathbf{x}_i^* + \mathbf{e}_i + \boldsymbol{\epsilon}_i, \quad \boldsymbol{\epsilon}_i \in \mathcal{N}(\mathbf{0}, \sigma_i^2 I) \quad (\text{I.5})$$

where \mathbf{x}_i is the measured coordinates, \mathbf{x}_i^* is the true point coordinates, \mathbf{e}_i is a systematic effect and $\boldsymbol{\epsilon}_i$ is a random effect, $i = 1, \dots, m$. The systematic effect \mathbf{e}_i is taken to be approximately constant over the duration of a measurement of a part while the random effect $\boldsymbol{\epsilon}_i$ represents (a sum of) effects that change over a very short timescale, effectively modelling the repeatability component of the CMM.

We generalise the model in (I.5) to cater for the possibility that the measurements may be subject to a number of independent systematic effects that combine additively to influence the measurement result, e.g.,

$$\mathbf{x}_i = \mathbf{x}_i^* + \mathbf{e}_{i,B} + \mathbf{e}_{i,C} + \mathbf{e}_{i,D} + \boldsymbol{\epsilon}_i. \quad (\text{I.6})$$

We assume that the behaviour of the systematic effects can be described by a statistical model which allows us to calculate (or estimate) the contribution to the variance matrix V_X associated with $\mathbf{x}_{1:m}$ from the various effects. We denote by $V_{X|B}$, the variance contribution arising from $\mathbf{e}_{1:m,B}$, etc. For the model in (I.5), the variance matrix V_X can be decomposed as

$$V_X = V_{X|E} + V_{X|R},$$

where $V_{X|E}$ is the variance contribution from the effects $\mathbf{e}_{1:m}$. For the model in (I.6), the variance matrix V_X can be decomposed as

$$V_X = V_{X|B} + V_{X|C} + V_{X|D} + V_{X|R}.$$

In both cases, we denote by $V_{X|R}$ the diagonal variance matrix representing the variance contribution from the random effects $\boldsymbol{\epsilon}_{1:m}$.

I.3.2 Propagation of variances

The law of propagation of uncertainty, the basis of the GUM [2], in its multivariate setting [7, 4] describes how uncertainties associated with the measured coordinates in (I.6) can be evaluated on the basis of uncertainties associated with the systematic and random effects. Suppose effects $\mathbf{e}_{i,B} = \mathbf{e}_i(\mathbf{b})$, $i = 1, \dots, m$, are specified by n_B parameters $\mathbf{b} = (b_1, \dots, b_{n_B})^\top$, and that a statistical model for \mathbf{b} specifies the $n_B \times n_B$ variance matrix V_B associated with \mathbf{b} . If $G_{X|B}$ is the $3m \times n_B$ sensitivity matrix of $\mathbf{x}_{1:m}$ with respect to \mathbf{b} constructed from $3 \times n_B$ matrices

$$G_{X|B,i} = \frac{\partial \mathbf{x}_i}{\partial \mathbf{b}^\top},$$

then

$$V_{X|B} = G_{X|B} V_B G_{X|B}^\top.$$

If V_B can be factored as $V_B = K_B K_B^\top$ where K_B is an $n_B \times p_B$ matrix (usually $p_B = n_B$), for example, from an eigenvalue decomposition or Cholesky decomposition [1, 26], then $V_{X|B}$ can be factored as

$$V_{X|B} = K_{X|B} K_{X|B}^\top, \quad K_{X|B} = G_{X|B} K_B.$$

If V_B is a diagonal matrix, then we factor V_B as $V_B = D_B^2$, where D_B is also a diagonal matrix. The j th diagonal element $d_{B,j}$ is the standard uncertainty associated with the effect b_j .

The role of the sensitivity matrix $G_{X|B}$ can be explained as follows. If the parameters \mathbf{b} describing the systematic effects are perturbed by $\Delta \mathbf{b}$, then the resulting perturbation on $\mathbf{e}_{1:m}$, and hence $\mathbf{x}_{1:m}$, is given by $\Delta \mathbf{x}_{1:m} = G_{X|B} \Delta \mathbf{b}$, to first order.

Often we are interested in quantities derived from a set of point coordinates. As a consequence of the chain rule in calculus, if $\mathbf{a} = (a_1, \dots, a_{n_A})^\top$ depends on $\mathbf{x}_{1:m}$ and $G_{A,X}$ is the $n_A \times 3m$ sensitivity matrix of \mathbf{a} with respect to $\mathbf{x}_{1:m}$ then the $n_A \times n_B$ sensitivity matrix $G_{A|B}$ of A with respect to influence factors \mathbf{b} is given by

$$G_{A|B} = G_{A|X} G_{X|B},$$

and the $n_A \times n_A$ variance matrix $V_{A|B}$ describing the variance contribution to \mathbf{a} arising from factors \mathbf{b} is given by

$$V_{A|B} = G_{A|B} V_B G_{A|B}^\top = K_{A|B} K_{A|B}^\top, \quad K_{A|B} = G_{A|B} K_B.$$

If the systematic effects \mathbf{b} are perturbed by $\Delta\mathbf{b}$, then the derived parameters \mathbf{a} are perturbed by $\Delta\mathbf{a} = G_{A|B}\Delta\mathbf{b}$, to first order.

An important example of quantities \mathbf{a} derived from point coordinates $\mathbf{x}_{1:m}$ is where \mathbf{a} are parameters associated with a Gaussian associated feature to $\mathbf{x}_{1:m}$, e.g., the least squares best-fit cylinder to a data set; see section I.5.2.

I.3.3 Random/repeatability component (R)

The simplest model of CMM behaviour is to consider only a random repeatability component constant throughout the working volume:

$$\mathbf{x}_i = \mathbf{x}_i^* + \boldsymbol{\epsilon}_i, \quad \boldsymbol{\epsilon}_i \in \mathcal{N}(\mathbf{0}, \sigma_R^2 I). \quad (\text{I.7})$$

This model has only one statistical (hyper-)parameter, σ_R . The variance matrix V_X associated with a set of measured coordinates \mathbf{x}_I is simply

$$V_X = V_R = \sigma_R^2 I = D_R^2, \quad D_R = \sigma_R I,$$

where represents the $3m \times 3m$ identity matrix with ones on the diagonal and zeros elsewhere. Despite its simplicity, this model is useful to determine how the uncertainties associated with geometric features depend on representative estimates of the CMM accuracy as represented by σ_R .

The uncertainty $u(d_{ij})$ associated with the distance $d_{ij} = \|\mathbf{x}_i - \mathbf{x}_j\|$ is given by

$$u^2(d_{ij}) = 2\sigma_R^2,$$

and is independent of the length of the distance d_{ij} .

I.3.4 Probe qualification effects (PQ)

For error models with an explicit dependence on the probe offset \mathbf{p}_k , the fact that the probe configuration geometry is usually determined in probe qualification experiments [?] means that there will be uncertainties associated with estimates of the offsets. If \mathbf{x}_i is a measurement using the k th probe, then the uncertainty contribution arising from the probe qualification can be modelled as

$$\mathbf{x}_i = \mathbf{x}_i^* + \mathbf{p}_k + \mathbf{e}_{PQ,k} + \boldsymbol{\epsilon}_i, \quad \mathbf{e}_{PQ,k} \in \mathcal{N}(\mathbf{0}, \sigma_{PQ,k}^2 I), \quad (\text{I.8})$$

where \mathbf{p}_k is the calibrated probe offset vector for the k th probe and $\mathbf{e}_{PQ,k}$ models the difference between the actual probe offset and its calibrated value, $k = 1, \dots, n_P$. An important feature of the model is that all measurements with the k th probe are associated with the same systematic effect $\mathbf{e}_{PQ,k}$. The variance contribution associated with probe qualification is given by

$$V_{X|PQ} = G_{X|PQ} V_{PQ} G_{X|PQ}^\top$$

where $V_{X|PQ}$ is the $3n_P \times 3n_P$ variance matrix associated with the systematic effects $\mathbf{e}_{PQ,k}$ and $G_{X|PQ}$ is the $3m \times 3n_P$ sensitivity matrix. The variance matrix V_{PQ} is a diagonal matrix with the 3×3 matrix $\sigma_{PQ,k}^2 I$ in the k th diagonal block. If the i th measurement is associated with the k th probe, then

$$G_{X|PQ}(3i - 2 : 3i, 3k - 2 : 3k) = I$$

the 3×3 identity matrix, and all other elements in these three rows are zero.

Estimating the variance associated with probe qualification effects

[This section needs some references]

Probe qualification according to ISO XXX involves measuring a reference sphere with a number of probe offsets \mathbf{p}_k and for each probe estimating the centre of the sphere, yielding estimates \mathbf{c}_k , $k = 1, \dots, n_P$. A measure of the spread of \mathbf{c}_k provides an estimate of the uncertainty contribution from probe qualification effects. One measure specified by ISO XXX is the diameter D_{MCS} of the minimum circumscribing sphere. Calculating the minimum circumscribing sphere to data can be posed as an optimisation problem to minimise a nonlinear function subject to linear inequality constraints. Such problems can be solved using standard optimisation techniques [24] but these algorithms are not entirely straightforward to implement. An alternative measure [?] is to use the maximum pairwise distance

$$D_{MP} = \max_{k_1, k_2} \|\mathbf{c}_{k_1} - \mathbf{c}_{k_2}\|.$$

If $n_{PQ} = 2$, then $D_{MP} = D_{MCS}$; if $n_{PQ} = 3$ then $D_{MP} \geq \sqrt{3/4} D_{MCS} \approx 0.87 D_{MCS}$ with equality given by three points on an equilateral triangle, and for $n_{PQ} \geq 4$, $D_{MP} \geq \sqrt{2/3} D_{MCS} \approx 0.82 D_{MCS}$ with equality given by points on the corners of a tetrahedron. Thus, in all cases

$$D_{MP} \geq 0.82 D_{MCS}.$$

We now describe a Bayesian approach for assessing the uncertainty contribution associated with probe qualification. It based on the model

$$\mathbf{c}_k \in \mathcal{N}(\mathbf{c}, \phi_{PQ}^{-1}I), \quad \phi_{PQ} = 1/\sigma_{PQ}^2, \quad k = 1, \dots, n_P,$$

where the parameter $\phi = 1/\sigma_{PQ}^2$ represents the σ_{PQ} in the model⁵. The model is such that the posterior distributions for \mathbf{c} and ϕ can be determined analytically [23]. Given non-informative prior $p(\mathbf{c}) \propto 1$ for \mathbf{c} and a Gamma prior

$$\phi_{PQ} \sim G(n_0/2, n_0\sigma_{PQ,0}^2/2),$$

then the posterior distribution for $\phi_{PQ}|\{\mathbf{c}_k\}$ is the Gamma distribution $G(\bar{n}/2, \bar{n}\bar{\sigma}_{PQ}^2/2)$ where

$$\bar{n} = n_0 + 3n_P - 3, \quad \bar{\sigma}_{PQ}^2 = \frac{n_0\sigma_{PQ,0}^2 + (3n_P - 3)\hat{\sigma}^2}{\bar{n}},$$

$$\hat{\sigma}^2 = \frac{1}{3n_P - 3} \sum_{k=1}^{n_P} (\mathbf{c}_k - \bar{\mathbf{c}})^\top (\mathbf{c}_k - \bar{\mathbf{c}}),$$

and

$$\bar{\mathbf{c}} = \frac{1}{n_P} \sum_{k=1}^{n_P} \mathbf{c}_k.$$

It is seen that $\bar{\sigma}_{PQ}^2$ is a weighted average of the prior estimate $\sigma_{PQ,0}^2$ and the estimate $\hat{\sigma}$ of the standard deviation of the residuals associated with the estimate $\bar{\mathbf{c}}$, the mean of $\{\mathbf{c}_k\}$. In this way, results from previous but similar probe qualification experiments can be incorporated into a current experiment. The quantity $\bar{\sigma}_{PQ}$ can be taken as an estimate of σ_{PQ} . We note that it is always defined if $n_P \geq 2$. If $n_P = 1$, then no new information about σ_{PQ} is generated.

I.3.5 Scale and squareness effects (S)

Scale and squareness effects are special cases of a class of models in which the systematic effects in (I.5) are taken to be functions $\mathbf{e}_i = \mathbf{e}(\mathbf{x}_i, \mathbf{b})$ of location \mathbf{x} and additional parameters $\mathbf{b} = (b_1, \dots, b_p)^\top$ that model some aspect of CMM behaviour. If V_S is a prior assignment of the $p \times p$ variance

⁵Working with ϕ rather than σ_{PQ} leads to simpler expressions for the statistical distributions involved.

matrix associated with \mathbf{b} and $G_{X|S}$ is the matrix $3m \times p$ of sensitivities of \mathbf{e}_i , $i = 1, \dots, m$, with respect to \mathbf{b} , then the variance contribution of \mathbf{b} to the variance associated with $\mathbf{x}_{1:m}$ is given by

$$V_{X|E} = G_{X|S} V_S G_{X|S}^\top.$$

From practical experience, it is well known that scale and squareness effects are a major component of CMM behaviour. The model below incorporates scale effects and three squareness effects through

$$\mathbf{x}_i = B(\mathbf{b})\mathbf{x}_i^* + \boldsymbol{\epsilon}_i. \quad (\text{I.9})$$

where

$$B(\mathbf{b}) = \begin{bmatrix} (1 + b_{aa} + b_{xx}) & b_{xy} & b_{xz} \\ 0 & (1 + b_{aa} + b_{yy}) & b_{yz} \\ 0 & 0 & (1 + b_{aa} + b_{zz}) \end{bmatrix}$$

depends on effects $\mathbf{b} = (b_{aa}, b_{xx}, b_{yy}, b_{zz}, b_{xy}, b_{xz}, b_{yz})^\top$. The term b_{aa} models a global scale effect while b_{xx} , b_{yy} and b_{zz} model scale effects for each axis and b_{xy} , b_{xz} and b_{yz} model the squareness effects. The $3m \times 7$ sensitivity matrix $G_{X|S}$ for this model is assembled from 3×7 matrices of the form

$$G(\mathbf{x}_i^*) = \begin{bmatrix} x_i^* & x_i^* & 0 & 0 & y_i^* & z_i^* & 0 \\ y_i^* & 0 & y_i^* & 0 & 0 & 0 & z_i^* \\ z_i^* & 0 & 0 & z_i^* & 0 & 0 & 0 \end{bmatrix}. \quad (\text{I.10})$$

In practice, \mathbf{x}_i^* is unknown but can be approximated accurately by the measured coordinate \mathbf{x}_i and the sensitivity matrix is approximated by

$$G_i = G(\mathbf{x}_i) = \begin{bmatrix} x_i & x_i & 0 & 0 & y_i & z_i & 0 \\ y_i & 0 & y_i & 0 & 0 & 0 & z_i \\ z_i & 0 & 0 & z_i & 0 & 0 & 0 \end{bmatrix}. \quad (\text{I.11})$$

The model is completed by specifying the variance matrix V_B associated with the scale and squareness effects, e.g.,

$$V_B = \begin{bmatrix} \sigma_S^2 & 0 & 0 & 0 & 0 & 0 & 0 \\ 0 & \sigma_{S,x}^2 & 0 & 0 & 0 & 0 & 0 \\ 0 & 0 & \sigma_{S,y}^2 & 0 & 0 & 0 & 0 \\ 0 & 0 & 0 & \sigma_{S,z}^2 & 0 & 0 & 0 \\ 0 & 0 & 0 & 0 & \sigma_Q^2 & 0 & 0 \\ 0 & 0 & 0 & 0 & 0 & \sigma_Q^2 & 0 \\ 0 & 0 & 0 & 0 & 0 & 0 & \sigma_Q^2 \end{bmatrix}. \quad (\text{I.12})$$

If we assume that the individual axis scale effects are associated with the same variance so that $\sigma_{S,x}^2 = \sigma_{S,y}^2 = \sigma_{S,z}^2 = \sigma_{S,a}^2$, the model is associated with four statistical hyper-parameters $\boldsymbol{\sigma} = (\sigma_S, \sigma_{S,a}, \sigma_Q, \sigma_R)^\top$. Given a data point \mathbf{x}_i , the variance matrix $V_{\mathbf{x}_i} = V_{\mathbf{x}_i}(\boldsymbol{\sigma})$ due to scale and squareness effects is given by

$$V_{\mathbf{x}_i} = \sigma_S^2 \mathbf{x}_i \mathbf{x}_i^\top + \begin{bmatrix} x_i^2 \sigma_{S,a}^2 + (y_i^2 + z_i^2) \sigma_Q^2 & 0 & 0 \\ 0 & y_i^2 \sigma_{S,a}^2 + z_i^2 \sigma_Q^2 & 0 \\ 0 & 0 & z_i^2 \sigma_{S,a}^2 \end{bmatrix}.$$

For a working volume of $[-L, L]^3$, the maximum variance in a coordinate of a point is given by $L^2(\sigma_S^2 + \sigma_{S,a}^2 + 2\sigma_Q^2)$. This maximum can be compared with statements of maximum permissible error.

Over modest working volumes⁶ over which straightness and rotational effects are not significant, the scale and squareness model is a useful approximation. For this model, the variance matrix V_X associated with a set of coordinates is given by

$$V_X = G_{X|S} V_S G_{X|S}^\top + \sigma_R^2 I, \quad (\text{I.13})$$

where $G_{X|S}$ is the $3m \times 7$ sensitivity matrix constructed from G_i defined as in (I.11) and V_S typically has the form in (I.12).

Scale and squareness effects for multiple probe configurations

For measurements involving multiple probe offsets \mathbf{p}_k , $k = 1, \dots, n_P$, the measured coordinates \mathbf{x}_i are related to the true point coordinates \mathbf{x}_i^* through a model of the form

$$\mathbf{x}_i = B(\mathbf{b}) \mathbf{x}_i^* + \mathbf{p}_{k(i)} + \boldsymbol{\epsilon}_i.$$

For this model, the sensitivity of \mathbf{x}_i with respect to \mathbf{b} is approximated by

$$G_i = G(\mathbf{x}_i - \mathbf{p}_{k(i)})$$

with G defined as in (I.10).

⁶See section I.3.9 for an extension of this model more appropriate for larger working volumes.

Scale and squareness effects in two dimensions

In two dimensions, the model has the form

$$\mathbf{x}_i = \begin{bmatrix} (1 + b_{aa} + b_{xx}) & b_{xy} \\ 0 & (1 + b_{aa} + b_{yy}) \end{bmatrix} \mathbf{x}_i^* + \boldsymbol{\epsilon}_i. \quad (\text{I.14})$$

depending on effects $\mathbf{b} = (b_{aa}, b_{xx}, b_{yy}, b_{xy})^\top$. The $2m \times 4$ sensitivity matrix $G_{X|B}$ for this model is assembled from 2×4 matrices of the form

$$G_i = \begin{bmatrix} x_i & x_i & 0 & y_i \\ y_i & 0 & y_i & 0 \end{bmatrix}, \quad (\text{I.15})$$

variance matrix V_B associated with the scale and squareness effects typically of the form

$$V_B = \begin{bmatrix} \sigma_S^2 & 0 & 0 & 0 \\ 0 & \sigma_{S,x}^2 & 0 & 0 \\ 0 & 0 & \sigma_{S,y}^2 & 0 \\ 0 & 0 & 0 & \sigma_Q^2 \end{bmatrix}. \quad (\text{I.16})$$

I.3.6 Kinematic error model

The kinematic error model for a CMM [32, 41] involves firstly the specification of 6 error functions associated with the 6 degrees of freedom motion of a rigid body along an axis, e.g., $(e_{xx}(x), e_{xy}, e_{xz}(x), r_{xx}(x), r_{xy}(x), r_{xz}(x))^\top$, where e_{xx} models the scale error along the axis, e_{xy} the straightness error in the xy -plane, and r_{xx} is the rotation about the x -axis, in this case, roll. Thus there is a scale error function, two straightness functions and three rotation functions corresponding to roll, pitch and yaw. There are six such functions associated with each axis, 18 in all, sometimes augmented by 3 scalar squareness parameters, depending on the convention for specifying the straightness error functions. These error functions are usually modelled in terms of empirical functions such as polynomials or splines, the coefficients of which are collectively represented by parameter vector \mathbf{b} . The combined contribution of these $18 + 3$ errors to the CMM measurement can be written as

$$\mathbf{x}_i = \mathbf{x}_i^* + \mathbf{e}(\mathbf{x}_i^*, \mathbf{b}) + R(\mathbf{x}_i^*, \mathbf{b})\mathbf{p} + \boldsymbol{\epsilon}_i \quad (\text{I.17})$$

involving a translation component $\mathbf{e}(\mathbf{x}_i^*, \mathbf{b})$ and a component $R(\mathbf{x}_i^*, \mathbf{b})$ modelling angular errors where R is a rotation matrix depending on \mathbf{b} and location \mathbf{x}^* . The rotational component also involves the probe offset \mathbf{p} , the

vector pointing from the centre of rotation of the probe housing to the probe tip centre. The explicit dependence on the probe offset allows different probe configurations to be modelled using the same kinematic error functions.

Estimates of the function coefficients \mathbf{b} along with their associated variance matrix can be determined from repeated measurements of calibrated artefacts such as ball or hole plates [9, 12, 31].

If V_B is the variance matrix associated with \mathbf{b} (derived from a ball plate exercise or otherwise) and $G_{X|B}$ is the sensitivity matrix of $\mathbf{x}_{1:m}$ with respect to \mathbf{b} , then the variance matrix associated with $\mathbf{x}_{1:m}$ is given by

$$V_X = G_{X|B} V_B G_{X|B}^\top.$$

The full kinematic error model and its use in generating variance matrices is very much a specialist undertaking and perhaps not suitable for developing *a priori* methods. Typically, each error function is defined in terms of 5 or so parameters, e.g., polynomial coefficients, so that the complete error model involves of the order of 100 parameters \mathbf{b} . Consequently, the assigning the associated variance matrix V_B involves estimating of the order of 10^4 elements. However, the kinematic error model can be used to assess the ability of simpler *a priori* methods to capture the uncertainty characteristics due to non-ideal geometry.

I.3.7 Gaussian process models incorporating spatial correlation

Gaussian process (GP) models [11, 38] can be used to develop empirical models of behaviour that do not explicitly involve sets of basis functions such as polynomials or splines. Spatial or temporal correlation associated with data points (\mathbf{x}_i, e_i) takes the form

$$\text{corr}(e, e') = k(\mathbf{x}, \mathbf{x}' | \boldsymbol{\sigma})$$

where k is a correlation kernel depending on statistical parameters $\boldsymbol{\sigma}$. Often k depends on \mathbf{x} and \mathbf{x}' through $\|\mathbf{x} - \mathbf{x}'\|$, e.g.

$$\text{cov}(e, e') = k(\mathbf{x}, \mathbf{x}') = \sigma_E^2 \exp\{-\|\mathbf{x} - \mathbf{x}'\|^2 / \lambda_E^2\}. \quad (\text{I.18})$$

The strength of the correlation between e and e' dependence to the distance between \mathbf{x} and \mathbf{x}' : the closer \mathbf{x} is to \mathbf{x}' , relative to σ_2 , the stronger the correlation between e and e' .

MPE and spatial correlation

The use of spatially-correlated error models can be motivated in terms of consequences of the statement of maximum permissible error (MPE) in measuring length. In measuring length along a single axis, say the x -axis, suppose the basic statistical model for the measurement of two points is

$$x_1 = x_1^* + e_1 + \epsilon_1, \quad x_2 = x_2^* + e_2 + \epsilon_2,$$

with

$$e_1, e_2 \in \mathcal{N}(0, \sigma_E^2), \quad \epsilon_1, \epsilon_2 \in \mathcal{N}(0, \sigma_R^2).$$

The MPE statement implies that the measured length \hat{d}_{12} is related to the true length d_{12} according to

$$|\hat{d}_{12} - d_{12}| \leq A + d_{12}/B.$$

The MPE implies

$$|e_2 - e_1 + \epsilon_2 - \epsilon_1| \leq A + d_{12}/B$$

so that $2\sigma_R^2 \leq A^2$, and for $\sigma_R \ll \sigma_E$,

$$e_1 - (A + d_{12}/B) \leq e_2 \leq e_1 + (A + d_{12}/B),$$

i.e., the similarity of e_1 and e_2 depends on the *spatial separation* d_{12} .

We can also use a model of the form

$$x = x^* + e(x) + \epsilon \approx x^* + e(x) + \epsilon, \quad \epsilon \in \mathcal{N}(0, \sigma_R^2)$$

where $e(x)$ is an error function with $|e(x)| \leq 2\sigma_E$ that encodes the local scale error. (The same concept can be applied to straightness errors, etc.) The MPE implies

$$|e(x_2) - e(x_1) + \epsilon_2 - \epsilon_1| \leq A + |x_2 - x_1|/B$$

so for $\sigma_R \ll \sigma_E$ and $x_1 \neq x_2$,

$$\left| \frac{e(x_2) - e(x_1)}{x_2 - x_1} \right| \leq \frac{A}{|x_2 - x_1|} + \frac{1}{B}.$$

In other words, the slope of the error function $e(x)$ cannot be too large imposing some measure of smoothness on the error function $e(x)$ in order to

be consistent with the MPE statement. From this point of view, in the MPE statement, A quantifies effects over short length scales, while d/B controls the size and smoothness of effects over longer length scales.

Figures I.1–I.4 give examples of spatially-correlated error functions generated using the correlation kernel in (I.18) with $\sigma_E = 0.005$ mm and $\lambda_E = 1000$ mm, 500 mm, 200 mm and 100 mm

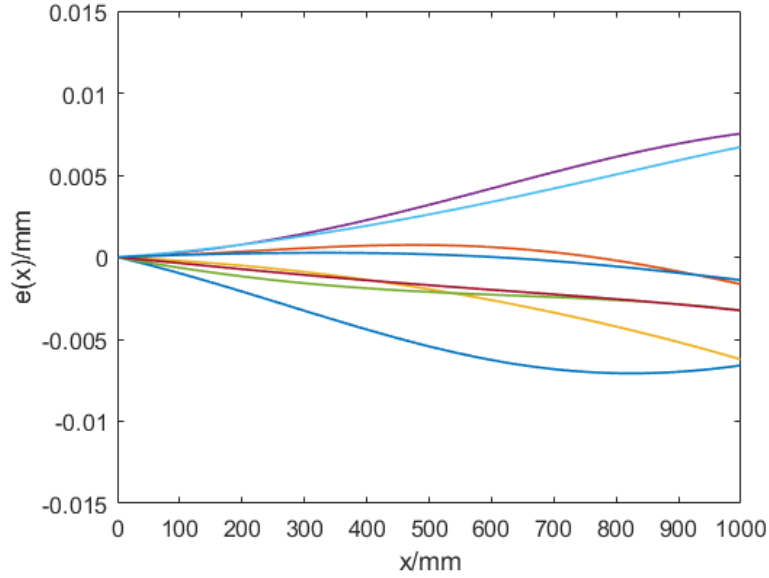


Figure I.1: Examples of spatially-correlated error functions generated using the correlation kernel in (I.18) with $\sigma_E = 0.005$ mm and $\lambda_E = 1000$ mm.

A GP model can be used to supplement a parametric model $\mathbf{e}(\mathbf{b})$ for the systematic effects, e.g., a scale and squareness error model considered in section I.3.5, in which the role of the GP model is to simulate behaviour not captured by the parametric model, such as uncorrected kinematic errors [17, 30]. The significant advantage of GP models for an *a priori* method is that the GP model can mimic the behaviour of empirical models in a non-parametric way and can be defined by a small number of statistical parameters. The point cloud variance matrices V_X are constructed from the point cloud $\mathbf{x}_{1:m}$ itself along with a few statistical parameters. In the models below, the geometric location errors, rotational errors and probing errors can each be modelled by specifying only two statistical parameters

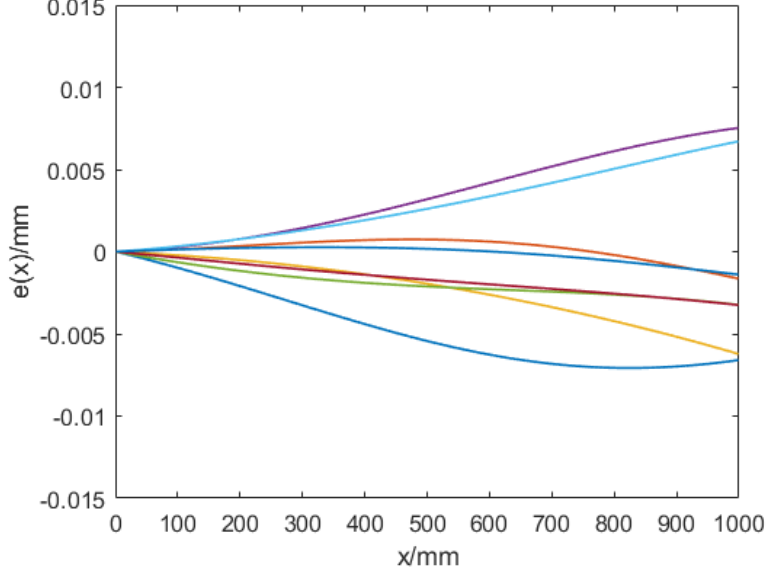


Figure I.2: As figure I.1 but with $\lambda_E = 500$ mm.

each. By contrast, kinematic error models, section I.3.6, typically involve 100 or so parameters.

GP models for location errors (ET)

We can apply a GP model for CMM behaviour as follows with

$$\mathbf{x}_i = \mathbf{x}_i^* + \mathbf{e}_i + \boldsymbol{\epsilon}_i, \quad (\text{I.19})$$

where the systematic effects are spatially (and sometimes temporally) correlated with the with the systematic effects \mathbf{e}_i spatially correlated. In general, the covariance applies only to the same coordinates, with the x -, y - and z -coordinates of \mathbf{e} mutually, independent. The covariance with e_x with e'_x could be modelled as

$$\text{cov}(e_x, e'_x) = k(\mathbf{x}, \mathbf{x}' | \boldsymbol{\sigma}_x) = \sigma_{ET,x}^2 \exp \left\{ -\|\mathbf{x} - \mathbf{x}'\|^2 / \lambda_{ET,x}^2 \right\}, \quad (\text{I.20})$$

for example, where $\lambda_{ET,x}$ defines the length scale for the correlation in the x -coordinate⁷. Note that in this model, there the strength of the correlation

⁷The ‘E’ and ‘T’ in ‘ET’ are meant to represent the error that acts translationally.

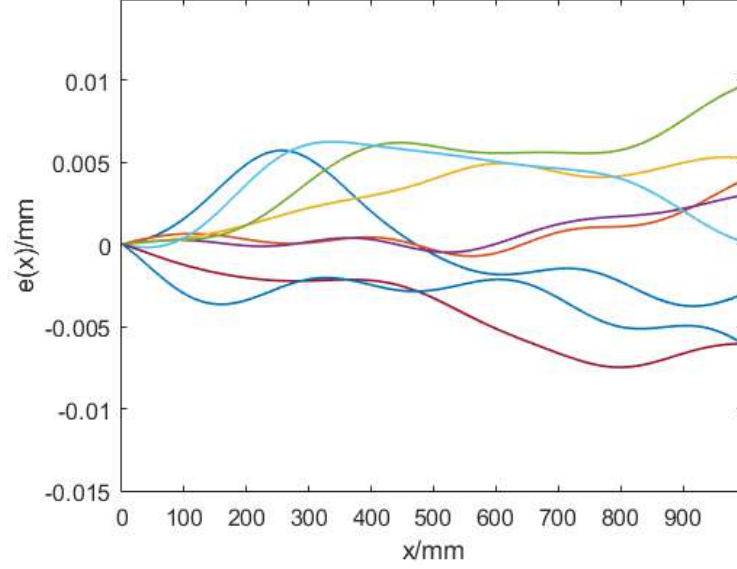


Figure I.3: As figure I.1 but with $\lambda_E = 200$ mm.

in the effects e_x depends on the distance $\|\mathbf{x} - \mathbf{x}'\|$ in 3D, not the distance along the x -axis.

Let D be the $m \times m$ matrix of distances with

$$D_{ij} = \|\mathbf{x}_i - \mathbf{x}_j\|.$$

The variance contribution V_{XT} from $\mathbf{e}_{1:m}$ to the x -coordinates of $\mathbf{x}_{i:m}$ is given by

$$V_{XT,x} = \sigma_{ET,x}^2 \exp \left\{ -D^2 / \lambda_{ET,x}^2 \right\}$$

where the calculations associated with D are made element-wise. The contribution to the y - and z -components are of exactly the same form. The matrix V_{XT} is assembled from $V_{XT,x}$, $V_{XT,y}$ and $V_{XT,z}$, with all other elements zeros since we assume that the systematic effects associated with the x -coordinates are independent from those associated with the y - and z -coordinates⁸.

⁸We assume that the GP model relates to uncorrected kinematic errors that are not likely to have a significant correlation between axes, even if the kinematic errors themselves are likely to produce such correlation. While the GP model assumes there is no inter-

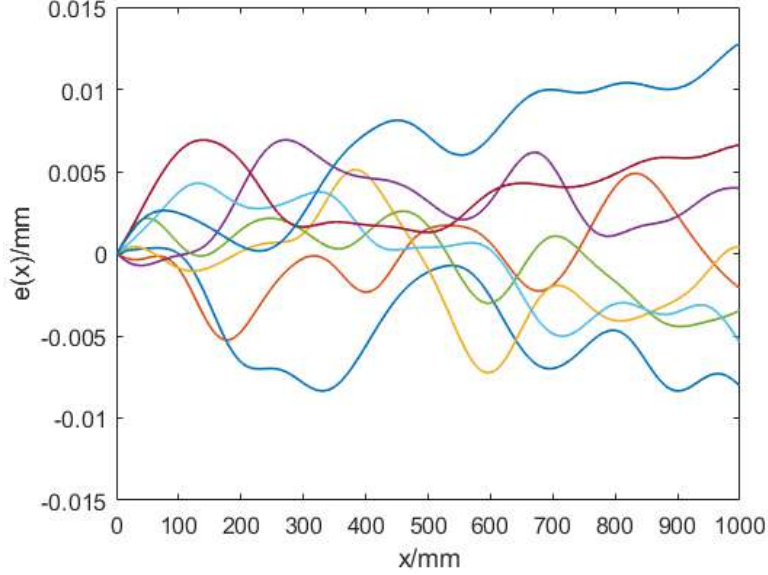


Figure I.4: As figure I.1 but with $\lambda_E = 100$ mm.

If it can be assumed that the systematic effects along each axis have the same behaviour, so that $\sigma_{ET,x} = \sigma_{ET,y} = \sigma_{ET,z} = \sigma_{ET}$, etc., then the model is specified by three statistical hyper-parameters $\boldsymbol{\sigma} = (\sigma_{ET}, \lambda_{ET}, \sigma_R)^\top$. The variance associated with any coordinate is σ_{ET}^2 . This variance can be compared with statements of maximum permissible error.

GP models for location errors incorporating multiple probes

Suppose that the point cloud $\mathbf{x}_{1:m}$ is gathered using multiple probes with offsets \mathbf{p}_k , $k = 1, \dots, n_P$. The measured coordinates \mathbf{x}_i are related to the true point coordinates \mathbf{x}_i^* through a model of the form

$$\mathbf{x}_i = \mathbf{x}_i^* + \mathbf{e}_i + \mathbf{p}_{k(i)} + \boldsymbol{\epsilon}_i,$$

where $\mathbf{p}_{k(i)}$ denotes the probe configuration associated with the i th measurement, etc. For this case, it is important to note that the spatial correlation

axes correlation, the GP model will model successfully behaviour that does have such correlation.

is dependent on $\|\mathbf{x}_i^* - \mathbf{x}_j^*\|$, not $\|\mathbf{x}_i - \mathbf{x}_j\|$. For different probe configurations we have

$$\|\mathbf{x}_i^* - \mathbf{x}_j^*\| \doteq \|(\mathbf{x}_i - \mathbf{p}_{k(i)}) - (\mathbf{x}_j - \mathbf{p}_{k(j)})\|.$$

Similar considerations apply to the model for scale and squareness errors with multiple probe offsets, section I.3.5, and for GP models for rotation errors, section I.3.7, below.

Gaussian process model for rotation errors

The GP models in section I.3.7 used, perhaps, with a simple parametric error model can simulate a wide range of plausible CMM behaviour but it relates only to one probing configuration and do not, without modification, allow us to evaluate the uncertainties associated with different probe configurations. An extension of the model is to use GP models to model both the location and rotation errors:

$$\mathbf{x}_i = \mathbf{x}_i^* + \mathbf{e}_i + R(\boldsymbol{\alpha}_i)\mathbf{p} + \boldsymbol{\epsilon}_i, \quad (\text{I.21})$$

where $\boldsymbol{\alpha}_i = (\alpha_{i,x}, \alpha_{i,y}, \alpha_{i,z})^\top$ represents three spatially correlated rotation errors acting on the probe offset vector \mathbf{p} through the rotation matrix

$$R(\boldsymbol{\alpha}_i) = R_z(\alpha_{i,z})R_y(\alpha_{i,y})R_x(\alpha_{i,x}), \quad (\text{I.22})$$

the product of rotations about each of the three coordinate axes:

$$R_x(\alpha_x) = \begin{bmatrix} 1 & 0 & 0 \\ 0 & \cos \alpha_x & -\sin \alpha_x \\ 0 & \sin \alpha_x & \cos \alpha_x \end{bmatrix}, \quad R_y(\alpha_y) = \begin{bmatrix} \cos \alpha_y & 0 & \sin \alpha_y \\ 0 & 1 & 0 \\ -\sin \alpha_y & 0 & \cos \alpha_y \end{bmatrix},$$

and

$$R_z(\alpha_z) = \begin{bmatrix} \cos \alpha_z & -\sin \alpha_z & 0 \\ \sin \alpha_z & \cos \alpha_z & 0 \\ 0 & 0 & 1 \end{bmatrix}.$$

We assume that the rotational effects about one axis are independent from the rotational effects about the other two axes, but other more general approaches are possible. For measurements involving multiple probes, the degree of spatial correlation associated with $\boldsymbol{\alpha}_i$ and $\boldsymbol{\alpha}_j$ depends on

$$\|\mathbf{x}_i^* - \mathbf{x}_j^*\| \doteq \|(\mathbf{x}_i - \mathbf{p}_{k(i)}) - (\mathbf{x}_j - \mathbf{p}_{k(j)})\|.$$

If the rotational errors are similar along each axis, then the GP model for the rotational errors is specified by two statistical hyper-parameters σ_{ER} , and λ_{ER} , say⁹.

The variance associated with location errors for any coordinate is σ_{ET}^2 . If the maximum probe length is P , then the maximum variance associated with rotational effects for a coordinate is given by $P^2\sigma_{ER}^2$. Hence the maximum variance associated with location and rotation errors for a coordinate is given by $\sigma_{ET}^2 + P^2\sigma_{ER}^2$. This maximum can be compared with statements of maximum permissible error.

We note that if the variance matrix associated with $\boldsymbol{\alpha} = (\alpha_x, \alpha_y, \alpha_z)^\top$ with $\boldsymbol{\alpha} = \mathbf{0}$ is $V_{\boldsymbol{\alpha}}$, then the variance matrix $V_{\mathbf{p}}$ associated with $R(\boldsymbol{\alpha})\mathbf{p}$, with $R(\boldsymbol{\alpha})$ as in (I.22), is given by $GV_{\boldsymbol{\alpha}}G^\top$ where

$$G = \begin{bmatrix} 0 & p_z & -p_y \\ -p_z & 0 & p_x \\ p_y & -p_x & 0 \end{bmatrix}, \quad \mathbf{p} = (p_x, p_y, p_z)^\top. \quad (\text{I.23})$$

As for the case of the kinematic error model, the explicit dependence on the probe offset allows different probe configurations to be modelled.

If V_{AR} is the $3m \times 3m$ variance matrix associated with $\boldsymbol{\alpha}_{1:m}$ determined from the correlation kernel (or otherwise), then the variance contribution V_{XR} to the measurements $\mathbf{x}_{1:m}$ is given by

$$V_{XR} = G_{XR}V_{AR}G_{XR}^\top,$$

where G_{XR} is a $3m \times 3m$ block-diagonal matrix. If the i th measurement is associated with the k th probe, then the 3×3 i th diagonal is equal to G_k , where G_k is constructed from \mathbf{p}_k as in (I.23). Although the model for the rotation angles about the three axes are mutually independent, the sensitivity matrices G_{XR} in general will introduce correlation between the effects applied to the x -, y - and z -coordinates.

Rotational errors and probe qualification effects

The model for rotational errors can be combined with that for probe qualification errors as follows. The model in (I.21) is a simplification of the

⁹The ‘E’ and ‘R’ in ‘ER’ are meant to represent the error that due to rotation effects.

following model. Firstly, we have

$$\mathbf{s}_i^* = \mathbf{x}_i^* + R(\boldsymbol{\alpha}^*)\mathbf{p}^*$$

relating a point \mathbf{s}^* on a surface to the point in the CMM working volume \mathbf{x}_i^* offset from \mathbf{s}_i^* by the true probe offset \mathbf{p}^* rotated by $R(\boldsymbol{\alpha}^*)$. The measurements \mathbf{x}_i of \mathbf{x}_i^* are modelled as

$$\mathbf{x}_i = \mathbf{x}_i^* + \mathbf{e}_i + \boldsymbol{\epsilon}_i,$$

and \mathbf{s}_i^* is estimated by

$$\mathbf{s}_i = \mathbf{x}_i + \mathbf{p},$$

where \mathbf{p} is the estimate of the probe offset determined in a probe qualification experiment. Combining these two equations, we have

$$\begin{aligned} \mathbf{s}_i &= \mathbf{x}_i^* + \mathbf{e}_i + \boldsymbol{\epsilon}_i + \mathbf{p}, \\ &= \mathbf{s}_i^* - R(\boldsymbol{\alpha}^*)\mathbf{p}^* + \mathbf{p} + \mathbf{e}_i + \boldsymbol{\epsilon}_i, \end{aligned}$$

which relates the true point on the surface to its estimate. For $\boldsymbol{\alpha}^*$ near zero and \mathbf{p} near \mathbf{p}^*

$$\mathbf{p} - R(\boldsymbol{\alpha}^*)\mathbf{p}^* \approx \mathbf{p} - \mathbf{p}^* - \begin{bmatrix} 0 & -\alpha_z^* & \alpha_y^* \\ \alpha_z^* & 0 & \alpha_x^* \\ -\alpha_y^* & \alpha_x^* & 0 \end{bmatrix} \mathbf{p}$$

showing that separation in to probe qualification effects and rotational errors.

Isotropic models for spatially correlated rotational errors

If the variances spatial correlation lengths are the same for each axis and equal to σ_{ER}^2 and λ_{ER} , respectively, then the variance matrix V_{XR} is constructed from 3×3 blocks of the form

$$V_{ij} = \sigma_{ER}^2 \left(\exp^{-d_{ij}^2/\lambda_{ER}^2} \right) G_{k(i)} G_{k(j)}^\top, \quad (\text{I.24})$$

where G_k is defined as in (I.23).

I.3.8 Gaussian process model for probing effects

The operation of the probe system will also make a variance contribution. While the CMM geometric errors are likely to vary smoothly with location, the probing errors are likely to vary smoothly with probing direction where the probing direction is usually designed to be normal to the surface being probed. We can augment the model in (I.19) to one of the form

$$\mathbf{x}_i = \mathbf{x}_i^* + \mathbf{e}_i + (e_{P,0} + e_{P,i})\mathbf{n}_i + \boldsymbol{\epsilon}_i, \quad (\text{I.25})$$

where $e_{P,0}$ is a fixed offset representing the the uncertainty in the estimate of the probe radius, $e_{P,i}$ is a spatially correlated systematic effect associated with probing and \mathbf{n}_i is the unit normal probing direction. The correlation between effects $e_{P,i}$ and $e_{P,j}$ depends the spatial separation $\|\mathbf{n}_i - \mathbf{n}_j\|$ if both measurements are made using the same probe. We assume that probing effects associated with different probes are statistically independent (although there may be situations where some statistical dependence would be expected). We assume that $e_{P,0}$ is associated with variance $\sigma_{P_0}^2$ and $e_{P,i}$ with variance σ_P^2 and length scale parameter λ_P . If V_{DP} is given by

$$V_{DP}(i, j) = \sigma_{P_0}^2 + \sigma_P^2 e^{-d_{P,ij}^2/\lambda_P^2}, \quad d_{P,ij} = \|\mathbf{n}_j - \mathbf{n}_i\|, \quad (\text{I.26})$$

then the variance contribution V_{XP} associated with probing effects is given by

$$V_{XP} = NV_{DP}N^\top$$

where N is the $3m \times m$ block diagonal matrix with \mathbf{n}_i in the i th diagonal block.

I.3.9 Spatially and temporally correlated systematic effects

This section discusses some possible extensions to the models described above.

Suppose that $\mathbf{x} = \mathbf{x}^* + \mathbf{e}(\mathbf{b}) + \boldsymbol{\epsilon}$ where $\mathbf{e}(\mathbf{b})$ are systematic effects specified by parameters \mathbf{b} . For measurements that naturally arise in distinct blocks X_q , $q = 1, \dots, n_Q$, representing measurements of different component surfaces or measurements taken over separate time intervals, it may be more realistic to assume that for each X_q , the effects \mathbf{e} are specified by different \mathbf{b}_q but that the parameters \mathbf{b}_q are correlated with each other and the strength of

correlation depends on where in the working volume the measurements are made or at what times the measurements were made. We can use Gaussian process models to represent this concept of spatio-temporal correlation. One simple approach is as follows. We assume that to each block of measurements X_q are assigned a representative location $\bar{\mathbf{x}}_q$ and a representative time t_q . For example we could take $\bar{\mathbf{x}}_q$ to be the centroid (mean) of the point coordinates X_q and t_q to be the mean time at which X_q was gathered. The correlation coefficient ρ_{qr} relating \mathbf{b}_q to \mathbf{b}_r can then be calculated according to $\rho_{qr} = k(\bar{\mathbf{x}}_q, \bar{\mathbf{x}}_r, t_q, t_r)$ for some correlation kernel k , e.g.,

$$k(\hat{\mathbf{x}}_q, \bar{\mathbf{x}}_r, t_q, t_r | \lambda_S, \tau) = e^{-d_{qr}^2 / \lambda_S^2} e^{-t_{qr}^2 / \tau^2},$$

where

$$d_{qr} = \|\mathbf{x}_r - \mathbf{x}_q\|, \quad t_{qr} = |t_r - t_q|,$$

and λ_S and τ are spatial and temporal correlation lengths, respectively. If V_B is the $n_B \times n_B$ variance matrix associated with one set of effects parameters \mathbf{b} , then the $(n_B n_Q) \times (n_B n_Q)$ variance matrix associated with $\mathbf{b}_{1:n_Q}$ is a tensor product of V_B with R , the matrix of correlation coefficients with submatrices $V_{B,qr} = \rho_{qr} V_B$. In practice only R and V_B need be stored, rather than the complete variance matrix. If $G_{X_q|B_q}$ is the sensitivity matrix of X_q with respect to \mathbf{b}_q , then the variance matrix associated with the complete point cloud is a block matrix with blocks

$$V_{X_{qr}|B} = G_{X_q|B} V_{B,qr} G_{X_r}^\top.$$

Temporal correlation can also be introduced to GP location, rotational and probing errors to model the fact that these effects may change over time and the degree of change depends on the temporal separation.

I.3.10 Length scales associated with the different influence factors

The influence factors considered in this report (section I.2.3) can be thought of as operating at different length scales. Effects associated with repeatability essentially operate at near zero length scales: knowing the effect at one location provides little information about the effect at a location nearby. Spatially-correlated location and rotation errors operate at medium length scales, controlled by the parameters λ_{ET} and λ_{ER} . Scale and squareness

effects operate at length scales of the order of the largest diameter of the machine working volume. Probe qualification and probe radius effects operate at infinite length scales in the sense that the effects are constant throughout the working volume. Effects that depend on probing direction also are associated with an infinite length scale in the sense that they are constant along any probing direction.

I.3.11 Combining effects

We can write the point cloud variance matrix V_X incorporating all the effects considered above as

$$V_X = V_{XT} + V_{XR} + V_{XP} + G_{X|PQ}V_{PQ}G_{X|PQ}^\top + G_{X|S}V_SG_{X|S}^\top + V_R, \quad (\text{I.27})$$

where the first three variance matrices on the right are derived from spatially correlated location, rotation and probing effects, and the second three are the contributions from probe qualification effects, scale and squareness effects, and independent random effects, respectively. For some cases, not all effects need to be considered. For example, for measurements using a single probe, rotational effects and probe qualifications need not be calculated. While the model does have some degree of complexity, all the variance matrices can be calculated using direct calculations based on, for example, the point coordinates, the distances between points, etc. All calculations have been implemented in spreadsheets, for example.

Contribution to the variances of derived features from different influence factors

If $G_{A|X}$ is the sensitivity matrix associated with a feature vector \mathbf{a} with respect to coordinates $\mathbf{x}_{1:m}$, then the variance matrix V_A associated with \mathbf{a} can also be decomposed as

$$V_A = V_{A|XT} + V_{A|XR} + V_{A|XP} + \dots \\ G_{A|PQ}V_{PQ}G_{A|PQ}^\top + G_{A|S}V_SG_{A|S}^\top + G_{A|X}V_RG_{A|X}^\top,$$

where $V_{A|XT} = G_{A|X}V_{XT}G_{A|X}^\top$, etc., and $G_{A|S} = G_{A|X}G_{X|S}$, etc. Thus $G_{A|PQ}V_{PQ}G_{A|PQ}^\top$ is the variance contribution to V_A arising from probe qualification effects, for example.

The uncertainty contributions to $u(\mathbf{a})$ from each of the influence factors can also be evaluated:

$$u^2(\mathbf{a}) = u_{ET}^2(\mathbf{a}) + u_{ER}^2(\mathbf{a}) + u_P^2(\mathbf{a}) + u_{PQ}^2(\mathbf{a}) + u_S^2(\mathbf{a}) + u_R^2(\mathbf{a}),$$

where $u_{ET}^2(\mathbf{a})$ is the set of diagonal elements of $V_{A|XT}$, etc.

Contributions to variances associated with position, size and shape from different influence factors

Appendix .1 shows how any point cloud variance matrix V_X can be analysed to separate out the positional, V_{PX} , size/scale, V_{ZX} , and shape, V_{SX} , components. The positional component is that which can be explained in terms an uncertain frame of reference for the point clouds, the size component that which can be explained in terms of an uncertainty global scale while the shape component essentially is that component remaining. The shape component is the dominant component in the contribution to form error. The decomposition into positional, size and shape components can be thought of as applying three sensitivity matrices $G_{PX|X}$, $G_{ZX|X}$ and $G_{SX|X}$ to V_X :

$$\begin{aligned} V_{PX|X} &= G_{PX|X} V_X G_{PX|X}^\top, & V_{ZX|X} &= G_{ZX|X} V_X G_{ZX|X}^\top, \\ V_{SX|X} &= G_{SX|X} V_X G_{SX|X}^\top. \end{aligned}$$

These sensitivity matrices can also be applied to the individual variance contributions arising from the various influence factors, e.g.,

$$\begin{aligned} V_{PX|PQ} &= G_{PX|X} V_{X|PQ} G_{PX|X}^\top, & V_{ZX|PQ} &= G_{ZX|X} V_{X|PQ} G_{ZX|X}^\top, \\ V_{SX|PQ} &= G_{SX|X} V_{X|PQ} G_{SX|X}^\top, \end{aligned}$$

separates the contribution probe qualification effects make to position, size and shape uncertainty and may be of interest for measurements involving multiple probes.

Point cloud variance factorisation

We note that V_X can always be factored as $V_X = K K^\top$ using a Cholesky factorisation or a eigenvalue decomposition [26]. If V_X is given as

$$V_X = \sum_{k=1}^{n_K} V_k, \quad V_k = K_k K_k^\top,$$

a sum of variance contributions V_k that are already factored, then

$$V_X = KK^\top, \quad K = [K_1 \ \cdots \ K_k \ \cdots \ K_{n_K}].$$

It is not necessary that the factor K is square and in general is a $3m \times p$ matrix. If $p > 3m$, then a QR factorisation [26] can be used to replace K by a $3m \times 3m$ factor.

Variance matrix associated with multiple features

It is often the case that multiple features \mathbf{a}_q are derived from distinct point sets X_q , $q = 1, \dots, n_Q$. Suppose V_X is the variance matrix associated with complete set of point coordinates $\mathbf{x}_{1:m}$ ordered so that X_1 is associated with $\mathbf{x}_{1:m_q}$, X_2 is associated with $\mathbf{x}_{m_1+1:m_2}$, etc., and $V_K = KK^\top$. Partition K row-wise so that

$$K = \begin{bmatrix} K_1 \\ \vdots \\ K_q \\ \vdots \\ K_{n_Q} \end{bmatrix},$$

so that the variance matrix associated with X_q is $V_{X_q} = K_q K_q^\top$. If $G_{A_q|X_q}$ is the sensitivity matrix of features \mathbf{a}_q with respect to X_q , then the variance matrix V_A associated with the complete set of feature vectors $\mathbf{a}_{1:n_Q}$ is

$$V_A = K_A K_A^\top, \quad K_A = \begin{bmatrix} G_{A_1|X_1} K_1 \\ \vdots \\ G_{A_q|X_q} K_q \\ \vdots \\ G_{A_{n_Q}|X_{n_Q}} K_{n_Q} \end{bmatrix}.$$

Note that in general V_A will be a full matrix with \mathbf{a}_{q_1} correlated to \mathbf{a}_{q_2} due to their common dependence on systematic effects.

I.4 Uncertainties associated with distances derived from point clouds

This section considers how uncertainties associated with a point cloud can be propagated through to the uncertainties associated the distance between pair of points.

If an *a priori* model determines the point cloud matrices $V_X(\boldsymbol{\sigma})$ associated with $\boldsymbol{x}_{i:m}$ in terms of statistical parameters $\boldsymbol{\sigma}$, then for any pair of points \boldsymbol{x}_i and \boldsymbol{x}_j we can calculate the variance associated with the distance d_{ij} according to

$$u^2(d_{ij}) = \begin{bmatrix} \boldsymbol{n}_{ij} \\ -\boldsymbol{n}_{ij} \end{bmatrix}^\top V_{ij} \begin{bmatrix} \boldsymbol{n}_{ij} \\ -\boldsymbol{n}_{ij} \end{bmatrix}, \quad \boldsymbol{n}_{ij} = \frac{1}{d_{ij}}(\boldsymbol{x}_i - \boldsymbol{x}_j)$$

where V_{ij} is the 6×6 variance matrix formed from the $3i - 2 : 3i$ th and $3j - 2 : 3j$ th rows and columns of V_X .

Often we are interested in the difference in distances, e.g., in comparing the distance associated with a test artefact with that associated with a calibrated reference artefact. Differences in distances also comes into the impact of CMM uncertainties in form errors, e.g., the uncertainties associated with the difference in two diameters of a spherical or cylindrical artefact. Using the same notation

$$u^2(d_{ij} - d_{rs}) = \begin{bmatrix} \boldsymbol{n}_{ij} \\ -\boldsymbol{n}_{ij} \\ -\boldsymbol{n}_{rs} \\ \boldsymbol{n}_{rs} \end{bmatrix}^\top V_{ijrs} \begin{bmatrix} \boldsymbol{n}_{ij} \\ -\boldsymbol{n}_{ij} \\ -\boldsymbol{n}_{rs} \\ \boldsymbol{n}_{rs} \end{bmatrix},$$

where V_{ijrs} is the 12×12 variance matrix formed from relevant rows and columns of V_X .

I.4.1 Distance measurement: uncertainty contribution associated with random effects

If $V_X = \sigma_S^2 I$, then

$$u^2(d_{ij}) = 2\sigma_R^2.$$

If $d_{ij} = \|\boldsymbol{x}_j - \boldsymbol{x}_i\|$ and $d_{rs} = \|\boldsymbol{x}_s - \boldsymbol{x}_r\|$, then

$$u^2(d_{ij} - d_{rs}) = 4\sigma_R^2.$$

Note that these uncertainties depend only on σ_R and are independent of location and separation of the points.

I.4.2 Distance measurement: uncertainty contribution from probe qualification effects

We assume that probe qualification effects are modelled as in section I.3.4:

$$\mathbf{e}_{PQ,k} \in \mathcal{N}(\mathbf{0}, \sigma_{PQ,k}^2 I).$$

If \mathbf{x}_i and \mathbf{x}_j are measured using the same probe, then the uncertainty contribution to the distance d_{ij} from probe qualification effects is zero. Otherwise

$$u^2(d_{ij}) = \sigma_{PQ,k(i)}^2 + \sigma_{PQ,k(j)}^2.$$

The uncertainty contribution associated with $d_{ij} - d_{rs}$ arises from the term

$$(\mathbf{e}_{k(i)} - \mathbf{e}_{k(j)})^\top \mathbf{n}_{ij} - (\mathbf{e}_{k(r)} - \mathbf{e}_{k(s)})^\top \mathbf{n}_{rs}.$$

If $k(i) = k(j)$ and $k(r) = k(s)$, then $u^2(d_{ij} - d_{rs}) = 0$. If $k(r) = k(s)$ but $k(i) \neq k(j)$, then

$$u^2(d_{ij} - d_{rs}) = u^2(d_{ij}) = \sigma_{PQ,k(i)}^2 + \sigma_{PQ,k(j)}^2.$$

If $k(i) = k(r)$ and $k(j) = k(s)$ but $k(i) \neq k(j)$, then

$$u^2(d_{ij} - d_{rs}) = (2 - 2\mathbf{n}_{ij}^\top \mathbf{n}_{rs}) \left(\sigma_{PQ,k(i)}^2 + \sigma_{PQ,k(j)}^2 \right),$$

so that

$$0 \leq u^2(d_{ij} - d_{rs}) \leq 4 \left(\sigma_{PQ,k(i)}^2 + \sigma_{PQ,k(j)}^2 \right),$$

depending on the angle between \mathbf{n}_{ij} and \mathbf{n}_{rs} . The uncertainty contribution is zero if $\mathbf{n}_{ij} = \mathbf{n}_{rs}$, e.g., when two gauge blocks are measured parallel to each other with both left faces measured by one probe and both right faces by the other. The uncertainty contribution is maximised when $\mathbf{n}_{ij} = -\mathbf{n}_{rs}$, e.g., when the left face of one gauge block is measured by one probe and the left face of a second parallel gauge block is measured by the other probe with the probes interchanged for the right face. If all four measurements are undertaken by different probes then

$$u^2(d_{ij} - d_{rs}) = u^2(d_{ij}) + u^2(d_{rs}) = \sigma_{PQ,k(i)}^2 + \sigma_{PQ,k(j)}^2 + \sigma_{PQ,k(r)}^2 + \sigma_{PQ,k(s)}^2.$$

I.4.3 Distance measurement: uncertainty contribution associated with scale and squareness effects

We consider scale and squareness model as in (I.9, involving seven random effects $\mathbf{b} = (b_{aa}, b_{xx}, b_{yy}, b_{zz}, b_{xy}, b_{xz}, b_{yz})^\top$. Given two data points \mathbf{x}_i and \mathbf{x}_j , let $d_{ij} = \|\mathbf{x}_j - \mathbf{x}_i\|$ and $x_{ij}x_j - x_i$, $y_{ij} = y_j - y_i$ and $z_{ij} = z_j - z_i$. Then the 1×7 sensitivity matrix $G_{D|ij}$ of d_{ij} with respect to the scale and squareness effects \mathbf{e} is given by¹⁰

$$G_{D|ij} = \frac{1}{d_{ij}} \begin{bmatrix} d_{ij}^2 & x_{ij}^2 & y_{ij}^2 & z_{ij}^2 & x_{ij}y_{ij} & x_{ij}z_{ij} & y_{ij}z_{ij} \end{bmatrix}.$$

If

$$b_{aa} \sim \mathcal{N}(0, \sigma_S^2), \quad b_{xx}, b_{yy}, b_{zz} \sim \mathcal{N}(0, \sigma_{S,a}^2),$$

and

$$b_{xy}, b_{xz}, b_{yz} \sim \mathcal{N}(0, \sigma_Q^2).$$

then

$$u^2(d_{ij}) = \sigma_S^2 d_{ij}^2 + \sigma_{S,a}^2 D_{S,a}^2 + \sigma_Q^2 D_Q^2, \quad (\text{I.28})$$

where

$$D_{S,a}^2 = \frac{1}{d_{ij}^2} [x_{ij}^4 + y_{ij}^4 + z_{ij}^4],$$

and

$$D_Q^2 = \frac{1}{d_{ij}^2} [x_{ij}^2 y_{ij}^2 + x_{ij}^2 z_{ij}^2 + y_{ij}^2 z_{ij}^2].$$

The expression for $u^2(d_{ij})$ in (I.28) shows non-isotropic behaviour in that the uncertainty depends not only on the distance but also the position of the points \mathbf{x}_i and \mathbf{x}_j . In particular, if \mathbf{x}_i and \mathbf{x}_j are aligned with an axis direction, the cross terms $x_{ij}y_{ij}$ are all zero along with two of x_{ij} , y_{ij} and z_{ij} . For this case, $u(d_{ij})$ is given by

$$u^2(d_{ij}) = (\sigma_S^2 + \sigma_{S,a}^2) d_{ij}^2,$$

and does not have a contribution from squareness effects.

¹⁰Strictly, $G_{D|ij}$ is the sensitivity matrix of $\delta_{ij} = (\mathbf{x}_j - \mathbf{x}_i)^\top \mathbf{n}_{ij}$ where $\mathbf{n}_{ij} = (\mathbf{x}_j - \mathbf{x}_i)/d_{ij}$. We note that δ_{ij} is a signed quantity with $\delta_{ij} = \pm d_{ij}$.

Two scale and squareness models with the same distance measurement behaviour

See also [15]. From the expressions for $u^2(d_{ij})$ in (I.28) we note that if $\sigma_Q^2 = 2\sigma_{S,a}^2 = \tau^2$, say, then

$$\sigma_{S,a}^2 D_{S,a}^2 + \sigma_Q^2 D_Q^2 = \frac{1}{d_{ij}^2} \tau^2 d_{ij}^4 = \tau^2 d_{ij}^2,$$

and so

$$u^2(d_{ij}) = (\sigma_S^2 + \tau^2) d_{ij}^2.$$

Thus, if $\sigma_Q^2 = 2\sigma_{S,a}^2 = \tau^2$ then the uncertainty associated with the measurement of *any* distance is exactly the same as for a CMM that has only a single global scale effect with $\tilde{\sigma}_S^2 = \sigma_S^2 + \tau^2$. While the measurement of distance has exactly the same behaviour, the measurement of other features could be quite different. For example, a global scale effect will have little contribution to the measurement of form error of a sphere while any squareness effect will have a contribution.

Limitations of MPE statements in characterising CMM uncertainty

The example above also shows that it is not possible to characterise the uncertainty contribution of CMM measurement purely on the basis of an MPE statement.

Uncertainty associated with the difference in two differences

If $d_{ij} = \|\mathbf{x}_j - \mathbf{x}_i\|$ and $d_{rs} = \|\mathbf{x}_s - \mathbf{x}_r\|$, then

$$u^2(d_{ij} - d_{rs}) = \sigma_S^2 (d_{ij} - d_{rs})^2 + \sigma_{S,a}^2 D_{S,a}^2 + \sigma_Q^2 D_Q^2,$$

where

$$D_{S,a}^2 = \left(\frac{x_{ij}^2}{d_{ij}} - \frac{x_{rs}^2}{d_{rs}} \right)^2 + \left(\frac{y_{ij}^2}{d_{ij}} - \frac{y_{rs}^2}{d_{rs}} \right)^2 + \left(\frac{z_{ij}^2}{d_{ij}} - \frac{z_{rs}^2}{d_{rs}} \right)^2$$

and $D_Q^2 =$

$$\left(\frac{x_{ij}y_{ij}}{d_{ij}} - \frac{x_{rs}y_{rs}}{d_{rs}} \right)^2 + \left(\frac{x_{ij}z_{ij}}{d_{ij}} - \frac{x_{rs}z_{rs}}{d_{rs}} \right)^2 + \left(\frac{y_{ij}z_{ij}}{d_{ij}} - \frac{y_{rs}z_{rs}}{d_{rs}} \right)^2.$$

For example is \mathbf{x}_1 and \mathbf{x}_2 and \mathbf{x}_3 and \mathbf{x}_4 are the end points of diameters with $d_{12} = d_{34} = d$ and $\mathbf{x}_2 - \mathbf{x}_1$ is parallel to the x -axis and $\mathbf{x}_4 - \mathbf{x}_3$ parallel to the y -axis, then

$$u^2(d_{12} - d_{34}) = 2d^2\sigma_{S,a}^2.$$

By contrast, if the four points are rotated by 45° then

$$u^2(d_{12} - d_{34}) = \sigma_Q^2 d^2.$$

If $\mathbf{x}_2 - \mathbf{x}_1$ is parallel to $\mathbf{x}_4 - \mathbf{x}_3$ and $d_{12} = d_{34} = d$, then $u^2(d_{12} - d_{34}) = 0$, showing that scale and squares effects make no significant contribution to the uncertainty in calibrating a test length standard against a reference length standard of nominally the same length if the two standards are aligned parallel to each other.

I.4.4 Distance measurement: uncertainty contribution from spatially correlated location effects

See section I.3.7. Suppose that

$$\mathbf{x}_i = \mathbf{x}_i^* + \mathbf{e}_i, \quad \mathbf{x}_j = \mathbf{x}_j^* + \mathbf{e}_j,$$

where \mathbf{e}_i and \mathbf{e}_j are correlated effects. Suppose the x -components of the correlated effects are such that

$$e_{i,x}, e_{j,x} \sim \mathcal{N}(0, \sigma_x^2),$$

and the the coefficient of correlation for these two effects is $\rho_{ij,x}$ and that the y - and z -components are similarly distributed. Assume that the x -, y - and z -components are mutually independent then

$$u^2(d_{ij}) = \frac{2}{d_{ij}^2} (x_{ij}^2 \sigma_x^2 (1 - \rho_{ij,x}) + y_{ij}^2 \sigma_y^2 (1 - \rho_{ij,y}) + z_{ij}^2 \sigma_z^2 (1 - \rho_{ij,z})).$$

(Here $x_{ij} = x_j - x_i$, etc., as before.) If the correlation is described in terms of a correlation kernel as in (I.20), then $\rho_{ij,x} = e^{-d_{ij}^2/\lambda_x^2}$. If the correlation behaviour is the same in each axis with $\sigma_x = \sigma_y = \sigma_z = \sigma_{ET}$ and $\rho_{ij,x} = \rho_{ij,y} = \rho_{ij,z} = \rho_{ij} = e^{-d_{ij}^2/\lambda_{ET}^2}$, then

$$u^2(d_{ij}) = 2\sigma_{ET}^2 \left(1 - e^{-d_{ij}^2/\lambda_{ET}^2}\right).$$

Let $r = d_{ij}/\lambda_{ET}$. Then

$$\begin{aligned} 1 - e^{-d_{ij}^2/\lambda_{ET}^2} &= 1 - \left\{ 1 - r^2 + \frac{r^4}{2!} - \frac{r^6}{3!} + \dots \right\}, \\ &= r^2 - \frac{r^4}{2!} + \frac{r^6}{3!} - \dots \end{aligned}$$

If λ_{ET} is much greater than d_{ij} then e^{-r^2} is close to 1 and the uncertainty is the distance is close to zero. For this case the effects $e_i \approx e_j$ act like a fixed offset associated with the measurements (similar to a probe qualification effect) and do not contribute the uncertainty associated with the distance. For d_{ij} somewhat less than λ_{ET} , the term on the right above is dominated by the first term r^2 so that

$$u^2(d_{ij}) \approx 2\sigma_{ET}^2 \frac{d_{ij}^2}{\lambda_{ET}^2}.$$

In this case, the uncertainty associated with d_{ij} is approximately proportional to d_{ij} showing that the correlated effects behave somewhat like a scale effect. If d_{ij} is much greater than λ_{ET} the $e^{-d_{ij}^2/\lambda_{ET}^2} \approx 0$ and

$$u^2(d_{ij}) \approx 2\sigma_{ET}^2.$$

For this case the correlated effects behave more like independent random effects. Figures I.1–I.4 also give insight into the dependence of uncertainties associated with distances on spatial correlation length.

Uncertainty associated with the difference in two distances

This section shows how the uncertainty $u(d_{12} - d_{34})$ in the difference in two distances associated with four points $\mathbf{x}_{1:4}$ can be evaluated for an isotropic spatial correlation model defined by statistical parameters σ_{ET} and length scale parameter λ_{ET} . Let \mathbf{n}_{12} be the unit normal point in the direction $\mathbf{x}_2 - \mathbf{x}_1$ and \mathbf{n}_{34} defined similarly. Then

$$u^2(d_{12} - d_{34}) = \sigma_{ET}^2 \mathbf{g}^\top V_N \mathbf{g}, \quad \mathbf{g} = (1, -1, -1, 1)^\top,$$

with

$$V_N = \begin{bmatrix} 1 & e^{-d_{12}^2/\lambda_{ET}^2} & ce^{-d_{13}^2/\lambda_{ET}^2} & ce^{-d_{14}^2/\lambda_{ET}^2} \\ e^{-d_{12}^2/\lambda_{ET}^2} & 1 & ce^{-d_{23}^2/\lambda_{ET}^2} & ce^{-d_{24}^2/\lambda_{ET}^2} \\ ce^{-d_{13}^2/\lambda_{ET}^2} & ce^{-d_{23}^2/\lambda_{ET}^2} & 1 & e^{-d_{34}^2/\lambda_{ET}^2} \\ ce^{-d_{14}^2/\lambda_{ET}^2} & ce^{-d_{24}^2/\lambda_{ET}^2} & e^{-d_{34}^2/\lambda_{ET}^2} & 1 \end{bmatrix},$$

where $c = \mathbf{n}_{12}^\top \mathbf{n}_{34}$, the cosine of the angle between the two normal vectors. Performing the matrix-vector multiplications, we end up with

$$u^2(d_{12} - d_{34}) = 2\sigma_{ET}^2 (2 - e_{12} - e_{34} + c(e_{23} + e_{14} - e_{13} - e_{24})),$$

where $e_{12} = e^{-d_{12}^2/\lambda_{ET}^2}$, etc.

Example: comparison of two gauge blocks. Suppose two gauge blocks of nominally the same length are measured side by side, parallel to each other. For this case $d_{12} \approx d_{34} = D$, say, $d_{13} \approx d_{24} = d$, say, and $n_{12} \approx n_{34}$ so that $c \approx 1$. If d is much smaller than D , then $d_{14} \approx d_{23} \approx d_{12}$, and

$$u^2(d_{12} - d_{34}) \approx 4\sigma_{ET}^2 \left(1 - e^{-d^2/\lambda_{ET}^2}\right).$$

This uncertainty can be thought of as a quantification of the Abbe contribution to the uncertainty due to the fact that the measuring lines associated with the two gauge blocks are displaced by d from each other.

I.4.5 Distance measurement: uncertainty contribution from spatially correlated rotation effects

See section I.3.7. We assume the spatial correlation is isotropic specified by variance σ_{ER}^2 and length scale parameter λ_{ER} . If \mathbf{x}_k is measured using probe offset \mathbf{p}_k , $k = 1, 2$, \mathbf{n}_{12} is the unit vector pointing from \mathbf{x}_1 to \mathbf{x}_2 , and G_k are the sensitivity matrices associated with $R(\boldsymbol{\alpha})\mathbf{p}_k$ with respect to $\boldsymbol{\alpha}$ evaluated at $\boldsymbol{\alpha} = 0$ as in (I.23), then the uncertainty $u(d_{12})$ in the distance d_{12} due to rotation effects is given by

$$u^2(d_{12}) = \sigma_{ER}^2 \left(\mathbf{m}_1^\top \mathbf{m}_1 + \mathbf{m}_2^\top \mathbf{m}_2 - 2(\mathbf{m}_1^\top \mathbf{m}_2) e^{-d_{12}^2/\lambda_{ER}^2} \right),$$

where $\mathbf{m}_k = G_k \mathbf{n}_{12}$, $k = 1, 2$. If the same probe is used for both measurements, then $\mathbf{p}_1 = \mathbf{p}_2 = \mathbf{p}$, say, $\mathbf{m}_1 = \mathbf{m}_2 = \mathbf{m}$, say, and

$$u^2(d_{12}) = 2\sigma_{ER}^2 \mathbf{m}^\top \mathbf{m} \left(1 - e^{-d_{12}^2/\lambda_{ER}^2}\right).$$

For this latter case, the quantity $\mathbf{m}^\top \mathbf{m}$ depends on the relationship between \mathbf{n}_{12} and \mathbf{p} . If \mathbf{p} is in same direction as \mathbf{n}_{12} (unlikely to be so in practice) $\mathbf{m} = \mathbf{0}$. If \mathbf{p} is orthogonal to \mathbf{n}_{12} (as is often the case) then $\mathbf{m}^\top \mathbf{m} = \mathbf{p}^\top \mathbf{p}$, so for the case of the measurement of a distance using the same probe,

$$u(d_{12}) \leq \sqrt{2}\sigma_{ER}\|\mathbf{p}\| \left(1 - e^{-d_{12}^2/\lambda_{ER}^2}\right).$$

More generally,

$$u(d_{12}) \leq \sqrt{2}\sigma_{ER}P \left(1 - e^{-d_{12}^2/\lambda_{ER}^2}\right) \leq \sqrt{2}\sigma_{ER}P,$$

where P is the length of the longest probe involved.

I.4.6 Distance measurement: uncertainty contribution from spatially correlated probing effects (P)

See section I.3.8. We assume the spatial correlation is isotropic and specified by variance σ_P^2 and length scale parameter λ_P . The spatial correlation parameter λ_P relates to chordal distance on the unit sphere and is usually chosen so that two points that are diametrically opposed on the unit sphere are associated with independent effects, i.e., λ_P is significantly smaller than 1. In general, a value of $\lambda_P = 1/2$ is appropriate. Suppose \mathbf{x}_k is measured in probing direction \mathbf{n}_k using probe offset \mathbf{p}_k with associated statistical parameters $\sigma_{P_0,k}$, $\sigma_{P,k}$ and $\lambda_{P,k}$, $k = 1, 2$, and \mathbf{n}_{12} is the unit vector pointing from \mathbf{x}_1 to \mathbf{x}_2 . For the case of different probes, the model in section I.3.8 assumes that the probing effects are independent so that

$$u^2(d_{12}) = \sigma_{P_0,1}^2 + \sigma_{P_0,2}^2 + \sigma_{P,1}^2 + \sigma_{P,2}^2.$$

For $\mathbf{p}_1 = \mathbf{p}_2 = \mathbf{p}$, etc.,

$$u^2(d_{12}) = \sigma_{P_0}^2(o_1^2 + o_2^2 - 2o_1o_2) + \sigma_P^2 \left(o_1^2 + o_2^2 - 2o_1o_2e^{-d_{P,12}^2/\lambda_P^2}\right),$$

where

$$o_1 = \mathbf{n}_1^\top \mathbf{n}_{12}, \quad o_2 = \mathbf{n}_2^\top \mathbf{n}_{12}, \quad d_{P,12} = \|\mathbf{n}_2 - \mathbf{n}_1\|.$$

It is usually the case that \mathbf{n}_1 and \mathbf{n}_2 are aligned with \mathbf{n}_{12} . In this case, $o_1, o_2 = \pm 1$, and we have

$$u^2(d_{12}) = 4\sigma_{P_0}^2 + 2\sigma_P^2, \quad \mathbf{n}_1 = -\mathbf{n}_2, \quad u^2(d_{12}) = 0, \quad \mathbf{n}_1 = \mathbf{n}_2. \quad (\text{I.29})$$

The relationships above in (I.29) shows how the model accounts for the differences between uni-directional and bi-directional probing. For example, in measuring a step gauge, the probing effects do not contribute to the uncertainties associated with the distances between left-facing faces or between right-faces faces but contribute to the uncertainties in distances between

left- and right-facing faces. In the comparison of two gauge blocks sitting side by side in which all four faces (two left-, two right-facing), are measured with the same probe, then the uncertainty contributions are such that

$$u^2(d_{12}) = u^2(d_{34}) = 4\sigma_{P_0}^2 + 2\sigma_P^2, \quad u^2(d_{12} - d_{34}) = 0.$$

I.4.7 Uncertainties associated with distances due to combined effects

In the sections above, we have considered the uncertainty contributions to distances due to a number of effects. In this section we summarise these results, giving typical uncertainty contributions in terms of a small number of statistical parameters.

Random effects (R). Statistical parameter σ_R .

$$u_R^2(d_{ij}) = 2\sigma_R^2.$$

Probe qualification effects (PQ). Statistical parameters σ_{PQ} representing the maximum probe qualification uncertainty. For distance measurements using the same probe, the contribution is zero. Otherwise

$$u_{PQ}^2(d_{ij}) \leq 2\sigma_{PQ}^2.$$

Scale and squareness effects (S). Statistical parameters σ_S , $\sigma_{S,a}$ and σ_Q . For this model, the uncertainty in distance is approximated by

$$u_S^2(d_{ij}) \approx (\sigma_S^2 + \sigma_{S,a}^2 + \sigma_Q^2) d_{ij}^2.$$

If the measurements are aligned with an axis the squareness component, represented by σ_Q , makes no contribution.

Spatially-correlated location effects (ET). Statistical parameters σ_{ET} and λ_{ET} .

$$u_{ET}^2(d_{ij}) = 2\sigma_{ET}^2 \left(1 - e^{-d_{ij}^2/\lambda_{ET}^2}\right) \leq 2\sigma_{ET}^2.$$

Spatially-correlated rotation effects (ER). Statistical parameters σ_{ER} , λ_{ER} and the maximum probe length P .

$$u_{ER}^2(d_{ij}) \leq 2\sigma_{ER}^2 P^2 \left(1 - e^{-d_{ij}^2/\lambda_{ER}^2}\right) \leq 2\sigma_{ER}^2 P^2.$$

Spatially-correlated probing effects (P). Statistical parameters σ_{P_0} , σ_P , and λ_P :

$$u_P^2(d_{ij}) \leq 4\sigma_{P_0}^2 + 2\sigma_P^2.$$

I.4.8 Plausible values for statistical parameters based on an MPE statement

Suppose the MPE statement is $|d - d^*| \leq A + d^*/B$. We can interpret this statement statistically as

$$Ku^2(d) \leq A + d/B$$

where K is, say, 2 or 3. From the summary information given in section I.4.7 above, for $d_{ij} \approx 0$, the uncertainty $u(d_{ij})$ is such that

$$u^2(d_{ij}) \leq 2(\sigma_R^2 + \sigma_{PQ}^2 + \sigma_P^2 + 2\sigma_{P_0}^2).$$

This implies

$$\sigma_A^2 = 2(\sigma_R^2 + \sigma_{PQ}^2 + \sigma_P^2 + 2\sigma_{P_0}^2) \leq A^2/K^2 \quad (\text{I.30})$$

which puts constraints on the size of σ_A , as defined above, and depending on the statistical parameters σ_R , σ_{PQ} , σ_{P_0} and σ_P . With σ_A defined as above, we can set

$$u^2(d) = \sigma_A^2 + (\sigma_S^2 + \sigma_{S,a}^2 + \sigma_Q^2) d^2 + 2\sigma_{ET}^2 \left(1 - e^{-d^2/\lambda_{ET}^2}\right) + 2\sigma_{ER}^2 P^2 \left(1 - e^{-d^2/\lambda_{ER}^2}\right), \quad (\text{I.31})$$

a summary estimate of the uncertainty in distance due to the combined effects, and evaluate

$$C(d) = \frac{Ku(d)}{A + d/B}. \quad (\text{I.32})$$

If $C(d) \leq 1$ over the working volume, then the values of the statistical parameters do not violate the MPE statement. If $C_{\max} = \max_{d \leq L_{\max}} C(d)$ is

Table I.3: Statistical parameters for calculating $u(d)$.

Effect	Parameter	Unit	Value
MPE	A	mm	0.002
	B	1	$1.25e5$
Repeatability	σ_R	mm	0.000 2
Scale, squareness	σ_S	1	$4.0e - 6$
	$\sigma_{S,a}$	1	$2.0e - 6$
	σ_Q	1	$2.0e - 6$
Probe qualification	σ_{PQ}	mm	0.000 5
Location	σ_{ET}	mm	0.000 5
	λ_{ET}	mm	100.0
Rotation	σ_{ER}	radians	$1.0e - 5$
	λ_{ER}	mm	200.0
	P	mm	40.0
Probing	σ_{P_0}	mm	0.000 2
	σ_P	mm	0.000 2
	λ_P	1	0.5

maximum value of $C(d)$ over the working volume, then the simple procedure of dividing all the statistical parameters representing standard deviations, σ_R , etc., by C_{\max} will lead to conformance with the MPE statement.

Graphs of the MPE and uncertainty of distance components as a function of d derived for statistical parameters in table I.3 and expansion factor $K = 2$ are shown in figure I.5. The figure shows that the statistical parameters conform to the MPE statement. The uncertainty contribution from scale and squareness effects is linear in d while the spatially-correlated location and rotation effects start off as linear in d but begin to level off for larger values of d . The spatially correlation length scale parameter λ_{ER} associated with the rotation effects is larger than that λ_{ET} for the location effects and the levelling off occurs later for the rotation effects. For $d < 200$ mm, the rotation effects look like a scale effect. Figures I.6 and I.7 graph the same functions but for the case $\lambda_{ET} = 50$ mm and $\lambda_{ER} = 100$ mm (shorter length scale, less smooth behaviour) and $\lambda_{ET} = 200$ mm and $\lambda_{ER} = 400$ mm, (longer length scale, smoother behaviour), respectively. The shorter length scales correspond to behaviour more similar to independent random effects (apart from over short distances) while the longer length scales correspond

to behaviour more similar to scale and squareness effects.

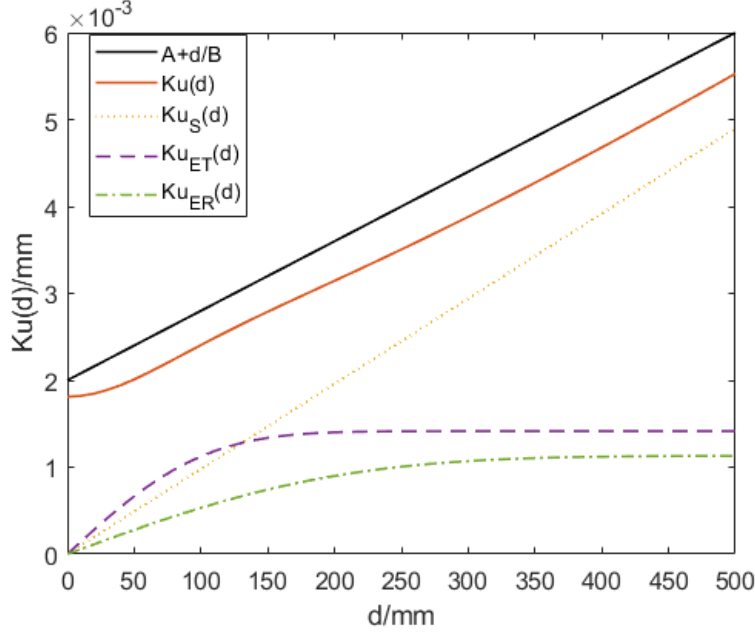


Figure I.5: Graphs of the MPE and uncertainty of distance components as a function of d . The upper solid line is $A + d/B$, the lower solid line is $Ku(d)$ with $u(d)$ evaluated as in (I.31) and uncertainty contributions $Ku_S(d)$ from scale and squareness effects, dotted line, $Ku_{ET}(d)$ from spatially correlated location effects, dashed line, and $Ku_{ER}(d)$ from spatially correlated rotation effects, dot-dashed line, derived for statistical parameters in table I.3 and expansion factor $K = 2$.

Plausible values for spatial correlation location effects

The MPE statement can be used to constrain a subset of the statistical parameters. In this section we consider random effects and spatially correlated location effects.

Suppose a CMM is modelled in terms of

$$\mathbf{x}_i = \mathbf{x}_i^* + \mathbf{e}_i + \boldsymbol{\epsilon}_i, \quad \boldsymbol{\epsilon}_i \in \mathcal{N}(\mathbf{0}, \sigma_R^2 \mathbf{I}),$$

where \mathbf{e}_i are isotropic spatially correlated effects with associated variance σ_{ET}^2 and length scale parameter λ_{ET} . The uncertainty $u(d)$ associated with

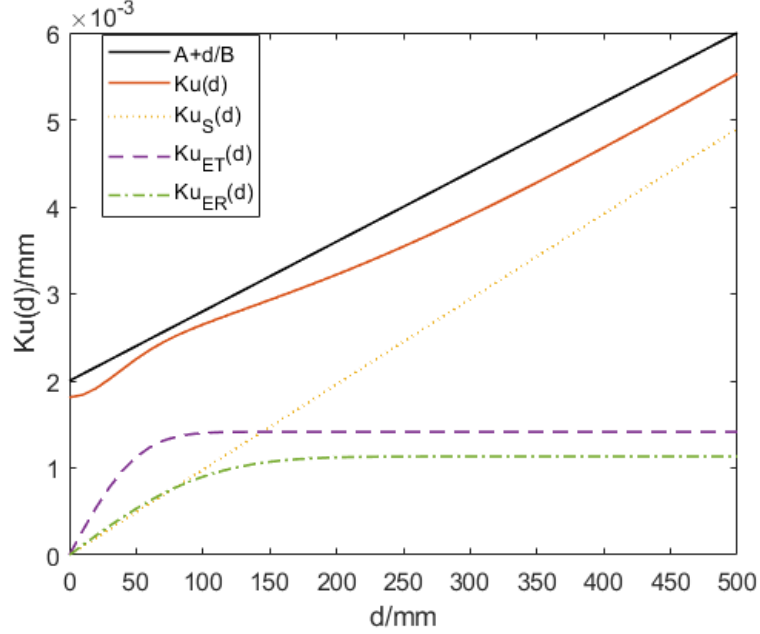


Figure I.6: As figure I.5, but for $\lambda_{ET} = 50$ mm and $\lambda_{ER} = 100$ mm corresponding to shorter length scales and less smooth behaviour of the error functions.

a distance measurement in this model is given by

$$u^2(d) = 2\sigma_R^2 + 2\sigma_{ET}^2 \left(1 - e^{-d^2/\lambda_{ET}^2}\right).$$

If the MPE statement is $|d - d^*| \leq A + d^*/B$, then we can interpret the MPE statement statistically as

$$u^2(d) = 2\sigma_R^2 + 2\sigma_{ET}^2 \left(1 - e^{-d^2/\lambda_{ET}^2}\right) \leq \frac{1}{K^2} (A + d/B)^2, \quad (\text{I.33})$$

where K is such that the chances of measuring a distance that fails the MPE test is small, say $K = 2$ or $K = 3$, correspond to a chance of 5 % or 0.27 %, respectively (assuming Gaussian distributions). The inequality in (I.33) constrains the possible choices for σ_R , σ_{ET} and λ_{ET} . In particular, for $d_{ij} \ll \lambda_{ET}$ and $d_{ij} \ll B$, we have

$$2\sigma_R^2 \leq A^2/K^2.$$

We can rewrite the inequality in (I.33) as

$$R(d|\sigma_R, \sigma_{ET}, \lambda_{ET}) \leq 1, \quad (\text{I.34})$$

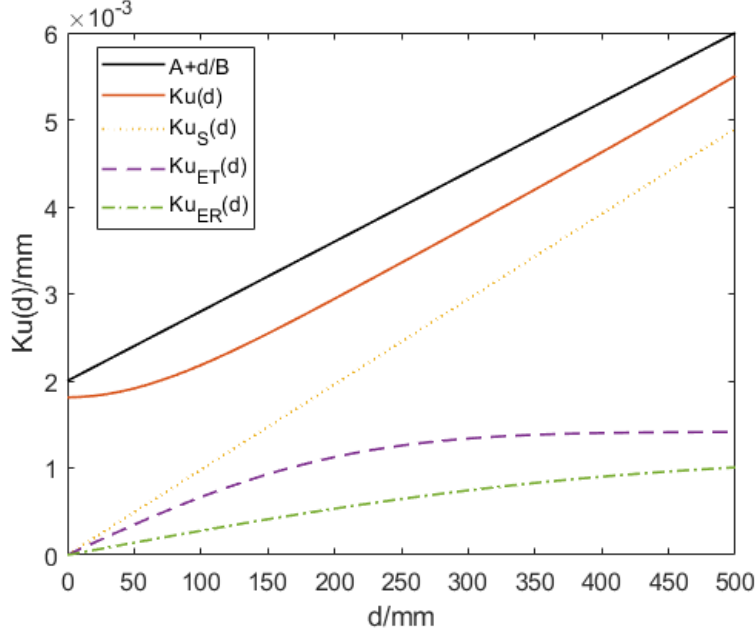


Figure I.7: As figure I.5, but for $\lambda_{ET} = 200$ mm and $\lambda_{ER} = 400$ mm corresponding to longer length scales and smoother behaviour of the error functions.

where

$$R(d|\sigma_R, \sigma_{ET}, \lambda_{ET}) = K^2 \frac{2\sigma_R^2 + 2\sigma_{ET}^2 (1 - e^{-d^2/\lambda_{ET}^2})}{(A + d/B)^2}.$$

As a function of d , $R(d|\sigma_R, \sigma_{ET}, \lambda_{ET})$ is unimodal taking the value of $2K\sigma_R^2/A^2$ at $d = 0$ and decaying like $1/d^2$ as $d \rightarrow \infty$. If L_{\max} is the longest distance in the working volume, then if $\dot{R}(L_{\max}) > 0$, where \dot{R} is the derivative of R with respect to d , it follows that $R(d) \leq 1$ for $0 \leq d \leq L_{\max}$. If $R(L_{\max}) \leq 1$ but $\dot{R}(L_{\max}) < 0$, then $R(d)$ has its maximum inside the interval $[0, L_{\max}]$. As d increases from 0, the numerator in $R(d)$ increases until the point where e^{-d^2/λ_{ET}^2} becomes small. From then the numerator is constant and the behaviour of $R(d)$ follows a $1/d^2$ decay. Let d_0 be such that $e^{-d_0^2/\lambda_{ET}^2} = 0.1$, i.e.,

$$d_0 = \sqrt{(-\log(0.1))\lambda_{ET}},$$

an approximation to the point where $R(d)$ takes its maximum. If $R_0 = R(d_0|\sigma_R, \sigma_{ET}, \lambda_{ET}) < 1$, then it is likely that the constraint on $R \leq 1$ is

valid for all $d \leq d_0$. If $R_0 > 1$, then reducing σ_{ET} to

$$\hat{\sigma}_M := \frac{1}{1.8} \left[\frac{(A + d_0/B)^2}{K^2} - 2\sigma_R^2 \right], \quad d_0 = \sqrt{\log(10)}\lambda_{ET}, \quad (\text{I.35})$$

will likely reduce $R(d)$ to be less than 1 over the range $0 \leq d \leq d_0$. These calculations give a useful approximate value for σ_{ET} so that $R(d|\sigma_R, \sigma_{ET}, \lambda_{ET}) \leq 1$, given estimates of σ_R and λ_{ET} .

Figure I.8 shows the graphs of the functions $R(d|\sigma_R, \sigma_{ET}, \lambda_{ET})$ and $R(d|\sigma_R, \hat{\sigma}_M, \lambda_{ET})$ defined in (I.34) for $\lambda_{ET} = 20$ mm, 50 mm and 100 mm. Each graph gives the function determined using the prior value of $\sigma_{ET} = 0.001$ mm, and the function determined using the adjusted value of $\hat{\sigma}_M$ calculated as in (I.35). The adjusted values are $\hat{\sigma}_M = 0.0006$ mm, 0.0007 mm, and 0.0009 mm, for the three values of λ_{ET} . For each of the three cases, it is seen that the estimate d_0 is reasonably close to where $R(d)$ is maximised, and that the adjusted function satisfies $R(d|\sigma_R, \hat{\sigma}_M, \lambda_{ET}) \leq 1$ to a good approximation.

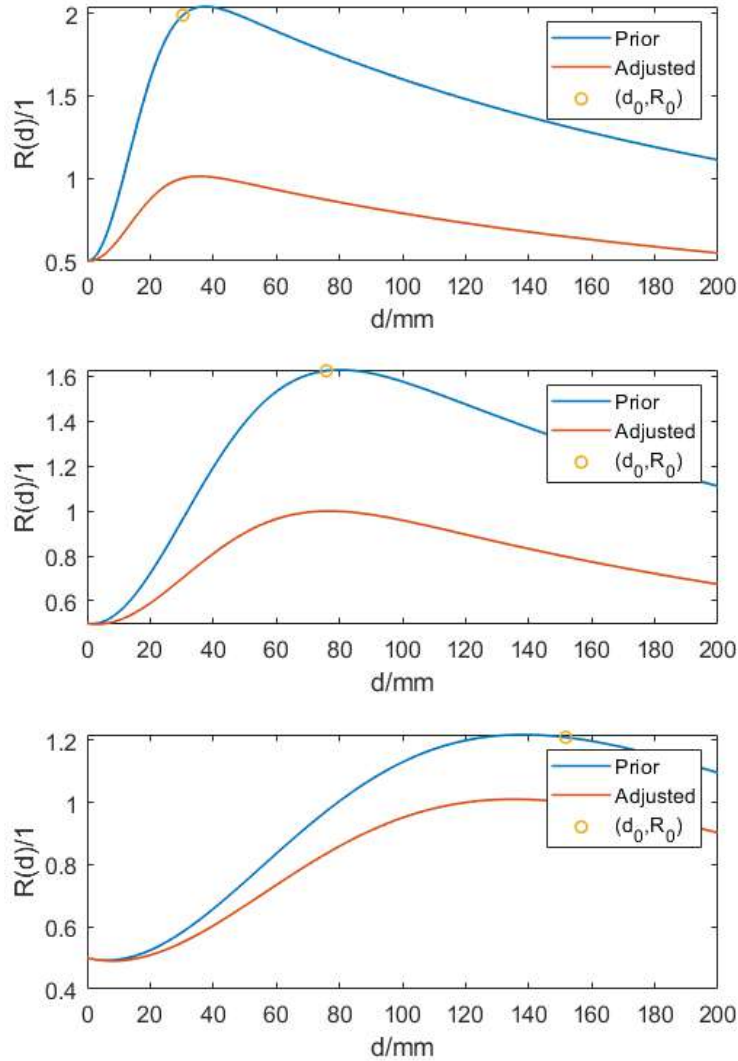


Figure I.8: Graphs of the functions $R(d|\sigma_R, \sigma_{ET}, \lambda_{ET})$ and $R(d|\sigma_R, \hat{\sigma}_M, \lambda_{ET})$ defined in (I.34) for $\lambda_{ET} = 20$ mm (top), $\lambda_{ET} = 50$ mm (middle) and $\lambda_{ET} = 100$ mm (bottom). Each graph gives the function determined using the prior value of σ_{ET} , and the function determined using the adjusted value of $\hat{\sigma}_M$ calculated as in (I.35).

I.5 Least squares (Gaussian) associated features

In this section we look at methods that derive features through fitting model to data by minimising a sum of squares objective function. Many of the calculations involve the distance to an axes or a plane and we consider those first.

I.5.1 Calculations associated with axes

Point on an axis

If $\mathbf{z}_A = \mathbf{x}_A + t_A \mathbf{v}_A$, is a point on the axis, then the sensitivity matrix $G_{Z|B}$ of \mathbf{z}_A with respect to $\mathbf{b}_A^\top = (\mathbf{x}_A^\top, \mathbf{v}_A^\top)$ is the 3×6 matrix

$$G_{Z_A|B_A} = \begin{bmatrix} 1 & 0 & 0 & t_A & 0 & 0 \\ 0 & 1 & 0 & 0 & t_A & 0 \\ 0 & 0 & 1 & 0 & 0 & t_A \end{bmatrix}.$$

Distance from a point to an axis

For an axis specified by \mathbf{x}_A and $\mathbf{v}_A = (u_A, v_A, w_A)^\top$ with $\|\mathbf{v}_A\| = 1$, the distance from a point \mathbf{x} to the axis is given by

$$d_A(\mathbf{x}, \mathbf{b}_A) = \|(\mathbf{x} - \mathbf{x}_A) \times \mathbf{v}_A\|, \quad (\text{I.36})$$

with

$$(\mathbf{x} - \mathbf{x}_A) \times \mathbf{v}_A = \begin{bmatrix} \xi \\ \eta \\ \zeta \end{bmatrix} = \begin{bmatrix} (y - y_A)w_A - (z - z_A)v_A \\ (z - z_A)u_A - (x - x_A)w_A \\ (x - x_A)v_A - (y - y_A)u_A \end{bmatrix}.$$

The 1×6 sensitivity matrix $G_{D_A|B_A}$ of $d_A = d_A(\mathbf{x}, \mathbf{b})$ with respect to $\mathbf{b}_A^\top = (\mathbf{x}_A^\top, \mathbf{v}_A^\top)$ is given by

$$G_{D_A|B_A}^\top = \frac{1}{d_A} \begin{bmatrix} \eta w_A - \zeta v_A \\ \zeta u_A - \xi w_A \\ \xi v_A - \eta u_A \\ \eta(z - z_A) - \zeta(y - y_A) \\ \zeta(x - x_A) - \xi(z - z_A) \\ \xi(y - y_A) - \eta(x - x_A) \end{bmatrix}. \quad (\text{I.37})$$

Distance from a point to a plane orthogonal to an axis

The distance $d_P(\mathbf{x}, \mathbf{b}_A)$ from a point \mathbf{x} to the plane $(\mathbf{x} - \mathbf{x}_A)^\top \mathbf{v}_A = 0$ specified by \mathbf{x}_A and $\mathbf{v}_A = (u_A, v_A, w_A)^\top$ with $\|\mathbf{v}_A\| = 1$, is given by

$$d_P(\mathbf{x}, \mathbf{b}_A) = (\mathbf{x} - \mathbf{x}_A)^\top \mathbf{v}_A. \quad (\text{I.38})$$

The 1×6 sensitivity matrix $G_{D_P|B_A}$ of $d_P = d_P(\mathbf{x}, \mathbf{b})$ with respect to $\mathbf{b}^\top = (\mathbf{x}_A^\top, \mathbf{v}_A^\top)$ is given by

$$G_{D_P|B_A}^\top = \begin{bmatrix} -u_A \\ -v_A \\ -w_A \\ x - x_A \\ y - y_A \\ z - z_A \end{bmatrix}. \quad (\text{I.39})$$

Intersection of axes with a fixed plane

Suppose $\mathbf{b} = (\mathbf{x}_A^\top, \mathbf{v}_A^\top)^\top$, with $\mathbf{v}_A^\top \mathbf{v}_A = 1$, specifying an axis \mathcal{L} has associated 6×6 variance matrix V_B and that a fixed plane \mathcal{P} is specified by locating point \mathbf{x}_P , with axis unit normal \mathbf{v}_P , with $\mathbf{v}_P^\top \mathbf{v}_P = 1$. The point intersection \mathbf{x}_L of the \mathcal{L} with \mathcal{P} is given by

$$\mathbf{x}_L = \mathbf{x}_A + t\mathbf{v}_A, \quad t = \frac{(\mathbf{x}_P - \mathbf{x}_A)^\top \mathbf{v}_P}{\mathbf{v}_A^\top \mathbf{v}_P}.$$

The 3×6 sensitivity matrix $G_{L|B}$ of \mathbf{x}_L with respect to \mathbf{b} is given by

$$G_{L|B} = [G \ tG], \quad G = I - \frac{\mathbf{v}_A \mathbf{v}_P^\top}{\mathbf{v}_A^\top \mathbf{v}_P}. \quad (\text{I.40})$$

If \mathbf{b}_1 and \mathbf{b}_2 specify two axes \mathcal{L}_1 and \mathcal{L}_2 that intersect the plane \mathcal{P} , then the 1×12 sensitivity matrix associated with the distance d_{12} between the two points of intersection with respect to $[\mathbf{b}_1^\top \ \mathbf{b}_2^\top]^\top$ is given by

$$G_{d_{12}, B} = \left[\mathbf{n}_{12}^\top G_1, \ t_1 \mathbf{n}_{12}^\top G_1, \ -\mathbf{n}_{12}^\top G_2, \ -t_2 \mathbf{n}_{12}^\top G_2 \right],$$

where $\mathbf{n}_{12} = (\mathbf{x}_{L,2} - \mathbf{x}_{L,1})/d_{12}$, the unit normal vector pointing from $\mathbf{x}_{L,1}$ to $\mathbf{x}_{L,2}$, t_1 and t_2 define the points of intersection, and G_1 and G_2 are the 3×3 sensitivity matrices calculated as in (I.40). If $\mathbf{v}_{A,1} \approx \mathbf{v}_{A,2} \approx \mathbf{v}_P$ as in

the case where both axes are approximately orthogonal to the plane, then $\mathbf{n}_{12}^\top \mathbf{v}_{A,1} \approx 0$, etc., and

$$G_{d_{12},B} \approx \begin{bmatrix} \mathbf{n}_{12}^\top & t_1 \mathbf{n}_{12}^\top & -\mathbf{n}_{12}^\top & -t_2 \mathbf{n}_{12}^\top \end{bmatrix}.$$

For this latter case, let $\mathbf{m}_{12} = \mathbf{n}_{12} \times \mathbf{v}_P$, the unit vector orthogonal to both \mathbf{n}_{12} and \mathbf{v}_P . Then $(\mathbf{v}_{A,2} - \mathbf{v}_{A,1})^\top \mathbf{n}_{12}$ is approximately the angle α_m of rotation between $\mathbf{v}_{A,1}$ and $\mathbf{v}_{A,2}$ about the axis \mathbf{m}_{12} and $(\mathbf{v}_{A,2} - \mathbf{v}_{A,1})^\top \mathbf{m}_{12}$ is approximately the angle rotation α_n between $\mathbf{v}_{A,1}$ and $\mathbf{v}_{A,2}$ about the axis \mathbf{n}_{12} . The 1×12 sensitivity matrices associated with α_m and α_n are approximated by

$$G_{\alpha_m,B} \approx \begin{bmatrix} \mathbf{0} & -\mathbf{n}_{12}^\top & \mathbf{0} & \mathbf{n}_{12}^\top \end{bmatrix},$$

$$G_{\alpha_n,B} \approx \begin{bmatrix} \mathbf{0} & -\mathbf{m}_{12}^\top & \mathbf{0} & \mathbf{m}_{12}^\top \end{bmatrix}.$$

These sensitivity matrices are useful in evaluating the uncertainty associated with the angles between two nominally parallel axes, and similar calculations.

I.5.2 Least squares (LS) feature assessment

Suppose $\mathbf{u} \mapsto \mathbf{s}(\mathbf{u}, \mathbf{a})$ defines a parametric curve or surface. The parameters \mathbf{u} determine the position of a point on the surface and the parameters \mathbf{a} determine the shape and position of the surface. We assume that set of measured coordinates, $\mathbf{x}_{1:m}$ nominally represent points on such a surface, so that

$$\mathbf{x}_i \approx \mathbf{s}(\mathbf{u}_i, \mathbf{a}), \quad (\text{I.41})$$

for some \mathbf{u}_i and some \mathbf{a} . The least squares (LS) estimates $\hat{\mathbf{u}}_{1:m}$ and $\hat{\mathbf{a}}$ of $\mathbf{u}_{1:m}$ and \mathbf{a} , respectively, can be found by minimising

$$\sum_{i=1}^m d^2(\mathbf{x}_i, \mathbf{a}), \quad d(\mathbf{x}_i, \mathbf{a}) = (\mathbf{x}_i - \mathbf{s}(\mathbf{u}_i^*, \mathbf{a}))^\top \mathbf{n}_i, \quad (\text{I.42})$$

where \mathbf{u}_i^* specifies the point $\mathbf{s}_i^* = \mathbf{s}(\mathbf{u}_i^*, \mathbf{a})$ on the surface closest to \mathbf{x}_i and \mathbf{n}_i is the normal vector at \mathbf{s}_i^* . The term least squares orthogonal distance regression (LSODR) is also used for this type of optimisation problem [6, 27] as $d(\mathbf{x}_i, \mathbf{a})$ is the (signed) distance of \mathbf{x}_i from the surface $\mathbf{s}(\mathbf{u}, \mathbf{a})$ measured orthogonally to the surface. For standard geometric elements, $d(\mathbf{x}, \mathbf{a})$ can

be evaluated analytically [13, 14]. For more general surfaces, numerical methods are required [21]. Let $J = J(\mathbf{x}_{1:m}, \mathbf{a})$ be the Jacobian matrix defined by

$$J_{ij} = \frac{\partial d}{\partial a_j}(\mathbf{x}_i, \mathbf{a}).$$

The optimality conditions for \mathbf{a} to minimise the sum of squares in (I.42) are of the form

$$J^\top \mathbf{d} = \mathbf{0}, \quad J = J(\mathbf{x}_{1:m}, \mathbf{a}), \quad d_i = d(\mathbf{x}_i, \mathbf{a}).$$

These optimality conditions implicitly define the solution \mathbf{a} as function of the data points $\mathbf{x}_{1:m}$ and allow us to evaluate the sensitivity matrix $G_{A|X}$ of \mathbf{a} with respect to the data [1, section 4.2.4]. If J is the Jacobian matrix and \mathbf{n}_i are the corresponding surface normals at the solution $\hat{\mathbf{u}}_{1:m}$ and $\hat{\mathbf{a}}$ then

$$G_{A|X} = G_{A|D} N^\top, \quad G_{A|D} = -(J^\top J)^{-1} J^\top, \quad (\text{I.43})$$

where N is the $3m \times m$ block diagonal matrix storing the normal vectors \mathbf{n}_i in the 3×1 diagonal blocks. The matrix $n \times m$ $G_{A|D}$ is the sensitivity matrix of the parameters \mathbf{a} with respect to changes in \mathbf{x}_i in the direction of \mathbf{n}_i , i.e, with respect to $\mathbf{n}_i^\top \mathbf{x}_i$, $i = 1, \dots, m$.

If J has QR factorisation [26]

$$J = QR = [Q_1 \ Q_2] \begin{bmatrix} R_1 \\ \mathbf{0} \end{bmatrix} \quad (\text{I.44})$$

where Q is orthogonal and R is upper-triangular, then

$$G_{A|D} = -R_1^{-1} Q_1^\top.$$

If V_X is the variance matrix associated with $\mathbf{x}_{1:m}$, then the variance matrix associated with the features \mathbf{a} is given by

$$V_A = G_{A|X} V_X G_{A|X}^\top.$$

If V_X is the diagonal matrix $\sigma^2 I$, then

$$V_A = \sigma^2 (J^\top J)^{-1} = \sigma^2 (R_1^\top R_1)^{-1}, \quad (\text{I.45})$$

using the fact that $N^\top N = I$. If the systematic effects $\mathbf{e}_{1:m}$ are defined in terms of parameters \mathbf{b} with associated variance matrix V_B , then the variance contribution $V_{A|B}$ to the variance V_A arising from the effects is given by

$$V_{A|B} = G_{A|B} V_B G_{A|B}^\top, \quad G_{A|B} = G_{A|X} G_{X|B}.$$

Uncertainties associated with residual distances

It is also possible to propagate the uncertainties associated with $\mathbf{x}_{1:m}$ through to the residual distances \mathbf{d} where $d_i = d(\mathbf{x}_i, \mathbf{a})$ evaluated at the solution. Taking into account the fact that the solution \mathbf{a} is implicitly defined as a function of $\mathbf{x}_{1:m}$, the sensitivity matrix $G_{\hat{D}|X}$ of \mathbf{d} with respect to $\mathbf{x}_{1:m}$ is given by

$$\begin{aligned} G_{\hat{D}|X} &= \left(I - J(J^\top J)^{-1} J \right) N^\top, \\ &= \left(I + JG_{A|D} \right) N^\top, \\ &= \left(I - Q_1 Q_1^\top \right) N^\top = Q_2 Q_2^\top N^\top, \end{aligned} \quad (\text{I.46})$$

where Q_1 and Q_2 are the submatrices of the orthogonal factor Q as in (I.44). We also write

$$G_{\hat{D}|D} = I + JG_{A|D} = I - Q_1 Q_1^\top \quad (\text{I.47})$$

to denote the sensitivity of the residual distances $d(\mathbf{x}_i, \hat{\mathbf{a}})$ with respect to changes in \mathbf{x}_i in the direction \mathbf{n}_i , i.e., with respect to $\mathbf{n}_i^\top \mathbf{x}_i$.

We can also evaluate the sensitivity matrix $G_{S|X}$ of the component of the surface points $\mathbf{s}(\mathbf{u}_i^*, \mathbf{a})$ orthogonal to the surface with respect to $\mathbf{x}_{1:m}$:

$$G_{S|X} = J(J^\top J)^{-1} J^\top N^\top = -JG_{A|X}. \quad (\text{I.48})$$

The sensitivity matrix

$$G_{S|D} = -J(J^\top J)^{-1} J^\top = -JG_{A|D}, \quad (\text{I.49})$$

is the sensitivity matrix of the component of the surface points $\mathbf{s}(\mathbf{u}_i^*, \mathbf{a})$ orthogonal to the surface with respect to $\mathbf{n}_i^\top \mathbf{x}_i$, $i = 1, \dots, m$.

The sensitivity matrices above, $G_{A|X}$, $G_{D|X}$ and $G_{S|X}$ can all be stored compactly and constructed from the $m \times n$ matrix J , the $n \times m$ matrix $(J^\top J)^{-1} J^\top$ and the normal vectors $\mathbf{n}_{1:m}$.

Weighted least squares orthogonal distance regression

It is sometimes useful to incorporate weights $w_i \geq 0$ into the orthogonal distance regression scheme so that the counterpart of (I.42) is

$$\sum_{i=1}^m w_i^2 d^2(\mathbf{x}_i, \mathbf{a}), \quad d(\mathbf{x}_i, \mathbf{a}) = (\mathbf{x}_i - \mathbf{s}(\mathbf{u}_i^*, \mathbf{a}))^\top \mathbf{n}_i. \quad (\text{I.50})$$

Let W be the diagonal matrix with w_i^2 in the i th diagonal element. Then the counterpart of (I.43) is

$$G_{A|X,W} = -(J^\top W J)^{-1} J^\top W N^\top, \quad (\text{I.51})$$

with $G_{D|X}$ and $G_{S|X}$ calculated as in (I.46) and (I.48) but with $G_{A|X,W}$ replacing $G_{A|X}$. Similarly,

$$G_{A|D,W} = -(J^\top W J)^{-1} J^\top W, \quad (\text{I.52})$$

is the sensitivity matrix of weighted least-squares fitted parameters \mathbf{a} with respect to $\mathbf{n}_i^\top \mathbf{x}_i$, and can be used to calculate $G_{\hat{D}|D}$ and $G_{S|D}$ as in (I.47) and (I.49).

I.5.3 Sensitivity matrix associated with a least-squares circle fit to data in a plane

If a circle is parametrized by $\mathbf{a} = (x_0, y_0, r_0)^\top$ specifying its centre \mathbf{x}_0 and radius r_0 , the signed distance $d(\mathbf{x}_i, \mathbf{a})$ from a data point \mathbf{x}_i to the sphere given by \mathbf{a} is

$$d(\mathbf{x}_i, \mathbf{a}) = r_i - r_0,$$

where

$$r_i^2 = (\mathbf{x}_i - \mathbf{x}_0)^\top (\mathbf{x}_i - \mathbf{x}_0) = (x_i - x_0)^2 + (y_i - y_0)^2.$$

The i th row Jacobian matrix J of partial derivatives of $d(\mathbf{x}_i, \mathbf{a})$ with respect to \mathbf{a}^\top is given by

$$J(i, :) = -\frac{1}{r_i} [x_i - x_0, y_i - y_0, r_i] = -[\mathbf{n}_i^\top, 1], \quad \mathbf{n}_i = (\mathbf{x}_i - \mathbf{x}_0)/r_i$$

The optimality conditions $J^\top \mathbf{d} = \mathbf{0}$ can be written as

$$\sum_{i=1}^m (r_i - r_0) \mathbf{n}_i = \mathbf{0}, \quad r_0 = \frac{1}{m} r_i,$$

showing that at the solution, the radius of the best fit circle is the average of all the distances of the points to the centre. The 3×3 matrix $H = J^\top J$ is given by

$$H = \begin{bmatrix} \sum_i \mathbf{n}_i \mathbf{n}_i^\top & \sum_i \mathbf{n}_i \\ \sum_i \mathbf{n}_i^\top & m \end{bmatrix}.$$

The sensitivity matrix $G_{A|X} = H^{-1} J^\top N^\top$ and

$$J^\top N^\top = - \begin{bmatrix} \mathbf{n}_1 \mathbf{n}_1^\top & \mathbf{n}_2 \mathbf{n}_2^\top & \cdots & \mathbf{n}_m \mathbf{n}_m^\top \\ \mathbf{n}_1^\top & \mathbf{n}_2^\top & \cdots & \mathbf{n}_m^\top \end{bmatrix}. \quad (\text{I.53})$$

showing that perturbing \mathbf{x}_i by $\Delta \mathbf{x}_i$ causes \mathbf{x}_0 to be perturbed by an amount that depends on extend to which $\Delta \mathbf{x}_i$ is aligned with the normal \mathbf{n}_i .

For points \mathbf{x}_i approximately uniformly distributed around the circle, H is approximately diagonal with

$$H \approx m \begin{bmatrix} 1/2 & 0 & 0 \\ 0 & 1/2 & 0 \\ 0 & 0 & 1 \end{bmatrix}, \quad H^{-1} \approx \frac{1}{m} \begin{bmatrix} 2 & 0 & 0 \\ 0 & 2 & 0 \\ 0 & 0 & 1 \end{bmatrix}. \quad (\text{I.54})$$

Thus if $V_X = \sigma_R^2 I$ then, from (I.45), $V_A = \sigma_R^2 H^{-1}$, showing that the variances associated with \mathbf{a} vary with $1/m$ and that the variance associated with \mathbf{x}_0 is twice that associated with r_0 , for a uniform distribution of points. We can argue that every data point contributes to estimating the radius but on average only half of the data points contribute to estimating each coordinate of the circle centre. This behaviour is made clear by looking at the sensitivity matrix $G_{A|X}$.

Analytical approximations for (an arc of) a circle

The calculation of H in (I.54) is for the case of points uniformly distributed around a complete circle. Similar but more complicated calculations can be made for a partial circle and the common and often problematic case of a small arc of a circle.

For points $(x_i, y_i)^\top = r_0(\cos \theta_i, \sin \theta_i)^\top$ on a circle, the corresponding contribution to the Jacobian matrix is the row $(-\cos \theta_i, -\sin \theta_i, -1)$ and the matrix $H = J^\top J$ is given by

$$H = \begin{bmatrix} \sum_i \cos^2 \theta_i & \sum_i \cos \theta_i \sin \theta_i & \sum_i \cos \theta_i \\ \sum_i \cos \theta_i \sin \theta_i & \sum_i \sin^2 \theta_i & \sum_i \sin \theta_i \\ \sum_i \cos \theta_i & \sum_i \sin \theta_i & m \end{bmatrix}.$$

The principle of Monte Carlo integration states that for a function $f(\theta)$ defined over a region A the integral of the function over the region can be approximated according to

$$\frac{1}{|A|} \int_A f(\theta) d\theta \approx \frac{1}{m} \sum_{i=1}^m f(\theta_i), \quad (\text{I.55})$$

where $\theta_{1:m}$ is a sample of points uniformly distributed over the region A and $|A|$ is the area/volume of the region. We can use this approximation in the other direction to approximate H derived from a discrete set of points from analytically derived integrals. For example, suppose points $\mathbf{x}_{1:m}$ are approximately uniformly distributed of the arc of the circle defined by $-\alpha \leq \theta_i \leq \alpha$. Then

$$\sum_{i=1}^m \cos^2 \theta_i \approx \frac{m}{2\alpha} \int_{-\alpha}^{\alpha} \cos^2 \theta d\theta = m \left(\frac{1}{2} + \frac{\sin 2\alpha}{4\alpha} \right);$$

see Appendix .3. Continuing in this way, let

$$H_\alpha = \begin{bmatrix} 1/2 + (\sin 2\alpha)/4\alpha & 0 & (\sin \alpha)/\alpha \\ 0 & 1/2 - (\sin 2\alpha)/4\alpha & 0 \\ (\sin \alpha)/\alpha & 0 & 1 \end{bmatrix}, \quad (\text{I.56})$$

and $V_\alpha = H_\alpha^{-1}$ given by

$$V_\alpha = \frac{1}{D_{13}} \begin{bmatrix} 1 & 0 & -(\sin \alpha)/\alpha \\ 0 & D_{13}/(1/2 - (\sin 2\alpha)/4\alpha) & 0 \\ -(\sin \alpha)/\alpha & 0 & (1/2 + (\sin 2\alpha)/4\alpha) \end{bmatrix},$$

where

$$D_{13} = 1/2 + (\sin 2\alpha)/4\alpha - ((\sin \alpha)/\alpha)^2,$$

the determinant of the 2×2 submatrix of H_α constructed from its first and third rows and columns. Then

$$(J^\top J)^{-1} \approx \frac{1}{m} V_\alpha.$$

If the variance matrix associated \mathbf{x}_{1_m} can be approximated by $\sigma_R^2 I$, then the variance matrix V_A associated with the fitted circle parameters is approximated by

$$V_A \approx \frac{\sigma_R^2}{m} V_\alpha,$$

and the standard uncertainties associated with \mathbf{a} are given by $\sigma_R \sqrt{v_{jj}/m}$, where v_{jj} is the j th diagonal element of V_α . The quantities $s(a_j) = \sqrt{v_{jj}}$ for selected values of α are given in table I.4. For α less than $10\pi/180$, i.e., less than 10 degrees, then D_{13} is approximated by $\alpha^4/45$ and the diagonal elements of V_α are approximated by $45/\alpha^4$, $3/\alpha^2$ and $45(1 - \alpha^2/3)/\alpha^4$; see also table I.4. The uncertainty associated with the y -coordinate of the circle centre scales with $1/\alpha$ while the uncertainties associated with the x -coordinate and radius scale with $1/\alpha^2$, for small α . The estimate of the x -coordinate of circle centre is almost perfectly negatively correlated with the estimate of the radius.

Table I.4: Square roots $s(\mathbf{a})$ of the diagonal elements of V_α . For points $\mathbf{x}_{1:m}$ approximately uniformly distributed on the arc of the circle defined by $-\alpha \leq \theta_i \leq \alpha$ and for point cloud variance matrix $\sigma_R^2 I$, the uncertainties $u(\mathbf{a}) = \sigma_R s(\mathbf{a}) / \sqrt{m}$.

$2\alpha/\text{deg}$	$s(x_0)$	$s(y_0)$	$s(r_0)$
360	1.41	1.41	1.00
270	1.81	1.28	1.14
180	3.25	1.41	2.30
160	3.96	1.51	2.97
140	5.00	1.65	3.98
120	6.62	1.85	5.56
100	9.30	2.14	8.23
80	14.25	2.61	13.16
60	24.95	3.40	23.85
40	55.54	5.02	54.42
20	220.70	9.95	219.58
$\alpha \leq 5 \text{ deg}$			
α/rad	$\approx \sqrt{45}/\alpha^2$	$\approx \sqrt{3}/\alpha$	$\approx \sqrt{45}/\alpha^2$

I.5.4 Sensitivity matrix associated with a least-squares sphere fit to data

If a sphere is parametrized by $\mathbf{a} = (x_0, y_0, z_0, r_0)^\top$ specifying its centre \mathbf{x}_0 and radius r_0 , the signed distance $d(\mathbf{x}_i, \mathbf{a})$ from a data point \mathbf{x}_i to the sphere given by \mathbf{a} is

$$d(\mathbf{x}_i, \mathbf{a}) = r_i - r_0,$$

where

$$r_i^2 = (\mathbf{x}_i - \mathbf{x}_0)^\top (\mathbf{x}_i - \mathbf{x}_0) = (x_i - x_0)^2 + (y_i - y_0)^2 + (z_i - z_0)^2.$$

The i th row Jacobian matrix J of partial derivatives of $d(\mathbf{x}_i, \mathbf{a})$ with respect to \mathbf{a}^\top is given by

$$J(i, :) = -\frac{1}{r_i} [x_i - x_0, y_i - y_0, z_i - z_0, r_i] = -[\mathbf{n}_i^\top, 1], \quad \mathbf{n}_i = (\mathbf{x}_i - \mathbf{x}_0)/r_i$$

The optimality conditions $J^\top \mathbf{d} = \mathbf{0}$ can be written as

$$\sum_{i=1}^m (r_i - r_0) \mathbf{n}_i = \mathbf{0}, \quad r_0 = \frac{1}{m} r_i,$$

showing that at the solution, the radius of the best fit sphere is the average of all the distances of the points to the centre. The 4×4 matrix $H = J^\top J$ is given by

$$H = \begin{bmatrix} \sum_i \mathbf{n}_i \mathbf{n}_i^\top & \sum_i \mathbf{n}_i \\ \sum_i \mathbf{n}_i^\top & m \end{bmatrix}.$$

For points \mathbf{x}_i approximately uniformly distributed around the sphere, H is approximately diagonal with

$$H \approx m \begin{bmatrix} 1/3 & 0 & 0 & 0 \\ 0 & 1/3 & 0 & 0 \\ 0 & 0 & 1/3 & 0 \\ 0 & 0 & 0 & 1 \end{bmatrix}, \quad H^{-1} \approx \frac{1}{m} \begin{bmatrix} 3 & 0 & 0 & 0 \\ 0 & 3 & 0 & 0 \\ 0 & 0 & 3 & 0 \\ 0 & 0 & 0 & 1 \end{bmatrix}.$$

Thus if $V_X = \sigma_R^2 I$ then, from (I.45), $V_A = \sigma_R^2 H^{-1}$, showing that the variances associated with \mathbf{a} vary with $1/m$ and that the variance associated with \mathbf{x}_0 three times that associated with r_0 , for a uniform distribution of points around the complete sphere.

The sensitivity matrix $G_{A|X} = H^{-1}J^T N^T$ and

$$J^T N^T = - \begin{bmatrix} \mathbf{n}_1 \mathbf{n}_1^T & \mathbf{n}_2 \mathbf{n}_2^T & \cdots & \mathbf{n}_m \mathbf{n}_m^T \\ \mathbf{n}_1^T & \mathbf{n}_2^T & \cdots & \mathbf{n}_m^T \end{bmatrix}. \quad (\text{I.57})$$

showing that perturbing \mathbf{x}_i by $\Delta \mathbf{x}_i$ causes \mathbf{x}_0 to be perturbed by an amount that depends on extend to which $\Delta \mathbf{x}_i$ is aligned with the normal \mathbf{n}_i .

Analytical approximations for a patch of a sphere

We can use the principle of Monte Carlo integration (I.55) to determine analytical approximations for matrices used to construct the sensitivity matrices. In polar coordinates with $(x, y, z) = (\cos \theta \cos \phi, \sin \theta \cos \phi, \sin \phi)$, for points approximately uniformly distributed on the sphere on the patch determined by $\pi \leq \alpha_1 \leq \theta \leq \alpha_2 \leq \pi$ and $-\pi/2 \leq \beta_1 \leq \phi \leq \beta_2 \leq \pi/2$ we have

$$\frac{1}{m} J^T J \approx \frac{1}{A} H_A,$$

where H_A is the symmetric matrix with

$$\begin{aligned}
 H_A(1,1) &= \int_{\alpha_1}^{\alpha_2} \cos^2 \theta d\theta \int_{\beta_1}^{\beta_2} \cos^3 \phi d\phi, \\
 H_A(1,2) &= \int_{\alpha_1}^{\alpha_2} \sin \theta \cos \theta d\theta \int_{\beta_1}^{\beta_2} \cos^3 \phi d\phi \\
 H_A(1,3) &= \int_{\alpha_1}^{\alpha_2} \cos \theta d\theta \int_{\beta_1}^{\beta_2} \sin \phi \cos^2 \phi d\phi, \\
 H_A(1,4) &= \int_{\alpha_1}^{\alpha_2} \cos \theta d\theta \int_{\beta_1}^{\beta_2} \cos^2 \phi d\phi, \\
 H_A(2,2) &= \int_{\alpha_1}^{\alpha_2} \sin^2 \theta d\theta \int_{\beta_1}^{\beta_2} \cos^3 \phi d\phi, \\
 H_A(2,3) &= \int_{\alpha_1}^{\alpha_2} \sin \theta d\theta \int_{\beta_1}^{\beta_2} \sin \phi \cos^2 \phi d\phi, \\
 H_A(2,4) &= \int_{\alpha_1}^{\alpha_2} \sin \theta d\theta \int_{\beta_1}^{\beta_2} \cos^2 \phi d\phi, \\
 H_A(3,3) &= (\alpha_2 - \alpha_1) \int_{\beta_1}^{\beta_2} \sin^2 \phi \cos \phi d\phi, \\
 H_A(3,4) &= (\alpha_2 - \alpha_1) \int_{\beta_1}^{\beta_2} \sin \phi \cos \phi d\phi, \\
 H_A(4,4) &= (\alpha_2 - \alpha_1) \int_{\beta_1}^{\beta_2} \cos \phi d\phi.
 \end{aligned}$$

These integrals can be evaluated according to the formulæ in Appendix .3. The elements of H_A take into account the change of variables from Cartesian to spherical coordinates and involve an additional $\cos \phi$ term.

Cap of a sphere

We consider here the case $-\pi \leq \theta \leq \pi$ and $-\pi/2 \leq \beta_1 \leq \phi \leq \pi/2$. For this case, the nonzero elements of $H_\gamma = \frac{1}{|A|}H_A$ are determined by

$$\begin{aligned} H_\gamma(1, 1) &= \frac{1}{2(1 - \cos \gamma)}(2/3 - \cos \gamma - \cos^3 \gamma/3), \\ H_\gamma(2, 2) &= \frac{1}{2(1 - \cos \gamma)}(2/3 - \cos \gamma - \cos^3 \gamma/3), \\ H_\gamma(3, 3) &= \frac{1}{1 - \cos \gamma}(1 - \cos^3 \gamma)/3, \\ H_\gamma(3, 4) &= \frac{1}{1 - \cos \gamma}(1 - \cos 2\gamma)/4, \\ H_\gamma(4, 4) &= 1, \end{aligned}$$

where $\gamma = \pi/2 - \beta_1$. The nonzero elements of $V_\gamma = H_\gamma^{-1}$ are determined by

$$\begin{aligned} V_\gamma(1, 1) &= 1/H_\gamma(1, 1), \\ V_\gamma(2, 2) &= 1/H_\gamma(2, 2), \\ V_\gamma(3, 3) &= \frac{1}{D_{34}}, \\ V_\gamma(3, 4) &= -\frac{1}{D_{34}}H_\gamma(3, 4), \\ V_\gamma(4, 4) &= \frac{1}{D_{34}}H_\gamma(3, 3), \end{aligned}$$

where

$$D_{34} = H_\gamma(3, 3) - H_\gamma^2(3, 4),$$

the determinant of the bottom right 2×2 submatrix of H_γ . If the point cloud data is associated with variance matrix $\sigma_R^2 I$, then the variance matrix V_A associated with the fitted sphere parameters \mathbf{a} is approximated by

$$V_A \approx \frac{\sigma_R^2}{m} V_\gamma.$$

For γ approaching zero, corresponding to measurements on a cap of a sphere, $D_{34} \approx \gamma^4/48$, and

$$V_\gamma \approx \begin{bmatrix} 4/\gamma^2 & 0 & 0 & 0 \\ 0 & 4/\gamma^2 & 0 & 0 \\ 0 & 0 & 48/\gamma^4 & -48(1 - \gamma^2/4)/\gamma^4 \\ 0 & 0 & -48(1 - \gamma^2/4)/\gamma^4 & 48(1 - \gamma^2/2)/\gamma^4 \end{bmatrix}. \quad (\text{I.58})$$

Table I.5: Square roots $s(\mathbf{a})$ of the diagonal elements of V_γ in (I.58). For points $\mathbf{x}_{1:m}$ approximately uniformly distributed on the sphere with elevation angle satisfying $\pi/2 - \gamma \leq \phi_i \leq \pi/2$ and for point cloud variance matrix $\sigma_R^2 I$, the uncertainties $u(\mathbf{a}) = \sigma_R s(\mathbf{a}) / \sqrt{m}$.

γ/deg	$s(x_0)$	$s(y_0)$	$s(z_0)$	$s(r_0)$
180	1.73	1.73	1.73	1.00
135	1.65	1.65	2.03	1.04
90	1.73	1.73	3.46	2.00
80	1.83	1.83	4.19	2.66
70	1.97	1.97	5.26	3.67
60	2.19	2.19	6.93	5.29
50	2.52	2.52	9.70	8.03
40	3.04	3.04	14.81	13.11
30	3.95	3.95	25.86	24.15
20	5.82	5.82	57.44	55.72
10	11.50	11.50	228.02	226.29
$\gamma \leq 5 \text{ deg}$				
γ/rad	$\approx 2/\gamma$	$\approx 2/\gamma$	$\approx \sqrt{48}/\gamma^2$	$\approx \sqrt{48}/\gamma^2$

The quantities $s(a_j) = \sqrt{V_\gamma(j, j)}$ for selected values of γ are given in table I.5. The uncertainty associated with the x and y -coordinates of the sphere centre scale with $1/\gamma$ while the uncertainties associated with the z -coordinate and radius scale with $1/\gamma^2$, for small γ . The estimate of the z -coordinate of sphere centre is almost perfectly negatively correlated with the estimate of the radius. These results are in line with results associated with an arc of a circle discussed in section I.5.3.

These calculations are also relevant to determining the radius of curvature for other surfaces such as paraboloids and aspherics that have low curvature.

Equatorial band of a sphere

The calculations in section I.5.4 can be used to estimate sensitivities associated with measurements distributed along an equatorial band of a sphere defined by $-\pi \leq \theta \leq \pi$ and $-\beta \leq \phi \leq \beta \leq \pi/2$. These calculations are also relevant to measurements using ball bar or machine checking gauge that

Table I.6: Square roots $s(\mathbf{a})$ of the diagonal elements of V_β in (I.59). For points $\mathbf{x}_{1:m}$ approximately uniformly distributed on a equatorial band of the sphere with elevation angle satisfying $-\beta \leq \phi_i \leq \beta \leq \pi/2$ and for point cloud variance matrix $\sigma_R^2 I$, the uncertainties $u(\mathbf{a}) = \sigma_R s(\mathbf{a}) / \sqrt{m}$.

β/deg	$s(x_0)$	$s(y_0)$	$s(z_0)$	$s(r_0)$
90	1.73	1.73	1.73	1.00
80	1.72	1.72	1.76	1.00
70	1.68	1.68	1.84	1.00
60	1.63	1.63	2.00	1.00
50	1.58	1.58	2.26	1.00
40	1.52	1.52	2.69	1.00
30	1.48	1.48	3.46	1.00
20	1.44	1.44	5.06	1.00
10	1.42	1.42	9.97	1.00
$\beta \leq 5 \text{ deg}$				
β/rad	$\approx \sqrt{2}$	$\approx \sqrt{2}$	$\approx \sqrt{3}/\beta$	1

rotates about a fixed point and defines points on a virtual sphere. The area over which the integration is performed is $|A| = 4\pi \sin \beta$. For points approximately uniformly distributed in an equatorial band, if the point cloud data is associated with variance matrix $\sigma_R^2 I$, then the variance matrix V_A associated with the fitted sphere parameters \mathbf{a} is approximated by

$$V_A \approx \frac{\sigma_R^2}{m} V_\beta$$

where

$$V_\beta = \begin{bmatrix} 2/(1 - \sin^2 \beta/3) & 0 & 0 & 0 \\ 0 & 2/(1 - \sin^2 \beta/3) & 0 & 0 \\ 0 & 0 & 3/\sin^2 \beta & 0 \\ 0 & 0 & 0 & 1 \end{bmatrix}. \quad (\text{I.59})$$

Points on a longitudinal segment of a sphere

The calculations in section I.5.4 can be used to estimate sensitivities associated with measurements distributed in a longitudinal segment of a sphere

defined by $-\pi \leq -\alpha \leq \theta \leq \alpha \leq \pi$ and $-\pi/2 \leq \phi \leq \pi/2$ (the curved surface of a segment of an orange). These calculations are also relevant to measurements using ball bar or machine checking gauge that rotates about a fixed point and defines points on a virtual sphere. The area over which the integration is performed is $|A| = 4\alpha$. For points approximately uniformly distributed over the segment, if the point cloud data is associated with variance matrix $\sigma_R^2 I$, then the variance matrix V_A associated with the fitted sphere parameters \mathbf{a} is approximated by

$$V_A \approx \frac{\sigma_R^2}{m} V_\alpha \quad (\text{I.60})$$

where the nonzero elements of V_α are specified by

$$\begin{aligned} V_\alpha(1,1) &= 1/D_{14}, \\ V_\alpha(1,4) &= -\pi \sin \alpha / (4\alpha D_{14}), \\ V_\alpha(2,2) &= 3\alpha / (\alpha - (\sin 2\alpha)/2), \\ V_\alpha(3,3) &= 3, \\ V_\alpha(4,4) &= 3\alpha / (D_{14}(\alpha + (\sin 2\alpha)/2)), \end{aligned}$$

with

$$D_{14} = \frac{\alpha + (\sin 2\alpha)/2}{3\alpha} - \left(\frac{\pi \sin \alpha}{4\alpha} \right)^2.$$

the determinant of the 2×2 submatrix of $H_\alpha = V_\alpha^{-1}$ comprising of rows and columns 1 and 4. For α near zero, $D_{14} \approx 2/3 - (\pi/4)^2 \approx 0.05$,

$$V_\alpha \approx \begin{bmatrix} 20 & 0 & 0 & -5\pi \\ 0 & 9/(2\alpha^2) & 0 & 0 \\ 0 & 0 & 3 & 0 \\ -5\pi & 0 & 0 & 40/3 \end{bmatrix}. \quad (\text{I.61})$$

The quantities $s(a_j) = \sqrt{V_\alpha(j,j)}$ for selected values of α are given in table I.5.4. The uncertainty associated with the y -coordinate of the sphere centre scales with $1/\alpha$, while all other parameters remain well defined. These calculations depend on measuring over the complete segment, including the two poles. Corresponding calculations for measurements reduced to an equatorial band of the segment can be made using the results in section I.5.4.

Table I.7: Square roots $s(\mathbf{a})$ of the diagonal elements of V_α in (I.60). For points $\mathbf{x}_{1:m}$ approximately uniformly distributed on a segment of the sphere with $-\alpha \leq \theta_i \leq \alpha \leq \pi$ and for point cloud variance matrix $\sigma_R^2 I$, the uncertainties $u(\mathbf{a}) = \sigma_R s(\mathbf{a}) / \sqrt{m}$.

$2\alpha/\text{deg}$	$s(x_0)$	$s(y_0)$	$s(z_0)$	$s(r_0)$
360	1.73	1.73	1.73	1.00
270	2.20	1.57	1.73	1.13
180	3.46	1.73	1.73	2.00
160	3.85	1.85	1.73	2.36
140	4.22	2.02	1.73	2.74
120	4.50	2.26	1.73	3.09
100	4.66	2.62	1.73	3.36
80	4.69	3.19	1.73	3.53
60	4.64	4.16	1.73	3.62
40	4.56	6.15	1.73	3.65
20	4.50	12.19	1.73	3.66
$\alpha \leq 5 \text{ deg}$				
α/rad	$\approx \sqrt{20}$	$\approx \sqrt{4.5}/\alpha$	$\approx \sqrt{3}$	$\approx \sqrt{40/3}$

Procedure for evaluating a sphere feature sensitivity matrix

The approach described in section I.5.2 allow us to evaluate the sensitivity matrix associated with a weighted least-squares sphere fit to data.

Inputs

1. Sphere centre \mathbf{x}_0 and radius r_0 .
2. Point coordinates $\mathbf{x}_{1:m}$ for points lying on or close to the sphere surface specified by $\mathbf{a}^\top = (\mathbf{x}_0^\top, r_0)$.
3. Weights $w_{1:m}$, $w_i \geq 0$.

Outputs

1. $4 \times m$ sensitivity matrix $G_{A|D}$ of \mathbf{a} with respect to changes in $\mathbf{x}_{1:m}$ normal to the sphere surface where \mathbf{a} is determined from a *weighted* least-squares fit to the data.
2. Point coordinates $\mathbf{x}_{1:m}^*$ of footpoints, i.e., \mathbf{x}_i^* is the point on the sphere surface specified by \mathbf{a} closest to \mathbf{x}_i .
3. Outward pointing unit normal vectors $\mathbf{n}_{1:m}$ corresponding to $\mathbf{x}_{1:m}^*$.
4. $m \times 4$ Jacobian matrix associated with an *unweighted* least-squares fit and parameters \mathbf{a} .

Procedure

1. For each $i = 1, \dots, m$, set $r_i = \|\mathbf{x}_i - \mathbf{x}_0\|$, $\mathbf{n}_i = (\mathbf{x}_i - \mathbf{x}_0)/r_i$ and $\mathbf{x}_i^* = r_0 \mathbf{n}_i$.
2. Assign the $m \times 4$ Jacobian matrix J : for each $i = 1, \dots, m$, set $J(i, 1 : 4) = [-\mathbf{n}_i^\top, -1]$ to
3. Form weighted Jacobian matrix J_W : for each $i = 1, \dots, m$, set $J_W(i, 1 : 4) = w_i^2 J(i, 1 : 4)$.
4. Form sensitivity matrix $G_{A|D} = -(J^\top J_W)^{-1} J_W^\top$.

I.5.5 Sensitivity matrix associated with a least-squares plane fit to data

The calculations associated with an axis give above in section I.5.1 allow us to evaluate the sensitivity matrix associated with a least-squares plane fit to data. Given a location point \mathbf{x}_A and unit direction vector \mathbf{v}_A , the equation of the associated plane can be written as

$$(\mathbf{x} - \mathbf{x}_A)^\top \mathbf{v}_A = 0.$$

The calculations involve a parametrization of the plane in terms of three parameters \mathbf{a} in which the k th coordinate of \mathbf{v}_A is held fixed and only the k th coordinate of \mathbf{x}_A is free.

Procedure for evaluating the plane feature sensitivity matrix

Inputs

1. Plane locating point \mathbf{x}_A and unit axis direction vector \mathbf{v}_A , $\|\mathbf{v}_A\| = 1$.
2. Point coordinates $\mathbf{x}_{1:m}$ for points lying on or close to the plane specified by \mathbf{b} where $\mathbf{b}^\top = (\mathbf{x}_A^\top, \mathbf{v}_A^\top)$.
3. Weights $w_{1:m}$, $w_i \geq 0$.
4. Coordinate index k specifying the parametrization of the plane to be used.

Outputs

1. $6 \times m$ sensitivity matrix $G_{B|D}$ of \mathbf{b} with respect to changes in $\mathbf{x}_{1:m}$ normal to the plane surface, where \mathbf{b} is determined from a *weighted* least squares fit to the data.
2. $3 \times m$ sensitivity matrix $G_{A|D}$ of \mathbf{a} with respect to changes in $\mathbf{x}_{1:m}$ normal to the plane surface, where \mathbf{a} are associated with the parametrization specified by k and is determined from a *weighted* least squares fit to the data.

3. Point coordinates $\mathbf{x}_{1:m}^*$ of footpoints, i.e., \mathbf{x}_i^* is the point on the plane surface specified by \mathbf{b} closest to \mathbf{x}_i .
4. Outward pointing unit normal vectors $\mathbf{n}_{1:m}$ corresponding to $\mathbf{x}_{1:m}^*$.
5. $m \times 3$ Jacobian matrix associated with an *unweighted* least-squares fit and parameters \mathbf{a} .

Procedure

1. For each $i = 1, \dots, m$, set $d_i = (\mathbf{x}_i - \mathbf{x}_A)^\top \mathbf{v}_A$, $\mathbf{n}_i = \mathbf{v}_A$, and $\mathbf{x}_i^* = \mathbf{x}_i - d_i \mathbf{n}_i$.
2. Assign the $m \times 6$ Jacobian matrix J_B : for each $i = 1, \dots, m$, set $J_B(i, 1 : 6) = [-\mathbf{n}_i^\top, (\mathbf{x}_i - \mathbf{x}_A)^\top]$.
3. Assign sensitivity matrix $G_{B|A}$ depending on k :

- (a) if $k = 1$, set

$$G_{B|A} = \begin{bmatrix} 1 & 0 & 0 \\ 0 & 0 & 0 \\ 0 & 0 & 0 \\ 0 & w_A & -v_A \\ 0 & 0 & u_A \\ 0 & -u_A & 0 \end{bmatrix}.$$

- (b) if $k = 2$, set

$$G_{B|A} = \begin{bmatrix} 0 & 0 & 0 \\ 1 & 0 & 0 \\ 0 & 0 & 0 \\ 0 & 0 & -v_A \\ 0 & -w_A & u_A \\ 0 & v_A & 0 \end{bmatrix}.$$

- (c) if $k = 3$, set

$$G_{B|A} = \begin{bmatrix} 0 & 0 & 0 \\ 0 & 0 & 0 \\ 1 & 0 & 0 \\ 0 & 0 & w_A \\ 0 & -w_A & 0 \\ 0 & v_A & -u_A \end{bmatrix}.$$

4. Form Jacobian matrix with respect to \mathbf{a} : $J = J_B G_{B|A}$.
5. Form weighted Jacobian matrix J_W : for each $i = 1, \dots, m$, set $J_W(i, 1 : 3) = w_i^2 J(i, 1 : 3)$.
6. Form sensitivity matrix $G_{A|D} = -(J^\top J_W)^{-1} J_W^\top$.
7. Form sensitivity matrix $G_{B|D} = G_{B|A} G_{B|D}$.

We note that the unit normals associated with $\mathbf{x}_{1:m}^*$ are given by $\mathbf{n}_i = \mathbf{v}_A$.

Analytical approximation for measuring a rectangular area

Suppose data points $\mathbf{x}_{1:m}$ are distributed approximately on the plane $z = 0$ with $-a \leq x_i \leq a$ and $-b \leq y_i \leq b$ and J is the $m \times 3$ Jacobian matrix associated with fitting a plane to the data with $J(i, 1 : 3) = (-1, x_i, y_i)$. This Jacobian matrix corresponds to parametrization in terms of the z -coordinate of \mathbf{x}_A and the x - and y -coordinates of \mathbf{v}_A , $\mathbf{a} = (z_A, u_A, v_A)^\top$. Then, using the principle of Monte Carlo integration (I.55),

$$\frac{1}{m} J^\top J \approx H_{ab},$$

where

$$H_{ab} = \begin{bmatrix} 1 & 0 & 0 \\ 0 & a^2/3 & 0 \\ 0 & 0 & b^2/3 \end{bmatrix}. \quad (\text{I.62})$$

Set

$$V_{ab} = H_{ab}^{-1} = \begin{bmatrix} 1 & 0 & 0 \\ 0 & 3/a^2 & 0 \\ 0 & 0 & 3/b^2 \end{bmatrix}. \quad (\text{I.63})$$

If the variance matrix associated with $\mathbf{x}_{1:m}$ is approximated by $\sigma_R^2 I$, then the standard uncertainties $u(\mathbf{a})$ associated with the parameters is given by

$$u(\mathbf{a}) = \frac{\sigma_R}{\sqrt{m}} (1, \sqrt{3}/a, \sqrt{3}/a)^\top. \quad (\text{I.64})$$

Thus, the uncertainty in the angle of rotation about the x -axis scales with $1/b$ by that associated with rotation about the y -axis scales with $1/a$.

I.5.6 Sensitivity matrix associated with a least-squares cylinder fit to data

The calculations associated with an axis give above in section I.5.1 allow us to evaluate the sensitivity matrix associated with a least-squares cylinder fit to data.

Procedure for evaluating the cylinder feature sensitivity matrix

Inputs

1. Cylinder axis locating point \mathbf{x}_A , unit axis direction vector \mathbf{v}_A , $\|\mathbf{v}_A\| = 1$, and cylinder radius r_0 .
2. Point coordinates $\mathbf{x}_{1:m}$ for points lying on or close to the cylinder surface specified by \mathbf{b} where $\mathbf{b}^\top = (\mathbf{x}_A^\top, \mathbf{v}_A^\top, r_0)$.
3. Weights $w_{1:m}$, $w_i \geq 0$.
4. Coordinate index k specifying the parametrization of the cylinder to be used.

Outputs

1. $7 \times m$ sensitivity matrix $G_{B|D}$ of \mathbf{b} with respect to changes in $\mathbf{x}_{1:m}$ normal to the cylinder surface, where \mathbf{b} is determined from a *weighted* least squares fit to the data.
2. $5 \times m$ sensitivity matrix $G_{A|D}$ of \mathbf{a} with respect to changes in $\mathbf{x}_{1:m}$ normal to the cylinder surface, where \mathbf{a} are associated with the parametrization specified by k and is determined from a *weighted* least-squares fit to the data.
3. Point coordinates $\mathbf{x}_{1:m}^*$ of footpoints, i.e., \mathbf{x}_i^* is the point on the cylinder surface specified by \mathbf{b} closest to \mathbf{x}_i .
4. Outward pointing unit normal vectors $\mathbf{n}_{1:m}$ corresponding to $\mathbf{x}_{1:m}^*$.
5. $m \times 5$ Jacobian matrix associated with an *unweighted* least-squares fit and parameters \mathbf{a} .

Procedure

1. For each $i = 1, \dots, m$, evaluate the vector cross product

$$\boldsymbol{\xi}_i = (\mathbf{x}_i - \mathbf{x}_A) \times \mathbf{v}_A,$$

calculating $\boldsymbol{\xi}_i = (\xi_i, \eta_i, \zeta_i)^\top$, and set $r_i = \|\boldsymbol{\xi}_i\|$ and $d_i = r_i - r_0$.

2. Assign the $m \times 7$ Jacobian matrix J_B : for each $i = 1, \dots, m$, set $J_B(i, 1 : 7)$ to be the vector

$$\frac{\partial d_i}{\partial \mathbf{b}}^\top = \frac{1}{r_i} \begin{bmatrix} \eta_i w_A - \zeta_i v_A \\ \zeta_i u_A - \xi_i w_A \\ \xi_i v_A - \eta_i u_A \\ \eta_i(z_i - z_A) - \zeta_i(y_i - y_A) \\ \zeta_i(x_i - x_A) - \xi_i(z_i - z_A) \\ \xi_i(y_i - y_A) - \eta_i(x_i - x_A) \\ -1 \end{bmatrix}^\top.$$

3. For each $i = 1, \dots, m$, set $\mathbf{n}_i = -J_B(i, 1 : 3)^\top$ and $\mathbf{x}_i^* = \mathbf{x}_i - d_i \mathbf{n}_i$.
4. Assign sensitivity matrix $G_{B|A}$ depending on k :

- (a) if $k = 1$, set

$$G_{B|A} = \begin{bmatrix} 0 & 0 & 0 & 0 & 0 \\ 1 & 0 & 0 & 0 & 0 \\ 0 & 1 & 0 & 0 & 0 \\ 0 & 0 & w_A & -v_A & 0 \\ 0 & 0 & 0 & u_A & 0 \\ 0 & 0 & -u_A & 0 & 0 \\ 0 & 0 & 0 & 0 & 1 \end{bmatrix};$$

- (b) if $k = 2$, set

$$G_{B|A} = \begin{bmatrix} 1 & 0 & 0 & 0 & 0 \\ 0 & 0 & 0 & 0 & 0 \\ 0 & 1 & 0 & 0 & 0 \\ 0 & 0 & 0 & -v_A & 0 \\ 0 & 0 & -w_A & u_A & 0 \\ 0 & 0 & v_A & 0 & 0 \\ 0 & 0 & 0 & 0 & 1 \end{bmatrix};$$

(c) if $k = 3$, set

$$G_{B|A} = \begin{bmatrix} 1 & 0 & 0 & 0 & 0 \\ 0 & 1 & 0 & 0 & 0 \\ 0 & 0 & 0 & 0 & 0 \\ 0 & 0 & 0 & w_A & 0 \\ 0 & 0 & -w_A & 0 & 0 \\ 0 & 0 & v_A & -u_A & 0 \\ 0 & 0 & 0 & 0 & 1 \end{bmatrix}.$$

5. Form Jacobian matrix with respect to \mathbf{a} : $J = J_B G_{B|A}$.
6. Form weighted Jacobian matrix J_W : for each $i = 1, \dots, m$, set $J_W(i, 1 : 5) = w_i^2 J(i, 1 : 5)$.
7. Form sensitivity matrix $G_{A|D} = -(J^\top J_W)^{-1} J_W^\top$.
8. Form sensitivity matrix $G_{B|D} = G_{B|A} G_{A|D}$.

Analytical approximation for measuring a cylindrical patch

Suppose data points $\mathbf{x}_{1:m} = (r_0 \cos \theta_i, r_0 \sin \theta_i, z_i)^\top$ are distributed approximately on a cylinder $x^2 + y^2 = r_0^2$ with $-\alpha \leq \theta_i \leq \alpha \leq \pi$ and $-a \leq z_i \leq a$. Let $\mathbf{x}_A = (x_A, y_A, z_A)^\top$ and $\mathbf{v}_A = (u_A, v_A, w_A)^\top$ specify the locating point and direction vector of the cylinder axis. Parametrizing the cylinder in terms of $\mathbf{a} = (x_A, y_A, u_A, v_A, r_0)^\top$, the associated $m \times 5$ Jacobian matrix has i th row given by

$$J(i, 1 : 5) = -[\cos \theta_i \quad \sin \theta_i \quad -z_i \sin \theta_i \quad z_i \cos \theta_i \quad 1].$$

Then, using the principle of Monte Carlo integration (I.55),

$$\frac{1}{m} J^\top J \approx H_{aa},$$

where the nonzero elements of $H_{a\alpha}$ are specified by

$$\begin{aligned} H_{a\alpha}(1,1) &= \frac{1}{2\alpha} (\alpha + (\sin 2\alpha)/2), \\ H_{a\alpha}(1,5) &= (\sin \alpha)/\alpha \\ H_{a\alpha}(2,2) &= \frac{1}{2\alpha} (\alpha - (\sin 2\alpha)/2), \\ H_{a\alpha}(3,3) &= \frac{a^2}{6\alpha} (\alpha - (\sin 2\alpha)/2), \\ H_{a\alpha}(4,4) &= \frac{a^2}{6\alpha} (\alpha + (\sin 2\alpha)/2), \\ H_{a\alpha}(5,5) &= 1. \end{aligned}$$

For $\alpha = \pi$, corresponding to data approximately uniformly space on the cylindrical surface then

$$H_{a\pi} = \begin{bmatrix} 1/2 & 0 & 0 & 0 & 0 \\ 0 & 1/2 & 0 & 0 & 0 \\ 0 & 0 & a^2/6 & 0 & 0 \\ 0 & 0 & 0 & a^2/6 & 0 \\ 0 & 0 & 0 & 0 & 1 \end{bmatrix},$$

and

$$V_{a\pi} = H_{a\pi}^{-1} = \begin{bmatrix} 2 & 0 & 0 & 0 & 0 \\ 0 & 2 & 0 & 0 & 0 \\ 0 & 0 & 6/a^2 & 0 & 0 \\ 0 & 0 & 0 & 6/a^2 & 0 \\ 0 & 0 & 0 & 0 & 1 \end{bmatrix},$$

showing that the uncertainties associated with the direction vector \mathbf{v}_A scale with $1/a$ (but are independent of the radius r_0). For general α , the elements in the first, second and fifth rows and columns of $H_{a\alpha}$ above are exactly the same as the elements of H_α in (I.56) associated with the analysis of measurements of an arc of a circle. In particular, the behaviour for measurements of a section of a cylinder subtending a small angle can be derived from the analysis on an arc of a circle. Let $V_{a\alpha} = H_{a\alpha}^{-1}$. The matrix V_α given by (I.60) is a submatrix of $V_{a\alpha}$. For points approximately uniformly distributed in $-\alpha \leq \theta_i \leq \alpha \leq \pi$, $-a \leq z_i \leq a$ and if the point cloud data is associated with variance matrix $V_X = \sigma_R^2 I$, then the variance matrix V_A associated with the fitted cylinder parameters \mathbf{a} is approximated by

$$V_A \approx \frac{\sigma_R^2}{m} V_{a\alpha}. \quad (\text{I.65})$$

Table I.8: Square roots $s(\mathbf{a})$ of the diagonal elements of $V_{a\alpha}$ in (I.65). For points $\mathbf{x}_{1:m}$ approximately uniformly distributed over a segment of a cylinder with $-\alpha \leq \theta_i \leq \alpha \leq \pi$ and $-a \leq z_i \leq a$, and point cloud variance matrix $V_X = \sigma_R^2 I$, the uncertainties $u(\mathbf{a}) = \sigma_R s(\mathbf{a}) / \sqrt{m}$.

$2\alpha/\text{deg}$	$s(x_A)$	$s(y_A)$	$as(u_A)$	$as(v_A)$	$s(r_0)$
360	1.41	1.41	2.45	2.45	1.00
270	1.81	1.28	2.22	2.76	1.14
180	3.25	1.41	2.45	2.45	2.30
160	3.96	1.51	2.61	2.31	2.97
140	5.00	1.65	2.85	2.18	3.98
120	6.62	1.85	3.20	2.06	5.56
100	9.30	2.14	3.71	1.96	8.23
80	14.25	2.61	4.51	1.88	13.16
60	24.95	3.40	5.89	1.81	23.85
40	55.54	5.02	8.70	1.77	54.42
20	220.70	9.95	17.24	1.74	219.58
$\alpha \leq 5 \text{ deg}$					
α/rad	$\approx \sqrt{45}/\alpha^2$	$\approx \sqrt{3}/\alpha$	$\approx 3/\alpha$	$\approx \sqrt{3}$	$\approx \sqrt{45}/\alpha^2$

Table I.5.6 shows the square roots $s(\mathbf{a})$ of the diagonal elements of $V_{a\alpha}$ as a function of a (the height of the cylinder is $2a$) and α . For $V_X = \sigma_R^2 I$, $u(\mathbf{a}) = \sigma_R s(\mathbf{a}) / \sqrt{m}$. For a small arc of a cylinder, α near zero, the uncertainties in the x -coordinate of the axis locating point and the radius scale with $1/\alpha^2$, the y -coordinate of the axis locating point and the angle of rotation about the x -axis scale with $1/\alpha$ while the angle of rotation of about the y -axis is well defined. The angles of rotation scale with $1/a$.

I.5.7 Sensitivity matrix associated with a least-squares cone fit to data

The calculations associated with an axis given above in section I.5.1 and a cylinder fit can be extended to evaluate the sensitivity matrix associated with a least-squares cone fit to data. The calculations below are based on specifying the cone in terms of an axes locating point \mathbf{x}_A , an axis unit direction vector \mathbf{v}_A , cone radius r_0 , and cone angle ϕ . The radius parameter is the radius of the circle defined by the intersection of the cone with the plane passing through \mathbf{x}_A and orthogonal to \mathbf{v}_A , i.e., the set of points \mathbf{x} satisfying $(\mathbf{x} - \mathbf{x}_A)^\top \mathbf{v}_A = 0$. The cone angle is the angle the cone generator makes with cone axis, i.e., half the vertex angle, with the convention that if $\phi > 0$, then the vertex of the cone lies at $\mathbf{x}_A + t\mathbf{v}_A$ with $t > 0$. While it may be natural to use the cone vertex as the axis locating point, the parametrization in terms of a radius remains stable for cone angles near zero.

The distance d from a point \mathbf{x} to a cone specified by $\mathbf{b}^\top = (\mathbf{x}_A^\top, \mathbf{v}_A^\top, r_0, \phi)^\top$ is given by

$$d = d(\mathbf{x}, \mathbf{b}) = (\cos \phi)d_C(\mathbf{x}, \mathbf{b}) + (\sin \phi)d_P(\mathbf{x}, \mathbf{a}), \quad (\text{I.66})$$

where $d_C(\mathbf{x}, \mathbf{b})$ is the distance of \mathbf{x} to the cylinder specified by \mathbf{x}_A , \mathbf{v}_A and r_0 and $d_P(\mathbf{x}, \mathbf{b})$ is the distance of \mathbf{x} to the plane specified by \mathbf{x}_A and \mathbf{v}_A .

Procedure for evaluating the cone feature sensitivity matrix

Inputs

1. Cone axis locating point \mathbf{x}_A , unit axis direction vector \mathbf{v}_A , $\|\mathbf{v}_A\| = 1$, and cone radius r_0 at \mathbf{x}_A , and ϕ , the angle the cone generator makes with the cone axes.
2. Point coordinates $\mathbf{x}_{1:m}$ for points lying on or close to the cylinder surface specified by \mathbf{b} where $\mathbf{b}^\top = (\mathbf{x}_A^\top, \mathbf{v}_A^\top, r_0, \phi)$.
3. Weights $w_{1:m}$, $w_i \geq 0$.
4. Coordinate index k specifying the parametrization of the cone to be used.

Outputs

1. $8 \times m$ sensitivity matrix $G_{B|D}$ of \mathbf{b} with respect to changes in $\mathbf{x}_{1:m}$ normal to the cone surface, where \mathbf{b} is determined from a *weighted* least squares fit to the data.
2. $6 \times m$ sensitivity matrix $G_{A|D}$ of \mathbf{a} with respect to changes in $\mathbf{x}_{1:m}$ normal to the cone surface, where \mathbf{a} are associated with the parametrization specified by k and is determined from a *weighted* least-squares fit to the data.
3. Point coordinates $\mathbf{x}_{1:m}^*$ of footpoints, i.e., \mathbf{x}_i^* is the point on the cone surface specified by \mathbf{b} closest to \mathbf{x}_i .
4. Outward pointing unit normal vectors $\mathbf{n}_{1:m}$ corresponding to $\mathbf{x}_{1:m}^*$.
5. $m \times 6$ Jacobian matrix associated with an *unweighted* least-squares fit and parameters \mathbf{a} .

Procedure

1. For each $i = 1, \dots, m$, evaluate the vector cross product

$$\boldsymbol{\xi}_i = (\mathbf{x}_i - \mathbf{x}_A) \times \mathbf{v}_A,$$

calculating $\boldsymbol{\xi}_i = (\xi_i, \eta_i, \zeta_i)^\top$, and set $r_i = \|\boldsymbol{\xi}_i\|$ and $d_{C,i} = r_i - r_0$.

2. Assign the $m \times 7$ Jacobian matrix $J_{C,B}$ associated with a cylinder fit: for each $i = 1, \dots, m$, set $J_{C,B}(i, 1 : 7)$ to be the vector

$$\frac{\partial d_{C,i}}{\partial \mathbf{b}}^\top = \frac{1}{r_i} \begin{bmatrix} \eta_i w_A - \zeta_i v_A \\ \zeta_i u_A - \xi_i w_A \\ \xi_i v_A - \eta_i u_A \\ \eta_i(z_i - z_A) - \zeta_i(y_i - y_A) \\ \zeta_i(x_i - x_A) - \xi_i(z_i - z_A) \\ \xi_i(y_i - y_A) - \eta_i(x_i - x_A) \\ -1 \end{bmatrix}^\top.$$

3. Set $d_{P,i} = (\mathbf{x}_i - \mathbf{x}_A)^\top \mathbf{v}_A$ and assign the $m \times 6$ Jacobian matrix $J_{P,B}$ associated with a plane fit: $J_{P,B}(i, 1 : 6) = [-\mathbf{v}_A^\top, (\mathbf{x} - \mathbf{x}_A)^\top]$.

$$\frac{\partial d_{C,i}}{\partial \mathbf{b}}^\top = \frac{1}{r_i} \begin{bmatrix} \eta_i w_A - \zeta_i v_A \\ \zeta_i u_A - \xi_i w_A \\ \xi_i v_A - \eta_i u_A \\ \eta_i(z_i - z_A) - \zeta_i(y_i - y_A) \\ \zeta_i(x_i - x_A) - \xi_i(z_i - z_A) \\ \xi_i(y_i - y_A) - \eta_i(x_i - x_A) \\ -1 \end{bmatrix}^\top.$$

4. Assign $d_i = (\cos \phi)d_{C,i} + (\sin \phi)d_{P,i}$ and assign the $m \times 8$ Jacobian matrix J_B :

- For $j = 1, \dots, 6$, set

$$J_B(i, j) = (\cos \phi)J_{C,B}(i, j) + (\sin \phi)J_{P,B}(i, j), \quad i = 1, \dots, m.$$

- For $j = 7$, set

$$J_B(i, j) = (\cos \phi)J_{C,B}(i, j), \quad i = 1, \dots, m.$$

- For $j = 8$, set

$$J_B(i, j) = -(\sin \phi)d_{C,i} + (\cos \phi)d_{P,i}, \quad i = 1, \dots, m.$$

5. For each $i = 1, \dots, m$, set $\mathbf{n}_i = -J_B(i, 1 : 3)^\top$ and $\mathbf{x}_i^* = \mathbf{x}_i - d_i \mathbf{n}_i$.

6. Assign 8×6 sensitivity matrix $G_{B|A}$ depending on k . Initialise all elements to zero, set $G_{B|A}(7, 5) = G_{B|A}(8, 6) = 1$ and:

- (a) if $k = 1$, set

$$G_{B|A}(1 : 6, 1 : 4) = \begin{bmatrix} 0 & 0 & 0 & 0 \\ 1 & 0 & 0 & 0 \\ 0 & 1 & 0 & 0 \\ 0 & 0 & w_A & -v_A \\ 0 & 0 & 0 & u_A \\ 0 & 0 & -u_A & 0 \end{bmatrix},$$

(b) if $k = 2$, set

$$G_{B|A}(1:6, 1:4) = \begin{bmatrix} 1 & 0 & 0 & 0 \\ 0 & 0 & 0 & 0 \\ 0 & 1 & 0 & 0 \\ 0 & 0 & 0 & -v_A \\ 0 & 0 & -w_A & u_A \\ 0 & 0 & v_A & 0 \end{bmatrix};$$

(c) if $k = 3$, set

$$G_{B|A}(1:6, 1:4) = \begin{bmatrix} 1 & 0 & 0 & 0 \\ 0 & 1 & 0 & 0 \\ 0 & 0 & 0 & 0 \\ 0 & 0 & 0 & w_A \\ 0 & 0 & -w_A & 0 \\ 0 & 0 & v_A & -u_A \end{bmatrix}.$$

7. Form Jacobian matrix with respect to \mathbf{a} : $J = J_B G_{B|A}$.

8. Form weighted Jacobian matrix J_W : for each $i = 1, \dots, m$, set

$$J_W(i, 1:6) = w_i^2 J(i, 1:6).$$

9. Form sensitivity matrix $G_{A|D} = -(J^\top J_W)^{-1} J_W^\top$.

10. Form sensitivity matrix $G_{B|D} = G_{B|A} G_{A|D}$.

Analytical approximation for measuring a patch of a cone

Suppose data points $\mathbf{x}_{1:m} = (r_i \cos \theta_i, r_i \sin \theta_i, z_i)^\top$, $r_i = r_0 - \tan \phi z_i$, are distributed approximately on a cone with $\mathbf{x}_A = \mathbf{0}$, $\mathbf{v}_A = (0, 0, 1)^\top$, with $-\alpha \leq \theta_i \leq \alpha \leq \pi$ and $-a \leq z_i \leq a$. Parametrizing the cone in terms of $\mathbf{a} = (x_A, y_A, u_A, v_A, r_0, \phi)^\top$, the associated $m \times 6$ Jacobian matrix has i th row given by

$$J(i, 1:6) = \begin{bmatrix} -\cos \phi \cos \theta_i \\ -\cos \phi \sin \theta_i \\ w_i \sin \theta_i \\ -w_i \cos \theta_i \\ -\cos \phi \\ z_i / \cos \phi \end{bmatrix}, \quad w_i = z_i / \cos \phi - r_0 \sin \phi.$$

Table I.9: Square roots $s(\mathbf{a})$ of the diagonal elements of $V_{a\alpha\phi}$ as a function of ϕ . For points $\mathbf{x}_{1:m}$ approximately uniformly distributed over cone with cone angle ϕ , $-\pi \leq \theta_i \leq \pi$ and $-a \leq z_i \leq a$, $a = 100$ and point cloud variance matrix $V_X = \sigma_R^2 I$, the uncertainties $u(\mathbf{a}) = \sigma_R s(\mathbf{a}) / \sqrt{m}$.

ϕ/deg	$s(x_A)$	$s(y_A)$	$s(u_A)$	$s(v_A)$	$s(r_0)$	$s(\phi)$
0	1.41	1.41	0.05	0.05	1.00	0.03
10	1.71	1.71	0.05	0.05	1.02	0.03
20	2.38	2.38	0.05	0.05	1.07	0.03
30	3.21	3.21	0.04	0.04	1.17	0.03
40	4.14	4.14	0.04	0.04	1.35	0.03
50	5.28	5.28	0.03	0.03	1.66	0.02
60	7.12	7.12	0.03	0.03	2.31	0.02
70	13.59	13.59	0.03	0.03	4.80	0.02

Then, using the principle of Monte Carlo integration (I.55),

$$\frac{1}{m} J^\top J \approx H_{a\alpha\phi},$$

where the nonzero elements of $H_{a\alpha\phi}$ are given by the integrals of functions of θ , z and ϕ determined from the form of the Jacobian matrix above. The integrals are somewhat more complicated than the other cases already considered but can be easily evaluated using one dimensional quadrature routines [37]. Here we give some example calculations. Table I.9 shows the square roots $s(\mathbf{a})$ of the diagonal elements of $V_{a\alpha\phi} = H_{a\alpha\phi}$ as a function of ϕ for the case $\alpha = \pi$, $r_0 = 50$ and $a = 100$. For $V_X = \sigma_R^2 I$, $u(\mathbf{a}) = \sigma_R s(\mathbf{a}) / \sqrt{m}$. As ϕ approaches 90 degrees, the uncertainties associated with x_A , y_A and r_0 increase markedly.

Table I.10 shows the square roots $s(\mathbf{a})$ of the diagonal elements of $V_{a\alpha\phi}$ as a function of α . For $V_X = \sigma_R^2 I$, $u(\mathbf{a}) = \sigma_R s(\mathbf{a}) / \sqrt{m}$. For a small arc of a cone, α near zero, the uncertainties associated with x_A , u_A , v_A , r_0 and ϕ scale with $1/\alpha^2$ while those associated with the y_A and u_A scale with $1/\alpha$. No parameter is well defined.

Table I.10: Square roots $s(\mathbf{a})$ of the diagonal elements of $V_{a\alpha\phi}$ as a function of α . For points $\mathbf{x}_{1:m}$ approximately uniformly distributed over a segment of a cone with cone angle $\phi = 45$ degrees, $-\alpha \leq \theta_i \leq \alpha \leq \pi$ and $-a \leq z_i \leq a$, and point cloud variance matrix $V_X = \sigma_R^2 I$, the uncertainties $u(\mathbf{a}) = \sigma_R s(\mathbf{a}) / \sqrt{m}$.

$2\alpha/\text{deg}$	$s(x_A)$	$s(y_A)$	$as(u_A)$	$as(v_A)$	$s(r_0)$	$s(\phi)$
360	4.06	4.06	0.04	0.04	1.73	0.03
270	5.21	3.69	0.04	0.05	1.97	0.03
180	9.33	4.06	0.04	0.10	3.98	0.07
160	11.37	4.34	0.05	0.12	5.14	0.09
140	14.37	4.73	0.05	0.15	6.89	0.12
120	19.01	5.30	0.06	0.20	9.64	0.17
100	26.72	6.15	0.06	0.28	14.25	0.25
80	40.94	7.48	0.08	0.43	22.79	0.39
60	71.67	9.77	0.10	0.75	41.31	0.72
40	159.51	14.43	0.15	1.67	94.27	1.63
20	633.90	28.59	0.30	6.62	380.32	6.59

I.5.8 Sensitivity matrix associated with fitting a point cloud to a CAD model

Suppose that $\mathbf{x}_{1:m}^*$ lie on a design surface \mathcal{S} given parametrically $\mathbf{u} \mapsto \mathbf{s}(\mathbf{u})$ and that the normal vector to the surface \mathcal{S} at \mathbf{x}_i^* is \mathbf{n}_i^* . Suppose $\mathbf{x}_{1:m}$ are measurements of $\mathbf{x}_{1:m}^*$ and that \mathbf{t} solves least squares orthogonal distance regression problem

$$\min_{\mathbf{t}} \sum_{i=1}^m d^2(\hat{\mathbf{x}}_i, \mathcal{S}),$$

where

$$\hat{\mathbf{x}}_i = \frac{1}{1+S} R(\boldsymbol{\alpha})(\mathbf{x}_i - \mathbf{x}_0), \quad \mathbf{t} = \begin{bmatrix} \mathbf{x}_0 \\ \boldsymbol{\alpha} \end{bmatrix}.$$

In these calculations, \mathbf{t} defines a transformation involving translation vector \mathbf{x}_0 , rotation angles $\boldsymbol{\alpha}$ and parameter S setting a global scale adjustment that maps the data $\mathbf{x}_{1:m}$ as close as possible to the design surface \mathcal{S} according to the least-squares criterion. Uncertainties associated with the measured data can be propagated through to the fitted parameters \mathbf{t} using the general scheme for least-squares fitting described in section I.5.2. If the solution \mathbf{t}

is given by $\mathbf{t} = 0$ then the $m \times 7$ Jacobian matrix at the solution is given by

$$J(i, 1 : 7)^\top = \begin{bmatrix} -\mathbf{n}_i^* \\ \mathbf{x}_i^* \times \mathbf{n}_i^* \\ -\mathbf{x}_i^\top \mathbf{n}_i^* \end{bmatrix}.$$

Note that this Jacobian matrix depends on the shape of the surface only through \mathbf{x}_i^* and \mathbf{n}_i^* . Hence, given any freeform surface and a measurement strategy defined by \mathbf{x}_i^* the associated normal vectors \mathbf{n}_i^* can then be calculated allowing J and derived sensitivity matrices to be evaluated.

If the surface \mathcal{S} has symmetries, e.g., with respect to translation along the z -axis or rotation about the z -axis, then the corresponding column of the Jacobian matrix can be removed. Similarly, if no global scale adjustment is desired, the final column of J can be removed.

The scheme above assumes that the solution parameter vector \mathbf{t} is near zero. For the more general case, suppose the solution \mathbf{t}_0 defines the 3×3 rotation matrix R_0 and that the global scale correction parameter is S_0 and that V_X is the $3m \times 3m$ variance matrix associated with the point cloud $\mathbf{x}_{1:m}$. Then the variance matrix $V_{\hat{\mathbf{x}}}$ associated with the transformed data $\hat{\mathbf{x}}_{1:m}$ is given by

$$V_{\hat{\mathbf{x}}} = \frac{1}{(1 + S_0)^2} R V_X R^\top,$$

where R is the $3m \times 3m$ block diagonal matrix with R_0 on the diagonal blocks. The variance matrix $V_{\hat{\mathbf{x}}}$ can then be propagated through to $\mathbf{t} = \mathbf{0}$ using the scheme above, where \mathbf{t} is now regarded as adjusting the fixed \mathbf{t}_0 . If $G_{T|\hat{\mathbf{x}}}$ is the sensitivity of \mathbf{t} with respect to $\hat{\mathbf{x}}_{1:m}$, then the sensitivity of \mathbf{t} with respect to $\mathbf{x}_{1:m}$ is given by

$$G_{T|X} = \frac{1}{(1 + S_0)^2} G_{T|\hat{\mathbf{x}}} R.$$

I.5.9 Uncertainty contribution associated with establishing a datum

See also [22, 18]. Many procedures to establish a datum frame of reference from measured coordinates $\mathbf{x}_{1:m}$ can be written in terms of establishing a rigid body transformation to satisfy six frame of reference constraints. For example, in the calibration of 3 dimensional reference artefacts such as ball-plates, it is usual to specify the frame of reference of the ball centres by having one ball centred at the origin, $\mathbf{x}_1 = \mathbf{0}$, a second centred on the x -axis, $y_2 = z_2 = 0$, and a third positioned in the xy -plane, $z_3 = 0$, six constraints in all. These constraints can usually be written as $C^\top \mathbf{x}_1 : m = \mathbf{c}_0$, where C is a $3m \times 6$ matrix.

Let $\mathbf{x}_{1:m}$, associated point cloud variance matrix V_X , constraint matrix C and \mathbf{c}_0 be given with the assumption that $C^\top \mathbf{x}_{1:m} \approx \mathbf{c}_0$, that is, $\mathbf{x}_{1:m}$ approximately satisfies the frame of reference constraints. Define $\hat{\mathbf{x}}$ by

$$\hat{\mathbf{x}}_i(\mathbf{t}) = T(\mathbf{x}, \mathbf{t}) = R(\boldsymbol{\alpha})(\mathbf{x}_i - \mathbf{x}_0), \quad (\text{I.67})$$

a rigid body transformation. We look for \mathbf{t} such that $\hat{\mathbf{x}}_{1:m}$ satisfies the frame of reference constraints exactly: $C^\top \hat{\mathbf{x}}_{1:m} = \mathbf{c}_0$. Since $\mathbf{x}_{1:m}$ approximately satisfies the constraints, to first order approximation, $\hat{\mathbf{x}}_{1:m} = \mathbf{x}_{1:m} + G\mathbf{t}$ where G is the $3m \times 6$ matrix of partial derivatives of $\hat{\mathbf{x}}_{1:m}$ with respect to \mathbf{t} evaluated at \mathbf{t} specifying the identity transformation. We note here that G constructed from 3×6 blocks

$$G_i = \begin{bmatrix} 1 & 0 & 0 & 0 & -z_i & y_i \\ 0 & 1 & 0 & z_i & 0 & -x_i \\ 0 & 0 & 1 & -y_i & x_i & 0 \end{bmatrix}. \quad (\text{I.68})$$

To first order, \mathbf{t} is defined by the equation $C^\top (\mathbf{x}_{1:m} + G\mathbf{t}) = \mathbf{c}_0$ so that $\mathbf{t} = (C^\top G)^{-1}(\mathbf{c}_0 - C^\top \mathbf{x}_{1:m})$. The $6 \times 3m$ sensitivity matrix $G_{T|X}$ of \mathbf{t} with respect to $\mathbf{x}_{1:m}$ is therefore

$$G_{T|X} = -(C^\top G)^{-1} C^\top. \quad (\text{I.69})$$

If the variance matrix associated with $\mathbf{x}_{1:m}$ is V_X , then the variance matrix $V_{T|X}$ associated with \mathbf{t} is given by

$$V_{T|X} = G_{T|X} V_X G_{T|X}^\top. \quad (\text{I.70})$$

Applying T defined by \mathbf{t} to $\mathbf{x}_{1:m}$, to first order,

$$\hat{\mathbf{x}}_{1:m} = \mathbf{x}_{1:m} + G(C^\top G)^{-1}(\mathbf{c}_0 - C^\top \mathbf{x}_{1:m}). \quad (\text{I.71})$$

This last equation defines $\hat{\boldsymbol{x}}_{1:m}$ as a linear function of $\boldsymbol{x}_{1:m}$ and allows us to propagate the variance V_X associated with $\boldsymbol{x}_{1:m}$ through to that, $V_{\hat{X}}$, associated with $\hat{\boldsymbol{x}}_{1:m}$:

$$V_{\hat{X}} = (I - G(C^\top G)^{-1}C^\top)V_X(I - G(C^\top G)^{-1}C^\top)^\top.$$

If the transformation T , defined by \boldsymbol{t} , is applied to another data set $\boldsymbol{z}_{1:p}$ with $\hat{\boldsymbol{z}}_q = T(\boldsymbol{x}_q, \boldsymbol{t})$ and G_Z is the $3p \times 6$ sensitivity matrix constructed from $\boldsymbol{z}_{1:p}$ as in (I.68), then the variance contribution to the transformed data $\hat{\boldsymbol{z}}_{1:m}$ is given by

$$V_{\hat{Z}} = G_Z V_{T|X} G_Z^\top = G_{Z|X} V_X G_{Z|X}^\top, \quad (\text{I.72})$$

where $G_{Z|X} = G_Z G_{T|X}$. In other words, $V_{\hat{Z}}$ is the variance contribution to the variance associated with $\boldsymbol{z}_{1:p}$ arising from the procedure to establish a datum frame of reference from $\boldsymbol{x}_{1:m}$. If $\boldsymbol{x}_{1:m}$ is correlated with $\boldsymbol{z}_{1:m}$, for example, if they are measured at the same time using the same CMM as is often the case and the joint variance matrix associated with them is given by

$$\begin{bmatrix} V_X & V_{XZ} \\ V_{XZ}^\top & V_Z \end{bmatrix},$$

then the variance matrix $V_{\hat{Z}|X}$ associated with $\hat{\boldsymbol{z}}_{1:m}$ is given by

$$V_{\hat{Z}|X} = G_{Z|X} V_X G_{Z|X}^\top + G_{Z|X} V_{XZ} + V_{XZ}^\top G_{Z|X}^\top + V_Z.$$

The expression for $V_{\hat{Z}|X}$ includes the variance contribution associated with both $\boldsymbol{x}_{1:m}$ and $\boldsymbol{z}_{1:p}$ taking into account their correlation.

I.6 Effect of form error on extracted features

Given surface points $\mathbf{s}_i = \mathbf{s}(\mathbf{u}_i, \mathbf{a})$ on idea design surface with normal vectors \mathbf{n}_i , $i \in I = \{1, \dots, m\}$, we can model form errors with an actual workpiece according to

$$\mathbf{x}_i^* = \mathbf{s}_i + f_i \mathbf{n}_i.$$

We provide statistical model for the form errors by assigning

$$\mathbf{f} \in \mathcal{N}(\mathbf{0}, V_F),$$

where V_F is an $m \times m$ variance matrix. The variance contribution to $\mathbf{x}_{1:m}^*$ is given by

$$V_{X|F} = N V_F N^\top,$$

where N the $3m \times m$ block-diagonal matrix constructed from $\mathbf{n}_{1:m}$, as before. We use a spatial correlation model for V_F of the form

$$V_F = \sigma_{F_0}^2 I + V_{EF}(\mathbf{s}_{1:m} | \sigma_F, \boldsymbol{\lambda}_F), \quad (\text{I.73})$$

with

$$V_{EF}(i, j) = \sigma_F^2 e^{-d_{F,ij}^2}, \quad (\text{I.74})$$

where

$$d_{F,ij}^2 = (\mathbf{s}_i - \mathbf{s}_j)^\top M_F (\mathbf{s}_i - \mathbf{s}_j)^\top, \quad M_F = \begin{bmatrix} 1/\lambda_{F,x}^2 & 0 & 0 \\ 0 & 1/\lambda_{F,y}^2 & 0 \\ 0 & 0 & 1/\lambda_{F,z}^2 \end{bmatrix}.$$

The first term on the right of equation models variation in the surface geometry over short length scales, that is, roughness effects. The form of M_F above allows spatially correlated components to be anisotropic, e.g., we may wish to assign different length scales to straightness and circularity components of the form error of a cylinder. Note that the spatial correlation is determined by the point of contact on the design surface where as spatially correlated location errors, section I.3.7, need to take into account probe offsets.

If $G_{A|X} = G_{A|D} N^\top$ is the sensitivity of features \mathbf{a} with respect to a point cloud $\mathbf{x}_{1:m}$ then the variance contribution $V_{A|F}$ for the form errors to \mathbf{a} is given by

$$\begin{aligned} V_{A|F} &= G_{A|X} V_{X|F} G_{A|X}^\top = G_{A|D} V_F G_{A|D}^\top \\ &= \sigma_{F_0}^2 G_{A|D} G_{A|D}^\top + G_{A|D} V_{EF} G_{A|D}^\top. \end{aligned} \quad (\text{I.75})$$

I.7 Uncertainties for derived features using Monte Carlo sampling and the point cloud variance matrix

The methods described in sections I.4 to I.5.9 are all based on deriving the sensitivity matrix $G_{A|X}$ that is used to construct the variance matrix V_A for the derived features \mathbf{a} from the variance matrix V_X associated with the point cloud $\mathbf{x}_{1:m}$. For the features involved, the functional relationship $\mathbf{a} = \mathbf{f}(\mathbf{x}_{1:m})$ of \mathbf{a} on the point cloud is smooth and almost linear so that the first order approximation of \mathbf{f} and the application of the law of propagation of uncertainty (I.1) is very effective in estimating uncertainties associated with the derived features. As noted in section I.2.1, for features derived according to Chebyshev and related criteria, the functional relationship is not smooth and the first order approximation of \mathbf{f} might not be fit for purpose.

An alternative approach is to use a Monte Carlo sampling approach [3] as summarised by (I.2), generating point cloud data sets $\mathbf{x}_{1:m,q}$ and derived features $\mathbf{a}_q = \mathbf{a}_q(\mathbf{x}_{1:m,q})$ for each data set, $q = 1, \dots, M$. The variance matrix associated with the sample $\mathbf{a}_{1:m}$ is an approximation to V_A . In order to implement the Monte Carlo approach, it is necessary to be able to generate data sets X_q that are samples from the distribution associated with the point cloud. This is quite straightforward to implement. If the point cloud variance matrix V_X associated with $\mathbf{x}_{1:m}$ can be factored as $V_X = KK^\top$ (for example, from an eigenvalue decomposition), then if $\boldsymbol{\delta}_{1:m}$ is a sample from the standard multivariate Gaussian distribution¹¹ $\boldsymbol{\delta}_{1:m,q} \in \mathcal{N}(\mathbf{0}, I)$ then

$$\mathbf{x}_{1:m,q} = \mathbf{x}_{1:m} + K\boldsymbol{\delta}_{1:m,q},$$

is associated with variance matrix V_X .

¹¹Each element of $\boldsymbol{\delta}_{1:m,q}$ is a sample from the standard normal distribution $\mathcal{N}(0, 1)$.

I.8 Example calculations

I.8.1 Three statistical characterisations based on MPE statements

The simulations involve characterisations of CMM behaviour based on three, MPE statements, the first, MPE1, with $A = 0.5 \mu\text{m}$ and $B = 500.0 \text{ mm}$, the second, MPE2, with $A = 1.0 \mu\text{m}$ and $B = 200.0 \text{ mm}$, the third, MPE3 with $A = 2.0 \mu\text{m}$ and $B = 125.0 \text{ mm}$. These MPE statements have been used to estimate the statistical parameters characterising the CMM influence factors. These prior estimates are given in table I.11. The second MPE characterisation is essentially twice the first and the derived statistical parameters, σ_R , σ_S , etc., in column 5 of table I.11 are twice those in column 4; the length scale parameters λ_{ET} , etc., are the same. The third MPE has a slightly different balance between A and B and the derived statistical parameters in column 6 in table I.11 are not a simple scaling of the parameters in columns 4 and 5. The statistical characterisations in terms of length measurement are illustrated in figures I.9–I.11. These figures show compares twice the estimated standard uncertainty $u(d)$ as a function of distance d , and contributions relating to scale and squareness effects (S), location effects (ET) and rotational effects (ER) compared with the MPE statement $A + d/B$ for the two characterisations.

Effect	Parameter	Unit	MPE1	MPE2	MPE3
MPE	A	μm	0.5	1.0	2.0
	B	mm	500.0	250.0	200.0
Repeatability	σ_R	μm	0.10	0.20	0.40
Scale, squareness	σ_S	10^{-6}	0.7	1.4	1.8
	$\sigma_{S,a}$	10^{-6}	0.7	1.4	1.8
	σ_Q	10^{-6}	0.7	1.4	1.8
Probe qualification	σ_{PQ}	μm	0.10	0.20	0.4
Location	σ_{ET}	μm	0.17	0.33	0.67
	λ_{ET}	mm	125.0	125.0	125.0
Rotation	σ_{ER}	μrad	2.0	4.0	5.0
	λ_{ER}	mm	125.0	125.0	125.0
Probing	σ_{P_0}	μm	0.07	0.14	0.28
	σ_P	μm	0.10	0.20	0.40
	λ_P	1	0.50	0.50	0.50

Table I.11: Three sets of statistical parameters estimated from MPE statements of the form $A + d/B$.

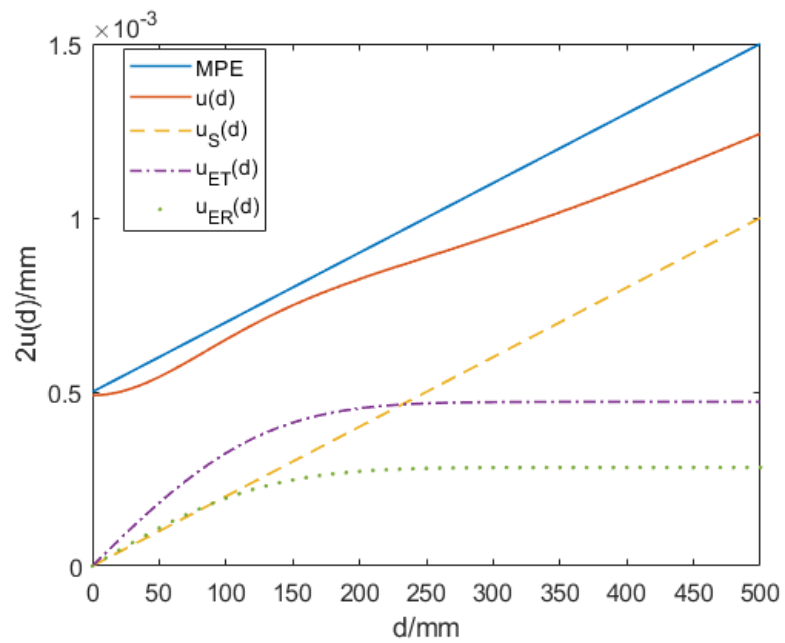


Figure I.9: Twice the estimated standard uncertainty $u(d)$ as a function of distance d , and contributions relating to scale and squareness effects (S), location effects (ET) and rotational effects (ER) compared with the MPE statement $A + d/B$ (upper straight line) for statistical parameters given in the third column in table I.11.

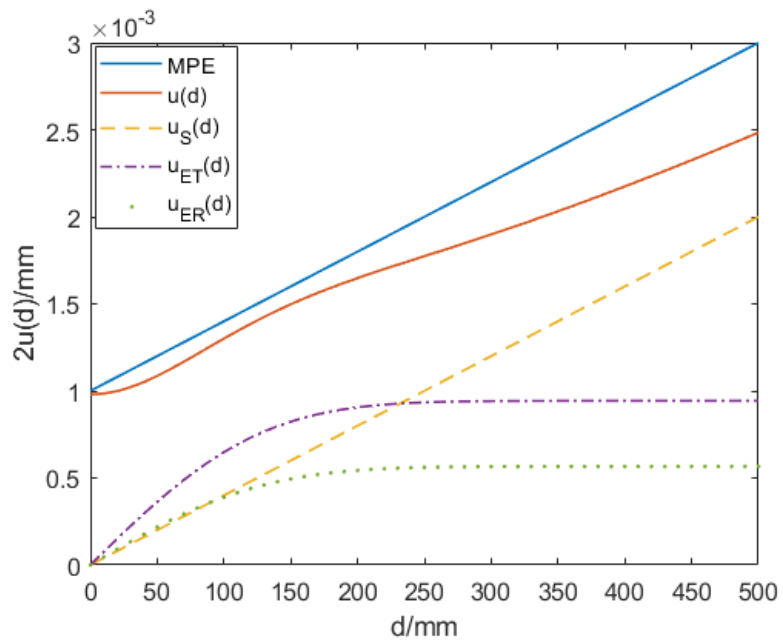


Figure I.10: As figure I.9 but with the statistical parameters given in the fourth column in table I.11.

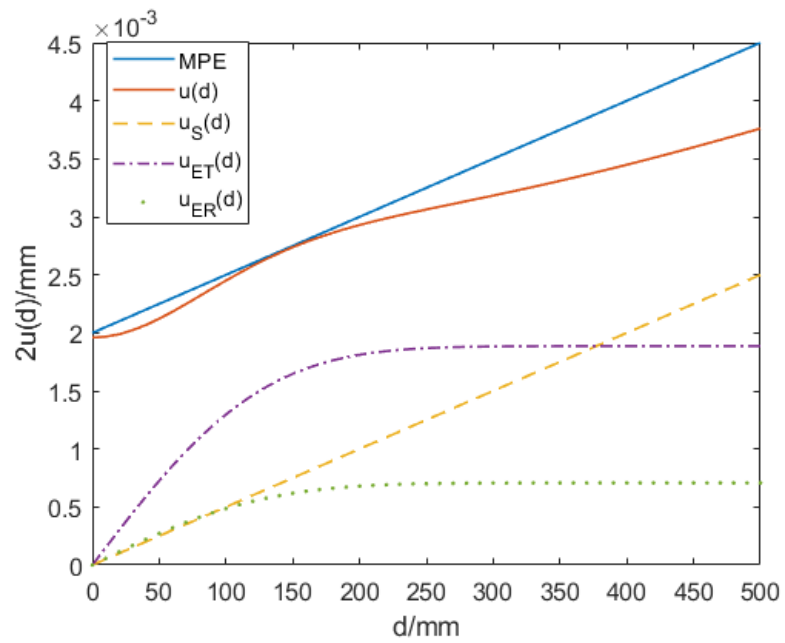


Figure I.11: As figure I.9 but with the statistical parameters given in the fifth column in table I.11.

I.8.2 Step gauge

The first set of calculations involve simulations measurements of a step gauge with 26 steps of nominal length 10 mm situated at 20 mm intervals along a measuring line. The simulations reported on here involve two scenarios. In each scenario the step gauge is aligned with the x -axis.

Scenario I. This scenario assumes i) the 52 step faces are measured with the same probe with probe offset $\mathbf{p} = (0.0, 0.0, -20.0)^\top$ mm.

Scenario II. This scenario assumes ii) the 26 left-facing faces are measured with a probe with offset $\mathbf{p}_L = (0.0, 20.0, 0.0)^\top$ mm and the 26 right-facing faces are measured with a probe with offset $\mathbf{p}_R = (0.0, -20.0, 0.0)^\top$ mm.

The extracted features derived from the measurements are:

d_{ij} The distances between all faces, with $d_{ij} = \|\mathbf{x}_i - \mathbf{x}_j\|$.

$d_{LL,ij}$ The distances between left-facing faces.

$d_{RR,ij}$ The distances between right-facing faces.

$d_{FF,k}$ The estimated length of each step.

Table I.12 gives the standard uncertainty associated with the location $\mathbf{x}_1^\top \mathbf{n}_1$ of the first face of the step gauge for the step gauge for scenario I and three sets of statistical parameters given in columns 3–5 of table I.11, along with the uncertainty contributions associated with the various effects. The contributions for scenario II are largely the same. Figures I.12–I.14 plot twice the estimated standard uncertainty $u(d)$ associated with distances derived from measurements of a step gauge under scenario I and statistical parameters given by columns 3–5 of table I.11 for the different extracted features discussed above. The label ‘LL’ relates to distances between left-facing faces, ‘RR’ to distances between right-facing faces and ‘FF’ to the distances between the step faces for each step. Also plotted is the MPE function $A + d/B$ (upper straight line). Figures I.15–I.17 provide the same information as figures I.12–I.14 but for scenario II. We note the following.

- Table I.12 shows that all influence factors contribute directly to the uncertainties associated with $\mathbf{x}_i^\top \mathbf{n}$. The rotational effects contribution (ER) is small but would be larger for a longer probe offset.

- Figures I.12–I.14 show the difference between measurements of distances using the same probing direction, ‘LL’, and ‘RR’ and measurements of distances involving both probing directions, ‘FF’, for example, in terms of associated uncertainties. For the former case, probing effects make no contribution; for the later case, they make a direct and full contribution. For both cases (in scenario I), the probe qualification effects make no contribution.
- Figures I.15–I.17 show the same behaviour as figures I.12–I.14 but also reflect the fact that probe qualification effects also contribute directly to the uncertainties associated with measurements for distances involving both probing directions.

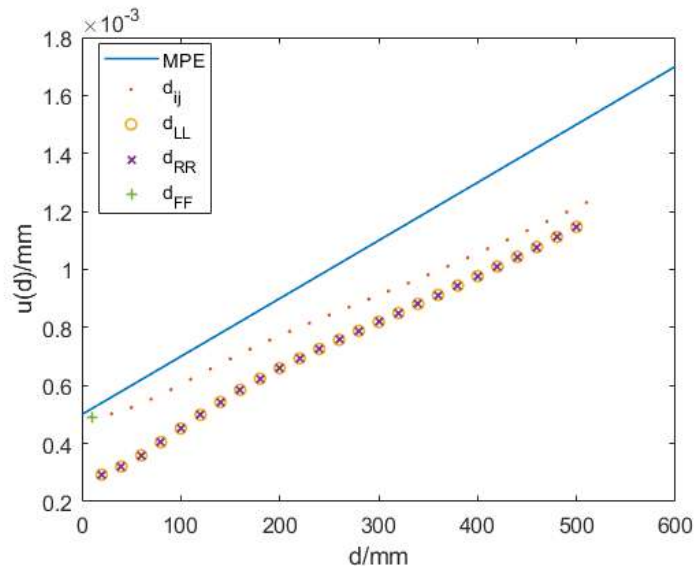


Figure I.12: Twice the estimated standard uncertainty $u(d)$ associated with distances derived from measurements of a step gauge under scenario I and statistical parameters given by the third column of table I.11, MPE1. The label ‘LL’ relates to distances between left-facing faces, ‘RR’ to distances between right-facing faces and ‘FF’ to the distances between the step faces for each step. Also plotted is the MPE function $A + d/B$ (upper straight line).

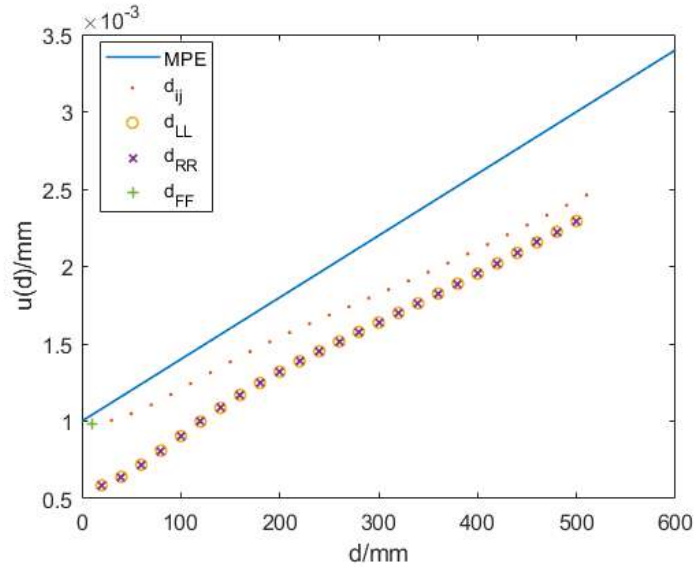


Figure I.13: As figure I.12 but for statistical parameters given by the fourth column of table I.11, MPE2.

	u	u_R	u_{PQ}	u_S	u_{ET}	u_{ER}	u_P
MPE1	0.36	0.10	0.10	0.26	0.17	0.04	0.12
MPE2	0.72	0.20	0.20	0.51	0.33	0.08	0.24
MPE3	1.19	0.40	0.40	0.64	0.67	0.10	0.49

Table I.12: Standard uncertainty associated with the location $\mathbf{x}_1^\top \mathbf{n}_1$ of the first face of the step gauge for the step gauge for scenario I and three sets of statistical parameters given in columns 3–5 of table I.11.

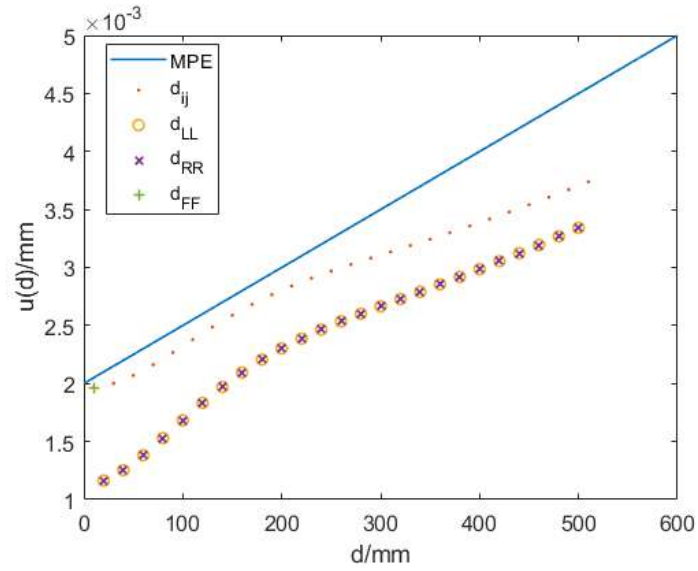


Figure I.14: As figure I.12 but for statistical parameters given by the fifth column of table I.11, MPE3.

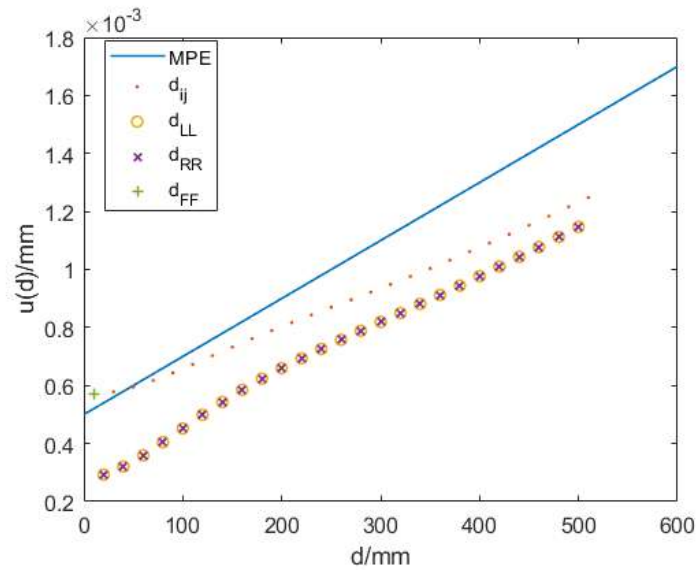


Figure I.15: As figure I.12 but for scenario II.

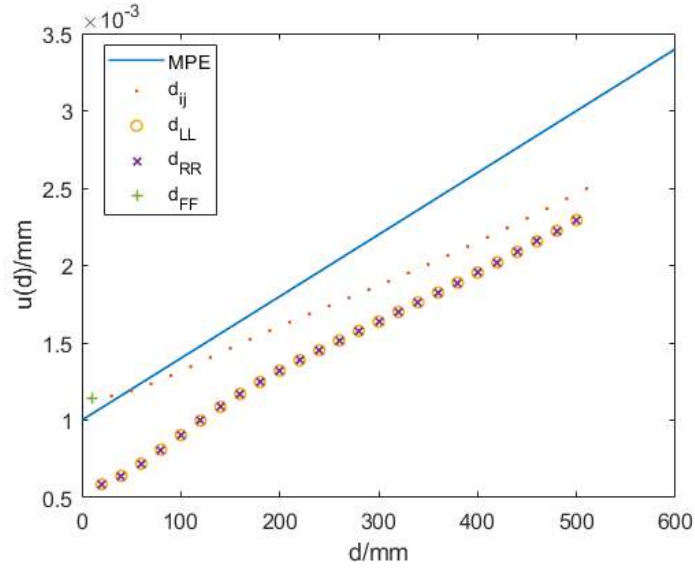


Figure I.16: As figure I.13 but for scenario II.

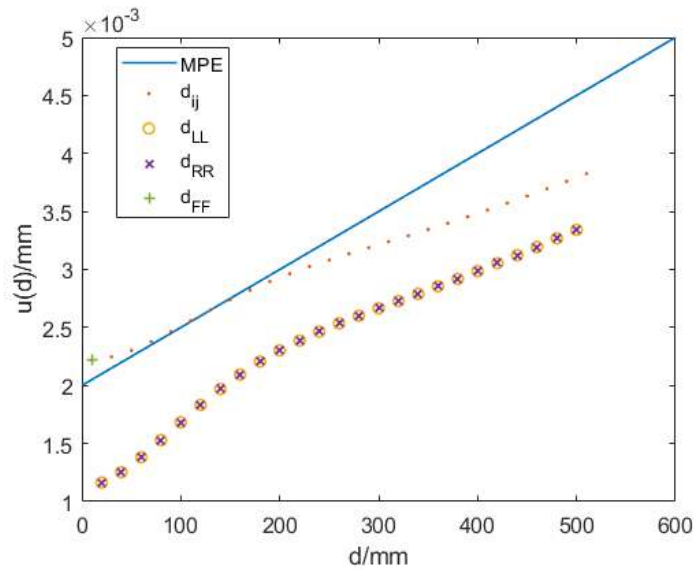


Figure I.17: As figure I.14 but for scenario II.

	\mathbf{b}_1	\mathbf{b}_2	\mathbf{b}_3
\mathbf{x}_A/mm	0.0	0.0	0.0
	0.0	140.0	0.0
	0.0	0.0	10.0
\mathbf{v}_A	0.0	0.0	0.0
	0.0	0.0	0.0
	1.0	1.0	1.0
r_0/mm	25.3	9.5	

Table I.13: Parameters specifying the geometric elements associated with the connecting rod.

I.8.3 Connecting rod

The second set of calculations involves the connecting rod involving two cylindrical geometric elements and one plane element (the datum plane), specified by locating points, direction vectors, and for the cylinders, radii; see diagram I.18. The parameter vectors associated with the elements are given in table I.13. The measurement strategy involved gathering 16 points at three parallel circles on each of the two cylinders and 8 points in a circular pattern on the planar surface.

The simulations reported on here involve two scenarios:

Scenario I. This scenario assumes i) the measured points on the cylinders are distributed uniformly around the cylindrical surface and that all elements (two cylinders, one plane) are measured using the same probe with probe offset $\mathbf{p} = (0, 0, -20)^\top$.

Scenario II. This scenario assumes ii) the measured points on the large cylinder are distributed on a 120° arc at bottom end of the connecting rod (figure I.18) and the measured points on the small cylinder are distributed on a 120° at the top end of the rod, and ii) the two cylinders are measured with two different probes, each with nominal probe offset $\mathbf{p}_k = (0, 0, -20)^\top$, $k = 1, 2$, but subject to different probe qualification effects.

Table I.14 shows the estimates of the uncertainties associated with the extracted features and derived features for scenario I and MPE1. The ex-

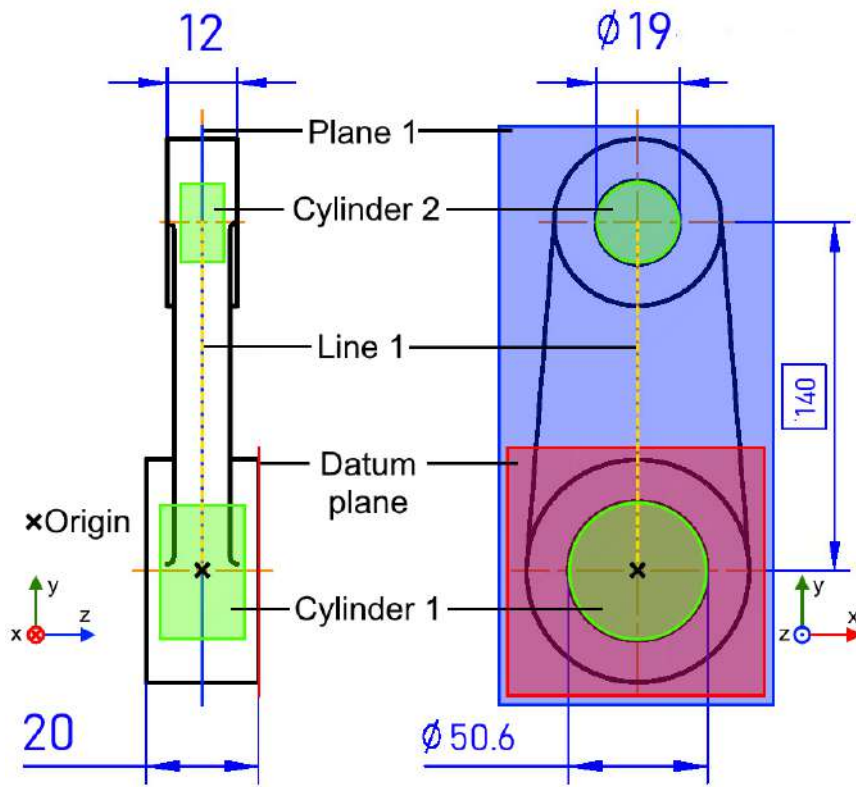


Figure I.18: Connecting rod workpiece with three geometric elements.

tracted features are related to the parameters associated with the two cylinders and plane:

x_A, y_A The x - and y -coordinates associated with the locating point \mathbf{x}_A associated with the two cylinders.

z_A The z -coordinate associated with the locating point \mathbf{x}_A associated with the plane.

u_A, v_A The x - and y -coordinates associated with the direction vectors \mathbf{v}_A associated with the two cylinders and the plane.

r_0 The radii associated with the two cylinders.

(All other elements of the locating points and direction vectors are held constant.) The uncertainties following derived features are also evaluated:

d_{12} the distance between the axis location points \mathbf{x}_A for the two cylinders as measured in the plane $z = 0$.

$\alpha_{12,x}$ the angle of rotation about the y -axis between the two cylinder direction vectors \mathbf{v}_A , i.e., the x -components of the direction vectors.

$\alpha_{12,y}$ the angle of rotation about the x -axis between the two cylinder direction vectors \mathbf{v}_A , i.e., the y -components of the direction vectors.

Table I.14 also shows the uncertainty contributions from the various influence factors: random effects (R), probe qualification effects (PQ), scale and squareness effects (S), and spatially correlated location (ET), rotation (ER) and probing effects (P), the latter three all assumed to be isotropic in that the behaviour for each axis is the same. We note the following.

R The random effects uncertainty contribution to the x - and y -coordinates of the cylinder location points (0.02 mm) is approximately $\sqrt{2}$ times that to radii r_0 in line with the analysis in section I.5.6. The contribution is small due to the averaging effect over $m = 48$ data points.

PQ The uncertainty associated with probe qualification contributes directly and in full to the uncertainties associated with the location point parameters, but does not contribute to the derived features since the probe qualification effect is modelled as a constant offset for measurements.

S The scale and squareness effects make minimal contribution to the locating point associated with the first cylinder since its location point is at the origin. The scale and squareness effects contribute more significantly to the location of the small cylinder \mathbf{b}_2 . The scale effects contribute directly to the uncertainty associated with the distance d_{12} between the two cylinder axes.

ET The spatially correlated location effects contribute to the uncertainties associated with the location point parameters. The spatial correlation length $\lambda_{ET} = 125$ mm is greater than the cylinder radii so that the location effects in the neighbourhood are significantly correlated and act somewhat like a probe qualification effect. For the same reason, they make minimal contribution to the uncertainties associated with the radii r_0 . The correlation length λ_{ET} is larger than the distance $d_{12} = 140$ mm between the two cylinder axes so that no significant cancellation of these effects arise, leading to a significant contribution to $u(d_{12})$.

ER Rotational effects contribute only modestly to the uncertainties associated with the features. Their contributions scale directly with probe offset length.

P The probe radius uncertainty represented by σ_{P_0} contributes directly and fully to the uncertainty associated with the cylinder radii r_0 . Since the probing directions for the two cylinders are exactly the same, the probing effects make no contributions to the uncertainties associated with the derived features d_{12} , $\alpha_{12,x}$ and $\alpha_{12,y}$.

Table I.15 gives the same uncertainty estimates but for scenario II with statistical parameters for MPE1 as in the third column of table I.11. We note the following.

R The uncertainty contribution from random effects to $u(y_A)$ and $u(r_0)$ are much greater due to the fact that only a 120° arc of the cylinder is measured, as discussed in section I.5.6; see also table I.5.6.

PQ Whereas for scenario I, probe qualification had no uncertainty contribution to $u(d_{12})$ since both cylinders were associated with the same probe qualification effect, in scenario II, these effects are independent and make a direct and full contribution to $u(d_{12})$.

P For scenario II, the probing directions for the two cylinders are completely different and probing effects contribute directly to $u(d_{12})$. They do not make a contribution to $u(\alpha_{12,x})$ and $u(\alpha_{12,y})$ since the probing strategy for each of the three circular profiles on each cylinder is the same.

Tables I.16 and I.17 give the uncertainty estimates but for scenarios I and II, respectively with statistical parameters for MPE3 as in the fifth column of table I.11. The tables show the same behaviour as tables I.14 and I.16 and the comments above apply.

	u	u_R	u_{PQ}	u_S	u_{ET}	u_{ER}	u_P
$x_A/\mu\text{m}$	0.20	0.02	0.10	0.01	0.16	0.04	0.05
$y_A/\mu\text{m}$	0.20	0.02	0.10	0.01	0.16	0.04	0.05
$u_A/\mu\text{rad}$	3.70	3.12	0.00	0.71	1.81	0.43	0.00
$v_A/\mu\text{rad}$	3.70	3.13	0.00	0.71	1.81	0.43	0.00
$r_0/\mu\text{m}$	0.09	0.01	0.00	0.02	0.03	0.01	0.08
$x_A/\mu\text{m}$	0.23	0.02	0.10	0.10	0.17	0.04	0.05
$y_A/\mu\text{m}$	0.25	0.02	0.10	0.14	0.17	0.04	0.05
$u_A/\mu\text{rad}$	6.58	6.25	0.00	0.71	1.87	0.45	0.00
$v_A/\mu\text{rad}$	6.58	6.25	0.00	0.71	1.87	0.45	0.00
$r_0/\mu\text{m}$	0.08	0.01	0.00	0.01	0.01	0.00	0.08
$z_A/\mu\text{m}$	0.23	0.04	0.10	0.03	0.16	0.00	0.12
$u_A/\mu\text{rad}$	2.60	1.87	0.00	0.00	1.80	0.00	0.00
$v_A/\mu\text{rad}$	2.60	1.87	0.00	0.00	1.80	0.00	0.00
$d_{12}/\mu\text{m}$	0.24	0.03	0.00	0.14	0.19	0.05	0.00
$\alpha_{12,x}/\mu\text{rad}$	7.34	6.99	0.00	0.00	2.19	0.53	0.00
$\alpha_{12,y}/\mu\text{rad}$	7.33	6.99	0.00	0.00	2.16	0.52	0.00

Table I.14: Standard uncertainties associated with derived features for the connecting rod for scenario I and statistical parameters for MPE1 as in the third column of table I.11.

	u	u_R	u_{PQ}	u_S	u_{ET}	u_{ER}	u_P
$x_A/\mu\text{m}$	0.22	0.03	0.10	0.02	0.17	0.04	0.10
$y_A/\mu\text{m}$	0.37	0.10	0.10	0.04	0.19	0.05	0.28
$u_A/\mu\text{rad}$	4.57	4.08	0.00	0.71	1.88	0.45	0.00
$v_A/\mu\text{rad}$	3.33	2.63	0.00	0.71	1.87	0.45	0.00
$r_0/\mu\text{m}$	0.26	0.08	0.00	0.03	0.08	0.02	0.23
$x_A/\mu\text{m}$	0.25	0.03	0.10	0.10	0.17	0.04	0.10
$y_A/\mu\text{m}$	0.38	0.10	0.10	0.15	0.17	0.04	0.28
$u_A/\mu\text{rad}$	8.43	8.17	0.00	0.71	1.88	0.45	0.00
$v_A/\mu\text{rad}$	5.64	5.25	0.00	0.71	1.88	0.45	0.00
$r_0/\mu\text{m}$	0.25	0.08	0.00	0.01	0.03	0.01	0.23
$z_A/\mu\text{m}$	0.23	0.04	0.10	0.03	0.16	0.00	0.12
$u_A/\mu\text{rad}$	2.60	1.87	0.00	0.00	1.80	0.00	0.00
$v_A/\mu\text{rad}$	2.60	1.87	0.00	0.00	1.80	0.00	0.00
$d_{12}/\mu\text{m}$	0.53	0.14	0.14	0.17	0.25	0.06	0.39
$\alpha_{12,x}/\mu\text{rad}$	9.47	9.13	0.00	0.00	2.42	0.58	0.00
$\alpha_{12,y}/\mu\text{rad}$	6.39	5.87	0.00	0.00	2.44	0.58	0.00

Table I.15: Standard uncertainties associated with derived features for the connecting rod for scenario II and statistical parameters for MPE1 as in the third column of table I.11. The uncertainty contribution from effects associated with probe qualification and probing are highlighted in bold.

	u	u_R	u_{PQ}	u_S	u_{ET}	u_{ER}	u_P
$x_A/\mu\text{m}$	0.79	0.08	0.40	0.04	0.64	0.10	0.21
$y_A/\mu\text{m}$	0.79	0.08	0.40	0.04	0.64	0.10	0.21
$u_A/\mu\text{rad}$	14.58	12.50	0.00	1.77	7.22	1.08	0.00
$v_A/\mu\text{rad}$	14.58	12.50	0.00	1.77	7.22	1.08	0.00
$r_0/\mu\text{m}$	0.36	0.06	0.00	0.05	0.13	0.02	0.32
$x_A/\mu\text{m}$	0.85	0.08	0.40	0.25	0.66	0.10	0.21
$y_A/\mu\text{m}$	0.88	0.08	0.40	0.35	0.66	0.10	0.21
$u_A/\mu\text{rad}$	26.18	25.00	0.00	1.77	7.49	1.12	0.00
$v_A/\mu\text{rad}$	26.18	25.00	0.00	1.77	7.49	1.12	0.00
$r_0/\mu\text{m}$	0.33	0.06	0.00	0.02	0.05	0.01	0.32
$z_A/\mu\text{m}$	0.91	0.14	0.40	0.07	0.64	0.00	0.49
$u_A/\mu\text{rad}$	10.39	7.48	0.00	0.00	7.21	0.00	0.00
$v_A/\mu\text{rad}$	10.39	7.48	0.00	0.00	7.21	0.00	0.00
$d_{12}/\mu\text{m}$	1.07	0.12	0.57	0.35	0.76	0.11	0.29
$\alpha_{12,x}/\mu\text{rad}$	29.32	27.95	0.00	0.00	8.75	1.31	0.00
$\alpha_{12,y}/\mu\text{rad}$	29.29	27.95	0.00	0.00	8.64	1.30	0.00

Table I.16: Standard uncertainties associated with derived features for the connecting rod for scenario I and statistical parameters as in the fifth column of table I.11.

	u	u_R	u_{PQ}	u_S	u_{ET}	u_{ER}	u_P
$x_A/\mu\text{m}$	0.88	0.11	0.40	0.05	0.66	0.10	0.38
$y_A/\mu\text{m}$	1.46	0.39	0.40	0.11	0.76	0.11	1.10
$u_A/\mu\text{rad}$	18.10	16.34	0.00	1.77	7.51	1.13	0.00
$v_A/\mu\text{rad}$	13.06	10.51	0.00	1.77	7.47	1.12	0.00
$r_0/\mu\text{m}$	1.04	0.32	0.00	0.09	0.32	0.05	0.93
$x_A/\mu\text{m}$	0.92	0.11	0.40	0.26	0.67	0.10	0.38
$y_A/\mu\text{m}$	1.46	0.39	0.40	0.37	0.68	0.10	1.10
$u_A/\mu\text{rad}$	33.60	32.68	0.00	1.77	7.53	1.13	0.00
$v_A/\mu\text{rad}$	22.42	21.02	0.00	1.77	7.53	1.13	0.00
$r_0/\mu\text{m}$	0.99	0.32	0.00	0.03	0.12	0.02	0.93
$z_A/\mu\text{m}$	0.91	0.14	0.40	0.07	0.64	0.00	0.49
$u_A/\mu\text{rad}$	10.39	7.48	0.00	0.00	7.21	0.00	0.00
$v_A/\mu\text{rad}$	10.39	7.48	0.00	0.00	7.21	0.00	0.00
$d_{12}/\mu\text{m}$	2.06	0.55	0.57	0.43	0.99	0.15	1.56
$\alpha_{12,x}/\mu\text{rad}$	37.83	36.53	0.00	0.00	9.69	1.45	0.00
$\alpha_{12,y}/\mu\text{rad}$	25.48	23.50	0.00	0.00	9.75	1.46	0.00

Table I.17: Standard uncertainties associated with derived features for the connecting rod for scenario II and statistical parameters for MPE3 as in the fifth column of table I.11.

I.9 Validation of the *a priori* method

I.9.1 Measurements of a calibrated artefact

Suppose an artefact has associated features $\mathbf{a} = (a_1, \dots, a_n)^\top$ and that prior information from a previous calibration is available and is summarised by

$$\mathbf{a}_C \in \mathcal{N}(\mathbf{a}, V_C).$$

We interpret this statement that the calibrated values \mathbf{a}_C is a draw from a multivariate Gaussian (normal) distribution with (unknown) mean \mathbf{a} and variance matrix V_C . Suppose also that a proposed measurement strategy $\mathbf{x}_{1:m}$ is defined and that a statistical characterisation of the CMM to be used to measure the artefact is also defined. For example, the statistical characterisation could be derived from an MPE statement, as discussed in section I.4.8. The statistical characterisation allows the point cloud variance matrix V_X to be estimated and, given the sensitivity matrix $G_{A|X}$ of \mathbf{a} with respect to $\mathbf{x}_{1:m}$, the variance matrix V_A associated with the estimate $\hat{\mathbf{a}}$ derived from V_X :

$$V_A = G_{A|X} V_X G_{A|X}^\top.$$

The statistical characterisation states that any estimate $\hat{\mathbf{a}}$ of \mathbf{a} derived from measurements of the artefact by the CMM is such that

$$\hat{\mathbf{a}} \in \mathcal{N}(\mathbf{a}, V_A).$$

Assuming that the calibration experiment and the CMM measurement are completely independent experiments (from the statistical point of view), we have

$$\hat{\mathbf{a}} - \mathbf{a}_C \in \mathcal{N}(\mathbf{0}, V_A + V_C). \quad (\text{I.76})$$

Letting

$$W_{AC} = (V_A + V_C)^{-1},$$

(assuming the inverse exists) the relationship (I.76) implies that

$$R^2 = (\hat{\mathbf{a}} - \mathbf{a}_C)^\top W_{AC} (\hat{\mathbf{a}} - \mathbf{a}_C) \in \chi_n^2,$$

a draw from a χ^2 distribution with n degrees of freedom. The observed value R^2 can be compared with quantiles of the χ^2 distribution to determine the probabilities

$$\alpha(R^2) = \Pr(\xi^2 \geq R^2 | \xi^2 \sim \chi_n^2), \quad \beta(R^2) = \Pr(\xi^2 \leq R^2 | \xi^2 \sim \chi_n^2).$$

If these probabilities are not too small, say greater than 0.05, the variance matrix V_A (and hence V_X) can be regarded as a plausible statement of the CMM uncertainty. Conversely, if $\alpha(R^2) < 0.05$, ($\beta(R^2) < 0.05$), there is evidence that V_A understates (overstates) the uncertainty associated with the CMM measurements (assuming that the calibration information is valid).

Relationship to normalised errors

For the case $n = 1$, the test of consistency of $\hat{\mathbf{a}}$ and V_A with the calibration information described above is related to the use of normalised errors in assessing consistency of a test result with a reference value [28]. For the univariate case we write

$$\hat{a} \in \mathcal{N}(a, u^2(a)), \quad a_C \in \mathcal{N}(a, u_C^2), \quad \hat{a} - a_C \in \mathcal{N}(0, u^2(a) + u_C^2)$$

and

$$R^2 = \frac{(\hat{a} - a_C)^2}{u^2(a) + u_C^2} \in \chi_1^2.$$

Since the probability density function $p_{\chi^2}(x|\nu = 1)$ associated with a χ^2 distribution with one degree of freedom is such that $p_{\chi^2}(x|\nu = 1) \propto e^{-x/2}$,

$$\alpha(R^2) = \Pr(\xi^2 \geq R^2 | \xi^2 \sim \chi_1^2) = \Pr(|\xi| \geq R | \xi \sim \mathcal{N}(0, 1)),$$

so that requiring $\alpha(R^2) \geq 0.05$ is equivalent to requiring that

$$\text{En} = \frac{|\hat{a} - a_C|}{2\sqrt{u^2(a) + u_C^2}} \leq 1.$$

Calibrated form error

While associated features such as the radius of a cylinder derived from CMM measurements can be used to valid an *a priori* uncertainty budget, if there are only a small number of calibrated features the information available for validation is small. The estimated form errors derived from fitting a geometric element, such as a cylinder, to data potentially is a richer source of validation information. Suppose $\mathbf{x}_{1:m}$ are measured points associated with a calibrated surface $\mathbf{u} \mapsto \mathbf{s}(\mathbf{u}, \mathbf{a})$, depending on parameters $\mathbf{a} = (a_1, \dots, a_n)^\top$, whose geometric form is known exactly, e.g., an ideal geometric element such

as a cylinder and that $d_{1:m} = d(\mathbf{x}_{1:m}, \hat{\mathbf{a}})$ are the residual distances associated with the least squares best-fit surface to $\mathbf{x}_{1:m}$ defined by parameter estimates $\hat{\mathbf{a}}$. Suppose also that V_X is the point cloud variance matrix associated with $\mathbf{x}_{1:m}$ derived using an *a priori* method (or otherwise). As discussed in section I.5.2, it is possible to derive the sensitivity matrix $G_{\hat{D}|X}$ of \mathbf{d} with respect to $\mathbf{x}_{1:m}$ and evaluate the variance matrix $V_{\hat{D}}$ associated with \mathbf{d} :

$$V_{\hat{D}} = G_{\hat{D}|X} V_X G_{\hat{D}|X}^\top.$$

As discussed in section I.5.2, the sensitivity matrix $G_{\hat{D}|X}$ can be factored as

$$G_{\hat{D}|X} = Q_2 Q_2^\top N^\top,$$

where Q_2 is an $m \times (m - n)$ orthogonal matrix. As a consequence, $V_{\hat{D}}$ is necessarily rank deficient and its inverse cannot be formed. However, the projected residuals $\tilde{\mathbf{d}} = Q_2^\top \mathbf{d}$ are such that

$$\tilde{\mathbf{d}} \in \mathcal{N}(\mathbf{0}, V_{\hat{D}}), \quad V_{\hat{D}} = Q_2^\top V_{\hat{D}} Q_2,$$

and $V_{\hat{D}}$ is (in almost all practical cases) full rank. Hence

$$\tilde{R}^2 = \tilde{\mathbf{d}}^\top V_{\hat{D}}^{-1} \tilde{\mathbf{d}} \in \chi_{m-n}^2$$

and can be used to assess the validity of V_X , assuming that the surface $s(\mathbf{u}, \mathbf{a})$ is free from form error.

More generally, if \mathbf{x}_i is measurement of $\mathbf{s}_i + f_i \mathbf{n}_i$ where f_i represents the form error measured orthogonally to the surface at \mathbf{s}_i (as discussed in section I.6), and the form error has been characterised as

$$\mathbf{f} \in \mathcal{N}(\mathbf{f}_0, V_F),$$

in a prior calibration exercise, for example, then

$$\tilde{\mathbf{d}} - \tilde{\mathbf{f}}_0 \in \mathcal{N}(\mathbf{0}, V_{\hat{D}} + V_{\hat{F}}), \quad \tilde{\mathbf{f}}_0 = Q_2^\top \mathbf{f}_0, \quad V_{\hat{F}} = Q_2^\top V_F Q_2,$$

enabling a validation assessment on the basis of the value of the hypothesis

$$\tilde{R}^2(\mathbf{f}_0) = (\tilde{\mathbf{d}} - \tilde{\mathbf{f}}_0)^\top W_{DF} (\tilde{\mathbf{d}} - \tilde{\mathbf{f}}_0), \quad W_{DF} = (V_{\hat{D}} + V_{\hat{F}})^{-1} \in \chi_{m-n}^2.$$

If the only available prior information about \mathbf{f} is that $|f_{1:m}| \leq F$, then we set $\mathbf{f}_0 = \mathbf{0}$ and V_F can be estimated by

$$V_F \approx \frac{F^2}{K^2} I,$$

for example, for $K = 2$, say.

I.9.2 Repositioning experiments

The validation approaches discussed above in section I.9.1 depend on having external calibration information available. In a repositioning experiment, the same artefact is measured using nominally the same measurement strategy in a number of positions, $k = 1, \dots, n_K$, in the working volume, possibly with repeat measurements in nominally the same position, gathering data sets X_k and associated extracted features \mathbf{a}_k . Since the artefact has is nominally the same in each position (although there may be influence factors relating fixturing and gravitational loading) and the points contacted on the artefact are nominally the same and involve the same form errors, any variation between X_k and associated features \mathbf{a}_k are due to CMM measurement effects and, importantly, are largely independent of form errors.

Let

$$X = \begin{bmatrix} X_1 \\ \vdots \\ X_k \\ \vdots \\ X_{n_K} \end{bmatrix}$$

and suppose the point cloud variance matrix V_X associated with X is partitioned accordingly,

$$V_X = \begin{bmatrix} V_{11} & V_{12} & \cdots & V_{1n_K} \\ V_{12}^\top & V_{22} & \cdots & V_{2n_K} \\ \vdots & & \ddots & \vdots \\ V_{1n_K}^\top & V_{2n_K}^\top & \cdots & V_{n_K n_K} \end{bmatrix}.$$

Let $G_{A_k|X_k}$ be the $n \times 3m$ sensitivity matrix of \mathbf{a}_k with respect to X_k and $G_{A|X}$ the block diagonal matrix with $G_{A_k|X_k}$ on the k th diagonal block. Then the variance matrix $V_{A|X}$ associated with $\mathbf{a}_{1:n_K}$ is given by

$$V_{A|X} = G_{A|X} V_X G_{A|X}^\top.$$

For two positions k and ℓ , the variance matrix $V_{A_{k\ell}}$ associated with $\mathbf{a}_{k\ell} = \mathbf{a}_k - \mathbf{a}_\ell$ is given by

$$V_{A_{k\ell}} = \begin{bmatrix} G_{A_k|X_k} & -G_{A_\ell|X_\ell} \end{bmatrix} \begin{bmatrix} V_{kk} & V_{k\ell} \\ V_{k\ell}^\top & V_{\ell\ell} \end{bmatrix} \begin{bmatrix} G_{A_k|X_k} & -G_{A_\ell|X_\ell} \end{bmatrix}^\top.$$

If the features \mathbf{a} are independent of position, e.g., the radius of a cylinder, then the observed difference $\mathbf{a}_{k\ell}$ is such that

$$\mathbf{a}_{k\ell} \in \mathcal{N}(\mathbf{0}, V_{A_{k\ell}}), \quad (\text{I.77})$$

from which a validity test can be constructed as above.

The approach can be applied to the case where the associated features are the projected residual distances $\tilde{\mathbf{d}}_k$ which are nominally independent of position. The relationship in (I.77) can be used to assess the *a priori* uncertainty estimate based on the pair-wise difference between projected residuals $\tilde{\mathbf{d}}_k$. It is also possible to assess validity based on all the measurements simultaneously as follows. Let $G_{\tilde{D}_k|X_k} = Q_{2,k}^\top G_{\hat{D}_k|X_k}$ be the sensitivity matrix associated with the projected residuals $\tilde{\mathbf{d}}_k = Q_{2,k}^\top \mathbf{d}_k$ with respect to X_k and $G_{\tilde{D}|X}$ the block diagonal matrix with $G_{\tilde{D}_k|X_k}$ on the k th diagonal block. Then the variance matrix $V_{\tilde{D}|X}$ associated with $\tilde{\mathbf{d}}_{1:n_K}$ is given by

$$V_{\tilde{D}|X} = G_{\tilde{D}|X} V_X G_{\tilde{D}|X}^\top.$$

The form errors \mathbf{f} associated with the artefact can be parametrized as $Q_2 \tilde{\mathbf{f}}$ where Q_2 is the orthogonal matrix associated with a fit to nominal data with the artefact in a nominal position and the model implies that

$$\tilde{\mathbf{d}}_{1:n_K} \in \mathcal{N}(C\tilde{\mathbf{f}}, V_{\tilde{D}|X}). \quad (\text{I.78})$$

Here C is the $n_K(m-n) \times (m-n)$ matrix constructed from $Q_{2,k}^\top Q_2$, $k = 1, \dots, n_K$. If $\tilde{\mathbf{f}}$ are the least squares estimates of $\tilde{\mathbf{f}}$ calculated by solving

$$\min_{\tilde{\mathbf{f}}} (\tilde{\mathbf{d}}_{1:n_K} - C\tilde{\mathbf{f}})^\top V_{\tilde{D}|X}^{-1} (\tilde{\mathbf{d}}_{1:n_K} - C\tilde{\mathbf{f}}),$$

then the model in (I.78) implies that

$$R^2 = (\tilde{\mathbf{d}}_{1:n_K} - C\tilde{\mathbf{f}})^\top V_{\tilde{D}|X}^{-1} (\tilde{\mathbf{d}}_{1:n_K} - C\tilde{\mathbf{f}})$$

is a sample from $\chi_{(n_K-1)(m-n)}^2$, enabling a validity test to be constructed.

Repeatability experiments

Repeatability experiments involve measuring the same artefact in the same nominal position using nominally the same measurement strategy $\mathbf{x}_{1:m}$ and

evaluating the same associated features \mathbf{a} . The experiments may involve remounting the artefact in the same position so that effects associated with fixturing can influence the results but other effects are nominally the same: geometric effects, probing effects, form errors, etc. Let X_r , $r = 1, \dots, n_R$, be the data sets recorded in the repeatability experiments and \mathbf{a}_r the associated features derived from X_r . The general model for CMM measurement in (I.5) separates out the systematic effects \mathbf{e}_i from the random effects $\boldsymbol{\epsilon}_i$ and the *a priori* method separates out point cloud variance matrix in a similar way:

$$V_X = V_R + V_E, \quad V_R = \sigma_R^2 I.$$

For repeatability experiments, we assume that the systematic effects are constant for each set of measurements

$$\mathbf{x}_{k,1:m} = \mathbf{x}_{k,1:m}^* + \mathbf{e}_{1:m} + \boldsymbol{\epsilon}_{k,1:m}.$$

Let $G_{A|X}$ be the sensitivity of the associated features \mathbf{a} with respect to $\mathbf{x}_{1:m}$ for the fixed measurement strategy. Then

$$\mathbf{a}_r = \mathbf{a}^* + \mathbf{e}_A + \boldsymbol{\delta}_r, \quad \mathbf{e}_A = G_{A|X} \mathbf{e}_{1:m},$$

with

$$\boldsymbol{\delta}_r \in \mathcal{N}(\mathbf{0}, V_{A|R}), \quad V_{A|R} = \sigma_R^2 G_{A|X} G_{A|X}^\top.$$

Letting

$$\bar{\mathbf{a}} = \frac{1}{n_R} \sum_{r=1}^{n_R} \mathbf{a}_r,$$

then

$$R^2 = \sum_{r=1}^{n_R} (\mathbf{a}_r - \bar{\mathbf{a}})^\top V_{A|R}^{-1} (\mathbf{a}_r - \bar{\mathbf{a}}) \in \chi_{(n_R-1)n}^2.$$

This relationship can be used to assess the validity of $V_{A|R}$ and since $V_{A|R}$ depends only on σ_R , the repeatability experiments can be used directly to assess the validity of σ_R (as one would expect).

I.9.3 Posterior adjustment of statistical parameters

See also [1], sections 4.1 and 4.1 and [16].

The *a priori* model of CMM behaviour allows the variance matrix V_X to be constructed, given a measurement strategy. The type of validation experiments described above involve using the fact that an observed sum of squares

residuals R^2 is modelled as a draw from a χ_ν^2 distribution with ν degrees of freedom. The mean of the distribution χ_ν^2 is ν . If the *a priori* method accurately modelled the CMM uncertainty behaviour and the validation experiments were carried out a number of times, then we expect that the average value of R^2 would be centred around ν . This fact leads to a posterior adjustment approach as follows.

Suppose a model predicts

$$R_0^2 = (\mathbf{a} - \hat{\mathbf{a}})^\top V_0^{-1} (\mathbf{a} - \hat{\mathbf{a}}) \in \chi_\nu^2, \quad (\text{I.79})$$

but that there is some doubt about the variance matrix V_0 in that it could be out by an unknown scale factor σ^2 , i.e., the true variance matrix V is given by $V = \sigma^2 V_0$ where σ^2 is unknown. Writing

$$R^2 = R^2(\sigma^2) = (\mathbf{a} - \hat{\mathbf{a}})^\top V^{-1} (\mathbf{a} - \hat{\mathbf{a}}) = \frac{R_0^2}{\sigma^2}$$

and equating R^2 with the expected value of ν , we arrive at a posterior estimate of

$$\hat{\sigma}^2 = \frac{R_0^2}{\nu} \quad (\text{I.80})$$

for σ^2 . Thus, multiplying the input uncertainties by $\hat{\sigma}$ leads to a residual sum of squares R^2 that accords (optimally in some sense) with the model predictions.

Repeatability experiments

If $\hat{\mathbf{d}}_r$ are residual error vectors associated with a set of repeated measurements, then the projected residual errors $\tilde{\mathbf{d}}_r = Q_2^\top \hat{\mathbf{d}}_r$ are such that

$$\tilde{\mathbf{d}}_r = Q_2^\top \mathbf{f} + Q_2^\top \mathbf{e}_D + \tilde{\mathbf{e}}_r, \quad \tilde{\mathbf{e}}_r \in \mathcal{N}(\mathbf{0}, \sigma_R^2 I),$$

where \mathbf{f} are the form errors associated with the artefact and \mathbf{e}_D are the fixed systematic effects associated with $\mathbf{x}_i^\top \mathbf{n}_i$. If $\bar{\mathbf{d}}$ is the mean of the $\tilde{\mathbf{d}}_r$, then a posterior estimate $\hat{\sigma}_R$ of σ_R is given by

$$\hat{\sigma}_R^2 = \frac{1}{n_R(m-n)} \sum_{r=1}^{n_R} (\tilde{\mathbf{d}}_r - \bar{\mathbf{d}})^\top (\tilde{\mathbf{d}}_r - \bar{\mathbf{d}}). \quad (\text{I.81})$$

Posterior adjustment with prior information

The posterior estimate of σ in (I.80) assumes that nothing is known about the scale factor σ^2 prior to the validation exercise. A more flexible approach is as follows, using a Bayesian hierarchical model [23, 35]. We suppose that the model predicts that estimates $\hat{\mathbf{a}}$ of parameters \mathbf{a} are such that

$$\hat{\mathbf{a}}|\phi \in \mathcal{N}(\mathbf{a}, \phi^{-1}V_0), \quad \phi = \sigma^{-2}, \quad (\text{I.82})$$

where ϕ is a scaling parameter defined in terms of σ^2 . We assume that a prior estimate σ_0^2 of σ^2 is available. If V_0 is our best estimate of the variance matrix, then σ_0^2 can be taken to be 1. Associated with the estimate σ_0^2 is a degree of belief parameter $m_0 > 0$ that model the confidence we have in the estimate σ_0^2 with large m_0 signifying more confidence. The parameter m_0 can be thought of as the number of repeat measurements taken to provide the estimate σ_0^2 . The prior information about σ^2 is encoded as

$$\phi \sim \mathcal{G}(m_0/2, m_0\sigma_0^2/2) \quad (\text{I.83})$$

where $\mathcal{G}(A, B)$ is a gamma distribution define in terms of shape parameter A and rate parameter B or, equivalently,

$$m_0\sigma_0^2\phi \sim \chi_{m_0}^2.$$

Table I.18 shows values of $s = s_{\alpha, m_0} = 1/\sqrt{\phi_{\alpha, m_0}}$ for ϕ_{α, m_0} such that $\Pr(\phi \leq \phi_{\alpha, m_0}) \leq \alpha$ for $\phi \sim \mathcal{G}(m_0/2, m_0/2)$. For example, if $m_0 = 10$, the table shows that there is 2.5 % prior probability that the true scaling factor $\sigma \leq 0.7$ or that $\sigma \geq 1.75$. Assuming a non-informative prior $p(\mathbf{a}) \propto 1$, the relationships (I.82) and (I.83) define the joint distribution

$$p(\mathbf{a}, \phi|\hat{\mathbf{a}}) = p(\mathbf{a}|\hat{\mathbf{a}}, \phi)p(\phi)$$

from which the marginalised distribution $p(\mathbf{a}|\hat{\mathbf{a}})$ can be calculated to be

$$\mathbf{a}|\hat{\mathbf{a}} \sim t_{m_0}(\hat{\mathbf{a}}, \sigma_0^2 V_0). \quad (\text{I.84})$$

If $\sigma_0^2 = 1$, as will be the case in our application, the fact that the scale parameter is not known exactly means that the instead of a Gaussian state of knowledge distribution for \mathbf{a} of the form $\mathbf{a} \sim \mathcal{N}(\hat{\mathbf{a}}, V_0)$, we have instead $\mathbf{a} \sim t_{m_0}(\hat{\mathbf{a}}, V_0)$. As $m_0 \rightarrow \infty$, the t -distribution approaches the corresponding Gaussian distribution. For modest values of m_0 , say less than 20, the t -distribution accords significantly more probability mass away from the mean

that the corresponding Gaussian distribution. For $m_0 > 2$, the variance matrix associated with $t_{m_0}(\hat{\mathbf{a}}, V_0)$ is $m_0/(m_0 - 2)$ representing the increase in variance due to the longer tails of the t -distribution.

Given observed sum of squares R_0^2 as in (I.79), the posterior adjusted estimate $\bar{\sigma}^2$ of σ^2 is given by

$$\bar{\sigma}^2 = \frac{m_0\sigma_0^2 + \nu\hat{\sigma}^2}{m_0 + \nu} = \left(\frac{m_0}{m_0 + \nu}\right)\sigma_0^2 + \left(\frac{\nu}{m_0 + \nu}\right)\hat{\sigma}^2, \quad (\text{I.85})$$

a weighted average of the prior estimate σ_0^2 and the estimate $\hat{\sigma}^2$ derived from the validation experiment as in (I.80). The posterior distribution for \mathbf{a} is given by

$$\mathbf{a} \sim t_{m_0+\nu}(\hat{\mathbf{a}}, \bar{V}), \quad \bar{V} = \bar{\sigma}^2 V_0.$$

The marginalised posterior distribution for ϕ is such that

$$\phi|\hat{\mathbf{a}} \sim \mathcal{G}(\bar{m}/2, \bar{m}\bar{\sigma}^2/2), \quad \bar{m} = m_0 + \nu.$$

If the prior information is weak in the sense that m_0 is small, relative to ν , then the posterior estimate $\bar{\sigma}^2$ is close to that determined from the validation experiment, namely $\hat{\sigma}^2$ in (I.80). Conversely, if the validation involves only a small number of measurements as represented by ν , relative to m_0 , then the posterior estimate is close to the prior estimate σ_0^2 .

Posterior adjustment of a number of statistical parameters

The posterior adjustment scheme described above in section I.9.3 relates to estimating a single scale adjustment parameters σ^2 . The *a priori* model for CMM measurement involves a number of statistical parameters. The one-parameter adjustment scheme can be applied to each of the statistical parameters, so that

$$\bar{\sigma}_R = \bar{\sigma}\sigma_R, \quad \bar{\sigma}_{ET} = \bar{\sigma}\sigma_{ET},$$

etc. However, we may be more confident in the estimates of some of the statistical parameters than others and applying a single scale adjustment to all the parameters may not be appropriate. Here, we consider the case where we want to apply separate adjustment schemes to the random effects and systematic effects.

We assume a validation experiments gives rise to data \mathbf{y} that can be modelled (after linearisation if necessary) according to

$$\mathbf{y} \in \mathcal{N}(C\mathbf{a}, \phi_R^{-1}V_R + \phi_E^{-1}V_E),$$

where C is a $m \times n$ observation matrix. Assuming a non-informative prior $p(\mathbf{a}) \propto 1$ for \mathbf{a} , it is possible to determine the posterior distribution $p(\phi_R, \phi_E | \mathbf{y})$ up to a normalising constant. Estimates $\hat{\phi}_R$ and $\hat{\phi}_E$ can then be determined finding the values that maximise $p(\phi_R, \phi_E | \mathbf{y})$. with prior information about scale factors ϕ_R and ϕ_E given by

$$\phi_R \sim \mathcal{G}(m_R/2, m_R/2), \quad \phi_E \sim \mathcal{G}(m_E/2, m_E/2),$$

(so that 1 is the prior expected value for both ϕ_R and ϕ_E).

$m_0 \backslash \alpha$	0.025	0.050	0.100	0.900	0.095	0.975
1.00	0.45	0.51	0.61	7.96	15.95	31.91
2.00	0.52	0.58	0.66	3.08	4.42	6.28
3.00	0.57	0.62	0.69	2.27	2.92	3.73
4.00	0.60	0.65	0.72	1.94	2.37	2.87
5.00	0.62	0.67	0.74	1.76	2.09	2.45
6.00	0.64	0.69	0.75	1.65	1.92	2.20
7.00	0.66	0.71	0.76	1.57	1.80	2.04
8.00	0.68	0.72	0.77	1.51	1.71	1.92
9.00	0.69	0.73	0.78	1.47	1.65	1.83
10.00	0.70	0.74	0.79	1.43	1.59	1.75
15.00	0.74	0.77	0.82	1.32	1.44	1.55
20.00	0.77	0.80	0.84	1.27	1.36	1.44
25.00	0.78	0.81	0.85	1.23	1.31	1.38
30.00	0.80	0.83	0.86	1.21	1.27	1.34
35.00	0.81	0.84	0.87	1.19	1.25	1.30
40.00	0.82	0.85	0.88	1.17	1.23	1.28
45.00	0.83	0.85	0.88	1.16	1.21	1.26
50.00	0.84	0.86	0.89	1.15	1.20	1.24
60.00	0.85	0.87	0.90	1.14	1.18	1.22
70.00	0.86	0.88	0.90	1.12	1.16	1.20
80.00	0.87	0.89	0.91	1.12	1.15	1.18
90.00	0.87	0.89	0.91	1.11	1.14	1.17
100.00	0.88	0.90	0.92	1.10	1.13	1.16
200.00	0.91	0.92	0.94	1.07	1.09	1.11
500.00	0.94	0.95	0.96	1.04	1.06	1.07

Table I.18: Values of $s = s_{\alpha, m_0} = 1/\sqrt{\phi_{\alpha, m_0}}$ for ϕ_{α, m_0} such that $\Pr(\phi \leq \phi_{\alpha, m_0}) \leq \alpha$ for $\phi \sim \mathcal{G}(m_0/2, m_0/2)$.

I.10 Numerical results

I.10.1 Repositioning and repeatability experiments

As part of an *a posteriori* (Type A) estimation of CMM uncertainty, a large number of experiments have been undertaken to measure a number of artefacts by a number of CMMs. In each experiment, the same artefact is measured in $n_K = 4$ different positions, with $n_R = 5$ repeat measurements in each position, making a total of $n_K n_R = 20$ measurements of the artefact. We denote by X_{kr} , $k = 1, \dots, n_K$, $r = 1, \dots, n_R$, the point cloud datasets and by \mathbf{a}_{kr} the features associated with data sets X_{kr} . The fact that the measurements involve repeat measurements means that posterior estimates $\hat{\sigma}_R$ can be derived using the approach described in section I.9.2. Given $\hat{\sigma}_R$, an estimate $\hat{\sigma}_E$ associated with the combined systematic effects can also be determined.

I.10.2 Hyperbolic paraboloid

The measurements of a hyperbolic paraboloid relate a surface [33] whose nominal shape is given by $z = xy/64$ in units of millimetres. The data set in the first position relates to the nominal surface

$$z - 27 = (x - 48)(y - 48)/64, \quad (\text{I.86})$$

with $m = 52$ gathered with xy -coordinates located as in figure I.19. The second, third and fourth locations of the artefact are nominally determined by rotating the artefact in position 1 through 90° about the x -, y - and z -axes.

The recorded data are distances \mathbf{d}_{kr}^o that are interpreted to be the orthogonal distances of the data \mathbf{x}_i to the nominal surface at \mathbf{x}_i^* , i.e., $d_i^o = \|\mathbf{x}_i - \mathbf{x}_i^*\|$. Given $\mathbf{x}_{1:m}^*$ lying on the nominal surface, associated normal vectors $\mathbf{n}_{1:m}$ we reconstruct the measured data according to $\mathbf{x}_i = \mathbf{x}_i^* + d_i^o \mathbf{n}_i$, so that \mathbf{d}_{kr}^o can be used to reconstruct the datasets X_{kr} , $k = 1, \dots, n_K = 4$, $r = 1, \dots, n_R = 5$.

A paraboloid is fitted to the datasets X_{kr} using a nonlinear least squares orthogonal distance regression algorithm [6, 21] to determine vectors $\hat{\mathbf{d}}_{kr}$ of residual orthogonal distances. The paraboloid is parametrized in terms of three rotation angles $\boldsymbol{\alpha}$ and six further parameters \mathbf{b} such that

$$\hat{z} = [\hat{x}^2, \hat{y}^2, \hat{x}\hat{y}, \hat{x}, \hat{y}, 1] \mathbf{b} \quad \hat{\mathbf{x}} = R(\boldsymbol{\alpha}) \mathbf{x}.$$

For the hyperboloid in (I.86), nominally $\mathbf{b}^\top = [0, 0, 1/64, -3/4, -3/4, 63]$.

Associated with each position of artefact is matrix $Q_{2,k}$ and sensitivity matrix $G_{\hat{D}|D} = Q_{2,k}Q_{2,k}^\top$. The projected residuals $\tilde{\mathbf{d}}_{kr} = Q_{2,k}^\top \mathbf{d}_{kr}$ are modelled according to

$$\tilde{\mathbf{d}}_{kr} = Q_{2,k}^\top Q_2 \tilde{\mathbf{f}} + Q_{2,k}^\top \mathbf{e}_k + \tilde{\boldsymbol{\epsilon}}_{kr}, \quad \tilde{\boldsymbol{\epsilon}}_{kr} \in \mathcal{N}(\mathbf{0}, \sigma_R^2 I), \quad (\text{I.87})$$

where \mathbf{e}_k relate to the combined systematic effects applying in the k th position. If

$$\bar{\mathbf{d}}_k = \frac{1}{n_R} \sum_{r=1}^{n_R} \tilde{\mathbf{d}}_{kr}, \quad k = 1, \dots, n_K,$$

then a posterior estimate of σ_R is given by

$$\hat{\sigma}_R^2 = \frac{1}{n_K n_R (m - n)} \sum_{k=1}^{n_K} \sum_{r=1}^{n_R} (\tilde{\mathbf{d}}_{kr} - \bar{\mathbf{d}}_k)^\top (\tilde{\mathbf{d}}_{kr} - \bar{\mathbf{d}}_k), \quad (\text{I.88})$$

derived from all $n_k n_R$ sets of measurements. With this posterior estimate of σ_R , we can also average (I.87) to yield

$$\bar{\mathbf{d}}_k = Q_{2,k}^\top Q_2 \tilde{\mathbf{f}} + \bar{\mathbf{e}}_k + \bar{\boldsymbol{\epsilon}}_k, \quad \bar{\boldsymbol{\epsilon}}_k \in \mathcal{N}(\mathbf{0}, (\hat{\sigma}_R^2/n_R)I), \quad \bar{\mathbf{e}}_k = Q_{2,k}^\top \mathbf{e}_k. \quad (\text{I.89})$$

If we make the simplifying assumption that $\bar{\mathbf{e}}_k \in \mathcal{N}(\mathbf{0}, \sigma_{E,0}^2)$, then, letting

$$\bar{\mathbf{f}} = \frac{1}{n_K} \sum_{k=1}^{n_K} \bar{\mathbf{d}}_k,$$

a posterior estimate $\hat{\sigma}_{E,0}$ of $\sigma_{E,0}$ is given by

$$\hat{\sigma}_{E,0}^2 = \frac{1}{n_K (m - n)} \sum_{k=1}^{n_K} (\bar{\mathbf{d}}_k - \bar{\mathbf{f}})^\top (\bar{\mathbf{d}}_k - \bar{\mathbf{f}}) - \hat{\sigma}_R^2/n_R. \quad (\text{I.90})$$

Given estimate $\hat{\sigma}_R$, equation (I.89) can be used to define the model

$$\bar{\mathbf{d}}_{1:n_K} \in \mathcal{N}\left(C \tilde{\mathbf{f}}, \sigma_0^2 (V_{\bar{D}|E} + \hat{\sigma}_R I)\right), \quad (\text{I.91})$$

where $V_{\bar{D}|E}$ is the variance matrix associated with the projected residuals due to the systematic effects and σ_0 is a single scale adjustment for the variance matrix. A posterior estimate $\hat{\sigma}_0$ of σ_0 can be determined following the general approach described in section I.9.3.

We note that the estimates $\hat{\sigma}_R$ and $\hat{\sigma}_{E,0}$ given in (I.88) and (I.90) are essentially those arising from an analysis of variance approach involving a random effect and a position effect, analogous to a repeatability and geometry effects in the *a posteriori* approach [39, 40].

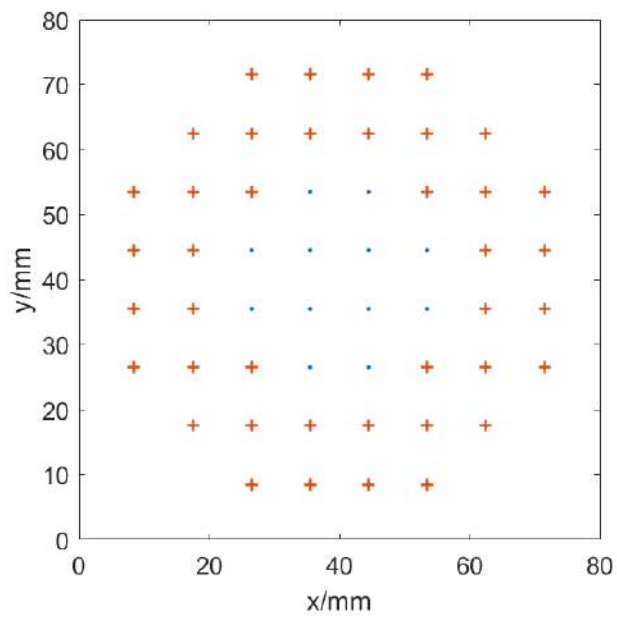


Figure I.19: Nominal xy -coordinates, of 52 points on a hyperbolic paraboloid given in (I.86). The points marked with a cross are those for which uncertainties are reported in the tables.

Analysis of the hyperbolic paraboloid data

The measurements using eight CMMs at different laboratories have been analysed. The main steps carried out in the analysis are:

1. From the $A + L/B$ statement, assign statistical parameters σ listed in table I.11. The spatial correlation lengths were set to be $\lambda_{ET} = \lambda_{ER} = 10$ mm, $\lambda_P = 0.3$.
2. Determine prior estimates of uncertainties associated with $\mathbf{x}_i^\top \mathbf{n}_i$ for measurements of the artefact in the first position.
3. Determine prior estimates of uncertainties associated with $\hat{\mathbf{d}}$, the fitted residual distances, for measurements of the artefact in the first position.
4. Reconstruct the datasets X_{kr} and calculate the residual error vectors $\hat{\mathbf{d}}_{kr}$ by fitting a paraboloid to X_{kr} .
5. Determine of a posterior estimate $\hat{\sigma}_R$ of σ_R based on all the repeatability measurements (I.88).
6. From $\hat{\sigma}_R$, determine estimate $\hat{\sigma}_{E,0}$ of the standard deviation of the combined systematic effects (I.90). This estimate is for information only.
7. With σ_R adjusted to be the posterior estimate $\hat{\sigma}_R$, determine a posterior estimate $\hat{\sigma}_0 = \hat{\sigma}_0 | \sigma$ of σ_0 , based on the model (I.91).
8. Use the posterior estimates to adjust all the statistical parameters (including σ_R for a second time), e.g., $\hat{\sigma}_{ET} = \hat{\sigma}_0 \sigma_{ET}$, etc., accept for those associated with probe qualification and scale effects. The estimate of σ_R is now $\hat{\sigma}_0 \hat{\sigma}_R$.
9. Verify that the posterior-adjusted $\hat{\sigma}$ statistical parameters are consistent with the measurement data by showing that the equivalent $\hat{\sigma}_{0,0} = \hat{\sigma}_0 | \hat{\sigma}$ is close to 1.

The uncertainty estimation assumes that four separate probes are used for each of the four positions, each of offset length 20 mm aligned with the main probing direction, i.e, aligned with the z -, y -, x - and z -axes.

CMI XENOS data

The prior estimates of the statistical parameters are given in the first numerical column of table I.19. Based on these estimates, the uncertainties $u_i = u(\mathbf{x}_i^\top \mathbf{n}_i)$ associated with measurements at nominal points \mathbf{x}_i , along with the contributions from various factors are given in table I.20. Table I.21 standard uncertainties $u(\hat{d}_i)$ associated with fitted residual distances along with uncertainty components relating to the various influence factors.

We note that while all the influence factors contribute to the uncertainties associated with $\mathbf{x}_i^\top \mathbf{n}_i$, table I.20, the probe qualification effects (PQ) and scale and squareness effects make no contribution to the uncertainties associated with $\hat{\mathbf{d}}$. Since only one probe is used in the simulation, the effect is the same as that of a fixed offset and does not contribute to the residual distances. Similarly, scale and squareness effects can be compensated by changing the position and shape of the fitted paraboloid.

The analysis of the repeatability data gives a posterior estimate $\hat{\sigma}_R = 0.034 \mu\text{m}$, about half the prior estimate of $\sigma_R = 0.06 \mu\text{m}$. The approximate estimate of the standard deviation $\sigma_{E,0}$ associated with the systematic effects is $\hat{\sigma}_{E,0} = 0.077 \mu\text{m}$. The posterior estimate of σ_0 is $\hat{\sigma}_0 = 0.45$, indicating that the prior estimates of the statistical parameters are pessimistic by a factor of about one half. The values of $\hat{\sigma}_R$ and $\hat{\sigma}_0$ are used to produce posterior estimates $\hat{\boldsymbol{\sigma}}$ of the statistical parameters and these have been used to provide estimates of the uncertainties $u(\hat{d}_i | \hat{\boldsymbol{\sigma}})$ associated with the residual distances $\hat{\mathbf{d}}$. These are given in table I.22. The prior estimates $\boldsymbol{\sigma}$ have been tuned to produce posterior estimates $\hat{\boldsymbol{\sigma}}$ that are optimally consistent with the data.

Validation of the prior estimates

The value of $\hat{\sigma}_0$ can be thought of as a single measure of the validity of the prior estimates of the point cloud uncertainties and associated features. A value of $\hat{\sigma}_0 = 1$ indicates optimal consistency of the prior model with the observed data. The values of σ_0 in the bottom row table I.19 range from 0.4 (laboratory 3) to 2.2 (laboratory 7). The results associated laboratory 7 have some anomalous aspects with some outlying data observed so that the value of $\hat{\sigma}_0$ for this laboratory is suspect. The next highest value of $\hat{\sigma}_0$ is 1.1, laboratory 5.

	1	2	3	4	5	6	7	8
A	0.300	0.400	0.700	0.800	0.800	1.200	1.300	2.700
B	1.000	0.900	0.600	0.400	0.400	0.770	0.300	0.300
σ_R	0.060	0.080	0.140	0.160	0.160	0.240	0.260	0.540
σ_S	0.354	0.393	0.589	0.884	0.884	0.459	1.179	1.179
$\sigma_{S,a}$	0.354	0.393	0.589	0.884	0.884	0.459	1.179	1.179
σ_Q	0.354	0.393	0.589	0.884	0.884	0.459	1.179	1.179
σ_{ET}	0.100	0.133	0.233	0.267	0.267	0.400	0.433	0.900
σ_{ER}	1.000	1.111	1.667	2.500	2.500	1.299	3.333	3.333
σ_{PQ}	0.060	0.080	0.140	0.160	0.160	0.240	0.260	0.540
σ_{P_0}	0.042	0.057	0.099	0.113	0.113	0.170	0.184	0.382
σ_P	0.060	0.080	0.140	0.160	0.160	0.240	0.260	0.540
$\hat{\sigma}_R$	0.036	0.069	0.120	0.111	0.042	0.182	0.093	0.214
$\hat{\sigma}_{E,0}$	0.034	0.077	0.052	0.205	0.109	0.164	0.574	0.423
$\hat{\sigma}_0$	0.464	0.703	0.405	1.141	0.440	0.646	2.241	0.730

Table I.19: Hyperboloid. Prior estimates the statistical parameters based on MPE statements and values of statistical parameters based on the measurement data. The units for σ_R , σ_{ET} , σ_{PQ} , σ_{P_0} , σ_P , $\hat{\sigma}_R$ and $\hat{\sigma}_{E,0}$ are μm , those for σ_S , $\sigma_{S,a}$, σ_Q and σ_{ER} are $\mu\text{m}/\text{m}$ and the unit for σ_0 is 1. The CMMs involved are 1 – CMI XENOS, 2 – Tekniker, 3 – PTB UPMC, 4 – PTB PMM, 5 – CUT PMM, 6 – CMI SIP, 7 – GUM, 8 – UNIPD (probing).

The following comments can be made:

1. The range of the values of σ_0 indicates approximate consistency of the prior model with observed data, with the majority indicating the prior model overestimates the uncertainty to some extent. The prior model is based on just two numbers, A and B, associated with the MPE statement. The statistical model we have used is based on scaling the A and B values by a factor of $K = 2$ as in (I.3). Since the MPE statement relates to the maximum permissible error, a larger value of K , say $K = 3$, may be more appropriate.
2. While the values of σ_0 indicate a possible overestimation of the uncertainties, the paraboloid experiments do not involve difficult probing strategies and multiple probe qualification effects so that other experiments could produce data that display more variation due to more effects have influence. As a consequence, the posterior estimates of the parameters characterising probe qualification and scale and squareness effects are set to be the same as their prior estimates as no new information about them is available.
3. Two of the laboratories, 4 and 5, have the same MPE statement, the values of $\hat{\sigma}_0$ are significantly different. Being based on the MPE statement alone, the prior estimates of the statistical parameters do not take into account different environmental conditions, or other influence factors such as fixturing, for example. However, if prior information is available on environment, then the statistical parameters could be adjusted appropriately.
4. The posterior estimates are based on the observed values of $\hat{\sigma}_R$ and $\hat{\sigma}_0$. Some averaging of the prior and observed values as in (I.85) might be more appropriate. Based on the values in table I.18, the prior estimates have a degree of belief value of $m_0 \approx 10$.

x_i	y_i	z_i	u_i	R	PQ	S	ET	ER	P	E
53.500	8.500	23.605	0.154	0.060	0.060	0.029	0.100	0.011	0.073	0.141
44.500	8.500	29.160	0.154	0.060	0.060	0.030	0.100	0.011	0.073	0.141
35.500	8.500	34.715	0.154	0.060	0.060	0.031	0.100	0.011	0.073	0.142
26.500	8.500	40.270	0.154	0.060	0.060	0.032	0.100	0.011	0.073	0.142
17.500	17.500	41.535	0.154	0.060	0.060	0.032	0.100	0.011	0.073	0.142
26.500	17.500	37.246	0.154	0.060	0.060	0.031	0.100	0.010	0.073	0.142
35.500	17.500	32.957	0.154	0.060	0.060	0.030	0.100	0.009	0.073	0.141
44.500	17.500	28.668	0.153	0.060	0.060	0.029	0.100	0.009	0.073	0.141
53.500	17.500	24.379	0.153	0.060	0.060	0.028	0.100	0.009	0.073	0.141
62.500	17.500	20.090	0.153	0.060	0.060	0.027	0.100	0.009	0.073	0.141
71.500	26.500	19.105	0.152	0.060	0.060	0.023	0.100	0.009	0.073	0.140
62.500	26.500	22.129	0.153	0.060	0.060	0.025	0.100	0.008	0.073	0.140
53.500	26.500	25.152	0.153	0.060	0.060	0.027	0.100	0.007	0.073	0.141
26.500	26.500	34.223	0.154	0.060	0.060	0.030	0.100	0.009	0.073	0.141
17.500	26.500	37.246	0.154	0.060	0.060	0.031	0.100	0.010	0.073	0.142
8.500	26.500	40.270	0.154	0.060	0.060	0.032	0.100	0.011	0.073	0.142
8.500	35.500	34.715	0.154	0.060	0.060	0.031	0.100	0.011	0.073	0.142
17.500	35.500	32.957	0.154	0.060	0.060	0.030	0.100	0.009	0.073	0.141
62.500	35.500	24.168	0.152	0.060	0.060	0.023	0.100	0.006	0.073	0.140
71.500	35.500	22.410	0.152	0.060	0.060	0.022	0.100	0.008	0.073	0.140
71.500	44.500	25.715	0.152	0.060	0.060	0.020	0.100	0.007	0.073	0.140
62.500	44.500	26.207	0.152	0.060	0.060	0.022	0.100	0.005	0.073	0.140
17.500	44.500	28.668	0.153	0.060	0.060	0.029	0.100	0.009	0.073	0.141
8.500	44.500	29.160	0.154	0.060	0.060	0.030	0.100	0.011	0.073	0.141
8.500	53.500	23.605	0.154	0.060	0.060	0.029	0.100	0.011	0.073	0.141
17.500	53.500	24.379	0.153	0.060	0.060	0.028	0.100	0.009	0.073	0.141
26.500	53.500	25.152	0.153	0.060	0.060	0.027	0.100	0.007	0.073	0.141
53.500	53.500	27.473	0.152	0.060	0.060	0.022	0.100	0.002	0.073	0.140
62.500	53.500	28.246	0.152	0.060	0.060	0.021	0.100	0.005	0.073	0.139
71.500	53.500	29.020	0.152	0.060	0.060	0.020	0.100	0.007	0.073	0.139
62.500	62.500	30.285	0.152	0.060	0.060	0.021	0.100	0.006	0.073	0.140
53.500	62.500	28.246	0.152	0.060	0.060	0.021	0.100	0.005	0.073	0.140
44.500	62.500	26.207	0.152	0.060	0.060	0.022	0.100	0.005	0.073	0.140
35.500	62.500	24.168	0.152	0.060	0.060	0.024	0.100	0.006	0.073	0.140
26.500	62.500	22.129	0.153	0.060	0.060	0.025	0.100	0.008	0.073	0.140
17.500	62.500	20.090	0.153	0.060	0.060	0.027	0.100	0.009	0.073	0.141
26.500	71.500	19.105	0.153	0.060	0.060	0.025	0.100	0.009	0.073	0.140
35.500	71.500	22.410	0.152	0.060	0.060	0.023	0.100	0.008	0.073	0.140
44.500	71.500	25.715	0.152	0.060	0.060	0.022	0.100	0.007	0.073	0.140
53.500	71.500	29.020	0.152	0.060	0.060	0.022	0.100	0.007	0.073	0.140

Table I.20: CMI XENOS data. Selected nominal point coordinates \mathbf{x}_i in mm and standard uncertainties $u_i = u(\mathbf{x}_i^\top \mathbf{n}_i)$ in μm along with uncertainty components relating to the various influence factors, based on prior estimates σ of the statistical parameters. The final column is the estimate uncertainty contribution from all the systematic effects with $u_i^2 = u_{R,i}^2 + u_{E,i}^2$.

x_i	y_i	z_i	$u(\hat{d}_i)$	R	PQ	S	ET	ER	P	E
53.500	8.500	23.605	0.097	0.050	0.000	0.000	0.078	0.008	0.028	0.084
44.500	8.500	29.160	0.098	0.054	0.000	0.000	0.079	0.008	0.023	0.082
35.500	8.500	34.715	0.098	0.054	0.000	0.000	0.079	0.008	0.023	0.082
26.500	8.500	40.270	0.098	0.050	0.000	0.000	0.079	0.008	0.027	0.084
17.500	17.500	41.535	0.096	0.052	0.000	0.000	0.078	0.009	0.019	0.081
26.500	17.500	37.246	0.098	0.057	0.000	0.000	0.077	0.008	0.019	0.080
35.500	17.500	32.957	0.102	0.057	0.000	0.000	0.081	0.007	0.021	0.084
44.500	17.500	28.668	0.101	0.057	0.000	0.000	0.081	0.007	0.021	0.084
53.500	17.500	24.379	0.097	0.057	0.000	0.000	0.077	0.007	0.020	0.079
62.500	17.500	20.090	0.096	0.052	0.000	0.000	0.077	0.007	0.021	0.080
71.500	26.500	19.105	0.096	0.049	0.000	0.000	0.077	0.007	0.029	0.082
62.500	26.500	22.129	0.097	0.057	0.000	0.000	0.076	0.006	0.021	0.079
53.500	26.500	25.152	0.109	0.058	0.000	0.000	0.087	0.006	0.030	0.092
26.500	26.500	34.223	0.109	0.058	0.000	0.000	0.088	0.007	0.029	0.093
17.500	26.500	37.246	0.098	0.057	0.000	0.000	0.077	0.008	0.019	0.080
8.500	26.500	40.270	0.098	0.050	0.000	0.000	0.079	0.008	0.027	0.084
8.500	35.500	34.715	0.098	0.054	0.000	0.000	0.079	0.008	0.023	0.082
17.500	35.500	32.957	0.102	0.057	0.000	0.000	0.081	0.007	0.021	0.084
62.500	35.500	24.168	0.101	0.057	0.000	0.000	0.080	0.005	0.024	0.083
71.500	35.500	22.410	0.096	0.053	0.000	0.000	0.075	0.006	0.024	0.079
71.500	44.500	25.715	0.096	0.053	0.000	0.000	0.075	0.005	0.025	0.079
62.500	44.500	26.207	0.100	0.057	0.000	0.000	0.079	0.004	0.024	0.083
17.500	44.500	28.668	0.101	0.057	0.000	0.000	0.081	0.007	0.021	0.084
8.500	44.500	29.160	0.098	0.054	0.000	0.000	0.079	0.008	0.023	0.082
8.500	53.500	23.605	0.097	0.050	0.000	0.000	0.078	0.008	0.028	0.084
17.500	53.500	24.379	0.097	0.057	0.000	0.000	0.077	0.007	0.020	0.079
26.500	53.500	25.152	0.109	0.058	0.000	0.000	0.087	0.006	0.030	0.092
53.500	53.500	27.473	0.109	0.058	0.000	0.000	0.086	0.003	0.032	0.092
62.500	53.500	28.246	0.097	0.056	0.000	0.000	0.075	0.004	0.022	0.078
71.500	53.500	29.020	0.095	0.049	0.000	0.000	0.076	0.005	0.030	0.082
62.500	62.500	30.285	0.095	0.052	0.000	0.000	0.076	0.005	0.023	0.079
53.500	62.500	28.246	0.097	0.056	0.000	0.000	0.075	0.004	0.022	0.078
44.500	62.500	26.207	0.100	0.057	0.000	0.000	0.079	0.004	0.024	0.083
35.500	62.500	24.168	0.101	0.057	0.000	0.000	0.080	0.005	0.024	0.083
26.500	62.500	22.129	0.097	0.057	0.000	0.000	0.076	0.006	0.021	0.079
17.500	62.500	20.090	0.096	0.052	0.000	0.000	0.077	0.007	0.021	0.080
26.500	71.500	19.105	0.096	0.049	0.000	0.000	0.077	0.007	0.029	0.082
35.500	71.500	22.410	0.096	0.053	0.000	0.000	0.075	0.006	0.024	0.079
44.500	71.500	25.715	0.096	0.053	0.000	0.000	0.075	0.005	0.025	0.079
53.500	71.500	29.020	0.095	0.049	0.000	0.000	0.076	0.005	0.030	0.082

Table I.21: CMI XENOS data. Selected nominal point coordinates x_i in mm and standard uncertainties $u(\hat{d}_i)$ associated with fitted residual distances in μm , along with uncertainty components relating to the various influence factors, based on prior estimates σ of the statistical parameters. The final column is the estimate uncertainty contribution from all the systematic effects with $u_i^2 = u_{R,i}^2 + u_{E,i}^2$.

x_i	y_i	z_i	$u(\hat{d}_i)$	R	PQ	S	ET	ER	P	E
53.500	8.500	23.605	0.041	0.014	0.000	0.000	0.036	0.004	0.013	0.039
44.500	8.500	29.160	0.041	0.015	0.000	0.000	0.037	0.004	0.011	0.038
35.500	8.500	34.715	0.041	0.015	0.000	0.000	0.037	0.004	0.011	0.038
26.500	8.500	40.270	0.041	0.014	0.000	0.000	0.037	0.004	0.013	0.039
17.500	17.500	41.535	0.040	0.015	0.000	0.000	0.036	0.004	0.009	0.038
26.500	17.500	37.246	0.040	0.016	0.000	0.000	0.036	0.004	0.009	0.037
35.500	17.500	32.957	0.042	0.016	0.000	0.000	0.038	0.003	0.010	0.039
44.500	17.500	28.668	0.042	0.016	0.000	0.000	0.037	0.003	0.010	0.039
53.500	17.500	24.379	0.040	0.016	0.000	0.000	0.036	0.003	0.009	0.037
62.500	17.500	20.090	0.040	0.015	0.000	0.000	0.036	0.003	0.010	0.037
71.500	26.500	19.105	0.041	0.014	0.000	0.000	0.036	0.003	0.013	0.038
62.500	26.500	22.129	0.040	0.016	0.000	0.000	0.035	0.003	0.010	0.037
53.500	26.500	25.152	0.046	0.016	0.000	0.000	0.040	0.003	0.014	0.043
26.500	26.500	34.223	0.046	0.016	0.000	0.000	0.041	0.003	0.013	0.043
17.500	26.500	37.246	0.040	0.016	0.000	0.000	0.036	0.004	0.009	0.037
8.500	26.500	40.270	0.041	0.014	0.000	0.000	0.037	0.004	0.013	0.039
8.500	35.500	34.715	0.041	0.015	0.000	0.000	0.037	0.004	0.011	0.038
17.500	35.500	32.957	0.042	0.016	0.000	0.000	0.038	0.003	0.010	0.039
62.500	35.500	24.168	0.042	0.016	0.000	0.000	0.037	0.002	0.011	0.039
71.500	35.500	22.410	0.040	0.015	0.000	0.000	0.035	0.003	0.011	0.037
71.500	44.500	25.715	0.040	0.015	0.000	0.000	0.035	0.002	0.011	0.037
62.500	44.500	26.207	0.042	0.016	0.000	0.000	0.037	0.002	0.011	0.038
17.500	44.500	28.668	0.042	0.016	0.000	0.000	0.037	0.003	0.010	0.039
8.500	44.500	29.160	0.041	0.015	0.000	0.000	0.037	0.004	0.011	0.038
8.500	53.500	23.605	0.041	0.014	0.000	0.000	0.036	0.004	0.013	0.039
17.500	53.500	24.379	0.040	0.016	0.000	0.000	0.036	0.003	0.009	0.037
26.500	53.500	25.152	0.046	0.016	0.000	0.000	0.040	0.003	0.014	0.043
53.500	53.500	27.473	0.046	0.016	0.000	0.000	0.040	0.001	0.015	0.043
62.500	53.500	28.246	0.040	0.016	0.000	0.000	0.035	0.002	0.010	0.036
71.500	53.500	29.020	0.040	0.014	0.000	0.000	0.035	0.002	0.014	0.038
62.500	62.500	30.285	0.040	0.014	0.000	0.000	0.035	0.002	0.010	0.037
53.500	62.500	28.246	0.040	0.016	0.000	0.000	0.035	0.002	0.010	0.036
44.500	62.500	26.207	0.042	0.016	0.000	0.000	0.037	0.002	0.011	0.038
35.500	62.500	24.168	0.042	0.016	0.000	0.000	0.037	0.002	0.011	0.039
26.500	62.500	22.129	0.040	0.016	0.000	0.000	0.035	0.003	0.010	0.037
17.500	62.500	20.090	0.040	0.015	0.000	0.000	0.036	0.003	0.010	0.037
26.500	71.500	19.105	0.041	0.014	0.000	0.000	0.036	0.003	0.013	0.038
35.500	71.500	22.410	0.040	0.015	0.000	0.000	0.035	0.003	0.011	0.037
44.500	71.500	25.715	0.040	0.015	0.000	0.000	0.035	0.002	0.011	0.037
53.500	71.500	29.020	0.040	0.014	0.000	0.000	0.035	0.002	0.014	0.038

Table I.22: CMI XENOS data. Selected nominal point coordinates \mathbf{x}_i in mm and standard uncertainties $u(\hat{d}_i)$ associated with fitted residual distances in μm , along with uncertainty components relating to the various influence factors, based on posterior estimates $\hat{\boldsymbol{\sigma}}$ of the statistical parameters. The final column is the estimate uncertainty contribution from all the systematic effects with $u_i^2 = u_{R,i}^2 + u_{E,i}^2$.

I.10.3 Connecting rod

The analysis of the connecting rod data follows a similar approach as that for the hyperboloid, but is much simpler in that it applies features \mathbf{a} rather than residual distances. Here we report on measurement results associated with the distance d_{12} between the two cylinder axes; see section I.8.3.

The analysis involves 5 repeated estimates of d_{12} in four positions. Table I.23 shows the prior estimates of the statistical parameters based on MPE statements, along with values of parameters based on the measurement data. The spatial correlation lengths were $\lambda_{ET} = \lambda_{ER} = 30$ mm, and $\lambda_P = 0.3$. Also shown in the table the estimate of $u(d_{12}|\boldsymbol{\sigma})$ based on the prior estimates of the statistical parameters and that $u(d_{12}|\hat{\boldsymbol{\sigma}})$ based on the adjusted estimates. The adjusted statistical parameters are on the basis of measurements of a single parameter in only four positions so that the number of degrees of freedom associated with the estimate of $\hat{\sigma}_0$ is three. If the prior models reflected the actual behaviour, we would expect $\hat{\sigma}_0$ to lie in the interval [0.27,1.77] with 95 % probability. The results associated with laboratory 7 seem anomalous as the standard deviation for all 20 estimates of d_{12} is 60 nm. The values of $\hat{\sigma}_0$ indicate that the uncertainties based on the prior estimates of the statistical parameters $\boldsymbol{\sigma}$ are plausible and reasonably consistent with the measurement data, given that only a limited amount of information is available for validation.

The estimates of d_{12} in the four positions are not statistically independent. For example, their correlation for the statistical characterisation of laboratory 8 in table I.23 is given by

$$C(d_{12}) = \begin{bmatrix} 1.00 & 0.15 & 0.60 & 0.15 \\ 0.15 & 1.00 & 0.15 & 0.15 \\ 0.60 & 0.15 & 1.00 & 0.15 \\ 0.15 & 0.15 & 0.15 & 1.00 \end{bmatrix}.$$

The correlation is strongest between position 1 and 3, the latter corresponding to rotation about the y -axis, i.e., about the long axis of the connecting rod. Relatively speaking, position 3 is approximately in the same region of the CMM as position 1 and the main scale effects are the same.

I.11 Conclusions

	1	2	3	4	5	6	7	8
A	0.300	0.400	0.500	0.700	0.700	0.800	0.900	1.200
B	1.000	0.900	0.500	0.600	0.400	0.400	0.400	0.770
σ_R	0.060	0.080	0.100	0.140	0.140	0.160	0.180	0.240
σ_S	0.354	0.393	0.707	0.589	0.884	0.884	0.884	0.459
$\sigma_{S,a}$	0.354	0.393	0.707	0.589	0.884	0.884	0.884	0.459
σ_Q	0.354	0.393	0.707	0.589	0.884	0.884	0.884	0.459
σ_{ET}	0.100	0.133	0.167	0.233	0.233	0.267	0.300	0.400
σ_{ER}	1.000	1.111	2.000	1.667	2.500	2.500	2.500	1.299
σ_{PQ}	0.060	0.080	0.100	0.140	0.140	0.160	0.180	0.240
σ_{P_0}	0.042	0.057	0.071	0.099	0.099	0.113	0.127	0.170
σ_P	0.060	0.080	0.100	0.140	0.140	0.160	0.180	0.240
$\hat{\sigma}_R$	0.082	0.095	0.027	0.220	0.163	0.035	0.057	0.186
$\hat{\sigma}_{E,0}$	0.038	0.261	0.548	0.208	0.388	0.330	0.037	0.498
$u(d_{12} \boldsymbol{\sigma})$	0.134	0.170	0.237	0.289	0.319	0.351	0.383	0.458
$u(d_{12} \hat{\boldsymbol{\sigma}})$	0.047	0.247	0.584	0.209	0.573	0.508	0.036	0.497
$\hat{\sigma}_0$	0.356	1.465	2.473	0.729	1.805	1.458	0.095	1.094

Table I.23: Connecting rod. Prior estimates of the statistical parameters based on MPE statements, along with values of parameters based on the measurement data. Also shown is the estimate of $u(d_{12}|\boldsymbol{\sigma})$ based on the prior estimates of the statistical parameters and that $u(d_{12}|\hat{\boldsymbol{\sigma}})$ based on the adjusted estimates. The units for σ_R , σ_{ET} , σ_{PQ} , σ_{P_0} , σ_P , $\hat{\sigma}_R$, $\hat{\sigma}_{E,0}$, $u(d_{12}|\boldsymbol{\sigma})$ and $u(d_{12}|\hat{\boldsymbol{\sigma}})$ are μm , those for σ_S , $\sigma_{S,a}$, σ_Q and σ_{ER} are $\mu\text{m}/\text{m}$ and the unit for σ_0 is 1. The CMMs involved are 1 – CMI XENOS, 2 – Tekniker, 3 – MG, 4 – ATH, 5 – Tubitak, 6 – PTB PMM, 7 – Metroser, 8 – CMI SIP (probing).

.1 Point cloud variance decomposition in terms of position, size and shape

See also [19, 18]. Suppose $V (= V_X)$ is a $3m \times 3m$ variance matrix associated with a set of coordinates $\mathbf{x}_{1:m}$ let J the $3m \times 7$ matrix constructed from J_i where

$$J_i = \begin{bmatrix} 1 & 0 & 0 & 0 & -z_i & y_i & x_i \\ 0 & 1 & 0 & z_i & 0 & -x_i & y_i \\ 0 & 0 & 1 & -y_i & x_i & 0 & z_i \end{bmatrix}. \quad (92)$$

Suppose J has QR factorisation $J = QR$ where Q is a $3m \times 3m$ orthogonal matrix with $Q^\top Q = QQ^\top = I$ and R is a $3m \times 7$ upper-triangular matrix [25]. Partition Q as $Q = [Q_1 \ Q_2 \ Q_3]$ where Q_1 is the submatrix comprised of columns 1 to 6, Q_2 corresponds to column 7 and Q_3 comprises columns 8 to $3m$. Finally, let

$$V_P = P_1 V P_1^\top, \quad V_Z = P_2^\top V P_2^\top, \quad V_S = P_3 V P_3^\top, \quad (93)$$

where $P_k = Q_k Q_k^\top$. Variance matrices V_P , V_Z and V_S represent the variance components with respect to Position, siZe (or scale) and Shape, respectively. Similarly, it is possible to isolate the variance components V_{PZ} and V_{ZS} associated with position and size, and size and shape [19], respectively, with

$$V_{PZ} = P_{12} V P_{12}^\top, \quad V_{ZS} = P_{23} V P_{23}^\top = (I - Q_1 Q_1^\top) V (I - Q_1 Q_1^\top)^\top, \quad (94)$$

where

$$P_{12} = [Q_1 \ Q_2][Q_1 \ Q_2]^\top, \quad P_{23} = [Q_2 \ Q_3][Q_2 \ Q_3]^\top.$$

The matrices P_k are projections with $P_k = P_k^\top$, $P_k P_k = P_k$, $k = 1, 2, 3$. Since Q is an orthogonal matrix

$$I = QQ^\top = [Q_1 \ Q_2 \ Q_3][Q_1 \ Q_2 \ Q_3]^\top = Q_1 Q_1^\top + Q_2 Q_2^\top + Q_3 Q_3^\top = P_1 + P_2 + P_3. \quad (95)$$

We can therefore write $\mathbf{x} = (P_1 + P_2 + P_3)\mathbf{x} = Q_1 \mathbf{p} + Q_2 \lambda + Q_3 \mathbf{s}$, where $\mathbf{p} = Q_1^\top \mathbf{x}$, $\lambda = Q_2^\top \mathbf{x}$ and $\mathbf{s} = Q_3^\top \mathbf{x}$ represent an alternative parametrization of \mathbf{x} in terms of six position parameters \mathbf{p} , one size parameter λ , and $3m - 7$ shape parameters \mathbf{s} .

A similar decomposition can be undertaken for point clouds in 2 dimensions.

.1.1 Traces of the variance matrices

Using (95), we can write

$$V = (P_1 + P_2 + P_3)V(P_1 + P_2 + P_3)^\top = V_P + V_Z + V_S + \sum_{k \neq j} P_k V P_j^\top.$$

This means that in general $V \neq V_P + V_Z + V_S$. However, we recall that for matrices for which AB and BA can be formed, $\text{trace}(AB) = \text{trace}(BA)$, [25], so that if $k \neq j$ then $\text{trace}(P_k V P_j^\top) = \text{trace}(P_k P_j^\top V) = 0$, since $P_k P_j^\top = \mathbf{0}$. Regarding the trace of a variance matrix as an aggregate measure of the total variance, we have

$$\text{trace}(V) = \text{trace}(V_P) + \text{trace}(V_Z) + \text{trace}(V_S) = \text{trace}(V_P) + \text{Tr}(V_Z),$$

so that in terms of this aggregate measure, no information is lost in the decomposition.

.1.2 Consistency of the decomposition

The projections P_k are determined by \mathbf{x} and, applying the process twice, we have $P_k P_j V P_j^\top P_k^\top = P_k V P_k^\top$, if $k = j$, and is zero otherwise. Thus, V_P has no component of variance relating to size or shape, V_Z has no component of variance relating to position or shape, etc.

.1.3 Decomposition for specific classes of variance matrix V

If $V = \sigma^2 I$, then $\text{trace}(V_P) = 6\sigma^2$, $\text{trace}(V_Z) = \sigma^2$ and $\text{trace}(V_S) = (3m - 7)\sigma^2$. For large m , the variance is dominated by the uncertainty in shape; random, uncorrelated perturbations will have only a small position and size component.

Suppose $\hat{\mathbf{x}}_i = R(\boldsymbol{\alpha})(\mathbf{x}_i - \mathbf{x}_0)$ is a rigid body transformation of \mathbf{x}_i depending on three rotation angles $\boldsymbol{\alpha}$ and three translation parameters \mathbf{x}_0 . Assuming $\mathbf{t} = \begin{bmatrix} \mathbf{x}_0 \\ \boldsymbol{\alpha} \end{bmatrix}$ is associated with variance matrix $V_{\mathbf{t}}$, let G be the $3m \times 6$ matrix of partial derivatives of $\hat{\mathbf{x}}$ with respect to \mathbf{t} and set $V = G V_{\mathbf{t}} G^\top$. Then V is the variance matrix associated with the $3m \times 1$ vector $\hat{\mathbf{x}}$ derived by propagating the variance associated with \mathbf{t} through to $\hat{\mathbf{x}}$. Then the variance decomposition for V has $V_P = V$ and $V_Z = V_S = \mathbf{0}$.

Now suppose $V = \sigma_Z^2 \mathbf{x} \mathbf{x}^\top$ so that V represents a variance matrix consisting solely in the uncertainty contribution from a scale parameter λ . In general the variance decomposition of V will have a non-zero position component V_P as well as a non-zero size component V_Z ; the shape component V_S will be zero. However, for mean centred data with $\sum x_i = \sum y_i = \sum z_i = 0$, then $V_Z = V$ and $V_P = V_S = \mathbf{0}$.

.1.4 Uncertainties associated with distances

If d_{ij} is the distance between \mathbf{x}_i and \mathbf{x}_j and \mathbf{g}_{ij} the $3m$ -vector of partial derivatives of d_{ij} with respect to \mathbf{x} , then

$$u^2(d_{ij}) = \mathbf{g}_{ij}^\top V \mathbf{g}_{ij} = \mathbf{g}_{ij}^\top V_{ZS} \mathbf{g}_{ij}, \quad \mathbf{g}_{ij}^\top V_P \mathbf{g}_{ij} = 0;$$

uncertainty in position does not contribute to uncertainty in distance.

.1.5 Uncertainties associated with angles

If α_{ijk} is the angle between $\mathbf{x}_i - \mathbf{x}_j$ and $\mathbf{x}_i - \mathbf{x}_k$ and \mathbf{g}_{ijk} the $3m$ -vector of partial derivatives of α_{ijk} with respect to \mathbf{x} , then

$$u^2(\alpha_{ijk}) = \mathbf{g}_{ijk}^\top V \mathbf{g}_{ijk} = \mathbf{g}_{ijk}^\top V_S \mathbf{g}_{ijk}, \quad \mathbf{g}_{ijk}^\top V_P \mathbf{g}_{ijk} = \mathbf{g}_{ijk}^\top V_Z \mathbf{g}_{ijk} = \mathbf{g}_{ijk}^\top V_{PZ} \mathbf{g}_{ijk} = 0;$$

uncertainty in angle depends only on the uncertainty in shape.

.2 Temporal correlation associated with systematic effects

The models so far have considered systematic effects \mathbf{e}_i and random effects $\boldsymbol{\epsilon}_i$. The distinction is important in the characterisation of repeated measurements: the systematic effects are considered constant while the random effects are re-sampled for each repeat measurement. One way to think of this is that the systematic effects are highly correlated over time while the random effects are completely independent with respect to time. In practice, it is more reasonable to regard the systematic effects as changing over time but do so over much longer timescales than the random effects. A GP model can be used to model this in which each systematic effect e is associated with

spatio-temporal coordinates (\mathbf{x}, t) and the correlation between effects e and e' depends both on the spatial and temporal separation:

$$\begin{aligned} \text{cov}(e, e') &= k(\mathbf{x}, \mathbf{x}')k(t, t') \\ &= \sigma_E^2 \exp\{-\|\mathbf{x} - \mathbf{x}'\|^2/\lambda_X^2\} \exp\{-(t - t')^2/\lambda_T^2\}. \end{aligned} \quad (96)$$

The temporal correlation can be important in uncertainty evaluation in comparator mode [20, 29] in which the CMM is used to measure of a calibrated master artefact and a test artefact nominally of the same geometry using the same measurement strategy. The test artefact can be calibrated under the assumption that the systematic effects are constant so that any difference in the the measurement results for the two artefacts is due to a difference in geometry and random effects. The temporal correlation model can be used to account for the fact that the systematic effects may have drifted in time resulting in a quantifiable increase in the uncertainties associated with the calibration of the test artefact due to instrument drift.

.2.1 Spatio-temporal correlation for scale and squareness effects

In section I.3.5, we considered a simple model for scale and squareness effects depending on seven parameters \mathbf{b} . The model is particularly appropriate for modelling the measurement of a workpiece at one location in the CMM measuring volume. Suppose the same workpiece is measured at a number of positions in the CMM. Is it plausible that exactly the same squareness and scale errors apply in each position? Similarly, suppose the same (or similar) workpiece is measured at a (much) later time. Can we be sure that the behaviour of the CMM has not drifted in the intervening period? We can use spatio-temporal correlation concepts to extend the model as follows.

Suppose there are n_K sets of measurements X_k , $k = 1, \dots, n_K$, each associated with a 7-vector \mathbf{b}_k of scale and squareness errors. The sets of measurements may involve different times or different positions or both. We assume that the variance matrix associated with each \mathbf{b}_k is the same, denoted by V_{B_0} . We control the degree of correlation between the parameters $\mathbf{b}_{1:n_K}$ through an $n_K \times n_K$ correlation matrix V_T with $0 \leq V_T(k, \ell) = t_{k\ell} \leq 1$ and $t_{kk} = 1$. For example, the correlation matrix could be constructed using spatio-temporal correlation kernel similar to that in (96). The $7n_K \times 7n_K$

variance matrix V_B associated with all the effects $\mathbf{b}_{1:n_K}$ is constructed as¹²

$$V_B = \begin{bmatrix} t_{11}V_{B_0} & t_{12}V_{B_0} & \cdots & t_{1n_K}V_{B_0} \\ t_{21}V_{B_0} & t_{22}V_{B_0} & \cdots & t_{2n_K}V_{B_0} \\ \vdots & & \ddots & \vdots \\ t_{n_K1}V_{B_0} & t_{n_K2}V_{B_0} & \cdots & t_{n_Kn_K}V_{B_0} \end{bmatrix}.$$

Let $G_{X_k|B_k}$ be the sensitivity matrix of X_k with respect to \mathbf{b}_k and $G_{X|B}$ the block diagonal matrix with $G_{X_k|B_k}$ on the k th diagonal block. Then the variance matrix $V_{X|B}$ associated with point coordinates $X_{1:n_K}$ due to the effects $\mathbf{b}_{1:n_K}$ is given by

$$V_{X|B} = G_{X|B}V_B G_{X|B}^\top.$$

The matrix $V_{X|B}$ is constructed from n_K^2 blocks

$$t_{k\ell}G_{X_k|B_k}V_{B_0}G_{X_\ell|B_\ell}^\top.$$

Similarly, let $G_{A_k|B_k}$ be the sensitivity matrix of parameters \mathbf{a}_k , derived from data set X_k , with respect to \mathbf{b}_k and $G_{A|B}$ the block diagonal matrix with $G_{A_k|B_k}$ on the k th diagonal block. Then the variance matrix $V_{A|B}$ associated with $\mathbf{a}_{1:n_K}$ due to the effects $\mathbf{b}_{1:n_K}$ is given by

$$V_{A|B} = G_{A|B}V_B G_{A|B}^\top.$$

The matrix $V_{A|B}$ is constructed from n_K^2 blocks

$$t_{k\ell}G_{A_k|B_k}V_{B_0}G_{A_\ell|B_\ell}^\top.$$

.3 Indefinite integrals

The following integral are relevant to estimating sensitivity matrices associated with fitting circles, spheres, cylinders and cones to data according to

¹²Thus V_B is the tensor product, $V_{B_0} \otimes V_T$, of V_{B_0} with V_T .

the least-squares criterion, section I.5.2:

$$\begin{aligned}\int \sin \theta d\theta &= -\cos \theta + C, \\ \int \cos \theta d\theta &= \sin \theta + C, \\ \int \sin^2 \theta d\theta &= \frac{1}{2}\theta - \frac{1}{4}\sin 2\theta + C, \\ \int \cos^2 \theta d\theta &= \frac{1}{2}\theta + \frac{1}{4}\sin 2\theta + C, \\ \int \sin \theta \cos \theta d\theta &= -\frac{1}{4}\cos 2\theta + C, \\ \int \cos^3 \theta d\theta &= \sin \theta - \frac{1}{3}\sin^3 \theta + C, \\ \int \sin^3 \theta d\theta &= \frac{1}{3}\cos^3 \theta - \cos \theta + C, \\ \int \sin^2 \theta \cos \theta &= \frac{1}{3}\sin^3 \theta + C, \\ \int \sin \theta \cos^2 \theta &= -\frac{1}{3}\cos^3 \theta + C.\end{aligned}$$

Bibliography

- [1] R. M. Barker, M. G. Cox, A. B. Forbes, and P. M. Harris. Software Support for Metrology Best Practice Guide no. 4: Modelling Discrete Data and Experimental Data Analysis. Technical Report DEM-ES 018, National Physical Laboratory, Teddington, 2007.
- [2] BIPM, IEC, IFCC, ILAC, ISO, IUPAC, IUPAP, and OIML. Evaluation of measurement data — Guide to the expression of uncertainty in measurement. Joint Committee for Guides in Metrology, JCGM 100:2008.
- [3] BIPM, IEC, IFCC, ILAC, ISO, IUPAC, IUPAP, and OIML. Evaluation of measurement data — Supplement 1 to the “Guide to the expression of uncertainty in measurement” — Propagation of distributions using a Monte Carlo method. Joint Committee for Guides in Metrology, JCGM 101:2008.
- [4] BIPM, IEC, IFCC, ILAC, ISO, IUPAC, IUPAP, and OIML. Evaluation of measurement data — Supplement 2 to the “Guide to the expression of uncertainty in measurement” — extension to any number of output quantities. Joint Committee for Guides in Metrology, JCGM 102:2011.
- [5] BIPM, IEC, IFCC, ISO, IUPAC, IUPAP, and OIML. *Guide to the Expression of Uncertainty in Measurement*. International Organization for Standardization, Geneva, second edition, 1995.
- [6] P. T. Boggs, R. H. Byrd, and R. B. Schnabel. A stable and efficient algorithm for nonlinear orthogonal distance regression. *SIAM Journal of Scientific and Statistical Computing*, 8(6):1052–1078, 1987.
- [7] M. G. Cox, M. P. Dainton, and P. M. Harris. Software Support for Metrology Best Practice Guide No. 6: Uncertainty and Statistical Mod-

- elling. Technical report, National Physical Laboratory, Teddington, 2001.
- [8] M. G. Cox and A. B. Forbes. Efficient solution of large scale calibration problems. In *SIMAI 98 Abstracts*, pages 337–340, Rome, 1998. SIMAI.
- [9] M. G. Cox, A. B. Forbes, P. M. Harris, and G. N. Peggs. Determining CMM behaviour from measurements of standard artefacts. Technical Report CISE 15/98, National Physical Laboratory, Teddington, March 1998.
- [10] M. G. Cox and P. M. Harris. SSfM Best Practice Guide No. 6, Uncertainty evaluation. Technical Report MS 6, National Physical Laboratory, Teddington, UK, 2010.
- [11] N. Cressie and C. K. Wikle. *Statistics for Spatio-Temporal Data*. Wiley, Hoboken, New Jersey, 2011.
- [12] P. C. Cresto. Self-calibration with application to CMMs geometry error correction. In P. Ciarlina, M. G. Cox, R. Monaco, and F. Pavese, editors, *Proceedings of the International Workshop on Advanced Mathematical Tools for Metrology, Turin*, pages 167–174. World Scientific, 1994.
- [13] A. B. Forbes. Least-squares best-fit geometric elements. Technical Report DITC 140/89, National Physical Laboratory, Teddington, 1989.
- [14] A. B. Forbes. Least squares best fit geometric elements. In J. C. Mason and M. G. Cox, editors, *Algorithms for Approximation II*, pages 311–319, London, 1990. Chapman & Hall.
- [15] A. B. Forbes. Evaluation of CMM measurements of hole plates in interlaboratory comparisons. In D. Pham, editor, *Laser Metrology and Machine Performance VIII*, pages 368–377, Bedford, 2007. euspen.
- [16] A. B. Forbes. Weighting observations from multi-sensor coordinate measuring systems. Technical report, National Physical Laboratory, Teddington, 2011. NIMTech Deliverable 3.3.3, version 1.
- [17] A. B. Forbes. Uncertainty associated with form assessment in coordinate metrology. *Int. J. of Metrol. and Qual. Eng.*, 4:17–22, 2013.
- [18] A. B. Forbes. Uncertainties associated with position, scale and shape. In *XXII World Congress of the International Measurement Confederation (IMEKO)*. IOP Conference Series: **1065**, 2018. doi:10.1088/1742-6596/1065/14/142023.

- [19] A. B. Forbes and P. M. Harris. Uncertainty associated with co-ordinate measurements. In P. Shore, editor, *Laser Metrology and Machine Performance VII*, pages 30–39, Bedford, 2005. Euspen.
- [20] A. B. Forbes, A. Mengot, and K. Jonas. Uncertainty associated with coordinate measurement in comparator mode. In *Laser Metrology and Machine Performance XI, University of Huddersfield, March 2015*, Bedford, 2015. euspen.
- [21] A. B. Forbes and H. D. Minh. Form assessment in coordinate metrology. In E. H. Georgoulis, A. Iske, and J. Levesley, editors, *Approximation Algorithms for Complex Systems*, Springer Proceedings in Mathematics, Vol 3, pages 69–90, Heidelberg, 2011. Springer-Verlag.
- [22] A. B. Forbes, A. Wilson, P. Saunders, and N. Orchard. Effect of form errors in datum features on evaluated geometries. In *16th International Congress of Metrology, 2013*. EDP Sciences, 2013. DOI: 10.1051/metrology/201308003.
- [23] A. Gelman, J. B. Carlin, H. S. Stern, D. B. Dunson, A. Vehtari, and D. B. Rubin. *Bayesian Data Analysis*. Chapman & Hall/CRC, Boca Raton, Fl., third edition, 2014.
- [24] P. E. Gill, W. Murray, and M. H. Wright. *Practical Optimization*. Academic Press, London, 1981.
- [25] G. H. Golub and C. F. Van Loan. *Matrix Computations*. John Hopkins University Press, Baltimore, third edition, 1996.
- [26] G.H. Golub and C.F. Van Loan. *Matrix Computations*. Johns Hopkins University Press, Baltimore, fourth edition, 2013.
- [27] H.-P. Helfrich and D. Zwick. A trust region method for implicit orthogonal distance regression. *Numerical Algorithms*, 5:535 – 544, 1993.
- [28] International Organization for Standardization, Geneva. *ISO/IEC 17043: Conformity Assessment – General Requirements for Proficiency Testing*, 2010.
- [29] ISO. *ISO 15530: Geometric Product Specifications (GPS) – Coordinate Measuring Machines (CMM): Technique for determining the uncertainty of measurement - Part 3: Use of calibrated workpieces or standards*. International Organization for Standardization, Geneva, 2011.

-
- [30] M. C. Kennedy and A. O’Hagan. Bayesian calibration of computer models. *J. Roy. Stat. Soc. B*, 64(3):425–464, 2001.
- [31] J. P. Kruth, P. Vanherk, and L. de Jonge. Self-calibration method and software error correction for three dimensional co-ordinate measuring machines using artefact measurements. *Measurement*, 14:1–11, 1994.
- [32] H. Kunzmann, E. Trapet, and F. Waldele. A uniform concept for calibration, acceptance test and periodic inspection of co-ordinate measuring machines using reference objects. *Annals of the CIRP*, 39:561–564, 1990.
- [33] A. Linkeova, P. Skalnik, and V. Zeleny. Calibrated CAD model of freeform standard. In *IMEKO World Congress XXI, 30 August – 4 September, 2015*, Prague, 2015. IMEKO.
- [34] D. J. C. MacKay. *Information Theory, Inference and Learning Algorithms*. Cambridge University Press, 2003.
- [35] H. S. Migon and D. Gamerman. *Statistical Inference: an Integrated Approach*. Arnold, London, 1999.
- [36] D. C. Montgomery and G. C. Runger. *Applied Statistics and Probability for Engineers*. John Wiley and Sons, 2003.
- [37] W. H. Press, S. A. Teukolsky, W. T. Vetterling, and B. P. Flannery. *Numerical Recipes: the Art of Scientific Computing*. Cambridge University Press, Cambridge, third edition, 2007.
- [38] C. E. Rasmussen and C. K. I. Williams. *Gaussian Processes for Machine Learning*. MIT Press, Cambridge, Mass., 2006.
- [39] O. Sato, T. Takatsuji, and A. Balsamo. Practical experiment design of task-specific uncertainty evaluation for coordinate metrology. In F. Pavese, A. B. Forbes, N.-F. Yang, and A. Chunovkina, editors, *Advanced Mathematical and Computational Tools for Metrology XII*, pages 381–389, Singapore, 2022. World Scientific.
- [40] Osamu Sato, Toshiyuki Takatsuji, Yuka Miura, and Shouichi Nakanishi. GD&T task specific measurement uncertainty evaluation for manufacturing floor. *Measurement: Sensors*, 18:100141, 2021.
- [41] G. Zhang, R. Ouyang, B. Lu, R. Hocken, R. Veale, and A. Donmez. A displacement method for machine geometry calibration. *Annals of the CIRP*, 37:515–518, 1988.

SECTION II

METHOD B2

An a priori method for CMM
uncertainty evaluation based on
essential sets of measurement
points

Table of contents

II-1	Introduction.....	2
II-2	Theoretical background.....	3
II-3	Comparison of method B2 with a pure geometrical approach.....	3
II-4	Essential sets of points and their relations	7
II-4.1	Angle between planes	7
II-4.2	Flatness.....	8
II-4.3	Coaxiality.....	9
II-4.4	Position of median lines relative to a datum system constructed from a plane, an axis and a symmetry plane	9
II-4.5	Complete list.....	10
II-5	Validation of the method B2	12
II-5.1	Procedure.....	12
II-5.2	Coaxiality.....	14
II-5.2.1	Validation plan.....	14
II-5.2.2	Summary of the validation plan.....	16
II-5.2.3	Results	17
II-5.3	Diameter of an external circle.....	25
II-5.3.1	Validation plan.....	25
II-5.4	Results	25
II-5.5	Diameter of an internal circle.....	26
II-5.5.1	Validation plan.....	26
II-5.5.2	Results	27
II-5.6	Diameter of the arc of a circle	28
II-5.6.1	Validation plan (single arcs)	28
II-5.6.2	Results (single arcs).....	28
II-5.6.3	Validation plan (average of multiple arcs)	30
II-5.6.4	Results (average of multiple arcs).....	31
II-5.7	Inter-method comparison	31
II-5.7.1	Validation plan.....	31
II-5.7.2	Connecting rod.....	32
II-5.7.3	MFC standard (high quality)	34
II-5.7.4	MFC standard (low quality)	36
II-6	Conclusions.....	37
II-7	References	39
	Annex II-A Details of the chi-squared analysis of the cylinder square	41

II-1 Introduction

In coordinate metrology, the elementary components of any measured geometry are features such as planes and cylinders. These features may be combined to form more complex measurands. For instance, a geometry consists of a pin nominally normal to a flat, and the measurand is how far the top of the pin is from the flat. This involves three features: the flat, and the lateral surface and the top of the pin. The points measured on these features are *associated* by best-fitting [1] (3.4.1.4) to as many ideal features, resulting in two planes (the flat and the pin top) and a cylinder. The measurand is, e.g., the distance to the bottom plane of the intersection of the cylinder axis with the top plane¹.

One of the difficulties in evaluating the uncertainty of such measurements is that there is no closed form for the association of ideal features to measured points by best-fitting. This prevents from starting GUM main-stream of operations, the first of which is defining a measurement model.

To overcome this problem, the approach of the method B2 is based on reducing the number of points to the essence of the geometry and the measurand. These essential points are not necessarily taken from those measured (or that will be measured), they are rather fabricated points representative of the geometry and of the evaluation of the measurand. In the above example of the pin and the flat, the representative points are three on the flat and one on the pin top. The measurand is then the distance of the latter to the plane through the former. The number of essential points is minimum, no approximation occurs, and the measurand can be expressed in closed form as a function of the essential points. This effectively constitutes the measurement model and enables to evaluate the uncertainty conventionally according to the GUM, by derivation of the sensitivity coefficients. The essential points may lay on integral features (surfaces; the three on the flat in the example) or on derived features (the one on the pin top, which lays of the cylinder axis). The exact location of the essential points is not immediately related to the sampling strategy. They are taken where significant for the geometry and in a reasonable and well-behaved fashion compatible with the nominal sizes and possible impediments. In the example, the three essential points on the flat will be 120° apart to each other (symmetrically disposed) at as long a distance to the pin axis as compatible with the pin and flat sizes. If any impediment prevents from this disposition, then the essential points are taken differently; for instance, not at 120° if an obstacle is there on one side, or not all at the same distance to the pin axis if the flat exhibits a high shape factor.

The loose relationship to the actual or planned probing strategy constitutes the main approximation underpinning method B2. The effect of the point redundancy, or of the exact location of individual points is not captured and then overlooked. The method overlooks also that essential points taken on derived features stem from a number of elementary points, as opposed to those taken on integral features. The challenge of this method is that few well-selected essential points dominate the geometry and are in fact enough for an approximated but relatively easy evaluation of the uncertainty.

In any measurement, there is no such measurand as the absolute position or orientation: any position or orientation is relative other features forming a datum (system). Ultimately, the fundamental pieces of information derived by measurements are *distances* between pairs of features. The measurand in the above example is explicitly a distance, but it could have been expressed as the *position* of the pin top when the flat is taken as datum. Distances can be decomposed to differences of coordinates of individual points. At the end, the measurand can be expressed as a function of the coordinate differences of the essential points.

The capability of a CMM to measure distances accurately is captured by the *length measurement error*, E_L , a metrological characteristic of the CMMs' defined in EN ISO 10360 [2]

¹ Alternative definitions of the measurand are possible, for example the distance between the intersections of the cylinder axis with the two planes.

likely available for most CMMs under metrological confirmation regime. E_L (or $E_{L,MPE}$) is used to derive the input uncertainties in the measurement model.

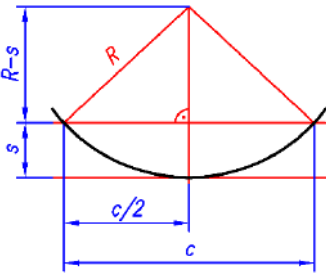
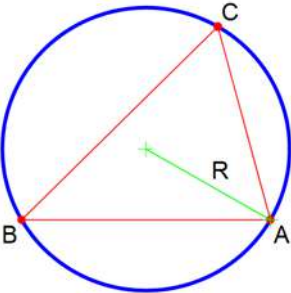
II-2 Theoretical background

Details on the assumptions as well as the analysis of some models developed for this approach (Method B2) was published in [3] and [4]. Their most important characteristics are the following:

- According to the classification of techniques for uncertainty estimation in coordinate metrology given in CEN ISO/TS 15530-1 [5], the method belongs to the "sensitivity analysis" category.
- The method is in line with the GUM [6]. A model is developed for individual coordinate measurements from which the sensitivity coefficients are derived. The input uncertainties are evaluated and propagated to the combined uncertainty by multiplication by the sensitivity coefficients.
- The input standard uncertainties are type B evaluated as suggested in EN ISO 14253-2 [7] (8.3.2). The largest possible error a is multiplied by a coefficient b that accounts for the known/assumed probability distribution of the error: $u = ab$. When the error is caused by a measuring instruments, [7] (8.4.5) suggests to give a the value of the MPE (*Maximum Permissible Error*) assigned to the instrument. In the case of a CMM measuring point-to-point distances—which is that of interest for the method—the relevant MPE is $E_{L,MPE}$ (EN ISO 10360-2 [2]): $a = E_{L,MPE}$. In the absence of other information, the probability distribution must be assumed: if uniform, then $b = 1/\sqrt{3}$; if normal, $b = 1/2$ or $b = 1/3$. When the actual results of the acceptance or reverification test of a specific CMM are available, then the values a and b can derived based on them instead of the more generic MPE value and assumption on the distribution. This documents illustrates this latter case.
- The method proceeds per closed form equations, and is similar in that to cases known from classical geometrical metrology.

II-3 Comparison of method B2 with a pure geometrical approach

Here below is a comparison between the measurement and uncertainty evaluation of the radius of a circle arc with pure geometry and GUM evaluation and coordinate measurement and method B2.

Pure geometry and GUM evaluation	Coordinate measurement and method B2
	
Measured quantities	
Sag s and chord c	Coordinates of points A, B, C

$R(c, s) = \frac{c^2}{8s} + \frac{s}{2}$	$R = \frac{abc}{4S}$ <p>where a, b, c are the side lengths; S is the area of the triangle.</p> <p>The sides lengths are the Cartesian distance between vertex pairs:</p> $a = \sqrt{x_{BC}^2 + y_{BC}^2 + z_{BC}^2}$ $b = \sqrt{x_{CA}^2 + y_{CA}^2 + z_{CA}^2}$ $c = \sqrt{x_{AB}^2 + y_{AB}^2 + z_{AB}^2}$ <p>where, e.g., $x_{BC} = x_C - x_B$ is the difference of the x coordinates of the vertexes B and C, and similarly for the others.</p> <p>The area S is calculated from the geometrical interpretation of the vector product</p> $S = \frac{\ \mathbf{AB} \times \mathbf{AC}\ }{2}$
--	---

Measurement model

$R(c, s) = \frac{c^2}{8s} + \frac{s}{2}$	$R(x_{AB}, y_{AB}, z_{AB}, x_{AC}, y_{AC}, z_{AC}, x_{BC}, y_{BC}, z_{BC}) = \frac{abc}{2M}$ <p>where</p> $M = \sqrt{M_x^2 + M_y^2 + M_z^2}$ $M_x = y_{AB} \cdot z_{AC} - z_{AB} \cdot y_{AC}$ $M_y = z_{AB} \cdot x_{AC} - x_{AB} \cdot z_{AC}$ $M_z = x_{AB} \cdot y_{AC} - y_{AB} \cdot x_{AC}$
--	--

Input quantities for models

<p>Lengths c and s</p>	<p>Differences of coordinates $x_{AB}, y_{AB}, z_{AB}, x_{AC}, y_{AC}, z_{AC}, x_{BC}, y_{BC}, z_{BC}$</p>
--	---

Combined standard uncertainty (assuming no correlation)

$$u_R = \sqrt{\left(\frac{\partial R}{\partial c} \cdot u_c\right)^2 + \left(\frac{\partial R}{\partial s} \cdot u_s\right)^2}$$

where

$$\frac{\partial R}{\partial c} = \frac{c}{4s}$$

$$\frac{\partial R}{\partial s} = \frac{-c^2}{8s^2} + \frac{1}{2}$$

$$u_R = \sqrt{\sum_{i=1}^9 \left(\frac{\partial R}{\partial x_i} u_{xi}\right)^2}$$

where the differences in x, y, z coordinates are generally designated as x_i , the standard uncertainties of their measurements are generally designated as u_{xi}

$$\frac{\partial R}{\partial x_{AB}} = \frac{abx_{AB}}{2cM} - \frac{abc(-M_y z_{AC} + M_z y_{AC})}{2M^3}$$

$$\frac{\partial R}{\partial y_{AB}} = \frac{aby_{AB}}{2cM} - \frac{abc(M_x z_{AC} - M_z x_{AC})}{2M^3}$$

$$\frac{\partial R}{\partial z_{AB}} = \frac{abz_{AB}}{2cM} - \frac{abc(-M_x y_{AC} + M_y x_{AC})}{2M^3}$$

$$\frac{\partial R}{\partial x_{AC}} = \frac{acx_{AC}}{2bM} - \frac{abc(M_y z_{AB} - M_z y_{AB})}{2M^3}$$

$$\frac{\partial R}{\partial y_{AC}} = \frac{acy_{AC}}{2bM} - \frac{abc(-M_x z_{AB} + M_z x_{AB})}{2M^3}$$

$$\frac{\partial R}{\partial z_{AB}} = \frac{acz_{AC}}{2bM} - \frac{abc(M_x y_{AB} - M_y x_{AB})}{2M^3}$$

$$\frac{\partial R}{\partial x_{CB}} = \frac{bcx_{CB}}{2aM}$$

$$\frac{\partial R}{\partial y_{CB}} = \frac{bcy_{CB}}{2aM}$$

$$\frac{\partial R}{\partial z_{CB}} = \frac{bcz_{CB}}{2aM}$$

The above equations are in scalar notation and may appear complicated. They can be expressed more compactly by using vectorial notation:

$$\nabla_{AB}R = \frac{ab}{4S} \mathbf{n}_{AB} - \frac{ab}{8S^2} (\mathbf{AC} \times \mathbf{m})$$

$$\nabla_{AC}R = \frac{ac}{4S} \mathbf{n}_{AC} - \frac{ab}{8S^2} (\mathbf{m} \times \mathbf{AB})$$

$$\nabla_{BC}R = \frac{bc}{4S} \mathbf{n}_{BC}$$

where

$\nabla_v R = \left(\frac{\partial R}{\partial v_i}\right)$ is the gradient of R with respect to the vectors of the triangle sides ($v = \{\mathbf{AB}, \mathbf{AC}, \mathbf{BC}\}$);

$\mathbf{n}_v = \frac{v}{\|v\|}$ are the unit vectors of the triangle sides ($v = \{\mathbf{AB}, \mathbf{AC}, \mathbf{BC}\}$);

	<p>$\mathbf{m} = \frac{\mathbf{AB} \times \mathbf{AC}}{\ \mathbf{AB} \times \mathbf{AC}\ }$ is the unit vector normal to the triangle.</p> <p>The above equations are derived considering that, in general, the gradient of the norm of a vector \mathbf{w} relative to a vector \mathbf{v} is</p> $\nabla_{\mathbf{v}} \ \mathbf{w}\ = \mathbf{J}_{\mathbf{w} \mathbf{v}}^T \mathbf{n}_{\mathbf{w}}$ <p>where</p> <p>$\mathbf{J}_{\mathbf{w} \mathbf{v}} = \left(\frac{\partial w_i}{\partial v_j} \right)$ is the Jacobian matrix of \mathbf{w} relative to \mathbf{v}</p> <p>$\mathbf{n}_{\mathbf{w}} = \frac{\mathbf{w}}{\ \mathbf{w}\ }$ is the unit vector of \mathbf{w}</p>
--	--

Example of numerical calculation

$R = 50 \text{ mm}, E_{L,MPE} = 2 + 0.004 L, b=1/3$

<p>$u_s = E_{L,MPE}/3 = (2 + 0,004s)/3$ $u_c = E_{L,MPE}/3 = (2 + 0,004c)/3$</p>	<p>$u_{x_i} = E_{L,MPE}/3 = (2 + 0,004x_i)/3$ A, B, C taken on a horizontal plane, B, C at the extremes and A at the midpoint of the arc</p>
---	--

Uncertainty budget for $s = 8 \text{ mm}$

	x_i/mm	$\frac{\partial R}{\partial x_i}$	$u_i/\mu\text{m}$	$\frac{\partial R}{\partial x_i} u_i/\mu\text{m}$		x_i/mm	$\frac{\partial R}{\partial x_i}$	$u_i/\mu\text{m}$	$\frac{\partial R}{\partial x_i} u_i/\mu\text{m}$	
s	8.000	-5.25	0.68	-3.56		x_{AB}	-27.129	-0.774	0.703	-0.544
c	54.259	1.70	0.75	1.25		y_{AB}	-8.00	2.625	0.677	1.778
			$u_R =$	3.77		z_{AB}	0.00	0.000	0.667	0.000
						x_{AC}	27.129	0.774	0.703	0.544
						y_{AC}	-8.00	2.625	0.677	1.778
						z_{AC}	0.00	0.000	0.667	0.000
						x_{BC}	54.259	0.922	0.739	0.681
						y_{BC}	0.00	0.000	0.667	0.000
						z_{BC}	0.00	0.000	0.667	0.000
								$u_R =$	2.72	

Uncertainty budget for $s = 25 \text{ mm}$

	x_i/mm	$\frac{\partial R}{\partial x_i}$	$u_i/\mu\text{m}$	$\frac{\partial R}{\partial x_i} u_i/\mu\text{m}$		x_i/mm	$\frac{\partial R}{\partial x_i}$	$u_i/\mu\text{m}$	$\frac{\partial R}{\partial x_i} u_i/\mu\text{m}$	
s	25.000	-1.00	0.70	-0.70		x_{AB}	-43.301	-0.289	0.724	-0.209
c	86.603	0.87	0.78	0.68		y_{AB}	-25.000	0.500	0.700	0.350
			$u_R =$	0.97		z_{AB}	0.000	0.000	0.667	0.000
						x_{AC}	43.301	0.289	0.724	0.209
						y_{AC}	-25.000	0.500	0.700	0.350
						z_{AC}	0.000	0.000	0.667	0.000
						x_{BC}	86.603	0.577	0.782	0.452
						y_{BC}	0.000	0.000	0.667	0.000
						z_{BC}	0.000	0.000	0.667	0.000
								$u_R =$	0.732	

Uncertainty budget for $s = 50$ mm

	x_i/mm	$\frac{\partial R}{\partial x_i}$	$u_i/\mu\text{m}$	$\frac{\partial R}{\partial x_i} u_i/\mu\text{m}$		x_i/mm	$\frac{\partial R}{\partial x_i}$	$u_i/\mu\text{m}$	$\frac{\partial R}{\partial x_i} u_i/\mu\text{m}$	
s	50.000	0	0.73	0	$u_R = 0.40$	x_{AB}	-50.000	0.0	0.733	0.000
c	100.001	0.5	0.8	0.40		y_{AB}	-50.000	0.0	0.733	0.000
						z_{AB}	0.000	0.0	0.667	0.000
						x_{AC}	50.000	0.0	0.733	0.000
						y_{AC}	-50.000	0.0	0.733	0.000
						z_{AC}	0.000	0.0	0.667	0.000
						x_{BC}	100.000	0.5	0.800	0.400
						y_{BC}	0.000	0.0	0.667	0.000
						z_{BC}	0.000	0.0	0.667	0.000
								$u_R =$	0.400	

Comparison of results

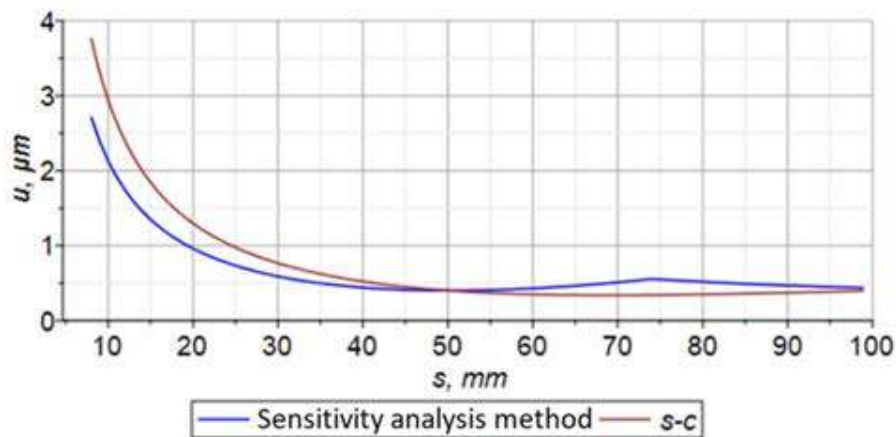


Figure II-1: Arc of a circle by three points. Comparison of uncertainties with a pure geometry approach (red) and method B2 (sensitivity analysis, blue).

The method (B2) leads to very similar uncertainties to those obtained with a pure geometry GUM-compliant analysis, when the assumption of the input uncertainty is the same (based on the point-to-point MPE).

II-4 Essential sets of points and their relations

Method B2 treats coordinate measurements as indirect measurements on an essential (minimal) set of points, with their differences in coordinates taken as input quantities in the measurement model. It allows to determine the measurement uncertainty of all geometric characteristics, namely distances, angles, form, orientation, location and run-out deviations [8].

Examples of essential sets of points and the basic equations for the derivation of such characteristics are given below.

II-4.1 Angle between planes

The minimum number of points is 6. They are divided in two triples, (A, B, C) and (K, L, M), each defining a plane.

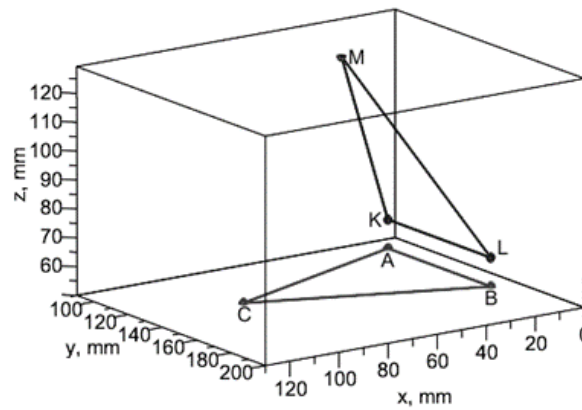


Figure II-2: Essential set of points for measuring an angle between planes.

The angle between planes is equal to that between any vectors v and w normal to the planes:

$$\cos \alpha = \frac{v^T w}{\|v\| \|w\|}$$

The vectors v and w normal to the planes through points A, B, C and K, L, M, respectively, can be calculated using the geometric interpretation of the vector product as

$$v = AB \times AC, \quad w = KL \times KM$$

II-4.2 Flatness

Two cases should be considered, one for convex or concave surfaces, and one for twisted surfaces. In both cases the minimum number of points is 4, but their distributions on the surface are different.

In the case of convex or concave surfaces, three points A, B, C define a plane and the fourth point S the peak of the form deviation.

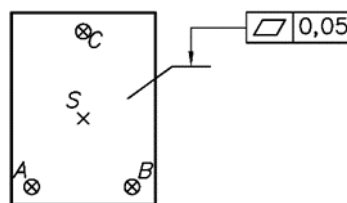


Figure II-3: Essential set of points for measuring flatness for convex or concave surfaces.

The form deviation is calculated as the distance of the central point S to the plane ABC:

$$l(AS, AB, AC) = \frac{|AS^T(AB \times AC)|}{\|AB \times AC\|}$$

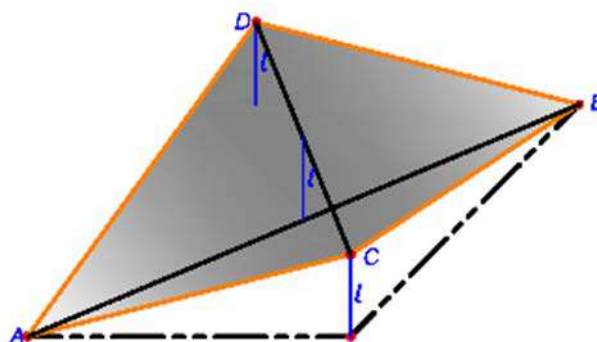


Figure II-4: Essential set of points for measuring flatness for twisted surfaces.

In the case of twisted surfaces, the points A, B defines the locus of the surface points whose local normal directions are parallel². The locus is a line, which is assumed straight so that two points define it completely. Points C, D are at the extremes of the twisted surface on opposite sides of the line AB.

The form deviation is calculated as the distance of two straight lines

$$l(AC, BA, DC) = \frac{|\mathbf{AC}^T(\mathbf{BA} \times \mathbf{DC})|}{\|\mathbf{BA} \times \mathbf{DC}\|}$$

II-4.3 Coaxiality

The minimum number of points is 3. A and B define the datum (axis of the cylinder on the left hand side in **Figure II-5**) and S defines the peak deviation of the median line of the cylinder on the right hand side in **Figure II-5** from the datum.

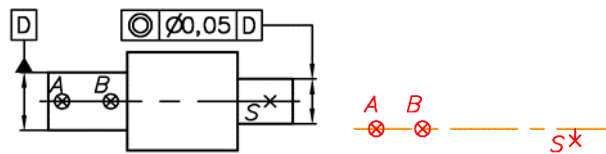


Figure II-5: Essential set of points for measuring coaxiality.

The coaxiality CX is twice the distance l of the point S to the axis AB:

$$CX = 2l(AS, AB) = 2 \frac{\|\mathbf{AS} \times \mathbf{AB}\|}{\|\mathbf{AB}\|}$$

II-4.4 Position of median lines relative to a datum system constructed from a plane, an axis and a symmetry plane

The primary datum X is a plane, which constrains the spatial orientation and orthogonally the location. The secondary datum Y is the axis of a cylinder, which constrains the location in the plane X. The tertiary datum Z is a symmetry plane, which constrains the planar orientation. As a result, the datum system fully constrains the tolerance zones.

The position of the median lines of three cylinders are toleranced and then are to be measured. They are the three bores around the workpiece centre ($\varnothing 12,5$, close to points A, B, C).

The minimum number of points is 7. A, B, C define the plane X, D the axis Y, E the plane Z, and S the peak deviation of the median line of one of the toleranced cylinders. Note that one point is sufficient for defining the axis Y because its orientation is already defined by the primary datum. Similarly, one point is sufficient for the symmetry plane Z because it is constrained to be through the axis Y.

² If the surface is regarded as a hill, the line is the crest of the hill.

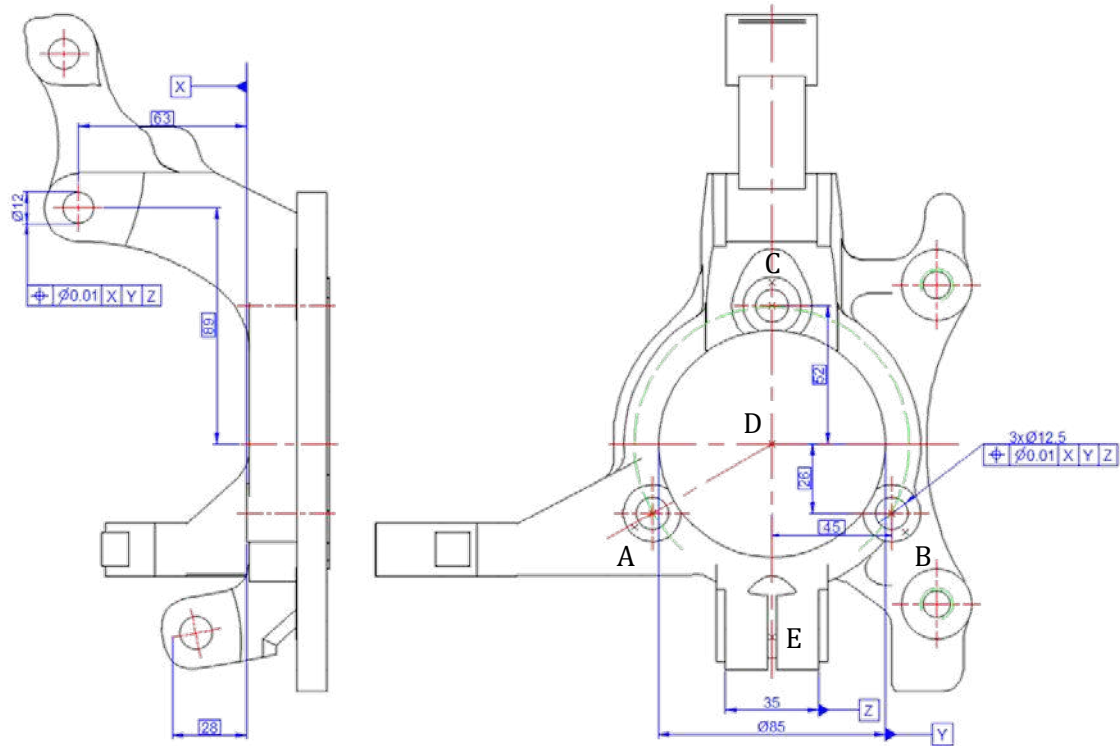


Figure II-6: Essential set of points for measuring the position of the median line relative to a datum system.

The coordinates of the point S in the plane X are³

$$S = \begin{pmatrix} ES \cdot \frac{(\mathbf{AB} \times \mathbf{AC}) \times \mathbf{DE}}{\|(\mathbf{AB} \times \mathbf{AC}) \times \mathbf{DE}\|} \\ DS \cdot \frac{[(\mathbf{AB} \times \mathbf{AC}) \times \mathbf{DE}] \times (\mathbf{AB} \times \mathbf{AC})}{\|[(\mathbf{AB} \times \mathbf{AC}) \times \mathbf{DE}] \times (\mathbf{AB} \times \mathbf{AC})\|} \end{pmatrix}$$

The position of the point S is relative to that of the theoretical exact axis of the tolerated bore. Because the position tolerance zone is defined by a diameter, the position value, POS, is twice the offset of S from the axis:

$$POS = 2\|S - C_{TED}\|$$

Where C_{TED} is the theoretical exact position of the axis. For instance, it is $C_{TED}^T = (45,26)$ for the cylinder indicated by the tolerance callout.

II-4.5 Complete list

13 models and 34 examples of their use have been identified (**Table II-1**).

Table II-1: List of geometrical relations among essential sets of points and examples of their use

#	Model	No of essential points	Examples
1	Distance between two points A and B	2	- distance between sphere centres, - distance between circle centres in a plane

³ The coordinate of S along the axis Y is not relevant. Let us consider the 2D projection onto the plane X.

2	Distance of a point S to the straight line through two points A and B	3	<ul style="list-style-type: none"> - straightness of an axis, - straightness of a generatrix, - straightness of a line on a plane - coaxiality of an axis with respect to a datum axis, - coaxiality of axes with respect to a common datum axis, - concentricity - distance between axes - position of an axis with respect to a datum axis - circular runout, - total circular runout
3	Distance of a point S to a straight line through a point A, parallel to that through two points A and B	4	<ul style="list-style-type: none"> - parallelism of axes with cylindrical tolerance zone
4	Distance of a point S to a straight line through a point A, normal to a plane through three points B, C, D	5	<ul style="list-style-type: none"> - perpendicularity of an axis with respect to a datum plane
5	Distance between of a point S to a plane through three points A, B, C	4	<ul style="list-style-type: none"> - flatness of a concave or convex surfaces - position of a point with respect to a datum plane - parallelism of an axis to a datum plane (nominally lying on the plane)
6	Distance between a point S to a plane through a point A, parallel to that through three points B, C, D	5	<ul style="list-style-type: none"> - parallelism of a plane to a datum plane - parallelism of an axis to a datum plane
7	Distance between a point S to a plane through a point A, normal to a straight line through two points B and C	4	<ul style="list-style-type: none"> - perpendicularity of a plane with respect to a datum axis, - perpendicularity of a line with respect to a datum axis, - axial run-out, - total axial run-out
8	Distance between a point S to a plane through a point A, parallel to a straight line through two points A and B, and perpendicular to a plane through three points C, D, E	6	<ul style="list-style-type: none"> - in-plane parallelism of axes
9	Distance between a point S to a plane through two points A and B, parallel to a straight line through two points C and D	5	<ul style="list-style-type: none"> - parallelism of a plane with respect to a datum axis
10	Distance of a point S to a plane through two points A and B, perpendicular to a plane through three points C, D, E	6	<ul style="list-style-type: none"> - position of a point with respect to a secondary datum plane - position of an axis with respect to a secondary datum in a datum system - position of the median plane with respect to secondary datum in a datum system - perpendicularity of a plane with respect to a datum plane

11	Distance of a point S to a plane through a point F, orthogonal to a plane through two points D and E, both planes orthogonal to a plane through three points A, B, C	7	- position of a point with respect to the tertiary datum plane, in a datum system made of three planes - position of an axis with respect to the tertiary datum plane, in a datum system made of three planes - position of a plane with respect to the tertiary datum plane, in a datum system made of three planes
12	Distance between two straight lines, each through two points (A, B) and (C, D)	4	- flatness of a twisted surface
13	Angle between two planes, each through three points (A, B, C) and (D, E, F)	6	- angle between two planes

II-5 Validation of the method B2

Case studies were investigated to validate the method B2. The experimental results gathered in the measurement campaign for validating the method A were used [9]. The procedure described in EN ISO/TS 15530-3 [10] based on 20 measurements of artefacts with known values of characteristics was followed. A deviation from it was due to the impossibility of correcting the bias.

The considered measurands were:

1. Size.
 - a. An external diameter was measured with one CMM. The artefact was an 80 mm diameter cylindrical square.
 - b. An internal diameter was measured with three CMMs. The artefacts were a 100 mm ring gauge for one CMM and a 45 mm ring gauge for the other two.
2. Size of a partial feature. The internal diameter of an arc of a circle was measured with three CMMs. The artefacts were a 100 mm ring gauge for one CMM and a 45 mm ring gauge for the other two. Four different arcs were measured.
3. Coaxiality. A cylindrical square was measured.
4. Others. In addition, uncertainties were evaluated according to the method B2 for most characteristics of the artefacts used in the project validation round-robin.

II-5.1 Procedure

The uncertainty evaluated according to [10] was compared with that evaluated according to the method B2. A chi-squared test was performed to confirm the null hypothesis of coincidence of the two methods.

The comparison was carried out in three main steps:

1. Evaluation of the uncertainty according to [10]. In turn, this was divided in two steps:

- a. The mean value \bar{y} , the bias b and the standard deviation of the measurement procedure u_p were evaluated⁴.
- b. The combined standard (u) and expanded (U) uncertainties were derived. [10] imposes to correct the bias and then to evaluate the uncertainty as⁵

$$U = 2\sqrt{u_{\text{cal}}^2 + u_p^2 + u_b^2}$$

In this logic, u_b is type B evaluated based on thermal effects only. Unfortunately, the correction of the bias was not possible, and an alternative equation to propagate the uncertainty was sought. Three were considered:

$$U_1 = 2\sqrt{u_{\text{cal}}^2 + u_p^2 + |b|}$$

$$U_2 = 2\sqrt{u_{\text{cal}}^2 + u_p^2 + b^2}$$

$$U_3 = 2\sqrt{u_{\text{cal}}^2 + u_{p0}^2}, \quad \text{with } u_{p0} = \sqrt{\frac{\sum_{i=1}^n (y_i - x_{\text{cal}})^2}{n-1}}$$

U_2 assigns b a bimodal distribution⁶. U_3 incorporates the bias into u_p (denoted as u_{p0} to avoid confusion) by calculating the root of the second-order moment about the known value x_{cal} rather than the mean value \bar{y} . It is worth noticing that the second and third equations yield practically identical results⁷, $U_2 \approx U_3$.

These equations are appropriate for errors distributed normally or at least symmetrically about the zero. This is a reasonable assumption for characteristics with nominal value (significantly) different from nought, such as dimensions and signed distances, whose errors may assume negative as well as positive values. For those errors assuming non-negative values only, such as nominally-null unsigned distances—so important in many geometrical specifications—evaluating the expanded uncertainty U as the 95 % quantile of the relevant distribution ($F^{-1}(0.95)$ where F is the cumulative distribution function) seems more appropriate. A strong candidate distribution is the Rayleigh distribution⁸, which characterises the norm of a 2D vector with independent equally-varied normally-distributed components. This results in a fourth option:

⁴ The mean value is that of the 20 measurements gathered during the procedure, $\bar{y} = \frac{1}{n-1} \sum_{i=1}^n y_i$. The bias is the deviation of the mean value from the known value, $b = \bar{y} - x_{\text{cal}}$. u_p is the standard deviation of the 20 measurements gathered during the procedure, $u_p = \sqrt{\frac{1}{n-1} \sum_{i=1}^n (y_i - \bar{y})^2}$.

⁵ The component u_w due to the workpiece is disregarded because the method B2 does not cover these effects.

⁶ A bimodal distribution with two possible discrete values, $\pm b$, with equal probability $\frac{1}{2}$ has variance $\sigma^2 = b^2$. This may be considered to match the case of uncorrected bias: the amount of bias $|b|$ is known and we pretend not to know the sign to justify the lack of correction.

⁷ The difference between the two is $U_3 - U_2 = \frac{1}{\sqrt{n-1}} \frac{b}{U}$, with $U = \frac{U_3 + U_2}{2}$. This is negligible for large n and when the bias is not dominant.

⁸ The Weibull distribution was used instead in the following analysis for practical reasons. The results are similar.

$$U_4 = 2 \sqrt{u_{\text{cal}}^2 + \left(\frac{F^{-1}(0.95)}{2}\right)^2}$$

2. The uncertainty was evaluated with the method B2.
3. Chi-square analysis was performed to test for equality the uncertainties estimated by method B2 and experimentally. The chi-squared variable was evaluated as

$$\chi^2 = \frac{n\sigma^2}{\sigma_0^2}$$

where σ and σ_0 are the standard uncertainties evaluated experimentally and with the Method B2, respectively, and n is the sample size (20). The critical values $\chi_{\text{cr1}}^2, \chi_{\text{cr2}}^2$ used as thresholds in the testing are the 2.5 % and 97.5 % quantiles, respectively, for a chi-squared distribution with 19 degrees of freedom. The test main characteristics are summarised in **Table II-2**.

The chi-squared values obtained in the analysis will be reported with a colour code (**Table II-3**).

Table II-2: Comparison of the uncertainties evaluated experimentally and with method B2: hypotheses and critical values for the chi-squared tests. σ and σ_0 are the standard uncertainties evaluated experimentally and with the Method B2, respectively.

Test	Null hypothesis, H_0	Alternative hypothesis, H_1	Null hypothesis criterion
Two-tailed	$\sigma^2 = \sigma_0^2$	$\sigma^2 \neq \sigma_0^2$	$\chi_{\text{cr1}}^2 \leq \chi^2 \leq \chi_{\text{cr2}}^2$ $\chi_{\text{cr1}}^2(0.025, 19) = 8.907$ $\chi_{\text{cr2}}^2(0.975, 19) = 32.852$

Table II-3: Colour-code for the results of the chi-squared analysis.

Colour	Criterion	Method B2 likely ...
	$\chi^2 \leq \chi_{\text{cr1}}^2$... overestimates the uncertainty
	$\chi_{\text{cr1}}^2 \leq \chi^2 \leq \chi_{\text{cr2}}^2$... properly estimates the uncertainty
	$\chi^2 > \chi_{\text{cr2}}^2$... underestimates the uncertainty

II-5.2 Coaxiality

II-5.2.1 Validation plan

A 80 mm diameter cylinder square (**Figure II-7**) was used for testing the method B2 on two characteristics: coaxiality and diameter. This section reports the outcomes for coaxiality; see the next section for the diameter.



Figure II-7: The cylinder square used for the testing.

The measurements were carried out with a CMM Aberlink - Zenith Too with PH10T probing system with specification $E_{L,MPE} = \pm(4 + 6L) \mu\text{m}$, and Aberlink 3D software. Measurements were repeated 20 times at long time intervals as recommended in .

The cylinder was measured as a sequence of 17 circles. They were as many right sections at intervals of 5 mm along the cylinder length, thus covering 80 mm of length.

To investigate the effect on the coaxiality of the distance of specific sections to the datum feature and of the datum feature extension, the datum feature A was taken on the leftmost portion of the cylinder with increasing lengths (**Figure II-8a**). Six datums were established with datum feature lengths of (10, 15, 20, 25, 30, 35) mm, respectively. A seventh datum was taken as a common datum A-B based on the two sections at the extremes (**Figure II-8b**). The coaxiality was evaluated at individual sections. Only the sections on the right hand side of the datum feature at increasing distances to it were evaluated for the case in **Figure II-8a**. All sections but the extreme two were evaluated for the common datum case in **Figure II-8b**.

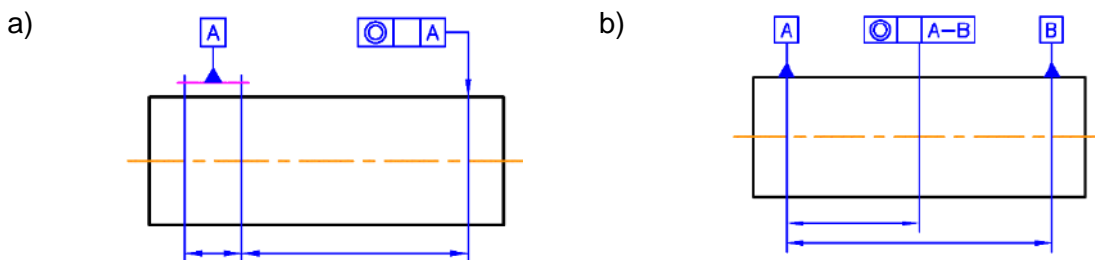


Figure II-8: Drawing of the cylinder with the indication of the datum and datum feature(s), and of a right section under coaxiality investigation. a) with a single datum; b) with a common datum.

The coaxiality known by calibration value was nought (nearly-perfect cylinder).

The experimental uncertainty U was evaluated [10] for each right section with the three equations U_1, U_2, U_4 . U_3 was disregarded because of its similarity to U_2 . The uncertainty was evaluated according to method B2 too with two values of the b coefficient to derive the standard uncertainty from the maximum error expressed by the MPE. They were $b_1 = \frac{1}{\sqrt{3}} \approx 0.577$ in the assumption of a uniform distribution and $b_2 = 0.459$ derived from the actual errors of indication incurred during a previous EN ISO 10360-2 test⁹.

⁹ The EN ISO 10360-2 test was not part of the current validation. The data used for evaluating b_2 had been stored during the test and retrieved and evaluated for the purpose.

The chi-square of the experimental uncertainty U_4 (quantile-based approach) with a Weibull distribution¹⁰ versus the method B uncertainty was calculated. U_4 only was used in the chi-square analysis as deemed as the most suited: coaxiality (and any other geometrical deviation) always hold positive values. **Figure II-9** illustrates an example of the experimental distribution of the expanded uncertainty values U_4 .

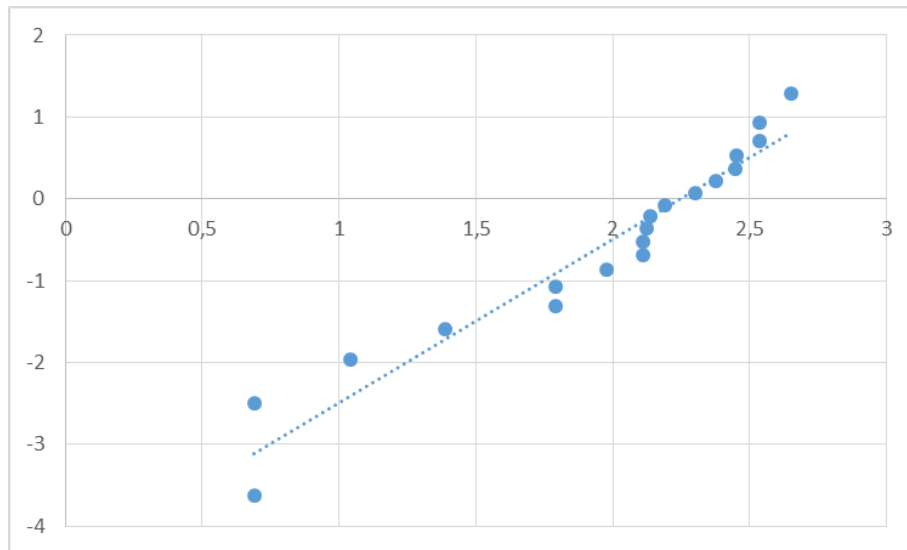


Figure II-9: Exemplar log-log plot of the distribution of uncertainties evaluated as 95 % quantiles of a Weibull distribution. The horizontal x axis is the logarithm of the measured values of coaxiality, ε , in micrometres, $x = \ln \frac{\varepsilon}{1 \mu\text{m}}$. The vertical y axis is $y = \ln\{-\ln[1 - F(\varepsilon)]\}$, where F is the cumulative Weibull distribution. The function y would exhibit a linear behaviour in case of perfectly Weibull-distributed data.

The evaluation was carried out by means of a MS Excel spreadsheet (cylindrical square.xlsx). Inputs to it were:

- Date and time of measurements;
- Values of the coefficients A and B in the expression of $E_{L,MPE}$;
- Values of the coefficients b_1 and b_2 to derive the standard uncertainty from the CMM MPE;
- Calibration standard uncertainty u_{cal} of the axis straightness of the cylindrical square;
- Value D and Standard uncertainty $u_{\text{cal}}(D)$ of the diameter of the cylindrical square;

II-5.2.2 Summary of the validation plan

The validation plan for the coaxiality is summarised in **Table II-4**.

¹⁰ Similar results would have been achieved with a Rayleigh distribution.

Table II-4: Summary of the validation plan for coaxiality.

Symbol	Dimension	Values	Description
l_A	Length of the datum (A) feature (leftmost cylinder portion)	(10, 15, 20, 25, 30, 35) mm	
l_{A-B}	Distance between the two common datum (A-B) features	80 mm	
d	Closest distance of a sections to the datum (A) feature	(5, 10, 15, 20, 25, 30, 35, 40, 45, 50, 55, 60, 65, 70) mm	Values for the shortest datum (A) feature ($l_A = 10$ mm). For longer datum features, the number of evaluated sections reduces (to fall within the total cylinder length)
h	Longitudinal coordinate of a section	(5, 10, 15, 20, 25, 30, 35, 40, 45, 50, 55, 60, 65, 70, 75) mm	Used only in the case of the common datum A-B
U	Evaluation method of the experimental uncertainty	U_1, U_2, U_4	See II-5.1 bullet 1.b
b	Coefficient to derive the method B2 standard uncertainty from the maximum error MPE	$b_1 = \frac{1}{\sqrt{3}}$ ≈ 0.577 $b_2 = 0.459$	(b_1) Uniform distribution (b_2) Derived from EN ISO 10360-2 testing data

The chi-squared analysis was performed for $U = U_4$ only.

II-5.2.3 Results

This section reports the many results obtained in the validation plan.

For each length of the datum feature, l_A , and for the common datum A-B, a synoptic table with the expanded uncertainties evaluated either experimentally or with the method B2 and its plot are reported.

Table II-5: Comparison of uncertainties. Length of the datum feature $l_A = 10$ mm.

d/mm	$U_1/\mu m$	$U_2/\mu m$	$U_4/\mu m$	$U_{B2}/\mu m$ ($b_1 = 0.577$)	$U_{B2}/\mu m$ ($b_2 = 0.459$)
5	8.71	9.62	7.92	10.328	8.211
10	10.71	11.32	11.37	13.064	10.386
15	11.16	13.04	9.98	16.653	13.240
20	15.59	17.81	14.30	20.656	16.422
25	15.60	18.26	14.38	24.873	19.774
30	22.20	25.54	20.37	29.212	23.224
35	24.07	28.74	22.00	33.625	26.733
40	26.48	30.34	24.44	38.088	30.280
45	25.82	31.57	23.71	42.583	33.854
50	30.60	36.60	28.09	47.103	37.447
55	32.58	39.72	30.25	51.640	41.054
60	33.45	40.30	30.78	56.190	44.672
65	37.20	45.52	34.21	60.751	48.298
70	37.95	45.73	35.04	65.320	51.930

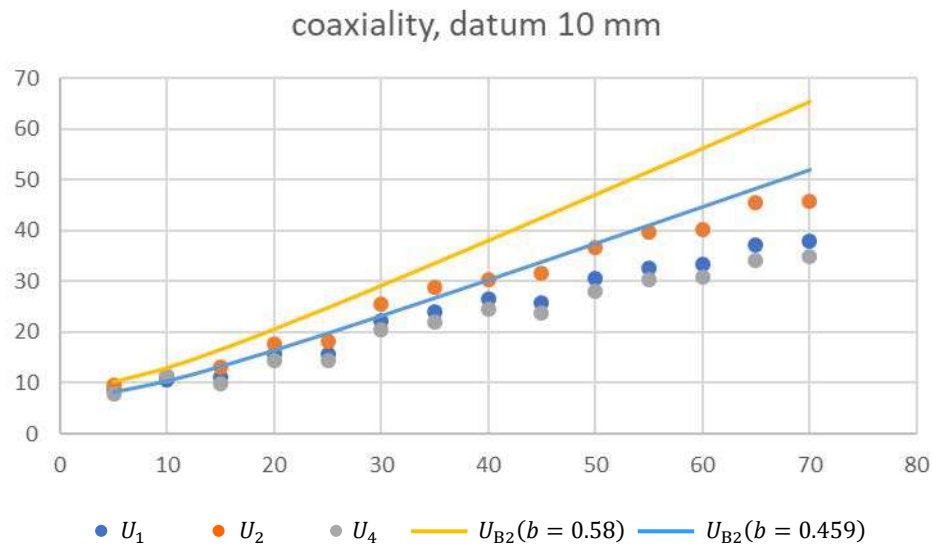


Figure II-10: Plot of the values in **Table II-5** ($l_A = 10$ mm). The horizontal axis is the distance of the right section to the datum feature, d (millimetres). The vertical axis is the expanded uncertainty (micrometres).

Table II-6: Comparison of uncertainties. Length of the datum feature, $l_A = 15$ mm.

d/mm	$U_1/\mu m$	$U_2/\mu m$	$U_4/\mu m$	$U_{B2}/\mu m$ ($b_1 = 0.577$)	$U_{B2}/\mu m$ ($b_2 = 0.459$)
5	8.72	9.02	8.07	9.737	7.741
10	10.00	10.24	9.32	11.102	8.826
15	10.91	12.17	10.07	13.064	10.386
20	13.52	14.09	12.78	15.396	12.240
25	19.33	20.64	18.07	17.955	14.274
30	21.39	23.85	20.09	20.656	16.422
35	22.55	24.21	20.98	23.450	18.643
40	21.43	24.77	19.96	26.309	20.916
45	23.26	26.82	21.74	29.212	23.224
50	25.37	29.60	23.63	32.148	25.558
55	25.71	30.64	24.31	35.108	27.911
60	28.45	34.55	26.83	38.088	30.280
65	28.42	34.47	26.52	41.082	32.660

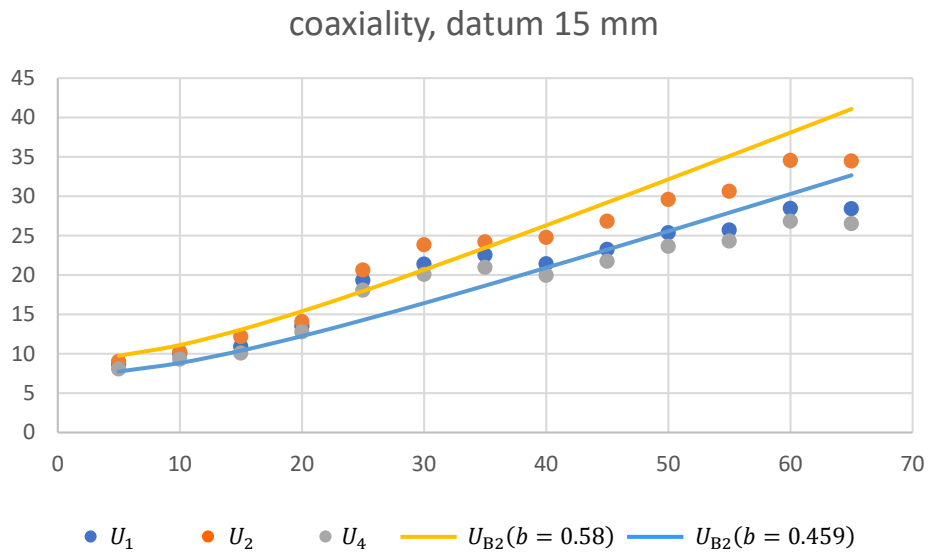


Figure II-11: Plot of the values in **Table II-6** ($l_A = 15$ mm). The horizontal axis is the distance of the right section to the datum feature, d (millimetres). The vertical axis is the expanded uncertainty (micrometres).

Table II-7: Comparison of uncertainties. Length of the datum feature, $l_A = 20$ mm.

d/mm	$U_1/\mu m$	$U_2/\mu m$	$U_4/\mu m$	$U_{B2}/\mu m$ ($b_1 = 0.577$)	$U_{B2}/\mu m$ ($b_2 = 0.459$)
5	7.13	7.49	6.48	9.52	7.57
10	7.73	8.69	6.98	10.33	8.21
15	9.17	9.68	8.43	11.55	9.18
20	14.71	15.60	13.88	13.06	10.39
25	18.76	19.27	17.79	14.79	11.76
30	17.03	17.73	15.96	16.65	13.24
35	15.97	17.08	14.93	18.62	14.80
40	19.20	20.42	21.43	20.66	16.42
45	18.90	21.27	17.42	22.74	18.08
50	19.51	21.72	18.20	24.87	19.77
55	22.12	25.00	20.41	27.03	21.49
60	21.67	23.76	20.23	29.21	23.22

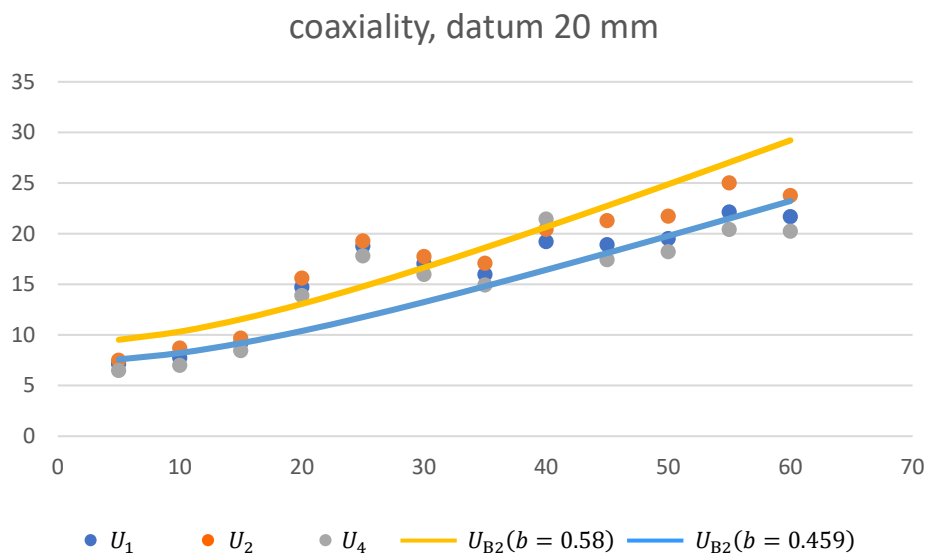


Figure II-12: Plot of the values in **Table II-7** ($l_A = 20$ mm). The horizontal axis is the distance of the right section to the datum feature, d (millimetres). The vertical axis is the expanded uncertainty (micrometres).

Table II-8: Comparison of uncertainties. Length of the datum feature, $l_A = 25$ mm.

d/mm	$U_1/\mu m$	$U_2/\mu m$	$U_4/\mu m$	$U_{B2}/\mu m$ ($b_1 = 0.577$)	$U_{B2}/\mu m$ ($b_2 = 0.459$)
5	8.76	9.20	8.20	9.42	7.49
10	8.84	9.73	8.04	9.95	7.91
15	12.82	13.66	12.07	10.77	8.56
20	14.85	16.50	13.78	11.83	9.40
25	14.35	15.79	13.28	13.06	10.39
30	13.73	14.70	13.30	14.43	11.47
35	15.20	17.82	13.94	15.89	12.64
40	18.27	20.14	16.97	17.43	13.86
45	16.89	19.63	15.41	19.02	15.12
50	18.68	22.79	16.89	20.66	16.42
55	17.81	21.17	16.27	22.32	17.75

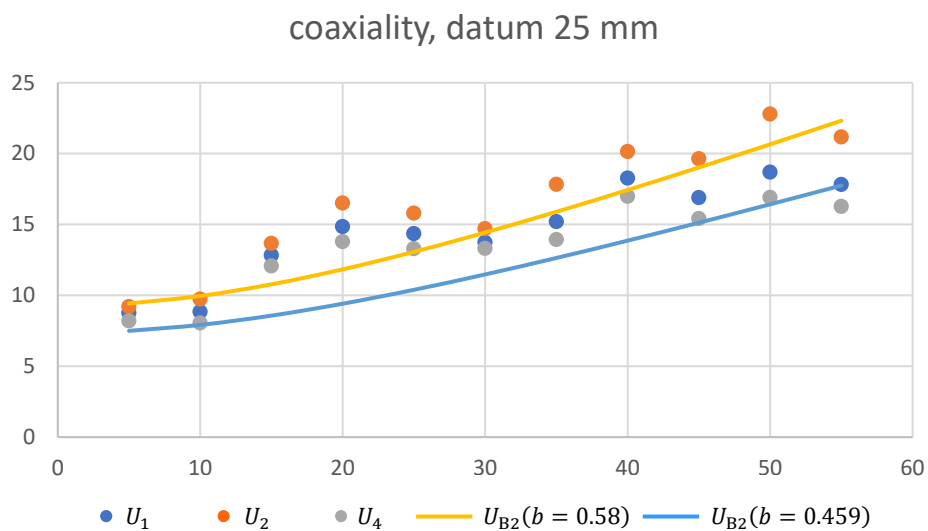


Figure II-13: Plot of the values in **Table II-8** ($l_A = 25$ mm). The horizontal axis is the distance of the right section to the datum feature, d (millimetres). The vertical axis is the expanded uncertainty (micrometres).

Table II-9: Comparison of uncertainties. Length of the datum feature, $l_A = 30$ mm.

d/mm	$U_1/\mu m$	$U_2/\mu m$	$U_4/\mu m$	$U_{B2}/\mu m$ ($b_1 = 0.577$)	$U_{B2}/\mu m$ ($b_2 = 0.459$)
5	7.73	8.09	7.19	9.37	7.45
10	13.05	13.03	12.83	9.74	7.74
15	13.03	13.39	12.06	10.33	8.21
20	12.13	12.53	11.21	11.10	8.83
25	12.36	13.00	11.54	12.02	9.56
30	12.90	13.52	14.01	13.06	10.39
35	15.90	16.06	14.77	14.19	11.28
40	12.50	13.36	11.60	15.40	12.24
45	14.31	14.79	13.51	16.65	13.24
50	14.47	15.44	13.46	17.95	14.27

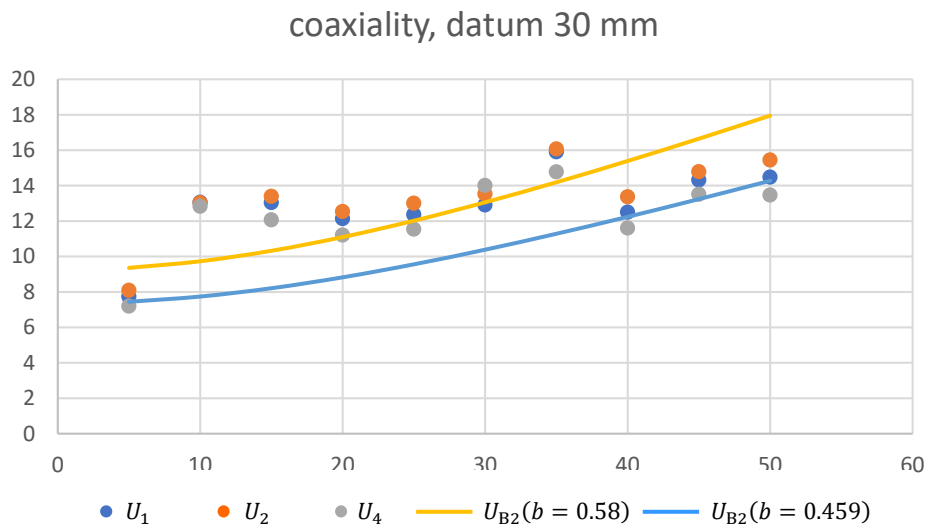


Figure II-14: Plot of the values in **Table II-9** ($l_A = 30$ mm). The horizontal axis is the distance of the right section to the datum feature, d (millimetres). The vertical axis is the expanded uncertainty (micrometres).

Table II-10: Comparison of uncertainties. Length of the datum feature, $l_A = 35$ mm.

d/mm	$U_1/\mu m$	$U_2/\mu m$	$U_4/\mu m$	$U_{B2}/\mu m$ ($b_1 = 0.577$)	$U_{B2}/\mu m$ ($b_2 = 0.459$)
5	12.77	13.73	11.84	9.33	7.42
10	15.00	14.92	13.92	9.61	7.64
15	13.65	13.46	12.67	10.05	7.99
20	11.73	12.93	10.87	10.64	8.46
25	14.37	15.16	13.60	11.35	9.03
30	14.94	16.14	13.96	12.17	9.67
35	14.20	14.78	13.39	13.06	10.39
40	16.00	17.09	14.89	14.03	11.15
45	14.78	15.05	14.08	15.05	11.96

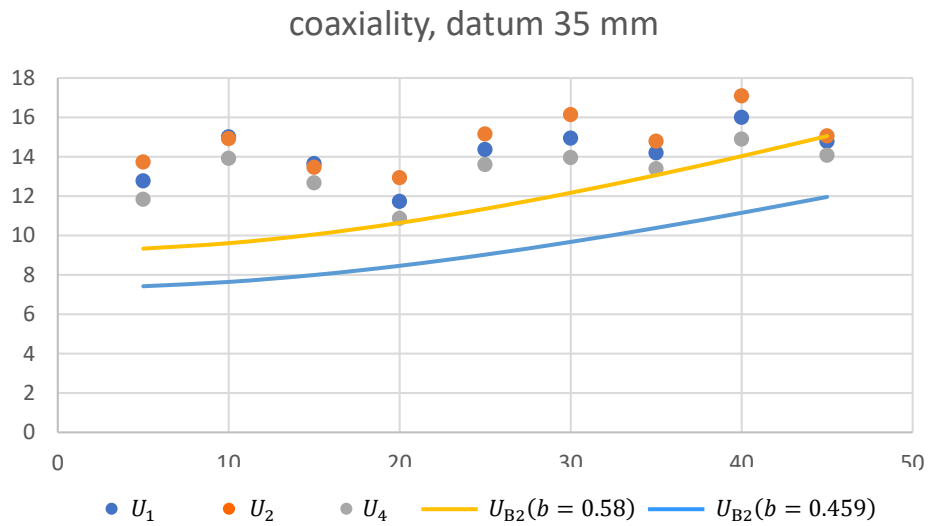


Figure II-15: Plot of the values in **Table II-10** ($l_A = 35$ mm). The horizontal axis is the distance of the right section to the datum feature, d (millimetres). The vertical axis is the expanded uncertainty (micrometres).

Table II-11: Comparison of uncertainties. Common datum A-B, $l_{A-B} = 80$ mm.

d/mm	$U_1/\mu m$	$U_2/\mu m$	$U_4/\mu m$	$U_{B2}/\mu m$ ($b_1 = 0.577$)	$U_{B2}/\mu m$ ($b_2 = 0.459$)
5	8.06	7.93	8.30	9.26	7.36
10	5.53	6.05	4.80	9.31	7.40
15	6.05	6.75	5.34	9.40	7.47
20	6.02	6.25	5.42	9.52	7.57
25	6.20	6.88	5.43	9.68	7.69
30	5.96	6.08	5.39	9.87	7.84
35	6.87	6.83	6.41	10.08	8.02
40	11.28	11.42	10.51	10.33	8.21
45	11.79	11.37	10.86	10.08	8.02
50	10.45	9.80	9.55	9.87	7.84
55	8.06	8.59	7.39	9.68	7.69
60	8.92	9.50	8.17	9.52	7.57
65	8.35	8.82	7.73	9.40	7.47
70	7.00	7.24	6.35	9.31	7.40
75	6.62	7.11	5.94	9.26	7.36

coaxiality, datum 80 mm,
element between datums

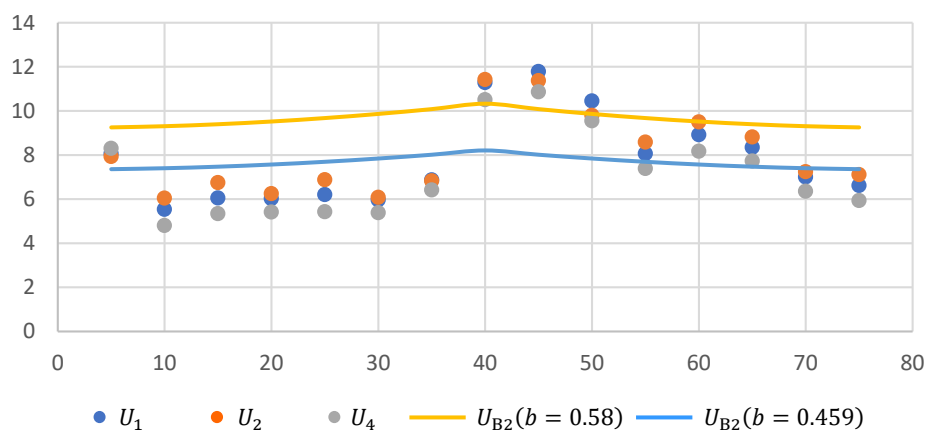


Figure II-16: Plot of the values in **Table II-11** ($l_{A-B} = 80$ mm). The horizontal axis is the longitudinal coordinate of the right section, h (millimetres). The vertical axis is the expanded uncertainty (micrometres).

The results show a strong dependence of the uncertainty on the datum feature length and on the distance of the section to the datum element. They also show a good compatibility of the proposed method B2 with the established experimental method [10].

The plots above use different scale magnifications. To help comparing, Figure II-17 merges them to one chart (for the case only of the method B2 uncertainty with $b_1 = 0.58$).

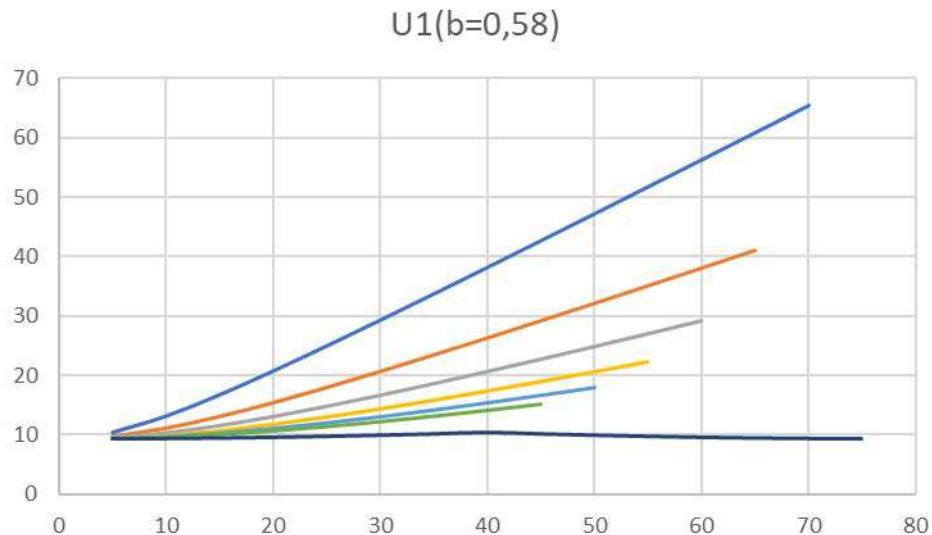


Figure II-17: Summary of the uncertainty evaluated with the method B2 in the case of a uniform distribution ($b_1 = 0.58$). Each curve illustrates a different datum feature length: the uppermost curve (in blue) is evaluated with $l_A = 10$ mm, the others below with progressively longer lengths up to $l_A = 35$ mm for the bottommost but one (in green). The bottommost in dark blue is with the common datum A-B. The horizontal axis is the distance of the section to the datum feature, d (millimetres), but for the bottommost curve is the longitudinal coordinate of the right section, h (millimetres). The vertical axis is the expanded uncertainty (micrometres).

II-5.3 Diameter of an external circle

II-5.3.1 Validation plan

The same cylindrical square used for validating the coaxiality (see II-5.2) was used for validating the external diameter too.

The validation plan was the same as described in II-5.1 for the coaxiality but adapted as follows:

- No datum was involved because the diameter is a feature of size;
- The measurements of all the 17 right sections of the cylinder were individually considered and their diameters were evaluated;
- The experimental uncertainty U_4 was not evaluated. The measurement errors of a diameter (characteristic of size) can be either positive or negative, and the approach based on the quantile of a one-sided distribution was not fit for purpose.

II-5.4 Results

The uncertainties evaluated experimentally (either U_1 or U_2) and with the method B2 (with either the value $b_1 = 0.577$ or $b_2 = 0.459$ of the coefficient b) are reported in **Table II-12**.

The chi-squared analysis of the experimental uncertainty U_1 and U_2 versus the uncertainty evaluated with method B2 (with either b_1 or b_2) is reported in **Table II-13**.

Table II-12: External diameter. Synopsis of the uncertainties evaluated for the chi-squared analysis.

Uncertainties/ μm			
Experimental	$U_1 \rightarrow$	(6.30 – 8.54)	$U_2 \rightarrow$ (6.07 – 7.68)
Method B2	$b_1 \rightarrow$	7.49	$b_2 \rightarrow$ 5.95

Table II-13: External diameter. Chi-squared analysis of the experimental uncertainty U_1 and U_2 versus the method B2 uncertainty (with either b_1 for a uniform distribution or the CMM-specific b_2). The values of χ^2 are colour-coded (**Table II-3**).

d/mm	Bias b/mm	$u_p/\mu\text{m}$	$U_1/\mu\text{m}$	χ_1^2 ($b_1 = 0.58$)	χ_2^2 ($b_2 = 0.46$)	$U_2/\mu\text{m}$	χ_1^2 ($b_1 = 0.58$)	χ_2^2 ($b_2 = 0.46$)
0	0.69	2.80	6.78	16.43	26.00	6.25	13.94	22.05
5	1.27	2.97	7.67	21.02	33.25	6.89	16.94	26.80
10	0.22	3.28	7.22	18.58	29.40	7.00	17.52	27.71
15	0.56	3.12	7.25	18.76	29.68	6.78	16.42	25.98
20	0.52	3.10	7.18	18.39	29.09	6.74	16.21	25.64
25	0.71	2.90	6.98	17.39	27.51	6.43	14.75	23.34
30	0.25	2.84	6.42	14.72	23.29	6.19	13.67	21.63
35	0.18	2.81	6.30	14.15	22.39	6.13	13.40	21.20
40	0.10	3.31	7.13	18.14	28.70	7.04	17.67	27.96
45	0.15	2.99	6.59	15.50	24.53	6.45	14.86	23.51
50	0.44	2.75	6.44	14.81	23.44	6.07	13.13	20.78
55	0.22	3.24	7.13	18.14	28.71	6.92	17.09	27.04
60	-0.55	3.26	7.49	20.00	31.65	7.03	17.62	27.88
65	-0.90	2.92	7.22	18.62	29.45	6.57	15.42	24.40
70	-1.57	2.84	7.74	21.37	33.80	6.92	17.09	27.05
75	-1.37	3.38	8.54	26.05	41.22	7.68	21.05	33.31
80	-1.47	3.01	7.95	22.56	35.69	7.11	18.07	28.59

The test chi-squared test was always passed with either experimental uncertainty U_1, U_2 in the (2×17) cases with uniform distribution assumption (b_1). It was too in 13 (U_1) and 16 (U_2) out of 17 cases based actual reverification test results (b_2). This is considered a satisfactory result, particularly in the case of U_2 , likely more reliable than U_1 .

II-5.5 Diameter of an internal circle

II-5.5.1 Validation plan

Two ring gauges (100 mm and 45 mm in diameter) were measured with three different CMMs, according to the experimental plan in **Table II-14**.

Table II-14: Experimental plan for the validation of the diameter of an internal circle.

CMM	$E_{L,MPE}/\mu\text{m}$ (L in millimetres)	Ring gauge 1 (\varnothing 100 mm)	Ring gauge 2 (\varnothing 45 mm)
1	$1.8 + L/300$	✓	
2	$1.5 + L/333$		✓
3	$1.8 + L/333$		✓

II-5.5.2 Results

Details of the uncertainty evaluation are reported in **Table II-15**. The uncertainties were evaluated experimentally with either U_1 or U_2 and with the method B2 with either the value $b_1 = 0.577$ (uniform distribution) or b_2 (for the specific CMM) of the coefficient b .

The chi-squared analysis is summarised in **Table II-16**. Values are colour-coded, see **Table II-3**.

Table II-15: Internal diameter. Details of the uncertainty evaluations: experimentally (with either U_1 or U_2) and with the method B2 (with either b_1 for a uniform distribution or b_2 for the specific CMM).

CMM	Ring \varnothing/mm	u_{cal} $/\mu\text{m}$	Bias b/mm	$u_p/\mu\text{m}$	b_1	b_2	U_1 $/\mu\text{m}$	U_2 $/\mu\text{m}$	U_{B2} $/\mu\text{m}$ (b_1)	U_{B2} $/\mu\text{m}$ (b_2)
1	100	0.5	0.29	0.17	0.577	0.228	1.35	1.21	3.52	1.39
2	45	0.7	0.05	0.56	0.577	0.249	1.84	1.80	2.75	1.19
3	45	0.7	-0.18	0.63	0.577	0.232	2.05	1.91	3.27	1.31

Table II-16: Internal diameter. Chi-squared analysis of the experimental uncertainty U_1 and U_2 versus the method B2 uncertainty (with either b_1 for a uniform distribution or b_2 for the specific CMM).

CMM	U_1		U_2	
	χ_1^2 (b_1)	χ_2^2 (b_2)	χ_1^2 (b_1)	χ_2^2 (b_2)
1	2.96	18.93	2.37	15.17
2	8.94	47.74	8.53	45.55
3	7.90	49.21	6.84	42.62

The large discrepancy between the two uncertainties with method B2 is due to the coefficient b_2 less than a half of b_1 . This occurred because the CMMs were in very good technical condition and performed in the EN ISO 10360-2 verification tests much better than their MPEs (**Figure II-18**).

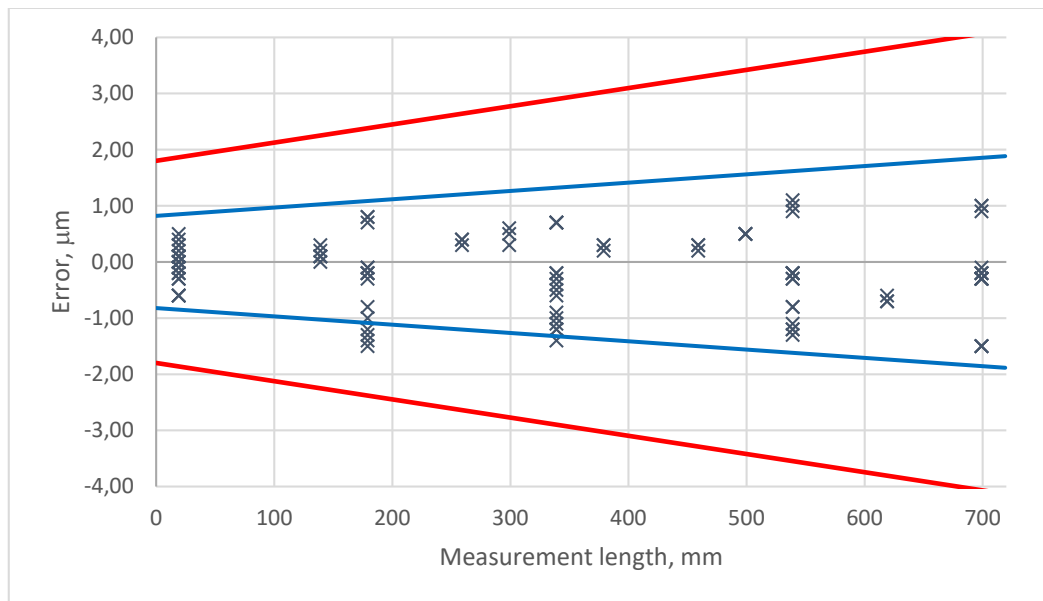


Figure II-18: Diagram of the errors of indication incurred in the EN ISO 10360-2 verification test of the CMM 1. The external red lines are the MPE. The internal blue lines symmetrically encompass 95 % of the errors and were used for the derivation of the coefficient b_2 .

For the CMM 1, the method B2 uncertainties were compatible with the experimental ones, with some overestimation versus U_1 .

For the CMMs 2 and 3, the order relationship $U_{B2,b_2} < U_2 < U_1 < U_{B2,b_1}$ could be observed. The method B2 uncertainties generally either overestimated (while using the MPE values, b_1) or underestimated (while using the actual test values, b_1) the uncertainty evaluated experimentally [10].

It is worth noticing that the value of u_{cal} was rather large and accounted for a large fraction (>50 %) of the uncertainty evaluated experimentally.

II-5.6 Diameter of the arc of a circle

Two validation exercises were carried out: on single arcs and on the average of multiple arcs rotated all along the circle.

II-5.6.1 Validation plan (single arcs)

The same ring gauges were measured with the same CMMs as for the validation of the internal diameter (**Table II-14**). Arcs with different central angles 2θ were measured.

II-5.6.2 Results (single arcs)

The results (both the uncertainties and the chi-squared values) are reported in **Table II-17**, **Table II-18** and **Table II-19** for the three CMMs.

Table II-17: Arc of a circle. Details of the experimental (with either U_1 or U_2) and the method B2 (with either b_1 for a uniform distribution or b_2 for the specific CMM) uncertainties, and chi-squared analysis. θ is half the central angle. Case of the CMM 1 and the 100 mm ring gauge.

CMM 1: $E_{L,MPE} = (1.8 + L/300) \mu\text{m}$							100 mm ring gauge; $u_{\text{cal}} = 0.5 \mu\text{m}$			
Half centr. angle, θ	Bias b/mm	$u_p/\mu\text{m}$	$U_1/\mu\text{m}$	$U_2/\mu\text{m}$	$U_{B2}/\mu\text{m}$ (b_1)	$U_{B2}/\mu\text{m}$ (b_2)	U_1		U_2	
							χ_1^2 (b_1)	χ_2^2 (b_2)	χ_1^2 (b_1)	χ_2^2 (b_2)
17°	5.37	1.64	8.79	11.26	65.77	25.99	0.36	2.29	0.59	3.76
25°	-3.02	0.89	5.05	6.37	29.89	11.81	0.57	3.66	0.91	5.81
40°	0.20	0.43	1.52	1.38	11.12	4.39	0.37	2.40	0.31	1.97
90°	0.25	0.21	1.33	1.19	2.46	0.97	5.84	37.37	4.68	29.94

Table II-18: Arc of a circle. Details of the experimental (with either U_1 or U_2) and the method B2 (with either b_1 for a uniform distribution or b_2 for the specific CMM) uncertainties, and chi-squared analysis. θ is half the central angle. Case of the CMM 2 and the 45 mm ring gauge.

CMM 2: $E_{L,MPE} = (1.5 + L/333) \mu\text{m}$							45 mm ring gauge; $u_{\text{cal}} = 0.7 \mu\text{m}$			
Half centr. angle, θ	Bias b/mm	$u_p/\mu\text{m}$	$U_1/\mu\text{m}$	$U_2/\mu\text{m}$	$U_{B2}/\mu\text{m}$ (b_1)	$U_{B2}/\mu\text{m}$ (b_2)	U_1		U_2	
							χ_1^2 (b_1)	χ_2^2 (b_2)	χ_1^2 (b_1)	χ_2^2 (b_2)
17°	-2.29	1.89	6.31	6.09	54.66	23.55	0.27	1.43	0.25	1.34
25°	-1.60	1.60	5.09	4.73	24.76	10.67	0.84	4.55	0.73	3.93
40°	-0.84	1.26	3.71	3.33	9.10	3.92	3.33	17.93	2.67	14.40
90°	-0.59	0.46	2.26	2.04	1.89	0.81	28.52	155.3	23.31	126.9

Table II-19: Arc of a circle. Details of the experimental (with either U_1 or U_2) and the method B2 (with either b_1 for a uniform distribution or b_2 for the specific CMM) uncertainties, and chi-squared analysis. θ is half the central angle. Case of the CMM 3 and the 45 mm ring gauge.

CMM 3: $E_{L,MPE} = (1.8 + L/333) \mu\text{m}$							45 mm ring gauge; $u_{\text{cal}} = 0.7 \mu\text{m}$			
Half centr. angle, θ	Bias b/mm	$u_p/\mu\text{m}$	$U_1/\mu\text{m}$	$U_2/\mu\text{m}$	$U_{B2}/\mu\text{m}$ (b_1)	$U_{B2}/\mu\text{m}$ (b_2)	U_1		U_2	
							χ_1^2 (b_1)	χ_2^2 (b_2)	χ_1^2 (b_1)	χ_2^2 (b_2)
17°	1.70	1.33	4.69	4.53	65.57	26.32	0.10	0.64	0.10	0.59
25°	0.50	1.25	3.36	3.03	29.68	11.92	0.26	1.59	0.21	1.29
40°	0.17	1.03	2.66	2.51	10.89	4.37	1.19	7.39	1.06	6.59
90°	0.31	0.61	2.17	1.96	2.23	0.90	18.86	115.8	15.42	94.64

The method B2 generally overestimated the uncertainty, particularly at small central angles. In the case of the semicircle ($\theta = 90^\circ$), the use of the validation-based coefficient b_2 led to a severe overestimation.

II-5.6.3 Validation plan (average of multiple arcs)

The ring gauge 100 mm was measured with a CMM with MPE $E_{L, MPE} = \pm(1.8 + L/333) \mu\text{m}$ (L in millimetres).

Eleven evenly spaced points were probed ($\Delta\theta = \frac{360^\circ}{11} \approx 32.7^\circ$ angular separation). Sets of three points were extracted out of the eleven and the diameter of the circle through them was evaluated. The selection of the three points followed a scheme aimed at investigating the effect of the central angle size with the impact of local form errors minimised by averaging (see Figure II-19). More precisely:

1. Increasing central angles $2\theta_k = k\Delta\theta$ were considered. The minimum and maximum values of k were selected to have at least three sampled points onto the subtending arc with non-coincident extreme points, that is, $k \in [2,10]$. In fact, $k = 1$ would have resulted in two points only, $k = 11$ in coincident extreme points. The corresponding 9 values of half central angles were $\theta_k = (32.7^\circ, 49.1^\circ, 65.5^\circ, 81.8^\circ, 98.2^\circ, 114.5^\circ, 130.9^\circ, 147.3^\circ, 163.6^\circ)$.
2. For each central angle $2\theta_k$, a set of three points was taken at the extremes and at the middle point of the subtending arc, the first point of the three being 1. This corresponded to the points $\left\{1, \frac{k}{2} + 1, k + 1\right\}$ ¹¹. For instance $\{1, 2, 3\}$ for $k = 2$ (Figure II-19a), or $\{1, 2, 4\}$ for $k = 3$, or $\{1, 6, 11\}$ for $k = 11$ (Figure II-19b).
3. Each set is progressively rotated about the centre in steps of $\Delta\theta$, resulting in 11 sets ($j \in [1,11]$) for each central angle ($k \in [2,10]$). The points in the sets resulted to be $\left\{j, \left(\frac{k}{2} + j\right), (k + j)\right\}$, with point indexes “wrapping around”¹² at the value of 12. The sequence resulted in

	$j = 1$	$j = 2$...	$j = 11$
$k = 2$	{1, 2, 3}	{2, 3, 4}	...	{11, 1, 2}
$k = 3$	{1, 2, 4}	{2, 3, 5}	...	{11, 1, 3}
\vdots	\vdots	\vdots	...	\vdots
$k = 10$	{1, 6, 11}	{2, 7, 1}	...	{11, 5, 10}

4. The 11 diameters computed for each central angle size were averaged to obtain $\bar{\varnothing}_k$.

¹¹ This is valid when k is even. When it is odd instead, the nearby point $\frac{k-1}{2} + 1$ rather than $\frac{k}{2} + 1$ is chosen as middle point point, resulting in $\left\{1, \frac{k-1}{2} + 1, k + 1\right\}$

¹² Indexes “wrap around” because of the point layout closed in a circle. The complete expression is

$$\left\{j, \left[\left(\frac{k}{2} + j - 1\right) \bmod 11\right] + 1, [(k + j - 1) \bmod 11] + 1\right\} \quad \text{for even values of } k$$

$$\left\{j, \left[\left(\frac{k-1}{2} + j - 1\right) \bmod 11\right] + 1, [(k + j - 1) \bmod 11] + 1\right\} \quad \text{for odd values of } k.$$

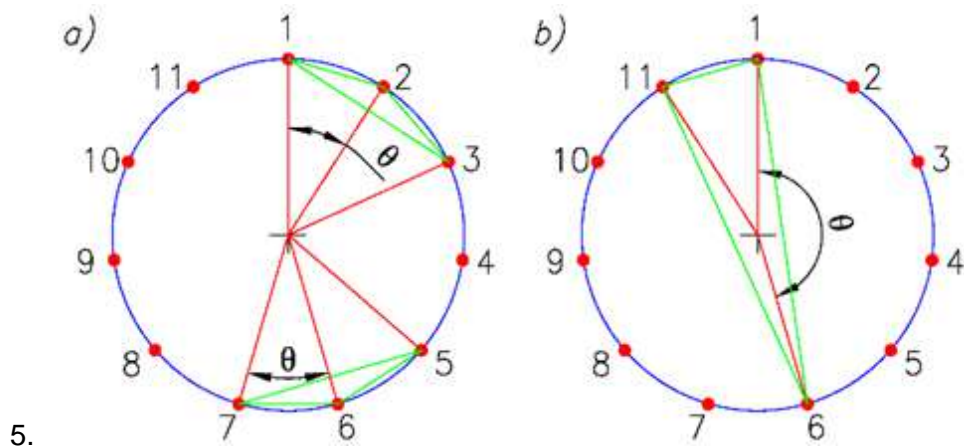


Figure II-19: Sampling of a circle used for the validation for arcs of circles. Examples of sets of extracted three points. Central angles 2θ : a) $\theta = 32.7^\circ$, b) $\theta = 163.6^\circ$.

Each experiment was repeated 20 times with measurements taken at long time intervals [10].

II-5.6.4 Results (average of multiple arcs)

Figure II-20 plots the evaluated uncertainties as a function of half the central angle θ .

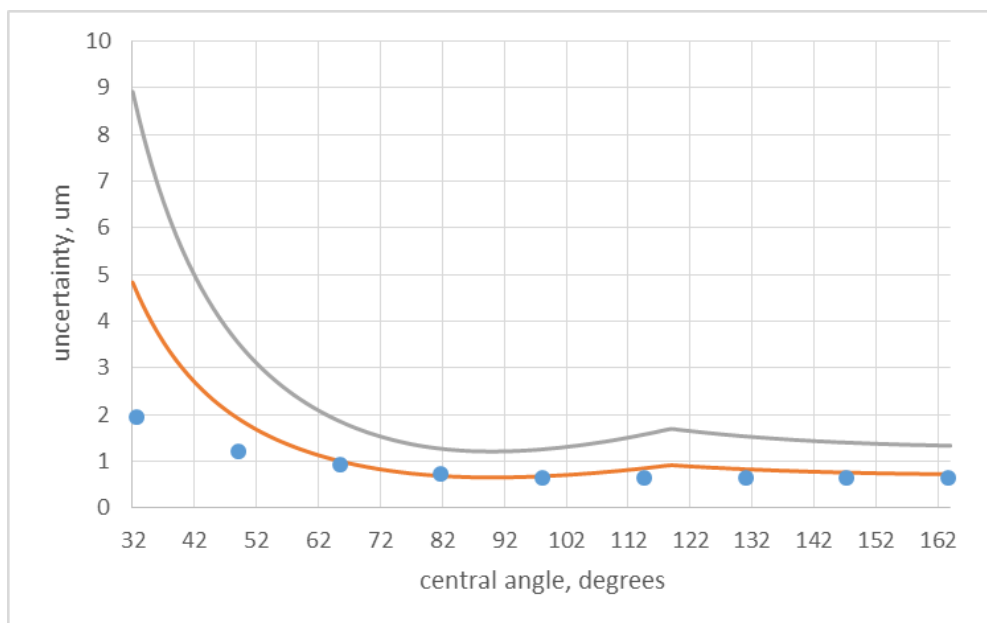


Figure II-20: Expanded measurement uncertainties of the diameter of a circle arc. The horizontal axis is half the central angle θ (degrees). The vertical axis is the evaluated expanded uncertainty (micrometres). Dots are the uncertainty evaluated experimentally [10]. Solid lines are uncertainties evaluated with the method B2: with $b_1 = 0.577$ for a uniform distribution (grey) and with $b_2 = 0.313$ based on actual CMM verification data.

A clear overestimation of method B2 uncertainty is observable for small central angles 2θ .

II-5.7 Inter-method comparison

II-5.7.1 Validation plan

The method B2 evaluations were compared with those with the method A also developed in the EUCoM project [11].

Three artefacts were investigated, namely an industrial connecting rod and two MFC standards (Multi-Feature Check) of high and low quality, respectively (**Figure II-21**). Details of these artefacts are given in [12].

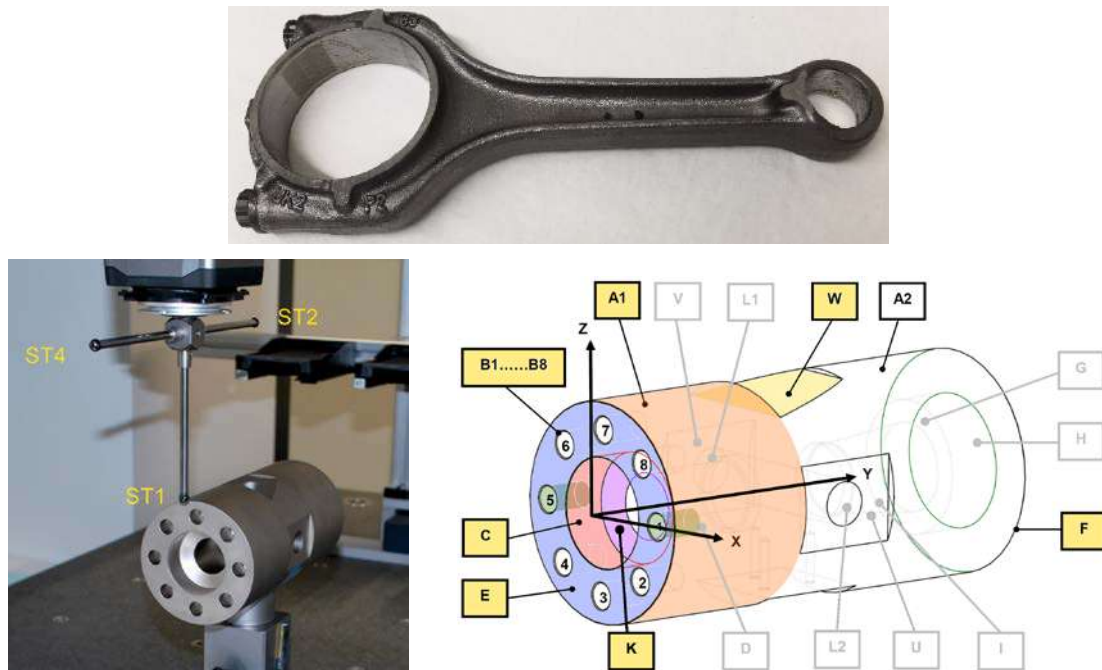


Figure II-21: Artefacts used for the inter-method comparison. An industrial connecting rod (top) and two MFC standards (Multi-feature Checks, bottom; one only is illustrated).

II-5.7.2 Connecting rod

Many characteristics could be defined in the geometry of a connecting rod. Six only were selected to keep the analysis effort viable.

To define the characteristics (measurands), a primary datum was established on the upper planar face of the big eye. This datum was parallel-shifted into the connecting rod to its nominal symmetry plane. Its intersections with the big and small eyes were nominally two circles (C3 and C4). The selected characteristics are reported in **Table II-20**.

Table II-20: Inter-method comparison – connecting rod. Definition of the measurands.

Symbol	Description	More precisely ...
\varnothing_{C3}	Diameter of the big eye	Diameter of C3
\varnothing_{C4}	Diameter of the small eye	Diameter of C4
d_{34}	Separation of the axes of the two eyes	Separation of the centres of C3 and C4
p_{BS}	Parallelism of the axes of the two eyes	
\varnothing_{Big}	Diameter of the big eye	Diameter of the cylinder associated to the big eye
\varnothing_{Small}	Diameter of the small eye	Diameter of the cylinder associated to the small eye

The expanded uncertainties evaluated with the methods A and B2 were compared. The latter was evaluated with $b_1 = 0.577$ for a uniform distribution and b_2 based on actual CMM verification data [2]. Usually $b_2 \leq b_1$, as all the involved CMMs were well-behaved.

The connecting rod was measured with 10 different CMMs. To keep the effort viable, the chi-squared analysis was carried out only for the four highest-accuracy CMMs.

The evaluation with the method A was based on four repeats of measurements of the connecting rod each in four orientations, resulting in 16 sets of data overall. Hence, the degrees of freedom were 15 in the chi-squared analysis (**Table II-21**).

Table II-21: Inter-method comparison – connecting rod. Critical values for the chi-squared analysis.

Null hypothesis criterion	Thresholds	
$\chi_{cr1}^2 \leq \chi^2 \leq \chi_{cr2}^2$	$\chi_{cr1}^2(0.025, 15) = 6.262$	$\chi_{cr2}^2(0.975, 15) = 27.488$

The resulting uncertainties and chi-squared analysis are reported in **Table II-22** and **Table II-23**, respectively.

Table II-22: Inter-method comparison – connecting rod. Uncertainties evaluated with the method A (U_A) and B2. The latter uncertainties were evaluated with $b_1 = 0.577$ for a uniform distribution ($U_{B2,b1}$) and with b_2 based on actual CMM verification data [2] ($U_{B2,b2}$). See **Table II-20** for the meaning of the symbols in the column headers (measurands).

CMM		\emptyset_{C3}	\emptyset_{C4}	d_{34}	p_{BS}	\emptyset_{Big}	\emptyset_{Small}
1 ($b_2 = 0.40$)	$U_{B2,b1}$	1.37	1.27	1.22	1.15	1.37	1.27
	$U_{B2,b2}$	0.94	0.88	0.84	0.79	0.94	0.88
	U_A	0.52	0.49	0.59	0.79	0.85	0.67
7 ($b_2 = 0.30$)		5.44	5.28	4.13	4.92	5.44	5.28
	$U_{B2,b2}$	2.81	2.73	2.14	2.55	2.81	2.73
	U_A	2.34	2.52	2.20	2.73	2.59	3.25
10 ($b_2 = 0.33$)	$U_{B2,b1}$	1.54	1.44	1.33	1.31	1.54	1.44
	$U_{B2,b2}$	0.88	0.82	0.76	0.75	0.88	0.82
	U_A	0.87	0.88	0.93	0.93	0.90	0.88
11 ($b_2 = 0.47$)	$U_{B2,b1}$	4.88	4.75	3.67	4.43	4.88	4.75
	$U_{B2,b2}$	3.95	3.85	2.98	3.59	3.95	3.85
	U_A	2.82	2.80	2.96	2.84	2.84	2.85

All values in micrometres

Table II-23: Inter-method comparison – connecting rod. Chi-squared values evaluated from the uncertainties reported in **Table II-22**. Values are colour-coded (**Table II-3**).

CMM	Comparison	\emptyset_{C3}	\emptyset_{C4}	d_{34}	p_{BS}	\emptyset_{Big}	\emptyset_{Small}
1	U_A vs $U_{B2,b1}$	2.29	2.36	3.78	7.58	6.11	4.40
	U_A vs $U_{B2,b2}$	4.82	4.96	7.95	15.94	12.84	9.26
7	U_A vs $U_{B2,b1}$	2.95	3.64	4.56	4.93	3.62	6.04
	U_A vs $U_{B2,b2}$	11.04	13.60	17.03	18.42	13.54	22.58
10	U_A vs $U_{B2,b1}$	5.14	5.97	7.77	7.95	5.40	5.96
	U_A vs $U_{B2,b2}$	15.89	18.44	23.99	24.57	16.67	18.41
11	U_A vs $U_{B2,b1}$	5.33	5.58	10.39	6.56	5.40	5.76
	U_A vs $U_{B2,b2}$	8.12	8.49	15.82	9.99	8.22	8.77

The chi-squared analysis results were very good for all four CMMs. The method B2 uncertainty based on actual CMM validation data, $U_{B2,b2}$, resulted compatible with the method A uncertainty in all cases but CMM 1 for two out of six measurands. The method B2 uncertainty based on MPEs, $U_{B2,b1}$, overestimated the uncertainty in most cases. No underestimation was observed.

II-5.7.3 MFC standard (high quality)

MFCs are designed to provide a variety of dimensional and geometrical characteristics, to provide a wide selection when testing CMM measuring capabilities. Twelve were considered in this exercise to keep the analysis effort viable. They are reported in **Table II-24**.

Table II-24: Inter-method comparison – MFC. Definition of the measurands. See **Figure II-21**. See [12] for more details.

Symb.	Nom. value /mm	Description	More precisely ...
\varnothing_{A1}	100	Diameter of the left external cylinder	External diameter of A1
\varnothing_C	50	Diameter of the left coaxial bore	Internal diameter of C
\varnothing_K	49,5	Diameter of the conical seat	Internal diameter of the right section of K, 20 mm apart from E
l_{EF}	200	Separation of the extreme ends	Length of the portion of the MFC axis between the intersections with the planes E and F
l_{B1B5}	75	Separation of diametrically opposed longitudinal bores	2D separation of the middle points of the axes of bores B1 and B5 in a plane orthogonal to the MFC axis
s_{A1}	-	Straightness of a generatrix of the left portion	Straightness of the generatrix of A closest to the bore B7.
v_C	-	Runout of the left coaxial bore	Runout of C with A1 taken as a datum
$v_{t,C}$	-	Total runout of the left coaxial bore	Total runout of C with A1 taken as a datum
c_{C-A1}	-	Concentricity of the left external and internal cylinders	Concentricity of C with A1 taken as a datum
f_E	-	Flatness of the left end	Flatness of E
p_{E-F}	-	Parallelism of the extreme ends	Parallelism of F with E taken as a datum
\perp_{E-C}	-	Perpendicularity of the coaxial bore axis to the left end	Perpendicularity of C with E taken as a datum

The expanded uncertainties evaluated with the methods A and B2 were compared. The latter was evaluated with $b_1 = 0.577$ for a uniform distribution.

The MFC was measured with three different CMMs. However, the chi-squared analysis was carried out only for two.

Similarly to the connecting rod, the degrees of freedom were 15 in the chi-squared analysis, resulting in the same critical values (**Table II-21**).

The resulting uncertainties and chi-squared analysis are reported in **Table II-25**.

Table II-25: Inter-method comparison – high quality MFC. Uncertainties evaluated with the method A (U_A) and B2 with $b_1 = 0.577$ for a uniform distribution ($U_{B2,b1}$). See **Table II-24** for the meaning of the symbols in the row headers (measurands). The chi-squared values are colour-coded (**Table II-3**) with the thresholds given in **Table II-21**.

Characteristic	CMM 1			CMM 10		
	U_A	$U_{B2,b1}$	χ^2	U_A	$U_{B2,b1}$	χ^2
\varnothing_{A1}	0.67	1.19	5.11	0.96	1.22	9.98
\varnothing_C	0.64	1.11	5.31	0.75	1.13	7.09
\varnothing_K	0.63	1.11	5.15	2.79	1.13	98.39
l_{EF}	0.74	1.08	7.47	0.85	1.16	8.58
l_{B1B5}	0.65	0.84	9.56	0.64	0.87	8.68
s_{A1}	0.60	0.78	9.51	0.56	0.78	8.30
v_C	0.65	0.74	12.20	0.65	0.75	11.78
$v_{t,C}$	0.85	0.82	17.12	1.51	0.83	52.68
c_{C-A1}	0.60	0.70	11.88	0.61	0.70	12.19
f_E	0.60	0.77	9.72	0.68	0.77	12.55
p_{E-F}	0.60	0.77	9.72	0.64	0.77	11.05
\perp_{E-C}	1.48	3.55	2.78	1.09	3.55	1.50

The results shown in **Table II-25** are good and satisfactory. Most evaluations were compatible with the method A, with a single case of underestimation and few overestimations.

The underestimation occurred for \varnothing_K , which is a diameter. The comparison among the three measured diameters (\varnothing_{A1} , \varnothing_C , \varnothing_K) shows that the uncertainty of \varnothing_K is quite larger than that of the other two with the method A, while it is in line with them with the method B2. A possible explanation is the following. \varnothing_K was taken on a cone and the measurement was sensitive to the directional response of the probing system. The method A is sensitive to the probing effects while the method B2 is not.

II-5.7.4 MFC standard (low quality)

The same comparison described in II-5.7.3 was carried out with a lower quality MFC standard. Measurands (**Table II-24**) and procedure were the same. The MFC standard was measured by different CMMs and the two highest-accuracy CMMs were selected for the chi-squared analysis.

The resulting uncertainties and chi-squared analysis are reported in **Table II-26**.

Table II-26: Inter-method comparison – low quality MFC. Uncertainties evaluated with the method A (U_A) and B2 with $b_1 = 0.577$ for a uniform distribution ($U_{B2,b1}$). See **Table II-24** for the meaning of the symbols in the row headers (measurands). The chi-squared values are colour-coded (**Table II-3**) with the thresholds given in **Table II-21**.

Characteristic	CMM 7			CMM 11		
	U_A	$U_{B2,b1}$	χ^2	U_A	$U_{B2,b1}$	χ^2
ϕ_{A1}	1.37	2.89	3.57	2.91	4.96	5.49
ϕ_C	1.38	2.74	4.04	2.87	4.82	5.69
ϕ_K	1.53	2.74	5.01	3.09	4.81	6.58
l_{EF}	1.59	2.51	6.44	4.05	3.91	17.24
l_{B1B5}	1.36	2.03	7.16	3.15	3.42	13.59
s_{A1}	1.37	1.95	7.98	2.94	3.50	11.25
v_C	1.41	1.84	9.49	3.77	3.23	21.85
$v_{t,C}$	1.41	2.03	7.75	3.77	3.59	17.69
c_{C-A1}	1.40	1.74	10.42	3.77	3.13	23.16
f_E	1.36	1.92	8.04	2.88	3.46	11.07
p_{E-F}	1.36	1.92	8.03	2.90	4.30	7.24
\perp_{E-C}	1.44	8.87	0.42	2.90	3.46	11.19

The results shown in **Table II-26** are good and satisfactory. Most evaluations were compatible with the method A, with no underestimation and a few overestimations, of which that relative to the perpendicularity \perp_{E-C} is severe for the CMM 7.

For both CMMs, better uncertainty estimation was achieved by taking the calibration rather than the method A values as reference¹³. The uncertainties of all characteristics were fully compatible with either CMM, apart from \perp_{E-C} , which remained overestimated significantly.

The datum feature size was small compared to that of the tolerated feature (measurand), resulting in high sensitivity of the datum. A possible explanation of the severe overestimation is the following. The method A imposed that the sampling was always the same for all repetitions and orientations. This applied to the datum feature as well, which was likely probed always at the same points, resulting in a lack of sensitivity of the method A.

II-6 Conclusions

An *a priori* method based on prior information of the CMM performance according to EN ISO 10360-2 [2] and on the geometry of the measurand was developed and presented in this Section 2. This method is referred to as B2 to distinguish it from the *a posteriori* method A—also developed in the EUCoM project but not part of this document [11]—and from the *a priori* method B1 dealt with in Section 1.

The method is based on the sensitivity analysis of an essential set of representative points. Closed-form equations for paradigmatic elementary measurement tasks were derived and reported. They are easily implemented with non-specialist software such as spreadsheets and listed in table for documentation, including a possible future international standard.

Extensive validation testing of the method B2 was performed. The tests were with several CMMs and the following artefacts: a cylinder square, a reference ring, an industrial connecting rod and two Multi-Feature-Check (MFC) standards. Uncertainties evaluated according either

¹³ The details are not reported here for brevity.

to the EN ISO 15530-3 [10] or to the Method A were compared with those evaluated with the method B2. The comparison was implemented through chi-squared testing.

The method B2 proved to be mostly compatible with the EN ISO 15530-3. The results obtained for the cylindrical square are particularly interesting. The investigation of the coaxiality when varying the length (longitudinal size) of the datum feature and the distance to it of the tolerated feature confirms the expectation that the uncertainties of different characteristics measured with the same CMM may differ significantly. Also confirmed was the expectation that the uncertainty of the diameter of a circle arc increases when the subtended central angle decreases. For small central angles, the method B2 overestimates the uncertainty, just like other methods.

The method B2 proved to be compatible with the method A too. Few cases were observed where overestimation occurred, with a single case of underestimation. They require further analysis.

The main characteristics of the method B2 are summarised below.

- The method takes data according to EN ISO 10360-2 testing as main input for the uncertainty evaluation; the data may be either the actual values incurred in testing or the MPEs. This information is likely available to any user of metrologically-confirmed CMMs.
- The method considers an essential set of representative points only, as opposed to the possibly many in the sampling plan. The points may be on either integral features (surface points) or derived features (such as axes, datums and sphere centres), the latter being in fact localisation points of features. The noise compression due to the redundancy of the many more sampling points does not take place in the method B2, leading to possible overestimation. This is acceptable, or even recommended, in view of the associated cost reduction or time shortening.
- The method is able to link the prior information on the CMM performance in size measurements [2] to that for any other dimensional or geometrical characteristic.
- The method currently disregards the effects due to the workpiece itself, such as the form error, but in principle it could be adapted to account for it too.
- Over twenty different cases of elementary characteristics were investigated. For each, the essential set of points and the closed-form sensitivity equations were given.
- The software validation procedure described in ISO/TS 15530-4 [13] and the suggestion therein to use a cylindrical square proved adequate for validating the method B2. However, the uncertainty comparison was carried through chi-squared analysis rather than the normalised error E_N .
- Experience in applying the method B2 to diverse geometric characteristics show that most uncertainty values fall within the range [0.8 – 2] of the A coefficient in the expression of the MPE ($E_{L,MPE} = A + L/B$). Exceptions were the coaxiality when a short datum feature is well separated from the tolerated feature, and the radius of the circle arc subtending a small central angle. In these cases, the uncertainty may be significantly larger.
- The expected B2 uncertainty's independence of the workpiece orientation in the CMM volume was confirmed. Any orientation can be assumed for the calculations, whichever is simplest. A good candidate is according to the drawing or CAD model.
- When applying the method to different CMMs—as long as the measurands remain the same—or when the b coefficient (to derive the uncertainty from the EN ISO 10360-2 data) is updated (e.g., to apply a different assumption on the error distribution), no re-evaluation of the partial derivatives is needed and the conversion can be done easily in a spreadsheet.
- Very importantly, this document did not consider all possible variants in deriving the measurand from an essential set of points. This applies particularly to deriving a normal vector to a plane through 3 points (A,B,C). This is evaluated as the cross product of two vectors having extremes in a combination of the three points, resulting in $\mathbf{AB} \times \mathbf{AC}$

or $BA \times BC$ or $CA \times CB$. The sensitivity equations are not the same for each option. To choose one properly, all three ought to be evaluated and that resulting in the smallest uncertainty chosen. This explains, e.g., the sharp change of slope in the graph of the uncertainty of a circle arc diameter in **Figure II-1** at $s = 74$ mm. The method, despite its simplicity, cannot be used effectively without suitable software.

II-7 References

- [1] *EN ISO 17450-1:2011 Geometrical product specifications (GPS) — General concepts — Part 1: Model for geometrical specification and verification*, 2011.
- [2] *EN ISO 10360-2:2009 Geometrical product specifications (GPS) - Acceptance and reverification tests for coordinate measuring machines (CMM) - Part 2: CMMs used for measuring linear dimensions*, 2009.
- [3] W. Płowucha, "Point-straight line distance as model for uncertainty evaluation of coordinate measurement," *Measurement*, vol. 135, pp. 83-95, 2019.
- [4] W. Płowucha, "Point-plane distance as model for uncertainty evaluation of coordinate measurement," *Metrology and Measurement Systems*, vol. 27, no. 4, p. 625–639, 2020.
- [5] *CEN ISO/TS 15530-1 Geometrical product specifications (GPS) — Coordinate measuring machines (CMM): Technique for determining the uncertainty of measurement — Part 1: Overview and metrological characteristics*, 2013.
- [6] *JCGM 100:2008 Evaluation of measurement data — Guide to the expression of uncertainty in measurement*, 2008.
- [7] *EN ISO 14253-2:2011 Geometrical product specifications (GPS) – Inspection by measurement of workpieces and measuring equipment - Part 2: Guidance for the estimation of uncertainty in GPS measurement, in calibration of measuring equipment and in product ve*, 2011.
- [8] P. Rosner, M. Wojtyła, E. G. Acedo and A. Balsamo, "Uncertainty evaluation for complex GPS characteristics," in *XXIII IMEKO World Congress "Measurement: sparking tomorrow's smart revolution"*, Yokohama, 2021.
- [9] M. Wojtyła, P. Rosner, A. B. Forbes, E. Savio and A. Balsamo, "Verification of sensitivity analysis method of measurement uncertainty evaluation," in *XXIII IMEKO World Congress "Measurement: sparking tomorrow's smart revolution"*, Yokohama, 2021.
- [10] *EN ISO 15530-3:2011 Geometrical product specifications (GPS) - Coordinate measuring machines (CMM): Technique for determining the uncertainty of measurement - Part 3: Use of calibrated workpieces or measurement standards*, 2011.
- [11] O. Sato and A. Balsamo, "Procedure for a posteriori (type A) evaluation of measurement uncertainty based on multiple measurement strategies," EUCoM project - Deliverable D1, 2022.

- [12] J. Frese, U. Neuschaefer-Rube and M. Bartscher, "Validation report of uncertainty evaluations for prismatic geometries," EUCoM project, Deliverable D3, 2022.
- [13] "ISO/TS 15530-4:2008 Geometrical Product Specifications (GPS) — Coordinate measuring machines (CMM): Technique for determining the uncertainty of measurement — Part 4: Evaluating task-specific measurement uncertainty using simulation". 2008.

Annex II-A Details of the chi-squared analysis of the cylinder square

The following tables are clustered in groups of three. Each group is about a different length of the datum feature, but the last group is about the common datum A-B. The three tables in each group report the analysis of U_1, U_2, U_4 , respectively, versus the uncertainty evaluated with the method B2.

The χ^2 values are reported in the last two columns of each table, derived for the values b_1 and b_2 , respectively, of the coefficient b .

The values of χ^2 are colour-coded (**Table II-3**).

Length of the datum feature, $l_A = 10$ mm

Table II-27: Chi-squared analysis with the experimental uncertainty U_1 . Length of the datum feature, $l_A = 10$ mm.

d/mm	Bias b/mm	$u_p/\mu\text{m}$	$U_1/\mu\text{m}$	$U_{B2}/\mu\text{m}$ ($b_1 = 0.58$)	$U_{B2}/\mu\text{m}$ ($b_2 = 0.459$)	χ_1^2 ($b_1 = 0.577$)	χ_2^2 ($b_2 = 0.459$)
5	4.26	1.99	8.71	10.3	8.2	14.23	22.52
10	4.84	2.76	10.71	13.1	10.4	13.45	21.29
15	5.99	2.39	11.16	16.7	13.2	8.99	14.22
20	8.08	3.62	15.59	20.7	16.4	11.39	18.03
25	8.39	3.47	15.60	24.9	19.8	7.87	12.45
30	11.63	5.19	22.20	29.2	23.2	11.55	18.28
35	13.33	5.28	24.07	33.6	26.7	10.25	16.22
40	13.78	6.27	26.48	38.1	30.3	9.67	15.29
45	14.79	5.42	25.82	42.6	33.9	7.35	11.63
50	16.99	6.73	30.60	47.1	37.4	8.44	13.36
55	18.59	6.92	32.58	51.6	41.1	7.96	12.59
60	18.76	7.27	33.45	56.2	44.7	7.09	11.21
65	21.33	7.87	37.20	60.8	48.3	7.50	11.86
70	21.29	8.27	37.95	65.3	51.9	6.75	10.68

Table II-28: Chi-squared analysis with the experimental uncertainty U_2 . Length of the datum feature, $l_A = 10$ mm.

d/mm	Bias b/mm	$u_p/\mu m$	$U_2/\mu m$	$U_{B2}/\mu m$ ($b_1 = 0.58$)	$U_{B2}/\mu m$ ($b_2 = 0.459$)	χ_1^2 ($b_1 = 0.577$)	χ_2^2 ($b_2 = 0.459$)
5	4.26	1.99	9.62	10.33	8.21	17.35	27.45
10	4.84	2.76	11.32	13.06	10.39	15.01	23.75
15	5.99	2.39	13.04	16.65	13.24	12.27	19.41
20	8.08	3.62	17.81	20.66	16.42	14.88	23.54
25	8.39	3.47	18.26	24.87	19.77	10.78	17.06
30	11.63	5.19	25.54	29.21	23.22	15.29	24.19
35	13.33	5.28	28.74	33.63	26.73	14.61	23.12
40	13.78	6.27	30.34	38.09	30.28	12.69	20.08
45	14.79	5.42	31.57	42.58	33.85	10.99	17.40
50	16.99	6.73	36.60	47.10	37.45	12.08	19.11
55	18.59	6.92	39.72	51.64	41.05	11.83	18.72
60	18.76	7.27	40.30	56.19	44.67	10.29	16.28
65	21.33	7.87	45.52	60.75	48.30	11.23	17.77
70	21.29	8.27	45.73	65.32	51.93	9.80	15.51

Table II-29: Chi-squared analysis with the experimental uncertainty U_4 . Length of the datum feature, $l_A = 10$ mm.

d/mm	Bias b/mm	$u_p/\mu m$	$U_4/\mu m$	$U_{B2}/\mu m$ ($b_1 = 0.58$)	$U_{B2}/\mu m$ ($b_2 = 0.459$)	χ_1^2 ($b_1 = 0.577$)	χ_2^2 ($b_2 = 0.459$)
5	4.26	1.99	7.92	10.33	8.21	11.77	18.62
10	4.84	2.76	11.37	13.06	10.39	15.14	23.95
15	5.99	2.39	9.98	16.65	13.24	7.19	11.37
20	8.08	3.62	14.30	20.66	16.42	9.58	15.16
25	8.39	3.47	14.38	24.87	19.77	6.68	10.57
30	11.63	5.19	20.37	29.21	23.22	9.73	15.39
35	13.33	5.28	22.00	33.63	26.73	8.56	13.55
40	13.78	6.27	24.44	38.09	30.28	8.24	13.03
45	14.79	5.42	23.71	42.58	33.85	6.20	9.81
50	16.99	6.73	28.09	47.10	37.45	7.11	11.25
55	18.59	6.92	30.25	51.64	41.05	6.86	10.86
60	18.76	7.27	30.78	56.19	44.67	6.00	9.50
65	21.33	7.87	34.21	60.75	48.30	6.34	10.03
70	21.29	8.27	35.04	65.32	51.93	5.75	9.10

Length of the datum feature, $l_A = 15$ mm

Table II-30: Chi-squared analysis with the experimental uncertainty U_1 . Length of the datum feature, $l_A = 15$ mm.

d/mm	Bias b/mm	$u_p/\mu m$	$U_1/\mu m$	$U_{B2}/\mu m$ ($b_1 = 0.58$)	$U_{B2}/\mu m$ ($b_2 = 0.459$)	χ_1^2 ($b_1 = 0.577$)	χ_2^2 ($b_2 = 0.459$)
5	3.77	2.26	8.72	9.7	7.7	16.04	25.37
10	4.23	2.71	10.00	11.1	8.8	16.22	25.67
15	5.43	2.55	10.91	13.1	10.4	13.96	22.09
20	5.94	3.66	13.52	15.4	12.2	15.42	24.40
25	8.91	5.11	19.33	18.0	14.3	23.18	36.67
30	10.65	5.28	21.39	20.7	16.4	21.44	33.93
35	10.50	5.94	22.55	23.5	18.6	18.49	29.25
40	11.30	4.96	21.43	26.3	20.9	13.27	21.00
45	12.22	5.43	23.26	29.2	23.2	12.68	20.07
50	13.57	5.82	25.37	32.1	25.6	12.46	19.71
55	14.19	5.67	25.71	35.1	27.9	10.72	16.97
60	16.14	6.07	28.45	38.1	30.3	11.16	17.66
65	16.09	6.08	28.42	41.1	32.7	9.57	15.15

Table II-31: Chi-squared analysis with the experimental uncertainty U_2 . Length of the datum feature, $l_A = 15$ mm.

d/mm	Bias b/mm	$u_p/\mu m$	$U_2/\mu m$	$U_{B2}/\mu m$ ($b_1 = 0.58$)	$U_{B2}/\mu m$ ($b_2 = 0.459$)	χ_1^2 ($b_1 = 0.577$)	χ_2^2 ($b_2 = 0.459$)
5	3.77	2.26	9.02	9.74	7.74	17.18	27.18
10	4.23	2.71	10.24	11.10	8.83	17.01	26.91
15	5.43	2.55	12.17	13.06	10.39	17.35	27.45
20	5.94	3.66	14.09	15.40	12.24	16.75	26.51
25	8.91	5.11	20.64	17.95	14.27	26.43	41.82
30	10.65	5.28	23.85	20.66	16.42	26.67	42.20
35	10.50	5.94	24.21	23.45	18.64	21.32	33.73
40	11.30	4.96	24.77	26.31	20.92	17.73	28.05
45	12.22	5.43	26.82	29.21	23.22	16.86	26.68
50	13.57	5.82	29.60	32.15	25.56	16.95	26.82
55	14.19	5.67	30.64	35.11	27.91	15.23	24.09
60	16.14	6.07	34.55	38.09	30.28	16.46	26.04
65	16.09	6.08	34.47	41.08	32.66	14.08	22.27

Table II-32: Chi-squared analysis with the experimental uncertainty U_4 . Length of the datum feature, $l_A = 15$ mm.

d/mm	Bias b/mm	$u_p/\mu m$	$U_4/\mu m$	$U_{B2}/\mu m$ ($b_1 = 0.58$)	$U_{B2}/\mu m$ ($b_2 = 0.459$)	χ_1^2 ($b_1 = 0.577$)	χ_2^2 ($b_2 = 0.459$)
5	3.77	2.26	8.07	9.74	7.74	13.73	21.72
10	4.23	2.71	9.32	11.10	8.83	14.09	22.29
15	5.43	2.55	10.07	13.06	10.39	11.89	18.82
20	5.94	3.66	12.78	15.40	12.24	13.78	21.80
25	8.91	5.11	18.07	17.95	14.27	20.26	32.05
30	10.65	5.28	20.09	20.66	16.42	18.92	29.93
35	10.50	5.94	20.98	23.45	18.64	16.01	25.33
40	11.30	4.96	19.96	26.31	20.92	11.51	18.22
45	12.22	5.43	21.74	29.21	23.22	11.08	17.53
50	13.57	5.82	23.63	32.15	25.56	10.81	17.10
55	14.19	5.67	24.31	35.11	27.91	9.59	15.17
60	16.14	6.07	26.83	38.09	30.28	9.92	15.70
65	16.09	6.08	26.52	41.08	32.66	8.33	13.18

Length of the datum feature, $l_A = 20$ mm

Table II-33: Chi-squared analysis with the experimental uncertainty U_1 . Length of the datum feature, $l_A = 20$ mm.

d/mm	Bias b/mm	$u_p/\mu m$	$U_1/\mu m$	$U_{B2}/\mu m$ ($b_1 = 0.58$)	$U_{B2}/\mu m$ ($b_2 = 0.459$)	χ_1^2 ($b_1 = 0.577$)	χ_2^2 ($b_2 = 0.459$)
5	3.18	1.70	7.13	9.5	7.6	11.21	17.73
10	3.90	1.64	7.73	10.3	8.2	11.21	17.73
15	4.13	2.31	9.17	11.5	9.2	12.61	19.95
20	6.69	3.88	14.71	13.1	10.4	25.36	40.13
25	7.99	5.29	18.76	14.8	11.8	32.19	50.93
30	7.46	4.68	17.03	16.7	13.2	20.92	33.11
35	7.38	4.17	15.97	18.6	14.8	14.71	23.27
40	8.78	5.11	19.20	20.7	16.4	17.29	27.35
45	9.56	4.56	18.90	22.7	18.1	13.81	21.84
50	9.69	4.81	19.51	24.9	19.8	12.30	19.46
55	11.26	5.34	22.12	27.0	21.5	13.39	21.19
60	10.48	5.50	21.67	29.2	23.2	11.00	17.41

Table II-34: Chi-squared analysis with the experimental uncertainty U_2 . Length of the datum feature, $l_A = 20$ mm.

d/mm	Bias b/mm	$u_p/\mu m$	$U_2/\mu m$	$U_{B2}/\mu m$ ($b_1 = 0.58$)	$U_{B2}/\mu m$ ($b_2 = 0.459$)	χ_1^2 ($b_1 = 0.577$)	χ_2^2 ($b_2 = 0.459$)
5	3.18	1.70	7.49	9.52	7.57	12.38	19.59
10	3.90	1.64	8.69	10.33	8.21	14.15	22.38
15	4.13	2.31	9.68	11.55	9.18	14.04	22.22
20	6.69	3.88	15.60	13.06	10.39	28.53	45.14
25	7.99	5.29	19.27	14.79	11.76	33.97	53.74
30	7.46	4.68	17.73	16.65	13.24	22.67	35.87
35	7.38	4.17	17.08	18.62	14.80	16.82	26.62
40	8.78	5.11	20.42	20.66	16.42	19.55	30.93
45	9.56	4.56	21.27	22.74	18.08	17.50	27.68
50	9.69	4.81	21.72	24.87	19.77	15.25	24.13
55	11.26	5.34	25.00	27.03	21.49	17.11	27.07
60	10.48	5.50	23.76	29.21	23.22	13.23	20.93

Table II-35: Chi-squared analysis with the experimental uncertainty U_4 . Length of the datum feature, $l_A = 20$ mm.

d/mm	Bias b/mm	$u_p/\mu m$	$U_4/\mu m$	$U_{B2}/\mu m$ ($b_1 = 0.58$)	$U_{B2}/\mu m$ ($b_2 = 0.459$)	χ_1^2 ($b_1 = 0.577$)	χ_2^2 ($b_2 = 0.459$)
5	3.18	1.70	6.48	9.52	7.57	9.26	14.66
10	3.90	1.64	6.98	10.33	8.21	9.14	14.46
15	4.13	2.31	8.43	11.55	9.18	10.67	16.88
20	6.69	3.88	13.88	13.06	10.39	22.57	35.71
25	7.99	5.29	17.79	14.79	11.76	28.96	45.82
30	7.46	4.68	15.96	16.65	13.24	18.37	29.06
35	7.38	4.17	14.93	18.62	14.80	12.85	20.34
40	8.78	5.11	21.43	20.66	16.42	21.52	34.06
45	9.56	4.56	17.42	22.74	18.08	11.74	18.57
50	9.69	4.81	18.20	24.87	19.77	10.71	16.95
55	11.26	5.34	20.41	27.03	21.49	11.40	18.04
60	10.48	5.50	20.23	29.21	23.22	9.59	15.17

Length of the datum feature, $l_A = 25$ mm

Table II-36: Chi-squared analysis with the experimental uncertainty U_1 . Length of the datum feature, $l_A = 25$ mm.

d/mm	Bias b/mm	$u_p/\mu\text{m}$	$U_1/\mu\text{m}$	$U_{B2}/\mu\text{m}$ ($b_1 = 0.58$)	$U_{B2}/\mu\text{m}$ ($b_2 = 0.459$)	χ_1^2 ($b_1 = 0.577$)	χ_2^2 ($b_2 = 0.459$)
5	3.91	2.21	8.76	9.4	7.5	17.28	27.35
10	4.31	2.03	8.84	9.9	7.9	15.77	24.96
15	5.88	3.32	12.82	10.8	8.6	28.31	44.80
20	7.35	3.61	14.85	11.8	9.4	31.50	49.83
25	6.98	3.55	14.35	13.1	10.4	24.13	38.18
30	6.36	3.55	13.73	14.4	11.5	18.10	28.63
35	8.19	3.36	15.20	15.9	12.6	18.29	28.94
40	8.92	4.57	18.27	17.4	13.9	21.97	34.77
45	8.99	3.82	16.89	19.0	15.1	15.76	24.94
50	10.66	3.88	18.68	20.7	16.4	16.36	25.89
55	9.80	3.88	17.81	22.3	17.7	12.73	20.14

Table II-37: Chi-squared analysis with the experimental uncertainty U_2 . Length of the datum feature, $l_A = 25$ mm.

d/mm	Bias b/mm	$u_p/\mu\text{m}$	$U_2/\mu\text{m}$	$U_{B2}/\mu\text{m}$ ($b_1 = 0.58$)	$U_{B2}/\mu\text{m}$ ($b_2 = 0.459$)	χ_1^2 ($b_1 = 0.577$)	χ_2^2 ($b_2 = 0.459$)
5	3.91	2.21	9.20	9.42	7.49	19.07	30.17
10	4.31	2.03	9.73	9.95	7.91	19.14	30.29
15	5.88	3.32	13.66	10.77	8.56	32.13	50.84
20	7.35	3.61	16.50	11.83	9.40	38.92	61.58
25	6.98	3.55	15.79	13.06	10.39	29.22	46.23
30	6.36	3.55	14.70	14.43	11.47	20.74	32.82
35	8.19	3.36	17.82	15.89	12.64	25.15	39.79
40	8.92	4.57	20.14	17.43	13.86	26.69	42.23
45	8.99	3.82	19.63	19.02	15.12	21.31	33.71
50	10.66	3.88	22.79	20.66	16.42	24.34	38.51
55	9.80	3.88	21.17	22.32	17.75	17.99	28.46

Table II-38: Chi-squared analysis with the experimental uncertainty U_4 . Length of the datum feature, $l_A = 25$ mm.

d/mm	Bias b/mm	$u_p/\mu\text{m}$	$U_4/\mu\text{m}$	$U_{B2}/\mu\text{m}$ ($b_1 = 0.58$)	$U_{B2}/\mu\text{m}$ ($b_2 = 0.459$)	χ_1^2 ($b_1 = 0.577$)	χ_2^2 ($b_2 = 0.459$)
5	3.91	2.21	8.20	9.42	7.49	15.14	23.95
10	4.31	2.03	8.04	9.95	7.91	13.06	20.67
15	5.88	3.32	12.07	10.77	8.56	25.09	39.70
20	7.35	3.61	13.78	11.83	9.40	27.14	42.94
25	6.98	3.55	13.28	13.06	10.39	20.68	32.72
30	6.36	3.55	13.30	14.43	11.47	17.00	26.90
35	8.19	3.36	13.94	15.89	12.64	15.38	24.33
40	8.92	4.57	16.97	17.43	13.86	18.97	30.01
45	8.99	3.82	15.41	19.02	15.12	13.13	20.78
50	10.66	3.88	16.89	20.66	16.42	13.38	21.17
55	9.80	3.88	16.27	22.32	17.75	10.62	16.80

Length of the datum feature, $l_A = 30$ mm**Table II-39:** Chi-squared analysis with the experimental uncertainty U_1 . Length of the datum feature, $l_A = 30$ mm.

d/mm	Bias b/mm	$u_p/\mu\text{m}$	$U_1/\mu\text{m}$	$U_{B2}/\mu\text{m}$ ($b_1 = 0.58$)	$U_{B2}/\mu\text{m}$ ($b_2 = 0.459$)	χ_1^2 ($b_1 = 0.577$)	χ_2^2 ($b_2 = 0.459$)
5	3.42	1.91	7.73	9.4	7.4	13.63	21.57
10	5.19	3.80	13.05	9.7	7.7	35.94	56.87
15	5.55	3.60	13.03	10.3	8.2	31.85	50.40
20	5.23	3.30	12.13	11.1	8.8	23.88	37.78
25	5.53	3.26	12.36	12.0	9.6	21.13	33.43
30	5.73	3.44	12.90	13.1	10.4	19.50	30.86
35	6.52	4.59	15.90	14.2	11.3	25.11	39.73
40	5.77	3.21	12.50	15.4	12.2	13.18	20.85
45	6.17	3.94	14.31	16.7	13.2	14.76	23.36
50	6.66	3.78	14.47	18.0	14.3	12.99	20.56

Table II-40: Chi-squared analysis with the experimental uncertainty U_2 . Length of the datum feature, $l_A = 30$ mm.

d/mm	Bias b/mm	$u_p/\mu m$	$U_2/\mu m$	$U_{B2}/\mu m$ ($b_1 = 0.58$)	$U_{B2}/\mu m$ ($b_2 = 0.459$)	χ_1^2 ($b_1 = 0.577$)	χ_2^2 ($b_2 = 0.459$)
5	3.42	1.91	8.09	9.37	7.45	14.92	23.61
10	5.19	3.80	13.03	9.74	7.74	35.80	56.63
15	5.55	3.60	13.39	10.33	8.21	33.62	53.20
20	5.23	3.30	12.53	11.10	8.83	25.49	40.33
25	5.53	3.26	13.00	12.02	9.56	23.38	36.99
30	5.73	3.44	13.52	13.06	10.39	21.43	33.90
35	6.52	4.59	16.06	14.19	11.28	25.62	40.53
40	5.77	3.21	13.36	15.40	12.24	15.07	23.84
45	6.17	3.94	14.79	16.65	13.24	15.77	24.94
50	6.66	3.78	15.44	17.95	14.27	14.78	23.39

Table II-41: Chi-squared analysis with the experimental uncertainty U_4 . Length of the datum feature, $l_A = 30$ mm.

d/mm	Bias b/mm	$u_p/\mu m$	$U_4/\mu m$	$U_{B2}/\mu m$ ($b_1 = 0.58$)	$U_{B2}/\mu m$ ($b_2 = 0.459$)	χ_1^2 ($b_1 = 0.577$)	χ_2^2 ($b_2 = 0.459$)
5	3.42	1.91	7.19	9.37	7.45	11.78	18.65
10	5.19	3.80	12.83	9.74	7.74	34.71	54.91
15	5.55	3.60	12.06	10.33	8.21	27.26	43.13
20	5.23	3.30	11.21	11.10	8.83	20.37	32.24
25	5.53	3.26	11.54	12.02	9.56	18.41	29.13
30	5.73	3.44	14.01	13.06	10.39	22.99	36.37
35	6.52	4.59	14.77	14.19	11.28	21.66	34.26
40	5.77	3.21	11.60	15.40	12.24	11.36	17.98
45	6.17	3.94	13.51	16.65	13.24	13.17	20.83
50	6.66	3.78	13.46	17.95	14.27	11.24	17.78

Length of the datum feature, $l_A = 35$ mm

Table II-42: Chi-squared analysis with the experimental uncertainty U_1 . Length of the datum feature, $l_A = 35$ mm.

d/mm	Bias b/mm	$u_p/\mu m$	$U_1/\mu m$	$U_{B2}/\mu m$ ($b_1 = 0.58$)	$U_{B2}/\mu m$ ($b_2 = 0.459$)	χ_1^2 ($b_1 = 0.577$)	χ_2^2 ($b_2 = 0.459$)
5	5.96	3.25	12.77	9.3	7.4	37.45	59.25
10	5.91	4.43	15.00	9.6	7.6	48.78	77.18
15	5.27	4.07	13.65	10.1	8.0	36.91	58.40
20	5.72	2.83	11.73	10.6	8.5	24.33	38.50
25	6.47	3.82	14.37	11.4	9.0	32.04	50.70
30	7.04	3.83	14.94	12.2	9.7	30.17	47.73
35	6.23	3.86	14.20	13.1	10.4	23.62	37.37
40	7.38	4.19	16.00	14.0	11.2	26.00	41.14
45	6.18	4.18	14.78	15.0	12.0	19.29	30.53

Table II-43: Chi-squared analysis with the experimental uncertainty U_2 . Length of the datum feature, $l_A = 35$ mm.

d/mm	Bias b/mm	$u_p/\mu m$	$U_2/\mu m$	$U_{B2}/\mu m$ ($b_1 = 0.58$)	$U_{B2}/\mu m$ ($b_2 = 0.459$)	χ_1^2 ($b_1 = 0.577$)	χ_2^2 ($b_2 = 0.459$)
5	5.96	3.25	13.73	9.33	7.42	43.29	68.50
10	5.91	4.43	14.92	9.61	7.64	48.22	76.30
15	5.27	4.07	13.46	10.05	7.99	35.89	56.78
20	5.72	2.83	12.93	10.64	8.46	29.54	46.74
25	6.47	3.82	15.16	11.35	9.03	35.65	56.40
30	7.04	3.83	16.14	12.17	9.67	35.20	55.69
35	6.23	3.86	14.78	13.06	10.39	25.62	40.53
40	7.38	4.19	17.09	14.03	11.15	29.67	46.94
45	6.18	4.18	15.05	15.05	11.96	20.02	31.68

Table II-44: Chi-squared analysis with the experimental uncertainty U_4 . Length of the datum feature, $l_A = 35$ mm.

d/mm	Bias b/mm	$u_p/\mu m$	$U_4/\mu m$	$U_{B2}/\mu m$ ($b_1 = 0.58$)	$U_{B2}/\mu m$ ($b_2 = 0.459$)	χ_1^2 ($b_1 = 0.577$)	χ_2^2 ($b_2 = 0.459$)
5	5.96	3.25	11.84	9.33	7.42	32.18	50.91
10	5.91	4.43	13.92	9.61	7.64	41.99	66.43
15	5.27	4.07	12.67	10.05	7.99	31.80	50.32
20	5.72	2.83	10.87	10.64	8.46	20.89	33.05
25	6.47	3.82	13.60	11.35	9.03	28.70	45.41
30	7.04	3.83	13.96	12.17	9.67	26.32	41.64
35	6.23	3.86	13.39	13.06	10.39	21.02	33.26
40	7.38	4.19	14.89	14.03	11.15	22.54	35.65
45	6.18	4.18	14.08	15.05	11.96	17.50	27.69

Common datum A-B, $l_{A-B} = 80$ mm

Table II-45: Chi-squared analysis with the experimental uncertainty U_1 . Common datum A-B, $l_{A-B} = 80$ mm.

h/mm	Bias b/mm	$u_p/\mu m$	$U_1/\mu m$	$U_{B2}/\mu m$ ($b_1 = 0.58$)	$U_{B2}/\mu m$ ($b_2 = 0.459$)	χ_1^2 ($b_1 = 0.577$)	χ_2^2 ($b_2 = 0.459$)
5	3.09	2.28	8.06	9.3	7.4	15.17	24.00
10	2.66	1.03	5.53	9.3	7.4	7.07	11.18
15	3.02	1.14	6.05	9.4	7.5	8.28	13.11
20	2.62	1.38	6.02	9.5	7.6	8.00	12.65
25	3.06	1.21	6.20	9.7	7.7	8.22	13.00
30	2.50	1.42	5.96	9.9	7.8	7.31	11.57
35	2.70	1.83	6.87	10.1	8.0	9.29	14.70
40	4.65	3.16	11.28	10.3	8.2	23.88	37.78
45	4.26	3.63	11.79	10.1	8.0	27.34	43.25
50	3.40	3.38	10.45	9.9	7.8	22.44	35.50
55	3.70	1.94	8.06	9.7	7.7	13.87	21.95
60	4.09	2.20	8.92	9.5	7.6	17.56	27.78
65	3.77	2.06	8.35	9.4	7.5	15.77	24.95
70	3.03	1.72	7.00	9.3	7.4	11.31	17.89
75	3.08	1.46	6.62	9.3	7.4	10.23	16.19

Table II-46: Chi-squared analysis with the experimental uncertainty U_2 . Common datum A-B, $l_{A-B} = 80$ mm.

h/mm	Bias b/mm	$u_p/\mu m$	$U_2/\mu m$	$U_{B2}/\mu m$ ($b_1 = 0.58$)	$U_{B2}/\mu m$ ($b_2 = 0.459$)	χ_1^2 ($b_1 = 0.577$)	χ_2^2 ($b_2 = 0.459$)
5	3.09	2.28	7.93	9.3	7.4	14.68	23.23
10	2.66	1.03	6.05	9.3	7.4	8.44	13.35
15	3.02	1.14	6.75	9.4	7.5	10.32	16.33
20	2.62	1.38	6.25	9.5	7.6	8.61	13.62
25	3.06	1.21	6.88	9.7	7.7	10.11	16.00
30	2.50	1.42	6.08	9.9	7.8	7.59	12.01
35	2.70	1.83	6.83	10.1	8.0	9.17	14.50
40	4.65	3.16	11.42	10.3	8.2	24.46	38.70
45	4.26	3.63	11.37	10.1	8.0	25.44	40.25
50	3.40	3.38	9.80	9.9	7.8	19.72	31.21
55	3.70	1.94	8.59	9.7	7.7	15.74	24.91
60	4.09	2.20	9.50	9.5	7.6	19.91	31.50
65	3.77	2.06	8.82	9.4	7.5	17.61	27.86
70	3.03	1.72	7.24	9.3	7.4	12.11	19.16
75	3.08	1.46	7.11	9.3	7.4	11.80	18.66

Table II-47: Chi-squared analysis with the experimental uncertainty U_4 . Common datum A-B, $l_{A-B} = 80$ mm.

h/mm	Bias b/mm	$u_p/\mu\text{m}$	$U_4/\mu\text{m}$	$U_{B2}/\mu\text{m}$ ($b_1 = 0.58$)	$U_{B2}/\mu\text{m}$ ($b_2 = 0.459$)	χ_1^2 ($b_1 = 0.577$)	χ_2^2 ($b_2 = 0.459$)
5	3.09	2.28	8.30	9.26	7.36	16.08	25.44
10	2.66	1.03	4.80	9.31	7.40	5.32	8.41
15	3.02	1.14	5.34	9.40	7.47	6.45	10.21
20	2.62	1.38	5.42	9.52	7.57	6.47	10.24
25	3.06	1.21	5.43	9.68	7.69	6.29	9.95
30	2.50	1.42	5.39	9.87	7.84	5.96	9.43
35	2.70	1.83	6.41	10.08	8.02	8.09	12.80
40	4.65	3.16	10.51	10.33	8.21	20.70	32.75
45	4.26	3.63	10.86	10.08	8.02	23.22	36.74
50	3.40	3.38	9.55	9.87	7.84	18.73	29.64
55	3.70	1.94	7.39	9.68	7.69	11.66	18.45
60	4.09	2.20	8.17	9.52	7.57	14.73	23.31
65	3.77	2.06	7.73	9.40	7.47	13.53	21.40
70	3.03	1.72	6.35	9.31	7.40	9.32	14.74
75	3.08	1.46	5.94	9.26	7.36	8.23	13.02

Conclusion

Conclusions

Two *a priori* methods were introduced in this document for the evaluation of the measurement uncertainty in coordinate metrology. They are *a priori* in that the information they use is known *prior to* any measurement is taken. Following the GUM's classification of uncertainty evaluations (Type A and B, founded on frequency and *a priori* distributions, respectively), these methods are referred to as *Methods B*.

These methods follow the main stream described in the GUM: the input uncertainty are identified and evaluated, and then propagated to the combined uncertainties. This requires two pieces of information: the input uncertainties and the sensitivity coefficients.

The input uncertainties are derived from known and standardized values of CMM metrological characteristics, either the measured values in actual EN ISO 10360 testing (when available) or their associated MPEs (*Maximum Permissible Error*) derived from data sheet or other sources.

The sensitivity coefficients are often conveniently arranged in matrices. They encode the information of the geometry of the problem, the sampling strategy and the selection and sequence of mathematical operators used to derive the results. The geometry is usually encoded in a drawing or CAD model and it is available as long as a specific measurement task is defined. The choice of the sampling and computational strategies is a valuable part of the metrologist's role. Different metrologists may favour different strategies deemed as most valuable for a specific characteristic. For instance, a very accurate strategy may be very expensive as well. Predicting the strategy-specific uncertainty is a valuable tool for designing and optimising experimental plans.

The proposed methods are unidirectional in their flow: given a strategy (and other information), they derive the uncertainty. The opposite (given a target uncertainty, define a strategy) would be very useful but difficult to do. The proposed approach leaves the optimisation to the metrologist's expert judgement, who decides which strategies to try out. The evaluation method helps in comparing alternatives by predicting the uncertainty of each, in a trial-and-error approach.

The two methods B proposed in this document share the same approach to the evaluation of the input uncertainties, based on EN ISO 10360-based information. They differ instead in the sensitivity analysis, resulting in completely independent methods.

- Method B1 divides the sensitivity analysis in two steps: from the input uncertainties to the sampled points (point cloud), and from the point cloud to the measurands. The former step is based on approximated models of the CMM behaviour, constrained to be consistent with the EN ISO 10360 performance. The latter step is independent of any CMM and is a pure geometrical problem.
- Method B2 is based on the careful selection of a small set of points. They may lay either on the workpiece surface or on a derived feature such as the axis of a cylinder. The set must be essential and paradigmatic: essential in that the measurands would not be achievable with lesser points; paradigmatic in that their locations represent reasonable sets of nearby measured points. As the set is essential (no redundancy and then no approximation), the measurands can be derived from the selected points in closed form. The sensitivity matrix is then formed by derivation of such analytical expressions.

Method B1 is very rigorous in its GUM-compliant approach. The price paid to dominate the intrinsic complexity of the problem is the approximation of the CMM error model. The rigid body model is well known in literature and well known is its very large number of error parameters, order of several hundreds. This would require a huge input variance matrix impossible to predict. The model is then simplified drastically based on the experience that few errors dominates and that close points are likely behaving similarly. The resulting few model parameters can be derived from the EN ISO 10360 values. Method B1 is able of tailoring the uncertainty evaluation to fine details of the sampling strategy, particularly when alternatives are evaluated. On the other hand, it requires dedicated software—all based on linear algebra

and implementable in common spreadsheets—whose development is usually not in the reach of CMM users.

The approximation underpinning Method B2 is completely different conceptually. Actual points are addressed collectively by means of the selected set. Subtleties in the probing strategies are disregarded by the method, which is then not suitable to discriminate among alternatives. On the other hand, the closed form enables derivation of the sensitivity coefficients once for all for any measurand. The resulting equations are simple enough that its coding in software is in the reach of educated CMM users. They can be recorded in tables and published in standards, so that no specific software is essential for applying the method.

The proposed methods are mature enough to be submitted for standardization to the competent ISO/TC 213/WG 10, as underpinned by the validation results reported in the project deliverables D3 and D4.